Seismic Geomorphology and Reservoir Characterization of Isolated Tertiary Reefs in the Eastern Sirt Basin, Libya

Abdeladim M. Asheibi

Submitted for the degree of Doctor of Philosophy

School of Energy, Geoscience, Infrastructure and Society (EGIS)
Heriot-Watt University
Scotland, UK

May 2018

ACADEMIC REGISTRY
Research Thesis Submission

Name*:*	Abdeladim M. Asheibi		
School:	School of Energy, Geoscience, Infrastructure and Society (EGIS)		
Version: *(i.e. First, Resubmission, Final)*	Final	Degree Sought:	PhD Petroleum Geoscience

Declaration

In accordance with the appropriate regulations I hereby submit my thesis and I declare that:

1) the thesis embodies the results of my own work and has been composed by myself
2) where appropriate, I have made acknowledgement of the work of others and have made reference to work carried out in collaboration with other persons
3) the thesis is the correct version of the thesis for submission and is the same version as any electronic versions submitted*.
4) my thesis for the award referred to, deposited in the Heriot-Watt University Library, should be made available for loan or photocopying and be available via the Institutional Repository, subject to such conditions as the Librarian may require
5) I understand that as a student of the University I am required to abide by the Regulations of the University and to conform to its discipline.
6) I confirm that the thesis has been verified against plagiarism via an approved plagiarism detection application e.g. Turnitin.

* *Please note that it is the responsibility of the candidate to ensure that the correct version of the thesis is submitted.*

Signature of Candidate*:*		Date:	

Submission

Submitted By *(name in capitals):*	
Signature of Individual Submitting:	
Date Submitted:	

For Completion in the Student Service Centre (SSC)

Received in the SSC by *(name in capitals):*			
Method of Submission (Handed in to SSC; posted through internal/external mail):			
E-thesis Submitted (**mandatory for final theses**)			
Signature:		Date:	

Please note this form should be bound into the submitted thesis.
Academic Registry/Version (1) August 2016

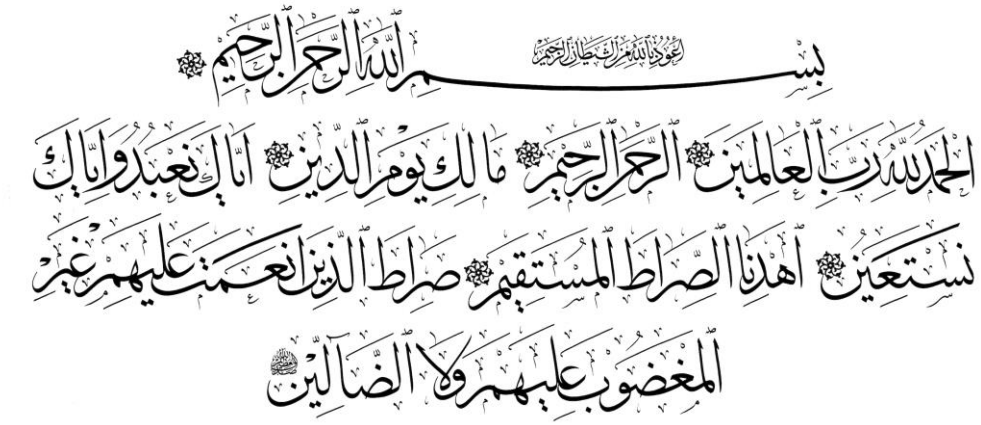

In the Name of Allah, the Most Beneficent, the Most Merciful

[All] praise is [due] to Allah, Lord of the worlds ۞ The Entirely Merciful, the Especially Merciful ۞ Sovereign of the Day of Recompense ۞ It is You we worship and You we ask for help ۞ Guide us to the straight path ۞ The path of those upon whom You have bestowed favor, not of those who have evoked [Your] anger or of those who are astray ۞

Surah Al-Fatihah, the Noble Quran

Abstract

The study area is situated on Ajdabiya trough, in the eastern part of Sirt basin, north-central Libya. The main play is Upper Sabil Carbonate, within large pinnacle reef traps. About twenty pinnacle reefs have been identified in the Ajdabiya trough within the Paleocene carbonates; some of these are oil bearing. The reservoirs are charged from the underlying mature Upper Cretaceous shales via faults and fractures. The aims of this study are to improve our understanding of the depositional and geomorphological processes, the reservoir characterization and the paleogeographic environment of the Paleocene reefs in the Sirt basin. In addition, it aims to provide a better understanding of the evolution of Sirt basin, which remains controversial. The present study is based on three-dimensional post-stack seismic and well logs. Well data have been used to indicate the lithological and petrophysical variations within the reefs. The seismic geomorphology has been used to assess how karst features have affected reservoir characterization. It is intended to improve the existing Intisar 'A' geological model using the properties estimated from the seismic inversion to enhance the interpolation and modelling, and to predict the properties of the Intisar 'B' and 'C' reservoirs, where minimum well control data is available. The study also provides a description of the Paleocene carbonate shelf and the opportunity to clarify and develop an understanding of the depositional processes, based on the combined interpretation of seismic attributes.

Karstification exhibits both positive and negative impacts on the quality of carbonate reservoirs. Carbonate dissolution can increase porosity and permeability, whereas seal quality may be reduced because of the collapse and deformation of strata overlying the karst features. Intisar 'B' and 'C' reefs contain only residual traces of oil, while Intisar 'A' has hydrocarbon fill factors as high as 85%. The seismic attributes indicate buried karst-collapse features within the Intisar 'B' and 'C' reefs, with an impact on the reservoir quality and the production of oil within these fields. These karst-collapse features provide pathways for upward movement of hydrocarbons into the Eocene reservoirs. This may be the main contributing factor to the escape of hydrocarbons from these two reef fields. The shale section above the reservoir is a weak cap rock and allows for upward hydrocarbon migration. The relationship of the karst-collapse features with an abnormally large upward movement of water explains the high water cuts in these two reef fields. The inverted impedance clearly highlighted variations in facies and porosity in the Intisar reefs which are not apparent in the

conventional seismic data. Five vertical facies units have been characterized in these reefs. The porosity of the south-eastern part of Intisar ‘A’ reef was significantly improved by faulting/fracturing and dissolution. The talus deposits are located on the north-eastern flank of Intisar ‘A’ reef. Well A6 on the southeast flank of the Intisar ‘A’ reef was the only remaining significant producer. It is most likely that it is draining oil from the talus zone.

The Intisar pinnacle reefs developed within the low energy outer-shelf environment in the protected southern embayment of the Ajdabiya trough. The distribution of the Intisar reefs is probably controlled by the Lower Sabil Carbonate paleo-highs’ topography. The Intisar ‘E’ and ‘L’ reefs may have developed along in the inner shelf margin where the broken discontinuous barrier reef complex has initiated a semi-lagoonal open marine area; this is the ideal condition for the continued growth of Intisar ‘E’ and ‘N’ pinnacle reefs in the inner shelf area. There are no evaporite sediments within the area surrounding or overlying these reefs, so the history of the Intisar reefs fits the Darwin transgressive type theory very well. The Intisar reefs have relatively the same size, shape and history as the Intisar ‘A’ reef. A practical geological model has been proposed that describes the evolution of these reefs.

Publications

Part of the work presented in this thesis is also presented in the following publications:

From Chapter 4:

Asheibi, A. and Shams, A. (2018). *Seismic geomorphology of Upper Sabil Carbonate reservoirs, Ajdabiya trough, Libya*. Marine and Petroleum Geology. Elsevier. *(under review)*

From Chapter 5:

Asheibi, A. and Shams, A. (2018). *The development of the Intisar reef in Sirt basin − An integrated seismic and petrophysics study*. Journal of Petroleum Science and Engineering. Elsevier. *(under review)*

From Chapter 6:

Asheibi, A. and Shams, A. (2018). *Paleoenvironmental interpretation of Paleocene carbonate Shelf, Ajdabiya trough, Libya*. Marine and Petroleum Geology. Elsevier. *(under review)*

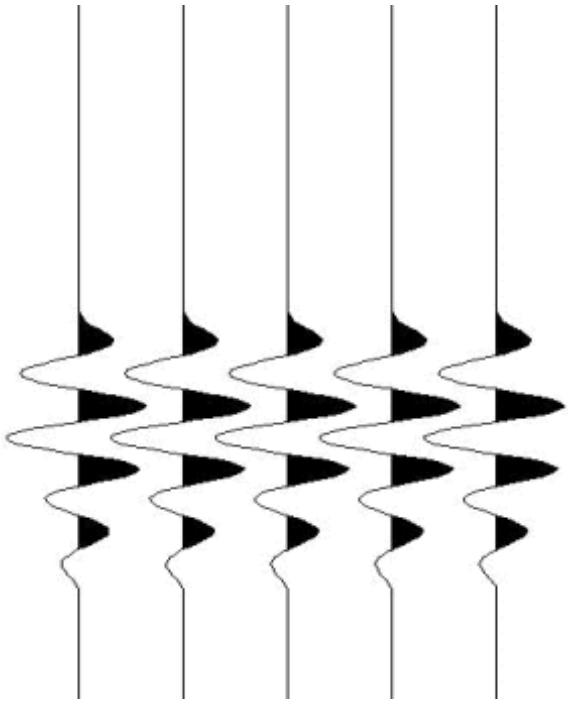

Dedication

to those

who love me

more than themselves...

My parents and my wife...

Acknowledgments

First and foremost, I would like to thank GOD for all that I have been given.

My special thanks go to the Libyan Ministry of Education and the University of Benghazi for the financial support. I would like to acknowledge the National Oil Corporation (NOC) of Libya and Zueitina Oil Company (ZOC) for providing the data for this work.

I would like to express my gratitude to Dr. Asghar Shams for being an extraordinary supervisor, and for all of the guidance and opportunities he has provided me. His constant guidance and advice were extremely helpful in completing my research. I gratefully acknowledge the great efforts of my second supervisor Professor Colin MacBeth for his help. I am very grateful to Professor Reza Rezaee from Curtin University, Dr. Mohamed Amish from Robert Gordon University and Dr. Hamed Amini from Heriot-Watt University for agreeing to be my examiners. I tried my best to keep the thesis as simple and interesting as I could. Thanks for your constructive criticism and the encouragement I received during the viva.

My deepest thanks are extend to Heriot-Watt University - UK for allowing the use of their facilities and software. Many thanks are also given to Abdul-Hamid Shahlol; the Arabian Gulf Oil Company (AGOCO), and Banour Dugdeg; Zueitina Oil Company (ZOC) for their help. I wish to thank my teachers and colleagues in the Earth Sciences Department, University of Benghazi - Libya for their advice, help and amusing conversation.

Um Zaid's support was infinite, I simply cannot thank you enough for always looking after me and my son. Finally, I am heavily indebted to my parents for every success in my life. Without your love, care and support I would have achieved nothing.

Abdeladim M. Asheibi

Edinburgh, UK

7 February 2018

ama111@hw.ac.uk

abdeladim.oshaiby@uob.edu.ly

Contents

Title *Page No.*

List of Figures

Figure ***Page No.***

List of Tables

Table ***Page No.***

Chapter 1. Introduction

Chapter 1
Introduction

1.1 Aims of the Thesis

The thesis presents a study of the large pinnacle reefs that formed along the north-central part of Libya during the Paleocene time. The aims of this thesis are to improve our understanding of the depositional and geomorphological processes, the reservoir characterization, and the paleogeographic environment of the Paleocene reefs in the Sirt basin using three-dimensional seismic and drilled well log data. Well log data have a higher resolution than seismic data and reveal more accurate information about petrophysical properties at well locations. On the other hand, seismic data provide a larger data coverage, but with much lower vertical resolution. One of the critical aspects in the evaluation of the prospectivity of an identified prospect or the development of a hydrocarbon discovery is the assessment of the reservoir quality beyond the areas covered by the wells. This issue becomes increasingly more difficult in carbonate reservoirs, where the distribution of porosity is more unpredictable compared to clastic reservoirs.

This study provides a description of the negative and positive effects of karstification on the quality of the Intisar reef reservoirs. Carbonate dissolution in the south-eastern part of Intisar ‘A’ reef has enhanced reservoir connectivity (increasing secondary porosity and improving permeability dramatically). However, dissolving large amounts of calcium carbonate preferentially continued moving the acidic water to

flow up through the fault zones, the seal unit within the Intisar ‘B’ and ‘C’ reefs has been breached, as overlying units collapsed into sinkholes under differential compaction. In addition, the study has allowed for a better determination of the main Intisar lithofacies units, and understanding of carbonate depositional environments and processes affecting the morphology of the reefs.

1.2 Location of the Study Area

The study area is situated on the Ajdabiya trough, in the eastern part of the Sirt basin, in north-central Libya. The study area represents the northern portion of Concession 103, with an area of 213 km^2. Concession 103 located between latitudes 28° 40´ and 29° 20´ N and between longitudes 20° 30´ and 21° 10´ E (Figure 1.1). The study area is 354 km south of Benghazi, and is restricted to onshore Libya and comprises predominantly desert terrain, with stony desert to the north and west, containing scattered sabkhas and large dune fields to the southeast and east.

Concession 103 contains an estimated 4.1 billion barrels of original oil in place (OOIP), and has produced 2.2 billion barrels of oil to date. There are six reefal fields in this concession; approximately 80% of the oil has been discovered in the Intisar ‘A’ and ‘D’ reef fields (Elag *et al.*, 2014). For the whole Intisar ‘A’ field, 58 wells have been drilled. Most of the wells were drilled in the late 1960’s to early 1970’s. The detailed reservoir characterization of this area has been concentrated on the reef core only and not outside reef and due to the depletion of oil in the reef this poses a challenge to find new discoveries to compensate for oil reduction in this area, where has a complete industry facility on surface.

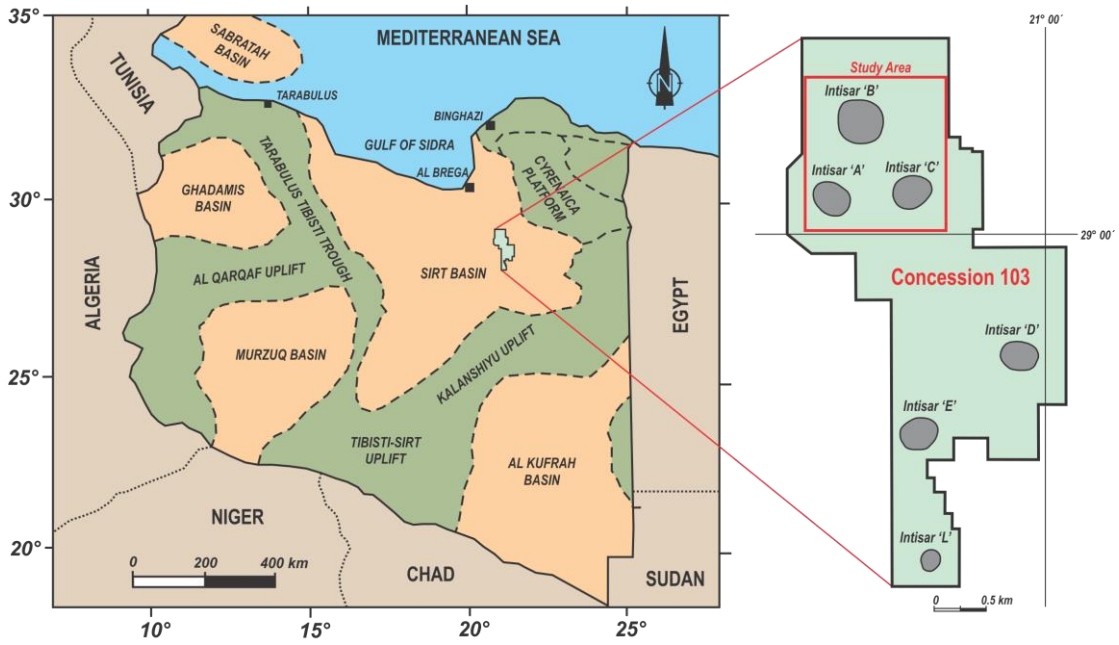

Figure 1.1. Libyan sedimentary basin and location of study area.

1.3 Database

Two main types of data were available for this study: three-dimensional post-stack seismic (covering an area of about 213 km^2) and well log data, including well locations (63 wells), as shown in Figure 1.2. All these data used in this study were provided by the *National Oil Corporation of Libya (NOC)*. The seismic data was first tied to the well log data. The second dataset was for a group of wells scattered over the area. Each of the wells had different types of logs. Gamma and density logs were available for every well, but no core data and neutron logs. Regional and global data for the stratigraphy, tectonics and lithology have been obtained from available published material.

The seismic data consist of 551 NS inlines and 621 EW crosslines. The inline and crossline intervals are 25 m. The seismic data show two-way travel times ranging down to 3-4 seconds, low amplitude and relatively low seismic resolution beneath the Tertiary. The well logs were acquired by *Schlumberger Co.* during 1967-1968. The formation tops between wells are not consistent and some wells penetrate only the tops of reefs, but do not penetrate completely to the reef platform. The basement has not yet been penetrated by the Intisar wells. The Intisar 'B' and 'C' reefs do not have a large amount of the well data.

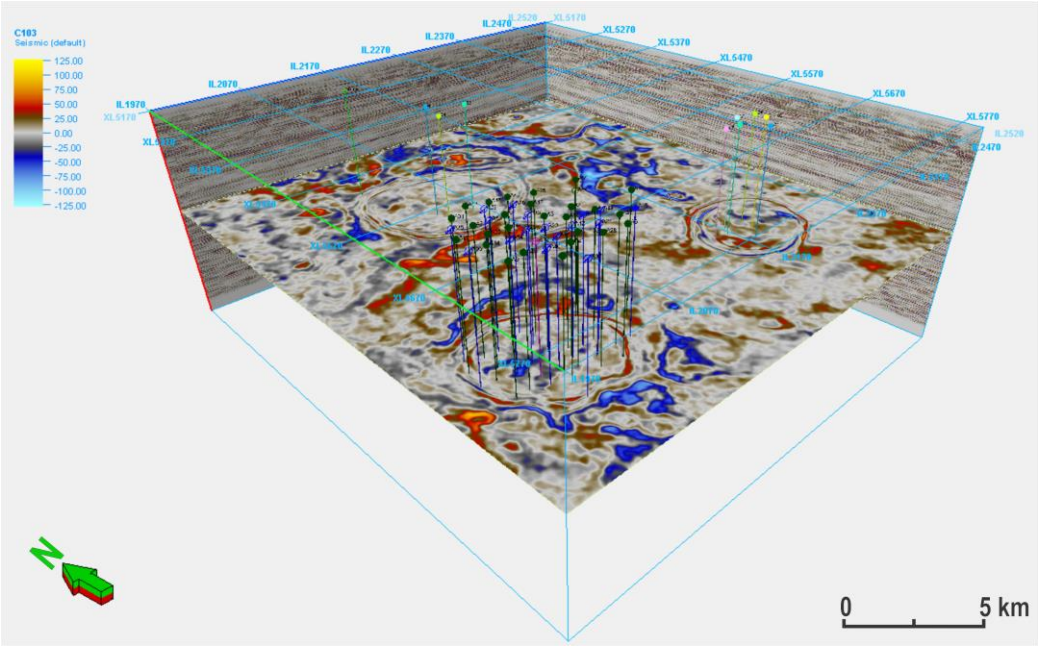

Figure 1.2. Three-dimensional seismic cube and wells for study area.

1.4 History of Concession

Oil exploration began in Libya in 1955, after a *Petroleum Law* was approved creating an independent *Petroleum Committee* to supervise the licenses for exploration. Between 1955 and 1968, the *Committee* approved 137 concessions to 42 international oil companies, once exploration set-ups were underway in 118 concessions covering an overall area of 586,000 km^2, one-third of the country's onshore area (APRC, 2004). The first oil discovery was made in 1957, close to the Algerian border (*ESSO Libya* – well Ashtan 1). The first commercial oil strikes in the Sirt basin were made in 1958, which marked an increase in exploration activity after the discovery of the giant Zelten field by *ESSO Libya* in 1959, and Libya started exporting crude two years later. The country became a member of *OPEC* (*Organization of the Petroleum Exporting Countries)* in 1962; in the following year, the *Ministry of Petroleum* was set up to take responsibility for the development of the oil industry.

Field	Well	Logs							Check Shot
		Gamma-ray	SP	Sonic	Bulk Density	Deep Resistivity	Medium Resistivity	Short Resistivity	
Intisar 'A'	A1	Yes	Yes	Yes	Yes	Yes	Yes	Yes	Yes
	A2	Yes*	Yes	Yes*	Yes*	Yes	No	Yes	Yes
	A3	Yes*	Yes*	Yes*	Yes	Yes	Yes*	Yes*	No
	A4	No	No	No	Yes*	No	No	No	No
	A5	Yes*	Yes	Yes*	Yes*	Yes	No	No	No
	A6	Yes*	Yes*	No	Yes*	Yes*	No	No	No
	A7	No	Yes*	Yes*	Yes*	Yes*	No	No	Yes
	A8	No	No	No	No	No	No	No	No
	A9	Yes	Yes	Yes	Yes	Yes	No	No	Yes
	A10	No	No	No	No	No	No	No	No
	A11	Yes*	Yes*	Yes*	Yes*	Yes*	Yes*	Yes*	Yes
	A12	Yes*	Yes*	No	Yes*	Yes*	Yes*	Yes*	No
	A13	Yes*	Yes*	No	Yes*	Yes*	Yes*	Yes*	No
	A14	Yes*	No	No	Yes*	No	No	No	No
	A15	Yes	Yes	Yes*	Yes	Yes	Yes	Yes	No
	A16	Yes*	Yes*	No	Yes*	Yes*	Yes*	Yes*	No
	A17	Yes*	Yes*	No	Yes*	Yes*	No	Yes*	No
	A18	Yes*	Yes*	No	Yes*	Yes*	No	Yes*	No
	A19	Yes	Yes	No	Yes	Yes	Yes	Yes	No
	A20	Yes	Yes	No	Yes	Yes	Yes	Yes	No
	A21	Yes	Yes	No	Yes	Yes	Yes	Yes	No
	A22	Yes	Yes	No	Yes	Yes	Yes	Yes	No
	A23	Yes*	Yes*	No	Yes*	Yes*	Yes*	Yes*	No
	A24	Yes	Yes	No	Yes	Yes	Yes	Yes	No
	A25	Yes	Yes	No	Yes	Yes	No	Yes	No
	A26	Yes	Yes	No	Yes	Yes	No	Yes	No
	A27	Yes	Yes	No	Yes	Yes	No	Yes	No
	A28	Yes	No	Yes	Yes	Yes	Yes	Yes	No
	A29	Yes*	Yes*	No	Yes*	Yes*	No	No	No
	A30	Yes*	Yes*	No	Yes*	Yes*	No	No	No
	A31	Yes	Yes	No	Yes	Yes	Yes	Yes	No
	A32	Yes*	Yes*	No	Yes*	Yes*	No	No	No
	A33	Yes*	Yes*	No	Yes*	Yes*	No	No	No
	A34	Yes*	Yes*	Yes*	Yes*	Yes*	No	No	No
	A35	Yes*	Yes*	No	Yes*	Yes*	No	No	No
	A36	Yes*	Yes*	No	Yes*	Yes*	No	No	No
	A37	Yes*	No	No	Yes*	No	No	Yes*	No
	A38	Yes*	No	No	Yes*	Yes*	No	No	No
	A39	Yes*	No	No	Yes*	No	No	No	No
	A40	Yes*	No	No	Yes*	No	No	No	No
	A41	Yes*	No	No	Yes*	No	No	No	No
	A42	Yes*	No	No	Yes*	No	No	No	No
	A43	Yes*	No	No	Yes*	No	No	No	No
	A44	Yes	Yes	No	Yes	Yes	Yes	Yes	No
	A45	Yes*	No	No	Yes*	No	No	No	No
	A46	Yes*	No	No	Yes*	No	No	No	No
	A47	Yes*	No	No	Yes*	No	No	No	No
	A48	Yes	Yes	Yes	Yes	Yes	Yes	Yes	No
	A51	Yes	Yes	Yes	Yes	Yes	Yes	No	Yes
	A52	Yes*	No	Yes*	Yes*	Yes*	Yes*	Yes*	Yes
Intisar 'B'	B1	Yes	Yes	Yes	Yes	Yes	No	Yes	No
	B2	Yes*	Yes*	Yes*	Yes*	Yes*	No	Yes*	No
	B3	Yes*	Yes*	No	Yes*	Yes*	Yes*	Yes*	No
	A4	Yes*	Yes*	Yes*	Yes*	Yes*	Yes*	Yes*	No
Intisar 'C'	C1	Yes	Yes	Yes	Yes*	Yes*	Yes*	Yes*	No
	C2	No	No	No	No	No	No	No	No
	C3	No	No	No	No	No	No	No	No
	C4	Yes	No	No	Yes	Yes	Yes	Yes	No
	C5	No	No	No	No	No	No	No	No
	C6	Yes	Yes	No	Yes	Yes	Yes	Yes	No
	C7	No	No	No	No	No	No	No	No
	C9	No	No	No	No	No	No	No	No
Off-reef	K1-12	No	Yes	Yes	No	No	Yes	No	No

Table 1.1. List of available well logs in this study. Yes means available, Yes* means partially available, and No means not available.

Concession 103 was awarded to *Occidental of Libya (Oxy), Inc*. by the *Libyan Ministry of Petroleum* on 29 March 1966. *Oxy* began seismic operations in Concession 103 early in 1967. A Geophysical Services International digital seismic recorder truck was shipped from Europe to Libya for work in *Oxy's* concessions; this was the first digital crew to work in Libya: a six-fold stack, dynamite charge sources, and 24 channels were used (Williams, 1972). The first two lines recorded crossed isolated reefs that eventually became the Intisar 'A' and 'B' oil fields. Seismic data allowed immediate identification of reefs, although the isolated pattern was not apparent until later. The Intisar 'A', 'B' and 'C' reefs were found and delineated by seismic data with Intisar 'A' and 'B' reefs being drilled before Intisar 'D' reef was detected on a seismic line; thus the type of prospect was well understood by the time Intisar 'D' reef was discovered.

In April 1967, the company drilled the first discovery well A1-103 on Concession 103, and discovered a major oil accumulation. The Intisar 'B' reef was explored in 1974. In September 1967, an exploratory well drilled in the concession discovered Intisar 'C'. Subsequently, in October 1967, the fourth drilling discovered a major oil accumulation in the Intisar 'D' reef (DesBrisay and Daniel, 1972).

The company drilled the A1-103 discovery well and pressure was maintained using water injection, which topped the pay at 9,416 ft. In May 1967, representatives from *Oxy* and the *Libyan Petroleum Ministry* tested the A1-103 well and estimated a flow rate of 43,000 barrels of oil per day from 689 ft, with 43.5° API oil. Following the completion of the discovery well, *Oxy* rapidly developed the Intisar 'A' field (Terry and Williams, 1969). By the end of 1967, eight wells were shut-in awaiting production outlets, and four rigs were drilling. During 1968, an additional nine wells were completed and a total of 17 wells were put on stream. Three rotary rigs were active at the end of the year. The production of the D1-103 discovery well was measured at rates up to 75,000 barrels of oil per day from 995 ft, with 40° API oil, and the field was estimated to contain more than one billion barrels of recoverable oil (Jenyon, 1990). The Intisar 'E' was discovered in 1968. The E1-103 well was drilled on a structure similar to the giant reef fields at Intisar 'A' and 'D'. A pipeline about 212 km long links the Intisar fields to the seaport of Zueitina.

The *Libyan General Petroleum Corporation* was operating under the overall charge of the *Ministry of Petroleum* in April 1968. It was authorized to operate at every level of the oil industry, from exploration to marketing. By 1969, Libya had become the world's 4th largest oil exporter, but it was getting the lowest per-barrel incomes in the

world. In 1970 the *Libyan General Petroleum Corporation* was replaced with the *National Oil Corporation (NOC) of Libya*. The new corporation was given wider powers than its precursor, including complete control of oil production, in order to decrease the rate of depletion of oil fields. The nationalization of the Libyan oil industry started in 1972. New sharing agreements provided *NOC of Libya* with a holding of a minimum of 51% in all concessions. *Occidental Petroleum, British Petroleum,* the *Oasis group* and *ENI* all accepted *NOC's* new sharing agreements. However, *Royal Dutch/Shell* and the U.S. companies – *Standard Oil of California, Mobil, Exxon* and *Texaco* – all refused. Their rejection of *NOC's* new terms led the government to decree in September 1973 that 51% of all their assets be nationalized and transferred to *NOC*, and the process was completed in April 1974 (APRC, 2004). In June 1986, the *Zueitina Oil Company (ZOC)* was formed after the departure of *Oxy* to control the six Intisar oil fields in Concession 103. Today, *NOC* has 87.5% and *OMV* (*Österr Mineralöl Verwaltung*) of Austria has 12.5% from *ZOC*. *OMV* had transported 25% into *Oxy* in 1985.

In 2001, there were 7 producing wells and 8 water injectors at Intisar 'A' field, and the production at this stage was 2400 barrels of oil per day at 83% water cut. Well A6 on the southeast flank of the Intisar 'A' reef was the only remaining significant producer at this time.

1.5 Previous Work

Several geological studies have been performed by various authors in Sirt basin, as a result of hydrocarbon exploration since the nineteen seventies. This previous work relating to Sirt basin were pioneered by an Italian geologist called *Ardito Desio (1897 – 2001)* who made a geological map of Libya in 1931 (Bagnold, 1933; Desio, 1935). The tectonic history and stratigraphy of the Sirt basin has been studied by several authors, among them Barr and Weegar (1972); Banerjee (1980); Anketell (1996); Hallett and El Ghoul (1996); Burwood, Cope and Redfern (2000), who examined the petroleum systems and geochemical evolution of the Eastern Sirt basin. Recent work by Hallett and Clark-Lowes (2016) also provided better understanding of the basin's evolution, tectonic, stratigraphic and hydrocarbon potential. A few new papers on the geology of the Ajdabiya trough area and particular on the Paleocene event have been published in recent years. For example, the Paleocene Sequence in the Sirt Basin was studied by

Bezan (1996). Gerdes *et al.* (2010) explained the effect of eustasy variation on the Tethyan carbonate sediments during Mesozoic and Cenozoic times.

Many reef fields occur in the Sirt basin of Libya, although only a small amount of work related to the Libyan reefs has been published. To date, only a couple of studies by Terry and Williams (1969); Brady, Campbell and Maher (1980) have described their petrographic and petrophysical properties, based on well data, from two reefs: Intisar 'A' and 'D', respectively. Only one study, by Gumati (1992) has defined the trend of pinnacle reefs within the late Paleocene sediments of the Ajdabiya trough. Later, Wang *et al.* (2016) described how and when submarine channels developed and how they were influenced by the presence of the Intisar 'E' reef, based on seismic attributes, while Faraj *et al.* (2016) analyzed crude oil samples from Intisar 'A', 'D' and 'E, fields by using organic geochemistry analysis.

1.6 Methodology and Objectives of the Research

The conventional seismic interpretation has identified the Intisar 'A', 'B' and 'C' pools as reefal bioherms. However, their detailed facies classification and reservoir characterization remain unresolved. The work programme is targeted to explain why some reefs are charged and some are not. A secondary objective of this work is to update the existing geological models in the Intisar 'A' reef field using the properties estimated from seismic inversion to enhance the interpolation and modelling. The study also provides a description of the Paleocene carbonate shelf and the opportunity to clarify and develop an understanding of the depositional process in this area. The methodology used for this study is summarized as a workflow chart in Figure 1.3.

All well logs were analysed in detail, and generally it was observed that the log quality was good, and the calculated porosity and saturation data were considered reliable. Water-based mud was used in the drilling fluid. Total porosity was calculated from density logs. Water saturation values were calculated from the logs using the Archie (1942) equation. Formation water resistivity was estimated using the Pickett (1973) plot within the water zone of the reservoir. This data was then used to identify the lithological and petrophysical variations within reefs, and to extract depositional facies from well logs to improve the geological/petrophysical models provided by Terry and Williams (1969) for the Intisar 'A' reef field.

Two main horizons (the top and base of the Upper Sabil Carbonate) were interpreted for the Paleocene reefs. Initially, auto-tracking of horizons was meant to be

utilized with the capability of skewing the horizon; however, it picks within a window restriction and does not always continue picking the correct reflector. This is most prevalent when the amplitude of the reflector varies throughout the survey. Given the above issues auto tracking of the horizons was not used in this study. Having these key formation tops picked allows me not only to create maps along that surface, but also to see subsurface stratigraphy within the seismic data and determine the reef extensions.

Seismic geomorphology helps to examine buried landforms (geomorphological features) using seismic attributes as a tool. In this study, seismic attributes helped to extract more information from conventional three-dimensional seismic data, to support the geomorphology and also interpretation of paleo-environments. Several seismic attributes have been generated to illuminate reef and karst features. Seismic attributes are a powerful tool when viewed in horizon and time slices. Thus, seismic geomorphology has been used to assess how karst features affected reservoir characterization, and to explain why the Intisar 'B' and 'C' reefs are not charged.

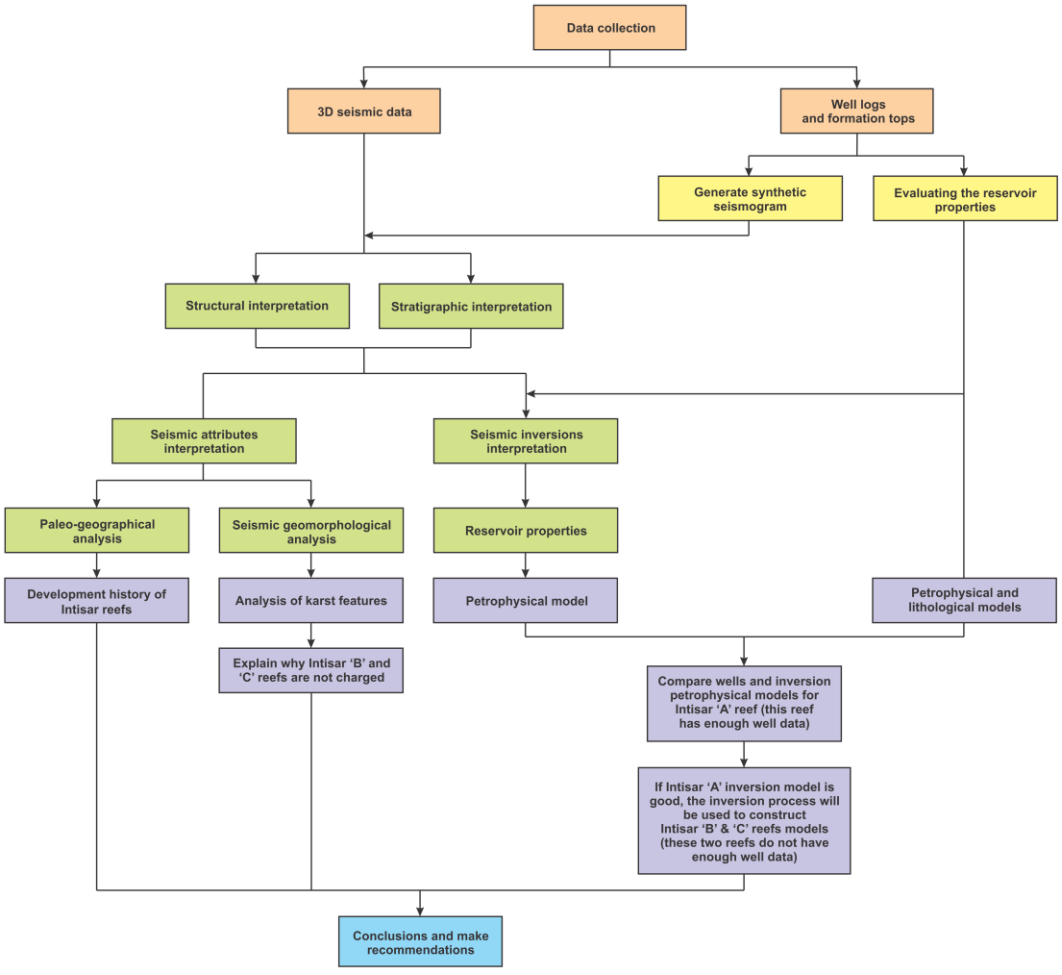

Figure 1.3. Flowchart of methodology for interpretation of Intisar reefs.

Seismic reservoir characterization is carried out to recognize reservoirs, define them and determine the distribution of their petrophysical properties, which will provide an early indication of the reservoir's potential. Well log data provide a high resolution estimation of the petrophysical properties of a reservoir and the surrounding layers. Nevertheless, properties can only be determined in the area local to the well. At the present time, it has become possible to calculate some of the petrophysical properties using seismic data, when those seismic data are calibrated with well control data. However, in many cases seismic data alone cannot provide a complete picture of the reservoir: for example, in some situations seismic data can be used to predict reservoir porosity but they may not give accurate information on saturation and fluid type. The objectives of this part are (a) to determine whether seismic inversion is an effective technique that can be used in the evaluation of the reservoir potential of the Intisar reefs, (b) to improve the existing Intisar 'A' reef geological/petrophysical model using the properties estimated from the inverted seismic to enhance the interpolation and modelling, and (c) predict the properties of Intisar 'B' and 'C' reservoirs, where minimum well control data is available. A detailed study of the petrophysical modelling, from seismic inversion and well information, could help in determining new prospective areas.

The seismic data has been used to predict, map and describe the depositional paleoenvironmental setting for Upper Sabil Carbonate (Figure 1.4) by classifying the seismic facies to define the seismic attribute variations caused by geological changes. About 1882 km^2 of seismic data was provided by *NOC Libya*, which merged the volume of various seismic surveys acquired over several years in Concession 103. The aims of paleoenvironmental interpretation are to clarify and develop an understanding of the depositional processes and the physical controlling factors affecting the distribution and morphology of the Intisar reefs, based on the combined interpretation of multi-seismic attributes. In addition, it is aimed to describe the development history of the Intisar pinnacle reefs. The results also provide new understandings on the paleogeographic, paleoenvironmental and tectonic evolution of the Sirt basin, which remain controversial. The Upper Sabil Carbonate reflector was tracked manually, and was then auto-tracked in the seismic cube using a selected time window. The seismic reflector was then gridded and a regional time-structure map was created. Along with conventional seismic time-structure and amplitude displays, dip illumination, the variance and the spectral decomposition seismic attribute time slices, and the RMS amplitude multi-attribute surface maps were created from the target horizons.

1.7 Thesis Layout

The thesis is divided into seven chapters. The current chapter has given a general introduction to the area and presented a background based on previous work that has been undertaken. This chapter has also defined the objectives and data preparation of this research. Chapter Two introduces the basic concepts of reef carbonate rocks, including classification of carbonate rocks, diagenesis, porosity and carbonate depositional environment, and the geophysical exploration of reef carbonates. Chapter Three reviews the geological setting of the Sirt basin, including its geology, tectonic frameworks, lithology, hydrocarbon potential and the sedimentological environment of the Ajdabiya trough, together with a review of the reef reservoirs in Sirt basin. Chapter Four presents an interpretation of reefal features that can be reverted from the seismic data and mapping these features and evaluates the reservoir within the context of the seismic geomorphology and depositional environment This chapter also interprets the seismic attribute maps to aid in reservoir delineation. Chapter Five discusses the seismic inversion and mapping porosity, describing reservoir compartmentalization, and evaluates the performance of seismic inversions by correlation with well data to verify the petrophysical model built only by using well data. Chapter Six describes the depositional paleoenvironmental setting for Upper Sabil Carbonate by classifying the seismic facies to define the seismic attribute variations caused by geological changes. This chapter also discusses the implications of the depositional processes and the physical controlling factors affecting the distribution and the morphology of the Intisar reefs. Finally, Chapter Seven summarises all of the innovative aspects of the thesis and the conclusions from the various studies in the thesis and provides some recommendations and suggestions for future work that might benefit the development in the study area.

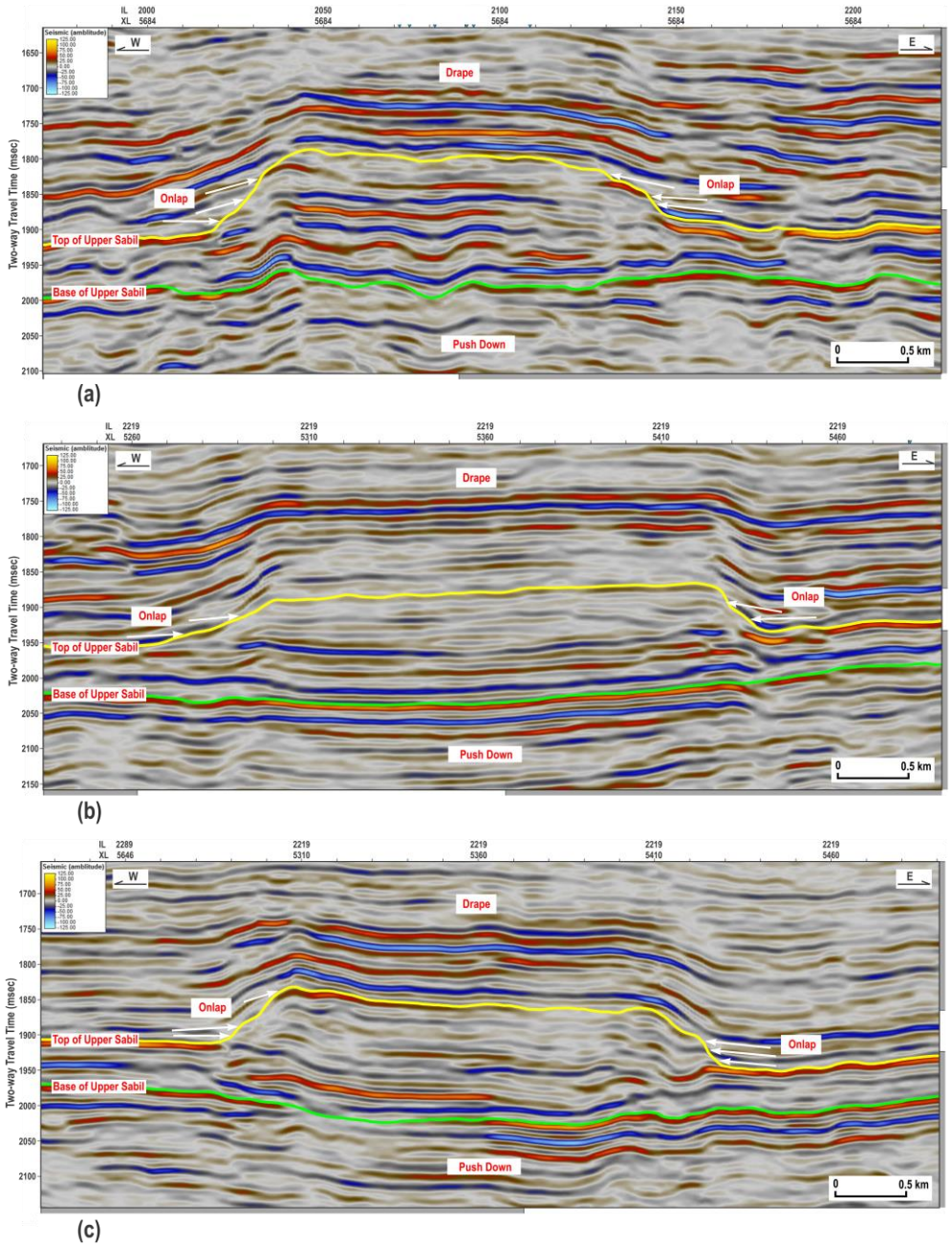

Figure 1.4 Seismic cross-sections over (a) Intisar 'A', (b) Intisar 'B' and (c) Intisar 'C' reefs, displaying the top and base of Upper Sabil Carbonate.

Chapter 2. Principles of Reef Carbonate Sedimentation

Chapter 2

Principles of Reef Carbonate Sedimentation

2.1 Introduction

Carbonate deposits happen naturally as reefs and sediments in recent tropical marine environments, as old sediments, and as significant hydrocarbon reservoir rocks (Ahr, 2008). About 20% of sedimentary rocks are carbonate, and they contain about 50% of the world's oil reserves (Flügel, 2004). About 90% of the carbonate rocks found in recent environments are supposed to be biotic in origin and formed under marine environments (Wilson, 1975; Tucker and Wright, 1990). Distribution of carbonate deposits is directly controlled by ecological parameters favourable for the precipitation of abiotic and biotic calcium carbonate. These parameters include: light, temperature, substrate, salinity and the presence or absence of siliciclastics (Lees, 1975). Carbonate sediments are anionic, consisting of $(CO_3)^2$. The link between the carbonate set and the metallic cation is not stronger than the inner links in the structure of CO_3 (carbon trioxide), which are not stronger than the covalent link in CO_2 (carbon dioxide). Thus, the carbonate set breaks down to produce CO_2 and H_2O (water) in the presence of hydrogen ions.

2.2 Classification of Carbonate Rocks

Practical classifications of carbonate rocks are based on descriptions obtained by using microscopes or hand lenses. Classifications of carbonate rocks often overlap. Therefore, the important sedimentary rock elements must be described in most classifications (e.g., if a limestone rock is composed of ooids and contains skeletal remains, it is called a skeletal-oolitic limestone). The most commonly used classifications in Libya are those by Folk (1962) and Dunham (1962), which are based on matrix content. Folk's classification is more detailed than other classifications, as it includes grain size, sorting, roundness, packing and grain composition (Figure 2.1). On the other hand, Dunham's classification is simple and easily used in the field by geologists. Thus, Folk's classification has been almost universally supplanted by that of Dunham (Moore and Wade, 2013).

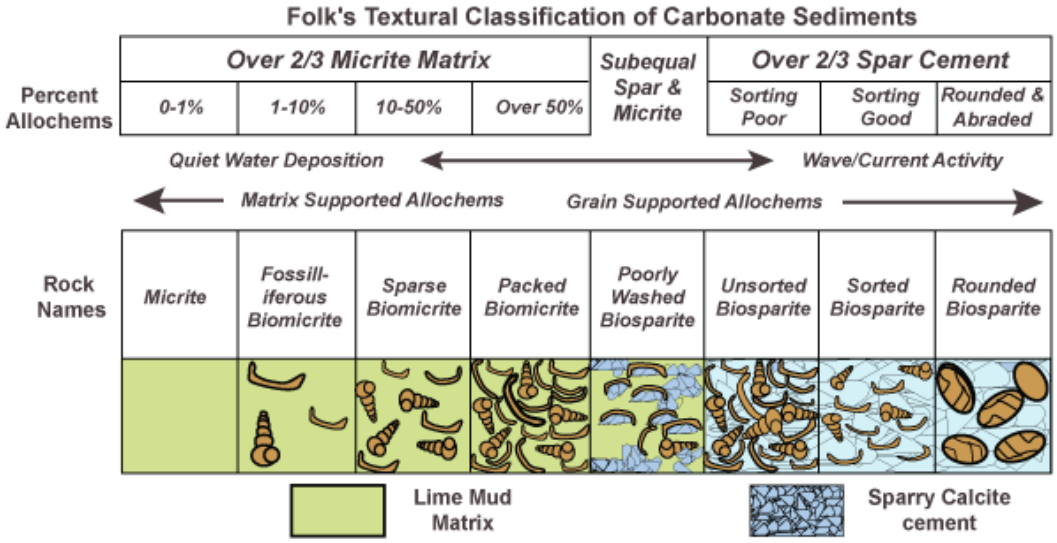

Figure 2.1. Carbonate rock classification of Folk (1962).

2.3 Diagenesis of Carbonate Rocks

The diagenesis of carbonates consists of several different processes and takes place in shallow marine environments, down into a deep-burial situation. It is most important in blocking and creating porosity in the sediments. The major diagenetic processes can be distinguished as dissolution, cementation, compaction, dolomitization, neomorphism and microbial micritization. Actually, depositional and diagenetic processes may be going on at the same time. For example, as a carbonate buildup is

growing or carbonate sand is being moved by the waves, cements may be caused in intra-skeletal voids and grains changed by *microbial micritization*. *Cementation* is the diagenetic process of making a hard limestone rock from a loose sediment, and takes place mainly where there is an important amount of pore fluid supersaturated with respect to the cement stage. *Neomorphism* is recrystallization and the replacement processes where there may have been a modification of the mineralogy. Many carbonates have suffered *dissolution* as a result of the passage of undersaturated pore fluids with respect to the present carbonate stage. The secondary porosity is created by carbonate dissolution. *Compaction* takes place during deep burial, resulting in a closer packing of grains under the pressure of overlying layers (Tucker, 1991). *Dolomitization* is a diagenetic process that changes limestone to dolomite over a micro-chemical process of calcium carbonate dissolution and dolomite precipitation. The shape of dolomitization will be controlled by the volume and source of the dolomitizing water, $CaMg(CO_3)_2$, and the flow path (Lucia, 2007). The distribution of dolomites may be characteristic for the type of flow system responsible for dolomitization (Figure 2.2). Carbonate buildup bodies have a number of possible dolomitization models related to (a) reflux, (b) costal mixing zones, (c) slope convection, (d) burial-compaction flow, and (e) regional-scale flow.

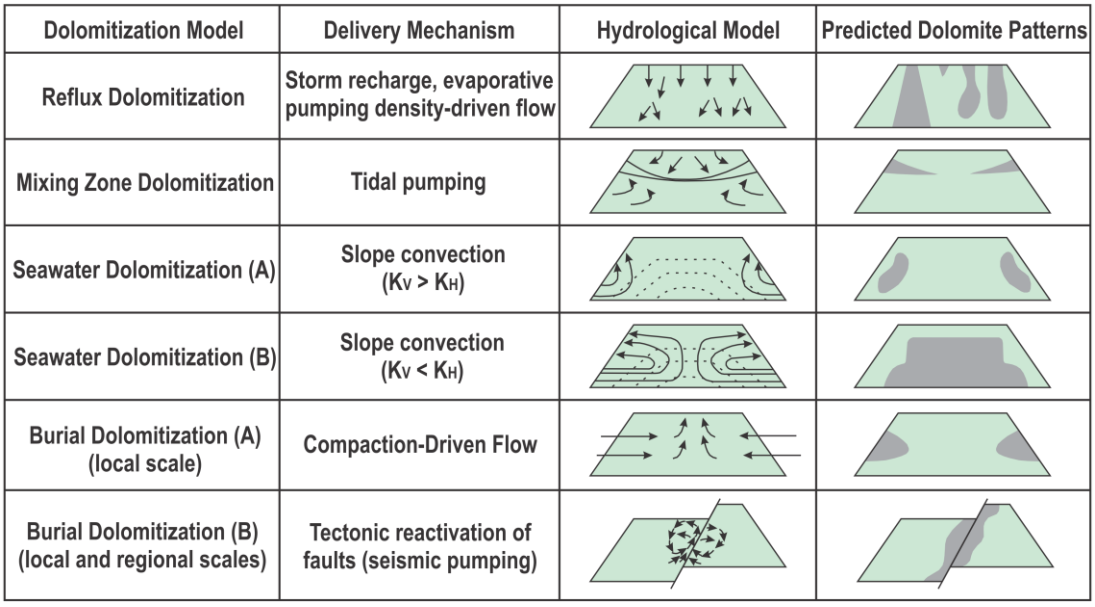

Figure 2.2. Diagrams of different models of dolomitization. Arrows denote flow direction and dashed lines are isotherms; modified after Machel (2004).

2.4 Porosity in Carbonate Rocks

Porosity is gained through tectonic fracturing, dolomitization and dissolution, and reduced or lost through compaction and cementation. Porosity in carbonates can be primary (or depositional) and/or secondary (or diagenetic – tectonic). Primary porosity includes framework porosity formed by rigid carbonate skeletons such as coral reefs and algae, and inter-particle porosity dependent on the shape and distribution of grain size. Secondary porosity comprises caverns, vugs and moulds produced by dissolution of rock grains, inter-crystalline porosity formed through dolomitization, and fracture porosity produced through compressions and tectonic activities (Tucker, 1991).

Many classifications of porosity in carbonate sediments have been suggested; however the classification proposed by Choquette and Pray (1970) has met with widespread approval. Their system of classification, of which Figure 2.3 is a graphic representation, is based on the fabric-selectivity of the porosity development, with additional distinctions being provided by modifiers indicating the genesis of the porosity and the size and abundance of pores.

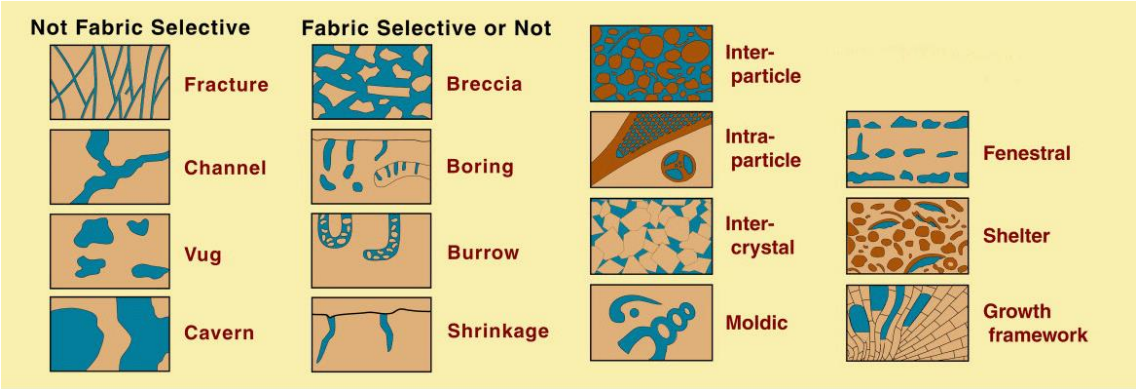

Figure 2.3. The classification of carbonate porosity provided by Choquette and Pray (1970).

2.5 Morphology of Carbonate Shelves

The term carbonate shelf in general refers to a thick sediment of shallow marine carbonates. Carbonate shelves develop in a variety of tectonic situations, such as foreland basins, rift systems and passive margins (Tucker and Wright, 1990). Many types of shelves are recognized as siliciclastic, rimmed and ramp shelfs.

A *rimmed carbonate shelf* is characterized by a pronounced disruption in the slope into a deeper marine area at the shelf margin. According to the nature of the shelf

margin, slope angles might vary from 1° to nearly 90° (Figure 2.4). The shelf margin is a high-energy shoal zone and/or shallow-water high-energy reefs. The rimmed shelf is often separated by a lagoon during development and becomes significantly deeper because of the higher growth rates of the carbonate marginal facies. The shore zone of the shelf interior may be dominated by siliciclastics, if there is a source of clastics (Ahr, 2008).

A *carbonate ramp* (Figure 2.4) is a gently sloping surface, in general less than 1°, on which a high-energy shoreline passes gradually into deeper marine environments with no obvious variation in slope (Ahr, 1973). Wilson (1975) suggested that carbonate ramps are an early stage in the development of a rimmed shelf. If the basin is relatively small and shallow with a low subsidence rate, such as many epeiric basins, a rimmed shelf may evolve into a ramp as the basin is filled and the slope angles off the shelf decrease.

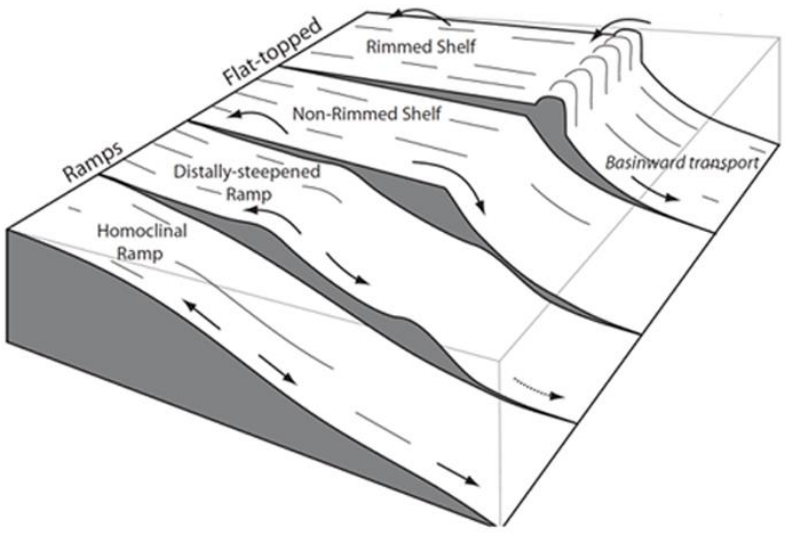

Figure 2.4 The structural view of the different types of carbonate shelf (Pomar, 2001).

2.6 Reefs, Banks and Buildups

The term *reef* has been used somewhat loosely on occasions, but it is defined here as a bioherm, that is, the creation of the actively structure and biotic ingredient sediments, which have the ability to form upstanding rigid and wave resistant relief structures (Lowenstam, 1950). Related terms sometimes confused with reef are biostrome and bioherm (Figure 2.5). The term *biostrome* is purely used for structures

such as coral beds, crinoid beds, shell beds, etc., containing and built mainly by sedentary organisms and without growth into lens-like or mound-like forms. A *bioherm* is a reef, bank or mound – of entirely organic origin, embedded in rocks of different lithology (Cumings, 1932; Braithwaite, 1973). Consequently, some bioherms are reefs and some are not, but all reefs are bioherms (Davis, 1983). A *bank* is a bioherm, created by organisms that do not have the ecological potential to create upstanding, rigid, wave resistant topographical structures (Nelson, Brown and Brineman, 1962). The term *buildup* is preferably applied to anybody of carbonate rock that has built up topographic relief above the surrounding environment (Prothero and Schwab, 2004).

According to the geometry of the reefs, Dunham (1970) suggested two different types of carbonate reefs; *stratigraphic reefs* and *ecologic reefs* (Figure 2.6). A stratigraphic reef is a thick, horizontally limited mass of carbonate rocks, often composed of several overlaid bioherms and/or biostromes, which individually had slight topographic structure above the surrounding sea floor at time of reef growth, while, an ecologic reef is a rigid, wave resistant topographic relief usually formed during one specific period. A stratigraphic reef may include ecologic stages.

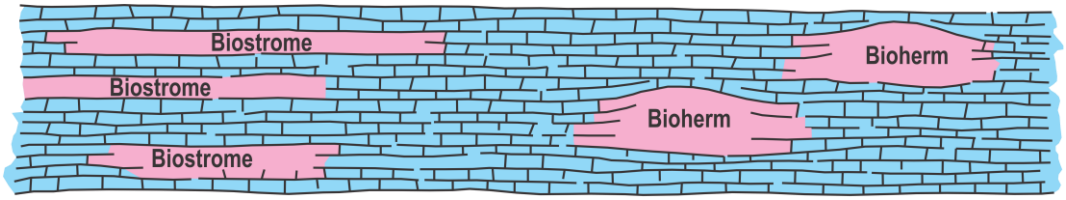

Figure 2.5. Showing the difference in geometry between a bioherm and biostrome (James, 1983).

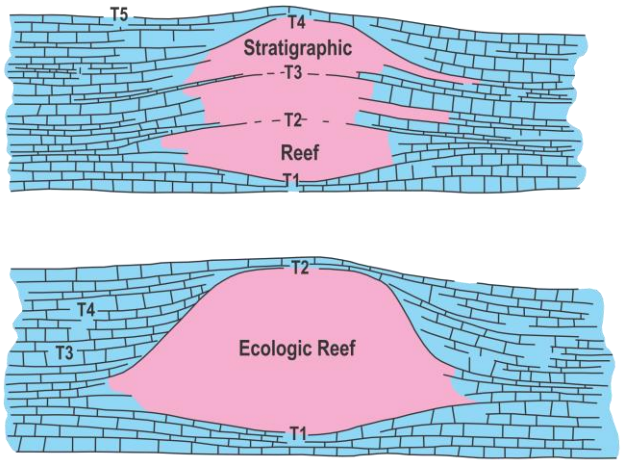

Figure 2.6. Showing the difference between ecologic and stratigraphic reefs (James, 1983).

2.7 Types of Reefs

The term reef itself is best restricted to a carbonate buildup which possesses a water-resistant framework constructed by organisms, but to be clear the term ecologic reef or organic framework reef should be used for this. A variety of reefs may be grouped into four main forms, shown in Figure 2.7. *Barrier reefs* are linear mounds, with comparatively deep marine on both flanks during growth. *Pinnacle reefs* are nearly equidimensional mounds and were enclosed by deep marine sediments during growth; this type of reef is common in the reservoirs in Sirt basin in Intisar (C103), Sahabi (NC73), Mheirigah (LP3C) and Shatirah (NC163). *Shelf-margin reefs* are linear mounds, with deep marine sediments on one flank, and shallow marine sediments on the other flank. *Patch reefs* are nearly equidimensional mounds and formed in shallow marine environments, either very close to shelf margins or over wide, shallow marine areas (Bubb and Hatlelid, 1978).

There are many factors controlling the growth of modern coral reefs and it is likely that these same factors exerted an influence on coral and other reefs in the past. For coral-reef growth, these factors are: (a) water temperature – optimum growth is around 25°, (b) water depth – most growth takes place within 10 m of the water depth, (c) salinity – corals cannot tolerate great fluctuations and (d) wave action and turbidity – coral growth is favoured by strong wave action and an absence of terrigenous silt and clay. Most reefs grow along shelf margins, an agitated zone where waves and currents of the open sea first impinge on the sea floor. Smaller patch reefs develop in open lagoons behind shelf-margin reefs, on carbonate ramps and epeiric platforms. Reefs, usually atolls, are also developed on submerged volcanic islands within the ocean basin. The configuration and morphology of some present-day reefs is a reflection of karstic dissolution of earlier reefs during glacial lowstands of sea level (Purdy, 1974).

Many modern reefs along shelf margins show a characteristic threefold division into back-reef, the reef itself/framework (reef flat/crest) and fore-reef (reef front/slope), as shown in Figure 2.8. The reef front is a steep slope, vertical in places, with organisms constructing the reef in the upper part, passing down to a talus slope of coarse reef debris. Reef-derived carbonate megabreccias, debrites and turbidites may be present in the adjoining basin. A prominent system of surge channels gives a spur and groove morphology along the reef front, extending up to the reef flat, in some cases. The reef crest, covered by no more than 1-2 m of water, is the site of prolific organic growth of corals and algae on modern reefs. Behind the crest is the reef-flat, a pavement of mostly

dead coral. The back-reef area consists of reef debris adjacent to the reef flat, passing shoreward to a quiet-water lagoon, where there may be patch reefs (Tucker, 1991).

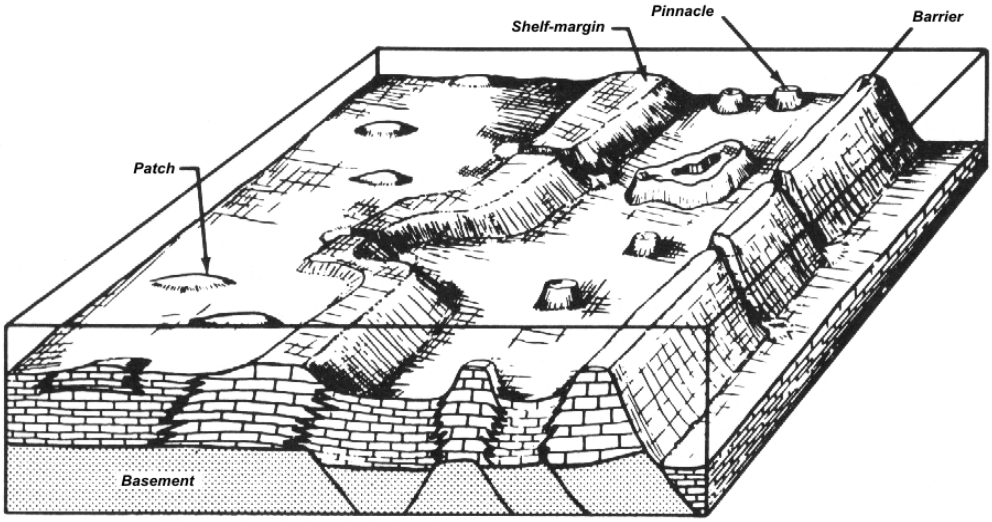

Figure 2.7. Types of reefs most easily recognized from seismic interpretation (Bubb and Hatlelid, 1978).

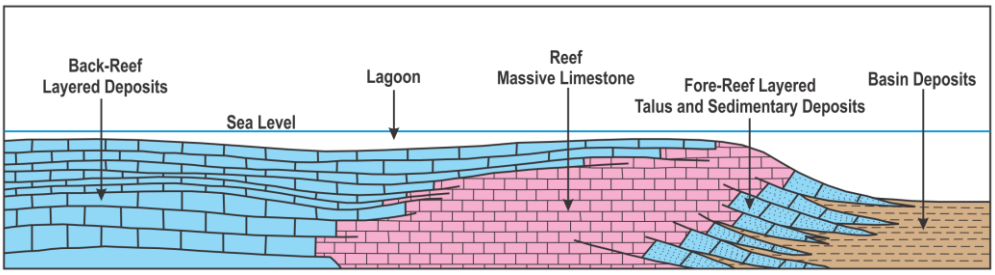

Figure 2.8. Sketch illustrating the major reef facies in cross-section.

Reefs are important oil reservoirs, with the most porous carbonate facies generally occurring in the upper fore-reef and facies of the reef itself. However, marine cementation is most prevalent in this zone and so porosities can be reduced from primary high values. The talus at the toe of reef slopes also makes good reservoirs. Many reefs are dolomitized, and this enhances their reservoir qualities.

2.8 Pinnacle and Patch Reefs

Patch reefs grow similarly to pinnacle reefs, in that they both reach mean sea-level; however, their rise from the substrate differs, in that patch reefs reach < 20 m depth, whereas pinnacle reefs have > 20 m relief (Blanchon, 2011). Typically, patch reefs occur within the lagoon behind the barrier rim. Sometimes, they can occur on the open shelf, as pinnacles. Pinnacle reefs grow during rapid sea-level rises during carbonate production. Three possible ways of accounting for the different heights to which pinnacle reefs grow within a limited area are indicated in Figure 2.9: (a) subsidence with tilting, (b) eustatic changes and (c) successive fault escarpments (Teichert and Fairbridge, 1948). Patch and pinnacle reefs are smaller, more symmetrical and relatively less oriented with respect to marine wave and current directions than other reef types. They are formed by frame builders, while the mounds are accumulations of lime mud and silt trapped by crinoids, algae and sponges. The fore-reef side commonly has more porous grain carbonates than the more back-reef side, but pore-filling marine cementation occurs more readily on the fore-reef side (seaward direction). The pinnacles are usually covered abruptly by basinal shales and marls similar to those deposited on the deeper parts of the margin and related to transgressive changes in sea-level (Kendall and Schlager, 1981).

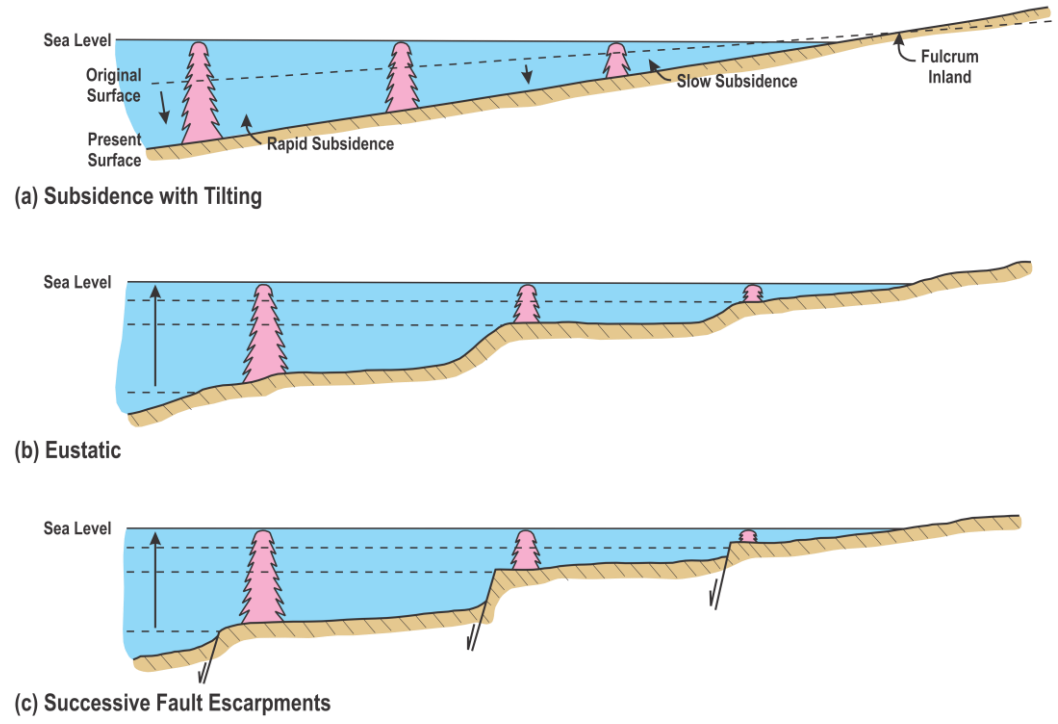

Figure 2.9. Three possible causes of different heights to which reefs grow (Teichert and Fairbridge, 1948).

2.9 Geophysical Exploration of Reef Carbonates

Seismic reflection events from the top of a carbonate rock boundary have a positive reflection coefficient because carbonates usually have high density and velocity compared to other sedimentary rocks. Only in cases where the carbonates are very fractured or porous are reflection coefficients of upper boundaries likely to be negative. The interpretation of reefs in seismic data may be simple, or it may be difficult. Occasionally, the expression of a reef on a seismic section may be very subtle, even if the seismic line passes right across the reef itself. Typical of such situations are the pinnacle and patch reefs (Badley, 1985). Because reefs vary so widely, the evidence for reefs shown by seismic data is extremely varied. We might hope to see diffraction from the top and/or flanks of the reef. Abrupt termination of reflections from the surrounding sediments may indicate the location of the reef. If the reef provided a barrier to sedimentation, the entire reflection pattern may differ on the two sides of the reef, reflecting the different sedimentary environments. Overlying reflections may show small relief because of the differential compaction. The velocity difference between the reef materials and the surrounding sediments may produce pseudo-structures on reflecting horizons below the reef. Usually the velocity in the reef limestone will be greater than that in the surrounding shales, so that there will be a pull-up under the reef. Sometimes, however, the reef will be surrounded by calcareous shale, anhydrite, or other rock that has a higher velocity than the porous reef limestone, so that the time anomaly is reversed: a ‘push-down anomaly’ (Telford, Geldart and Sheriff, 1990).

Seismic resolution distinguishes between horizontal (from trace to trace) and vertical (in time or in depth) resolutions. Sheriff (1991) defines the Fresnel zone as the part of a reflector from which reflected energy can reach a detector within 1/2 wavelength (λ) of the first reflected energy (Figure 2.10). Vertical resolution concerns the minimum thickness of a layer, and thus that reflections from the layer’s top and base interfaces can be separated, so that one can identify a layer of limited thickness from a single interface. The Rayleigh limit of vertical resolution is that the layer thickness must be 1/4 of the wavelength (Sheriff, 1997).

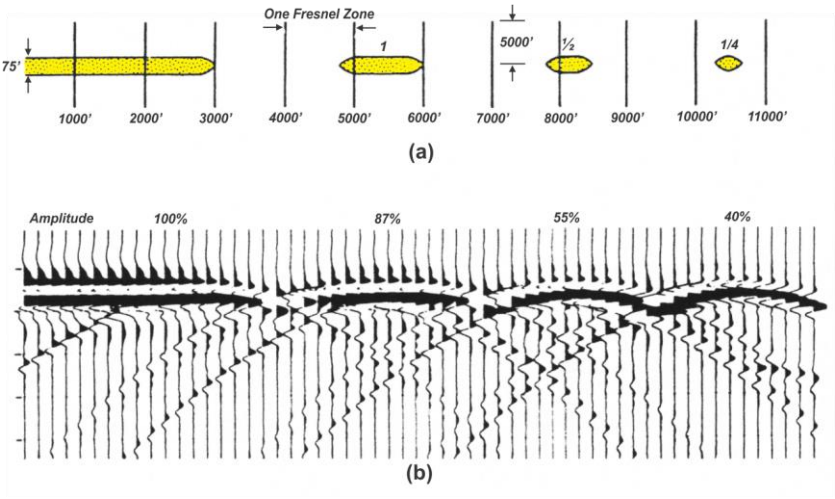

Figure 2.10 Illustrations the reflections from various reflector lengths measured in terms of the Fresnel-zone size; (a) geological model and (b) seismic record (Meckel Jr and Nath, 1977).

A grid of good seismic data with special processing and meticulous interpretation is required to define the shape and depositional environment of reefs. The relatively small size of the reefs compared to horizontal and vertical resolution limits is always a potential problem. Indirect methods, using for example, velocity pull-up or push-down effects beneath a reefs, or differential compaction of overlying layers, can sometimes be used to overcome the problem. The loss of reflection amplitude often associated with reefs is not always a good indication of lower acoustic impedance and high porosity. Isopach maps can be used to search for these subtle reefs, for example, where a pinnacle reef has grown on the carbonate platform and has been enclosed by shales (Figure 2.11a). The latter are more compactible than the reef, so that the differential compaction of later sediments causes the appearance of draping over the reef. Even if the reef is not directly visible on the seismic section, its presence can be inferred by mapping the time interval between the reflections from interfaces A and B: the reef is represented by a thick pattern on the map. Another special situation is where the reef has a higher velocity than that of the surrounding sediments, so that a reflection from below the reef shows velocity pull-up (Figure 2.11b). By mapping the time interval between interfaces B and A, it may be possible to infer the presence of the reef from a local thinning. Sometimes the effect of velocity and the effect of differential compaction exist together; in that case, one tends to cancel out the other (Badley, 1985).

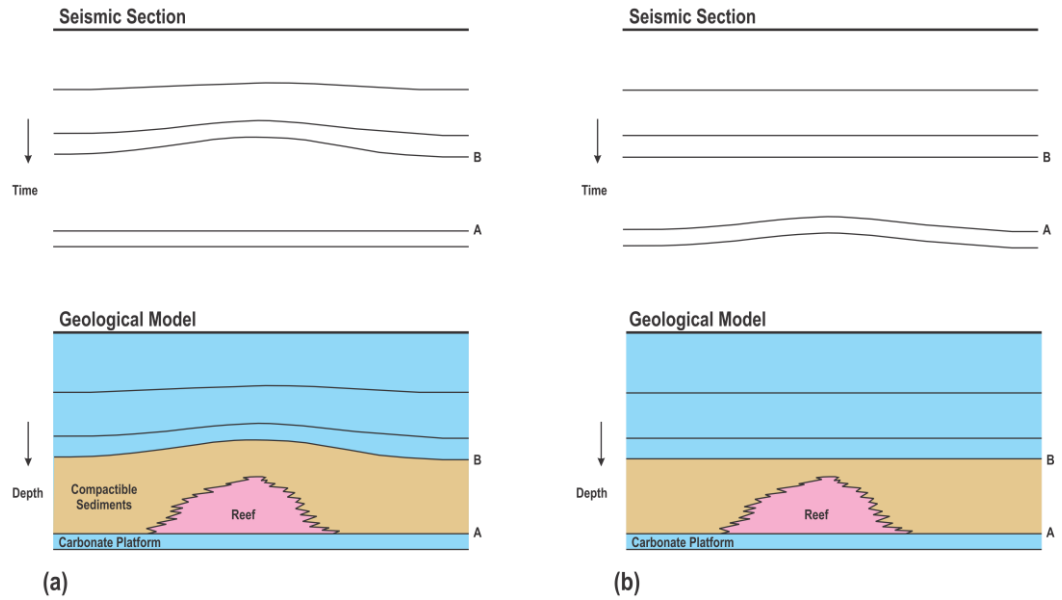

Figure 2.11. Seismic sections over a reef, (a) where the flanking sediments are more compactible than the reef, and (b) when the flanking sediments have a velocity less than that of the reef; re-printed from Badley and Anstey (1984).

Seismic properties of carbonate rocks are affected in complex ways by many parameters, such as pore type and shape, porosity, pore fluid, and saturation, and especially by pore type. In reality, most carbonate rocks contain more than one type of pores. The most compliant pores affect seismic properties the most.

The thinning of layers as well as the variations in the interval velocity, which are found over many reefs, can often cause observable differences between the frequencies of seismic data recorded across a reef and those recorded above off-reef sediments. Because of differential compaction, erosion and deposition, the layers above the reef typically are thinner and have a higher interval velocity than the off-reef sediments. Typically, reefs have rigid skeletal structures and deposits laid down over reefs tend to drape across the reef edges. Differential compaction usually happens when the rigid reef material is covered and enclosed by shales. Thus, from a statistical viewpoint reflections from the zone just above the reef would show a generally higher frequency over the reef body than above its flanks, an effect which usually diminishes rapidly with smaller time intervals (Figure 2.12). The sedimentary sequence below the reef should be normal and no frequency anomaly would be expected (Fitton and Long, 1967).

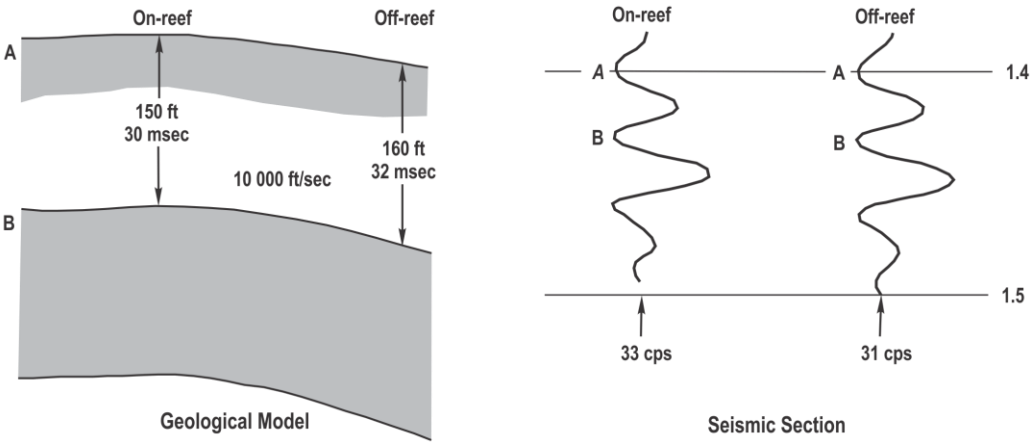

Figure 2.12. Relationship between thickness changes to frequency variations resulting from thinning and compaction over a reef (Fitton and Long, 1967).

Some authors have concluded that clear relationships between porosity, depth and seismic velocity cannot be established for carbonate sediments. One of the main reasons for this is seen in the presence of vugular porosity and, to a lesser extent, fracture porosity, which affects the compressibility of a rock in a different way from that of inter-granular porosity (Jankowsky, 1970). Most carbonate sediments are in reality a mixture of several lithological components. Generally, the seismic velocity of carbonate sediments depends on: (a) the type, size and distribution of their porosity, and (b) their lithologic composition. Most computer velocity analysis procedures assume that the subsurface consists of isotropic and non-dipping layers. The seismic velocities are therefore incorrect uncorrected in the field, for the following reasons: (a) the dipping reflectors in the reef flanks where the dip becomes steep (about 32°) influence the calculated velocity values; (b) the interval velocities that represent the physical property of the rocks are calculated by using Dix's equation, which is valid only for horizontal layers; (c) anisotropy, where the stacking velocities were correct, but gave an error in computing the true interval velocity and true average velocity (using time-to-depth conversion); (d) noise, acquisition geometry errors and static errors, and (e) errors in picking the spectrum (Salem, 1996).

Similarities between reefs and salt dome features also cause problems at times. The lagoonal areas behind reefs may provide conditions for evaporite deposition, so that salt may be present in the same portion of the sedimentary column. Differential solution of salt beds, followed by the collapse of the overlying sediments into the void thus created, may produce seismic features that are similar in many ways to those that indicate reefs (Telford, Geldart and Sheriff, 1990).

According to Mitchum Jr and Vail (1977); Mitchum Jr, Vail and Sangree (1977); Mitchum Jr, Vail and Thompson III (1977); Sangree and Widmier (1977); Mancini, Parcell and Har (2006), seismic facies analysis includes delineating and interpreting seismic reflection parameters, such as interval velocity, reflection configuration, amplitude, continuity, geometry, frequency, and the external form of reflectors within the framework of depositional units. Each of these parameters contains information of stratigraphic impact. Several steps are involved in visual analysis of reflection configuration. The relations between carbonate depositional environments and seismic facies are summarized in Figure 2.13.

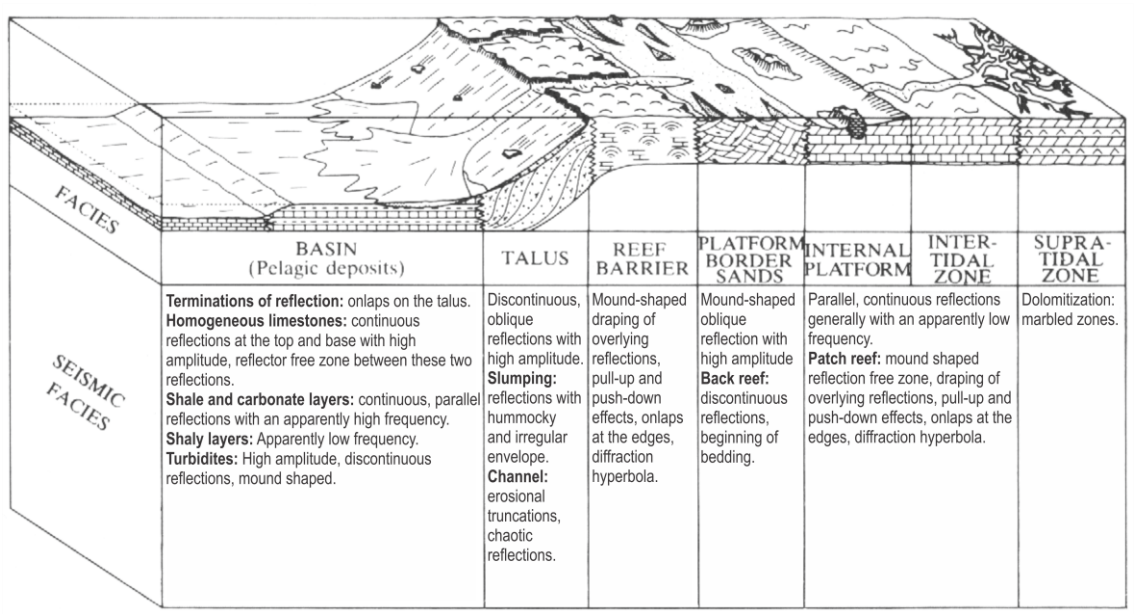

Figure 2.13. Seismic and depositional facies interpretation of carbonate environments (Wilson, 1975).

Shallow gravity anomalies are often associated with deeper tectonic structures. The density and porosity of reef limestone and the material it replaces can be so variable that it is not possible to specify what the contrast will generally be (Dobrin, 1976). The anomalies are produced by vertically extending density increases caused by differential compaction over underlying buried topography. The reef is more resistant to compaction than the enclosed shales. In fact, the layers just above the reef are always draped downward off the reef. The amount of draping is primarily an indication of the amount of compaction rather than depositional thinning (Figure 2.14). Recognition that differential compaction is the key to many reef anomalies requires appreciation of two phenomena: (a) differential compaction below the level of the top of the reef will cause lateral density contrasts for overburden layers, and (b) very minor changes in

sedimentary thickness due to compaction will cause recognizable gravity anomalies when they extend to shallow depths. The compaction should exist over tectonic structures as well as reefs; it would be even more difficult to separate the gravity anomaly caused by a reef body or tectonic structure. Reefs most usually show recognizable gravity anomalies, which may be a (a) simple high, (b) high with a negative rim around it, (c) low with a positive tendency in the centre, or (d) simple low (Haye, 1967). The Bouguer gravity anomaly over a reef is usually small, in the range of +0.2 to +0.5 milligals, according to (Yungul, 1961), who published one of the best articles on reefs and gravity.

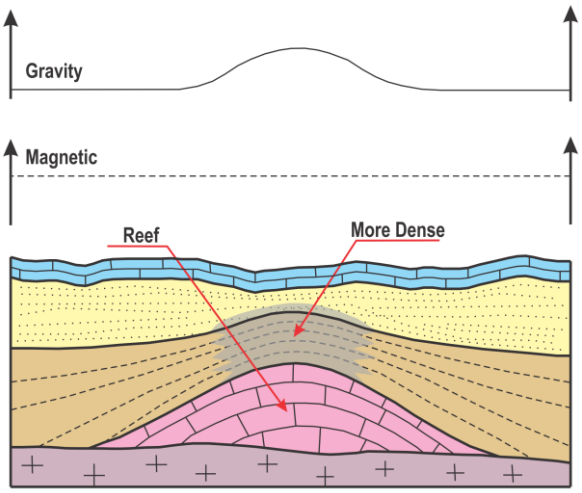

Figure 2.14. Gravity and magnetic anomalies' responses over the reef body (Selley and Sonnenberg, 2014).

The gamma-ray log measures the natural radiation of potassium, thorium and uranium. Many carbonate facies can be correlated with current energy and thus with potassium and thorium radiation. Grainstones and grain-dominated packstones are deposited in high-energy environments and typically have low gamma-ray activity. Mud-dominated packstones, wackestones and mudstones are deposited in low-energy environments and typically have higher gamma-ray activity (Lucia, 2007).

Porosity may be estimated in three ways: directly from cores, indirectly from well logs or at high resolution from seismic data. The neutron and density logs are responses to pores of all sizes.

In carbonate rocks having primary porosity, the Wyllie time-average formula (Wyllie, Gregory and Gardner, 1956) still applies; however, when a secondary porosity exists, i.e. of the vuggy type or when there are fractures, the velocity of sound seems to depend mostly on the primary porosity and the porosity derived from the sonic reading

will tend to be too low by an amount approaching the secondary porosity (Schlumberger, 1989).

The dipmeter log in particular measures the conductivity of rock in a number of directions around the borehole (Smith and Baker, 1983). Carbonate reef interpretation from a dipmeter log is fairly straightforward for reef facies, but becomes rather complex in back reef facies. The drape structure over the reef can be discriminated with ease on dipmeter logs run in wells located less than a quarter of a mile from the reef (Figure 2.15). The dip sequences in the overlying shales at flank positions form an upward-decreasing (red) pattern, in which dips diminish upward to an overlying uniform (green) pattern representing local structural dip. The crest of the reef is therefore located up-dip from the pattern trend and the reef axis parallels their strike. Within the reef core itself, the dips are generally highly inclined but chaotically oriented (random or white pattern), and are caused by fractures, vugs and other diagenetic features of no regional significance. Below and seaward of the reef core, a sequence of fore-reef talus ideally shows an upward-increasing (blue) pattern of downward decreasing dips sloping away from the reef. In detailed studies from several wells, the fore-reef and back-reef sides of the structure can often be determined. The fore-reef dips are usually greater, ‘up to 35°’, than most of the more gently sloping back-reef flanks, which are ‘up to 25°’ (Doveton, 1986).

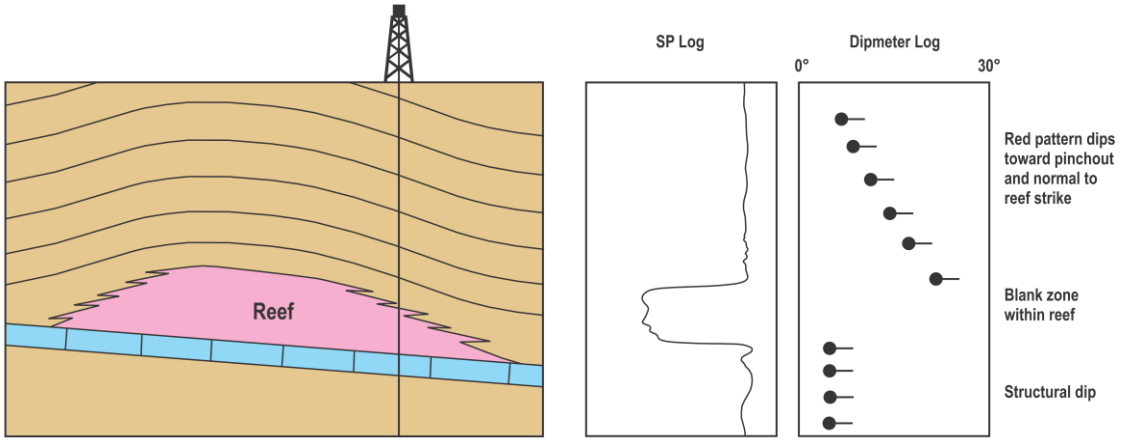

Figure 2.15. Dip patterns associated with draping over a barrier reef; modified after Campbell Jr (1968).

Chapter 3. Regional Setting and Stratigraphy

Chapter 3

Regional Setting and Stratigraphy

3.1 Introduction

Several major geologic sedimentary basins are present in Libya, namely the Sirt, Al Kufrah, Murzuq, Ghadamis and Sabratah basins. The Sirt basin is situated in the north-central part of Libya, within the North African passive margin (Saheel, Bin Samsudin and Bin Hamzah, 2010). It covers an area of about 600,000 km^2. The sedimentary record indicates that the filling of the basin belongs to the Mesozoic and Cenozoic ages (Figure 3.1). The basin is characterized by a series of troughs and platforms (Hallett, 2002), with the major structural trend running northwest-southeast. The basin deepens to the east, reaching the largest depression in the Ajdabyia trough (Craig *et al.*, 2008). The Sirt basin is surrounded to the north by the Mediterranean Sea, by the Cyrenaica platform to the northeast, by the Kalanshiyu uplift to the southeast, by the Tibisti-Sirt uplift to the south, and by the Tarabulus Tibisti trough and Al Qarqaf uplift to the west (Figure 1.1).

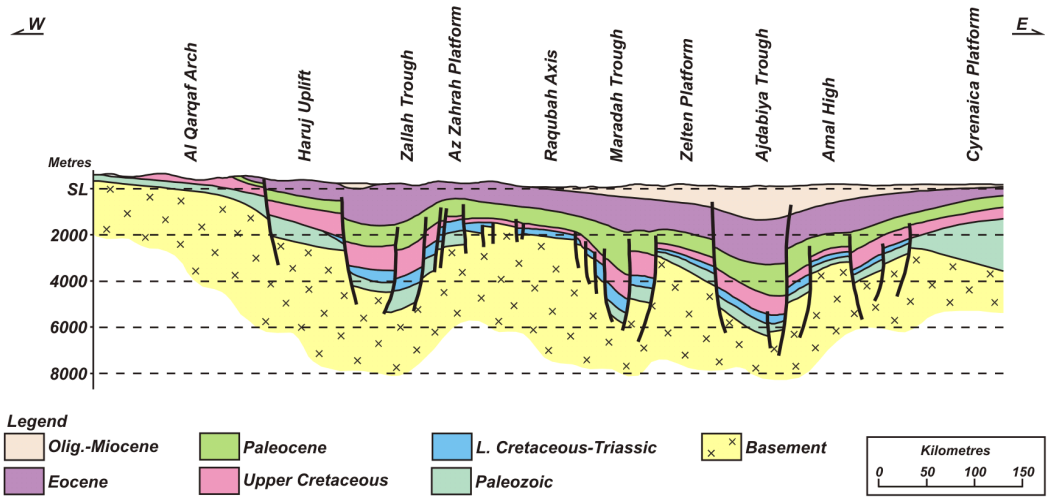

Figure 3.1. An east-west cross section of Sirt basin (Bonnefous, 1972; Parsons, Zagaar and Curry, 1980; Massa and Delort, 1984; Peterson, 1986; Gumati, Kanes and Schamel, 1996).

3.2 History of the Sirt Basin

The origin of the Sirt basin has been attributed to various causes by different scientists. Burk and Dewey (1974) suggested that in the Late Jurassic to Early Cretaceous, a drift-way movement over a fixed mantle hot-spot produced an extension and consequent collapse of what had been the Sirt uplift. The elasticity and stretch of the crust made the massive blocks of the Sirt arch move downward and break along the weak planes, forming a system of horsts and grabens. The origin of the Sirt basin and the neighbouring Libyan marginal basins has been related not only to inter-plate motion between Africa and Europe but also to intra-plate movements within the African plate (Anketell, 1996).

The broad geological history and main structural elements of the Sirt basin were clearly explained by Klitzsch (1970) and further clarified by Massa and Delort (1984). During the Cambro-Ordovician, a layer about 1,000 m thick of quartzarenites and sandstones comprising the Gargaf Formation was deposited in northern Libya (Figure 3.2). Thinning of the Silurian sequence across the Sirt area, with magmatism appears to have led to uplift of the Tibisti-Sirt arch throughout the Hercynian orogeny (Klitzsch, 1970). Deposition continued in the adjacent basins, while inversion of the area and increased igneous activity continued throughout the Devonian to reach a maximum during the Permo-Carboniferous period.

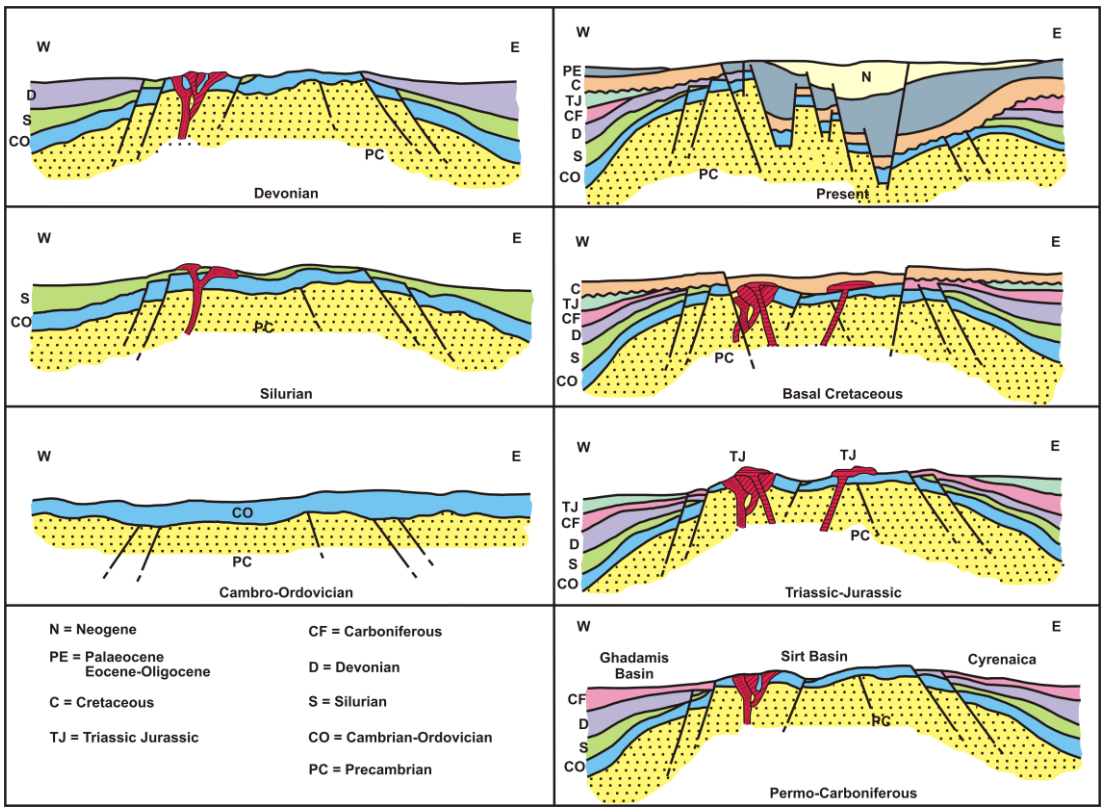

Figure 3.2. Structural development of Sirt region through Cambro-Ordovician to present (Massa and Delort, 1984).

Post-Hercynian movements (Triassic-Jurassic) were accompanied by the eruption of basic lavas. Relief inversion and the development of the Mesozoic basin began in the Early Cretaceous (Bonnefous, 1972; Burk and Dewey, 1974) with the collapse of Tibisti-Sirt arch (Klitzsch, 1971). Following the initial Early Cretaceous phase of faulting, the grabens underwent re-activation in the Late Cretaceous to Early Paleocene period (Van Houten, 1983) and throughout the Oligocene to the Miocene (Mikbel, 1977; Mikbel, 1979). Van Houten (1983) suggests that the Sirt rifting took place at a time in the Early Cretaceous, when a significant shift in the absolute motion of the African plate, from a westward to northward motion, coincided with the region passing over a fixed mantle hotspot. The alteration in movement of the plate caused the region to pivoting, and therefore remain over the hotspot for a long time, leading to thinning of the cratonic lithosphere and fragmentation.

3.3 Ajdabiya Trough

The Ajdabiya trough is the largest and deepest of the troughs in the Sirt basin; it covers an area of 22,500 km^2. The trough is the most prolific part of the Sirt basin,

containing about 60% of the entire hydrocarbon volume found in this basin. The Ajdabiya trough represents the main source kitchen area for oil and gas generation in the Sirt basin (Hallett, 2002). It represents the principal focus of crustal weakness in the Sirt basin and shows a more complex history than the other troughs within the basin. The trough has an axis orientated in a NW-SE direction. It was comparatively inactive throughout the Paleocene, but was re-activated again throughout the Eocene, and the subsidence has continued to the present time (Anketell, 1996).

The Ajdabiya trough is surrounded to the west by the Zelten platform; to the east it is bounded by the Amal and Messlah highs before connecting with the Hameimat trough. The Ajdabiya trough is flanked to the south by the Sarir trough and south depression and to the north by the Mediterranean Sea (Figure 3.3). The southern part of the trough, which includes the Intisar, Sahabi, Mheirigah and Shatirah oil fields, has been fairly well explored, but the northern part is very poorly understood.

3.4 Lithology and Lithostratigraphy

The stratigraphic columnar section of the study is shown in Figure 3.4. The terminology is identical to that proposed by Barr and Weegar (1972) and updated by Banerjee (1980). This is at variance with previously published papers, which used terminology developed by individual oil companies. Harding (1984) divided the depositional history of the Sirt basin into three phases: pre-rift, syn-rift and post-rift sediments.

The Paleocene section in the Sirt basin (Figure 3.5) represents a time of major carbonate banks and reefal growth and provides potential hydrocarbon plays associated with excellent reservoirs sealed with Paleocene shales and possibly charged from Cretaceous and Paleocene sources.

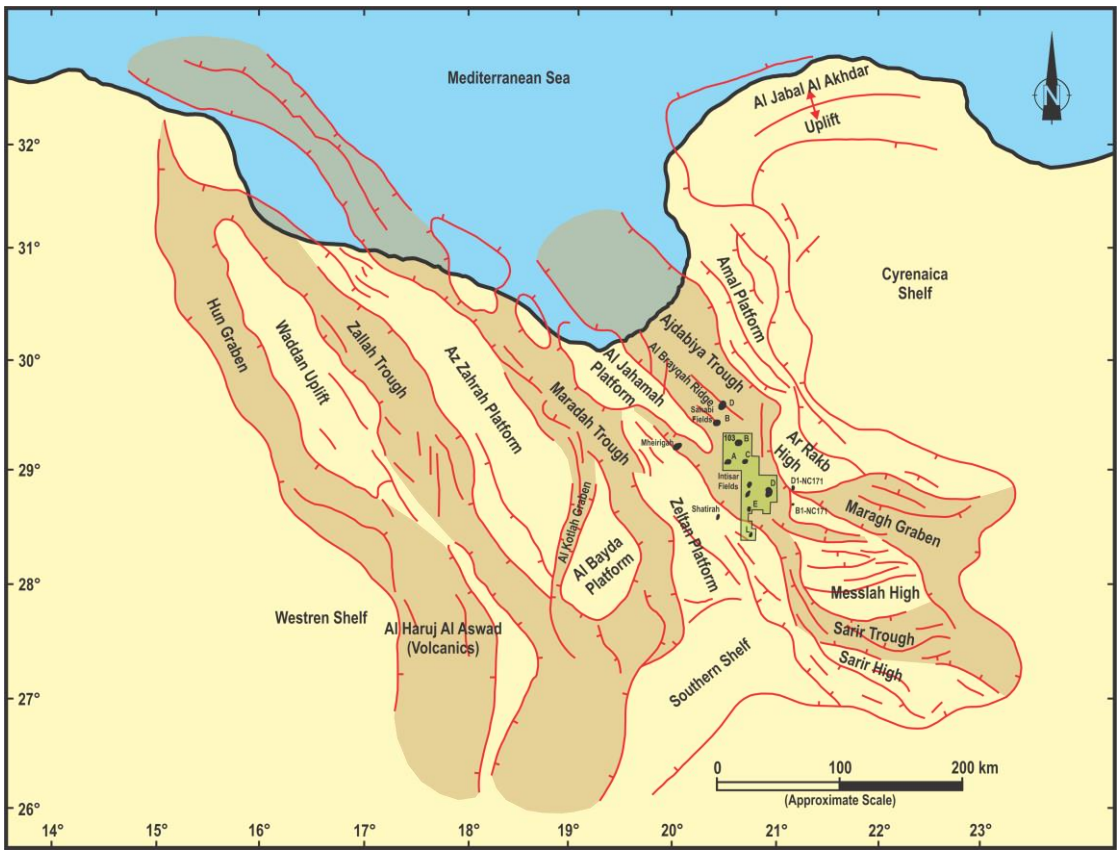

Figure 3.3. Tectonic elements of the Sirt basin and location of study area; modified after Mouzughi and Taleb (1981).

3.4.1 Pre-rift deposition

The Lower Cretaceous represents the final stage of the pre-rift phase deposited during the initial crustal stretching but before the major rifting and graben formation.

Virtually no data is available from the Ajdabiya trough where the Lower Cretaceous is for the most part too deep to be reached by the drill, but it seems likely that this area could represent a marine embayment connected around the western flank of the Cyrenaica ridge with the marine facies of northern Cyrenaica. This is supported by evidence from an offshore well drilled on the eastern flank of the Ajdabiya trough, which bottomed in marine rock of Cenomanian-Albian age (Hallett and El Ghoul, 1996).

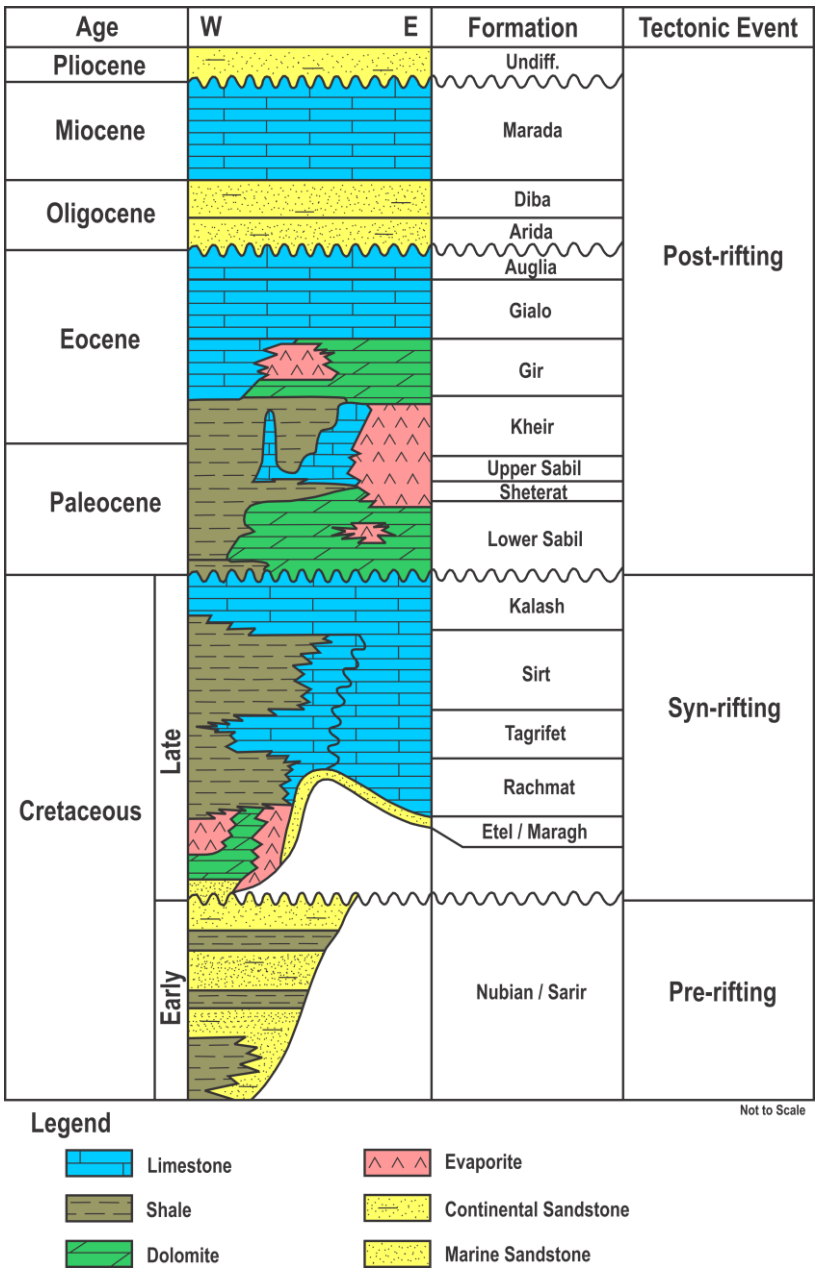

Figure 3.4. Lithostratigraphic framework of the eastern Sirt basin (Spring and Hansen, 1998).

3.4.2 Syn-rift deposition

Crustal stretching in the primordial Sirt basin eventually led to major rifting and structural collapse and the formation of major grabens; Hameimat, Ajdabiya, Maradah, Zallah and Hun, in which syn-rift sediments were deposited. The northward extension of these troughs into the offshore area is not entirely clear, but the work of Finetti (1982) shows that in general they debouch onto the upper Sirt slope increases. The marine transgression reached its peak during the Maastrichtian, marking the end of the

syn-rift deposition. The syn-rift sediments are divided into the following formations, from bottom to top:

3.4.2.1 Sirt Shale Upper Cretaceous (Campanian)

This is dominantly a shale sequence with thin limestone interbeds. The shales are carbonaceous and calcareous (Banerjee, 1980). It represents the main oil source rocks of the Sirt basin. The Sirt Shale conformably underlies the Kalash Limestone, and the contact can be picked up either by lithologic or electric-log characteristics (Barr and Weegar, 1972).

3.4.2.2 Kalash Limestone Upper Cretaceous (Maastrichtian)

This is mainly calcilutite, with the upper part occasionally being calcarenite, with some calcareous shale interbeds (Banerjee, 1980). It was deposited in a low-energy, shallow-water environment (Hallett, 2002). The contact with the Lower Sabil Carbonates is usually gradational, often being located at the base of the lowest dolomitic beds, which are apparent by their high electric-log resistivity (Barr and Weegar, 1972).

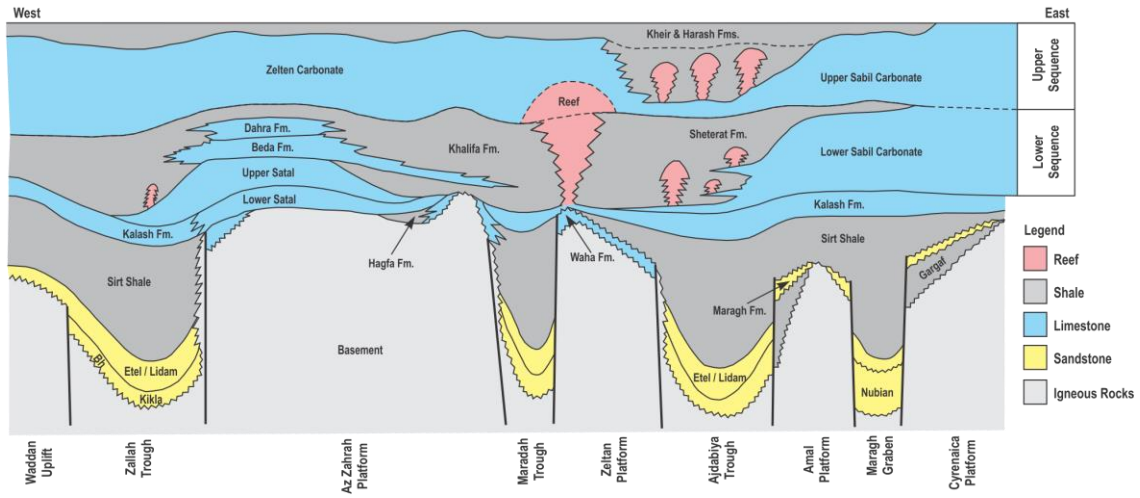

Figure 3.5. Schematic cross section of the Sirt basin, showing the Paleocene sequences; top: Paleocene datum (Bezan, 1996).

3.4.3 Post-rift deposition

The major tectonic events that formed the Sirt basin had nearly ceased by the end of the Cretaceous. The subsequent history of the basin was on a much gentler scale and

represents the post-rift depositional phase of the basin's development in an interior sag basin. The subsidence rate in the western troughs was reduced, and the distribution of the principal lithostratigraphic units in the Tertiary was less influenced by trough subsidence than by regional tilting towards the northeast, which became the dominant tectonic feature of the late Tertiary. Rapid deposition continued in the Maradah and Ajdabiya troughs (Hallett and El Ghoul, 1996). The post-rift sediments are divided into the following formations, from bottom to top:

3.4.3.1 Lower Sabil Carbonates Lower Paleocene (Danian)

These consist mainly of dolomite with subordinate limestone and occasional chalk and anhydrite (Banerjee, 1980) that were deposited in a quiet, low-energy, shallow-water environment (Terry and Williams, 1969). The Lower Sabil Carbonates are conformably overlain by the Sheterat Formation and the upper contact is placed at a resistivity increase and a prominent negative deflection of the SP curve. Where the Sheterat Shale is not present, the Upper and Lower Sabil Carbonates may be vertically contiguous, making the contact difficult to recognize (Barr and Weegar, 1972).

3.4.3.2 Sheterat Formation Middle Paleocene (Danian)

This is composed of fossiliferous calcilutite and some chalk with interbeds of fossiliferous calcareous shale (Banerjee, 1980). The upper contact is placed at the change from the calcilutites of the Upper Sabil to the shales of the Sheterat Formation. The upper contact is noticeable by an increase in resistivity as well as by a positive deflection of the SP curve (Barr and Weegar, 1972).

3.4.3.3 Upper Sabil Carbonates Upper Paleocene (Thanetian)

This is predominantly a limestone sequence with very subordinate amounts of shale, becoming biohermal in places (Banerjee, 1980). The Upper Sabil Carbonates have oil reservoirs at the Intisar, Sahabi, Mheirigah and Shatirah fields, where reefs have developed. East of the Amal field the sequence becomes increasingly dolomitic and anhydritic. The upper contact is placed at the change from the grey-green to brown shale of the Kheir Formation to pink fossiliferous calcilutite, and the top contact occurs at a resistivity decrease accompanied by a sharp negative deflection in the SP curve (Barr and Weegar, 1972).

3.4.3.4 Kheir Marl Upper Paleocene (Thanetian)

This is predominately shale with some marl, clay and limestone (Banerjee, 1980). The Kheir Formation is conformably overlain by the Gir Formation, and the top contact occurs at a resistivity increase accompanied by a sharp positive deflection in the SP curve (Barr and Weegar, 1972).

3.4.3.5 Gir Formation Lower Eocene (Ypresian)

This is predominantly a sequence of interbedded anhydrites and dolomites with subordinate amounts of shale and limestone (Banerjee, 1980). The Gialo Limestone is conformably superjacent to the Gir Formation.

3.4.3.6 Gialo Limestone Middle Eocene (Lutetian)

This consists of a thick sequence of limestone, mainly muddy nummulitic calcilutite and calcarenite (Banerjee, 1980). The Augila Formation is disconformable to the Gialo Limestone (Barr and Weegar, 1972).

3.4.3.7 Auglia Formation Upper Eocene (Priabonian)

This formation can often be divided into three members, the lower predominantly limestone with a thin shale unit. The middle member is a quartz sandstone. The upper member is slightly limestone to sandy, and occasionally very argillaceous. The environment of deposition was probably inner to middle neritic open sea for the shale member, and a shallower, more restricted environment for the sandstone and limestone members (Banerjee, 1980).

3.5 Regional Paleocene Geologic Setting

The top of the Kalash Limestone represents the base of the Paleocene section in the Ajdabiya trough, while the top of the Paleocene section is located within the Kheir Formation, of which the earliest formations are from the Eocene epoch (Barr and Weegar, 1972). The lithologies of the Paleocene age in the Sirt basin were controlled by transgressions and regressions of an epeiric sea across a broad shelf region that dipped gently into a deep and persistent shale basin. This basin was located NW of the study area.

The criteria for reef growth were satisfied in the Ajdabiya trough throughout the Paleocene epoch; these criteria were shallow-marine settings in an open-marine

environment with basin subsidence (Gumati, 1992). There were two major marine transgressions across Sirt basin shelves during the Paleocene time (Figure 3.6), the first major marine transgression occurring in the very early Upper Paleocene and the second major marine transgression occurring in the remaining part of the Upper Paleocene (Terry and Williams, 1969).

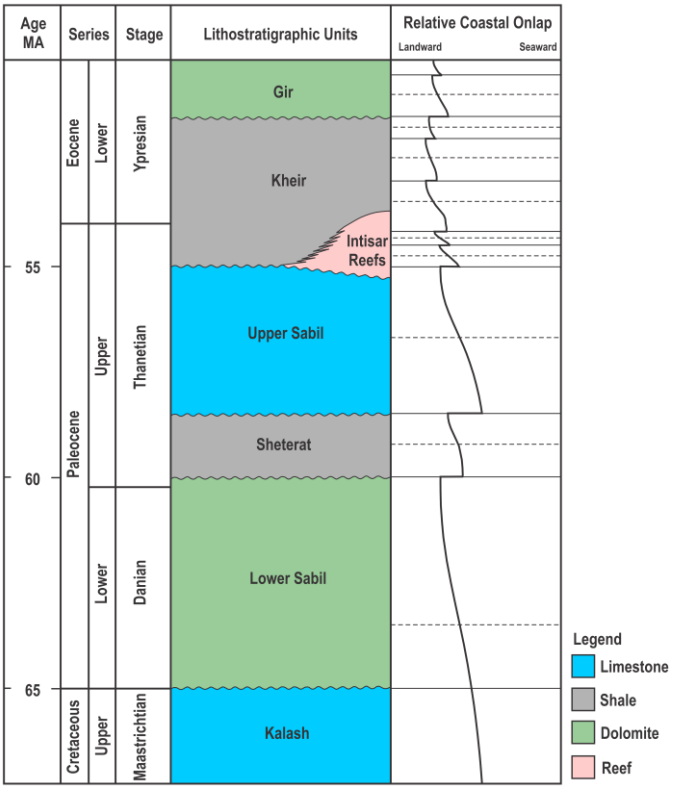

Figure 3.6. Chronostratigraphic, lithostratigraphic and sequence stratigraphic framework for the Upper Paleocene-Lower Eocene of the Eastern Sirt Basin (Haq, Hardenbol and Vail, 1987; Spring and Hansen, 1998).

Lower Sabil Carbonate was deposited in a quiet, low-energy, shallow-water environment with infrequent stages of development. The character of the carbonate shelf margin for Lower Sabil has not been definitely recognized, but by its similarity with the Upper Sabil it may signify a barrier-reef type margin (Terry and Williams, 1969). A barrier reef grew on the shelf edge of the Lower Sabil platform and grew basin-ward throughout its depositional period (Gumati, 1992).

The close of Lower Sabil deposition is marked by the influx of the Sheterat Shale (Figure 3.7a). The interpretation by Brady, Campbell and Maher (1980) suggests that the appearance of Sheterat Shales represents the existence of a far distant provenance that suddenly supplied argillaceous material into a previously clear-water environment.

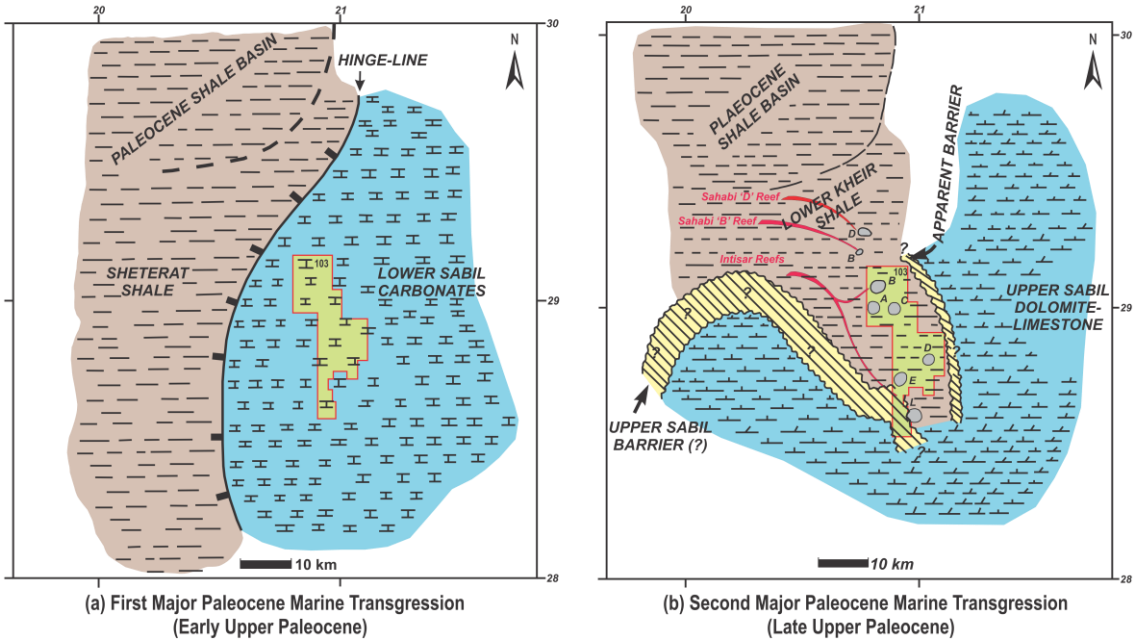

Figure 3.7. Upper Paleocene lithofacies map of central and NE Sirt basin prior to the first and the second major Paleocene marine transgressions; modified after Terry and Williams (1969).

The sea began a very slow and oscillating retreat from the forelands, which were far removed from the area of interest. The result over the high areas was a deposition of mud supporting the biomicrites of the Upper Sabil Carbonate.

As water continued to shoal, the paleo-highs on the Lower Sabil bank top and temperature, salinity and water agitation through the broken discontinuous barrier created an ideal condition for the establishment of isolated bioherms. Reefs developed in the semi-lagoonal area or along the bank slope between the bank and the barrier reef. The Sahabi and Intisar reefal complexes are located within such a bay (Figure 3.7b). The pinnacle reefs started as foraminiferal mounds and developed into coral reefs (Terry and Williams, 1969).

The close of the Paleocene was marked by a major incursion of the sea. The consequent deepening of the water in the study area drowned isolated reefs and capped them with upper Kheir Marl.

3.6 Hydrocarbon Potential

The Paleocene section is one of the major targets in the Ajdabiya trough, the carbonates within this section have good reservoir qualities and the reefs within this section form productive oil reservoirs at the Sahabi, Intisar, Shatirah and Mheirigah oilfields; more than 12 pinnacle reefs have been discovered in the Ajdabiya trough,

most of which are oil bearing. The reefs were developed in the Upper Sabil carbonates with the Kheir Formation as the top seal (Brady, Campbell and Maher, 1980). Paleocene traps also draped anticline features over reefs with lateral permeability barriers (Rusk, 2001). Good intergranular porosity resulted in these reefs, and further improvements in porosity resulted from a solution process, which both enlarged the existing pore spaces and dissolved the aragonite skeletons (Brady, Campbell and Maher, 1980).

The Ajdabiya trough is the focal depocentre in the East Sirte basin, with in excess of 20,000 ft of Mesozoic and Tertiary sediments. The potential Upper Cretaceous source interval is very thick, in excess of 4,500 ft and thus there is a substantial variation in the maturity between the basal shales and the top section, and consequently a range in the timing of the start of oil generation. Basin modelling of the southern part of the basin (Figure 3.8), close to the Intisar oilfields, indicates present-day peak oil generation at 12,250 ft and gas generation at 16,000 ft. The basal Upper Cretaceous Rachmat shales entered the oil window in the Middle Eocene and the gas window by the end of the Oligocene (Burwood, Cope and Redfern, 2000).

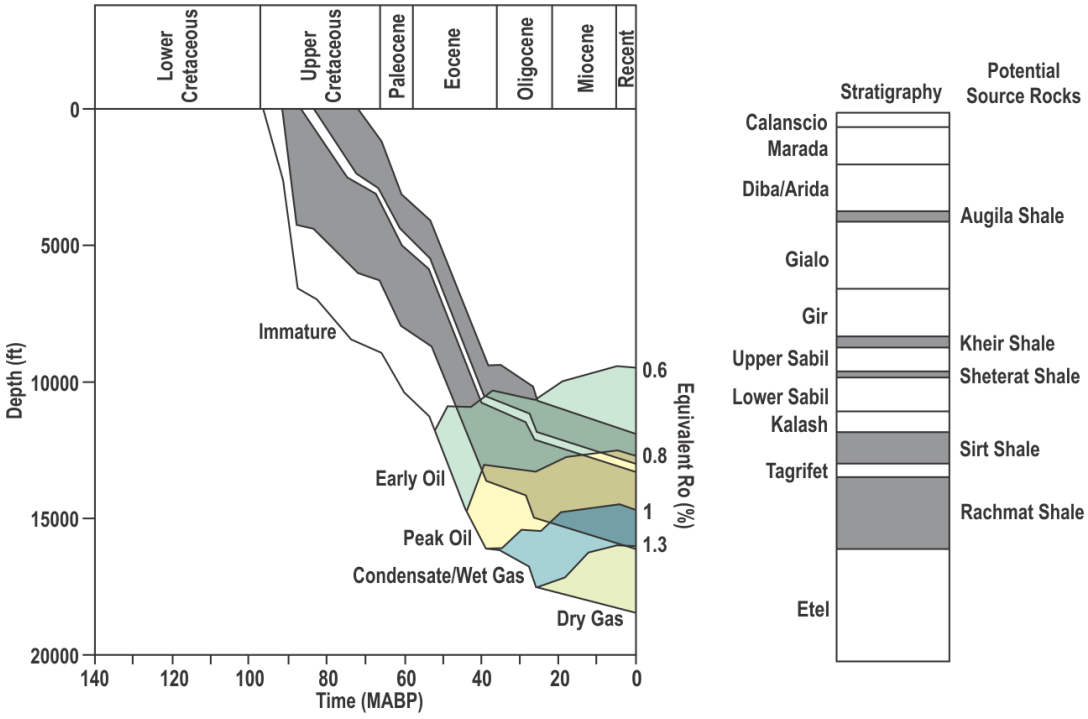

Figure 3.8. Burial history profile and petroleum generation history for a near-depocentre location within the southern Ajdabiya trough (Burwood, Cope and Redfern, 2000).

The main play in the southern part of the Ajdabiya trough is for Paleocene (Upper Sabil) carbonates, within large reefal buildups and smaller carbonate buildup traps.

Reservoir development in the latter is primarily associated with the higher energy carbonate facies which rim the main depocentre (Figure 3.9). These reservoirs are charged from the underlying mature Upper Cretaceous shales via faults and fractures (Burwood, Cope and Redfern, 2000).

Brady, Campbell and Maher (1980) believed the Intisar reefs to be sourced from the Late Paleocene shale (Sheterat Shale). However, this is most improbable since Sheterat Shale has neither the volume nor the organic fertility to generate the hydrocarbons found in the Intisar fields. Moreover, the Kheir shale is not a practical candidate, since it has been shown to be thin (Hallett, 2002). The geochemical analysis suggests that the oil of the Intisar fields was derived from Sirt Shales (Upper Cretaceous), which are the only source rocks with passable potential in the Ajdabiya trough. Burwood, Cope and Redfern (2000) favoured the idea that the oil was derived from Sirt Shale. The Paleocene reefs were charged by vertical, fault-controlled migration from Upper Cretaceous source rocks during the late Eocene to Oligocene (Hallett and Clark-Lowes, 2016). Barr and Weegar (1972) suggest that the vertical migration perhaps took place through Kalash Limestone, Lower Sabil Carbonate and through the Sheterat Shale which is may not be an effective cap rock in the Intisar area (Figure 3.10).

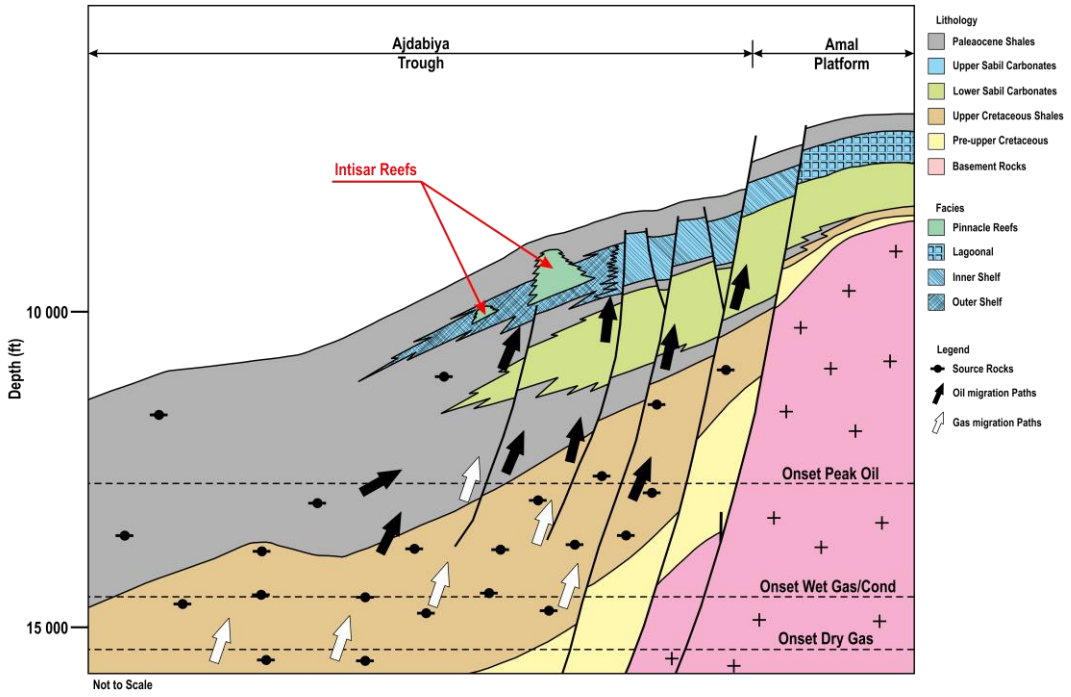

Figure 3.9. Petroleum systems charge model for the southern Ajdabiya Trough (Burwood, Cope and Redfern, 2000).

Circumstantial evidence indicates that the petroleum accessed these reefs via a combination of factors, possibly including faults and fractures across underlying seals and basal aquifers extending laterally; the access faults or fractures need not necessarily be at the field location but they may be anywhere within a reasonable distance from which regional aquifers or other tectonic discontinuities offer migrational pathways to the trap, keeping in mind the limitations of many carbonates for long-range migration. Some of Intisar reefs have developed rim-syncline features which may have affected the migration paths. Some of the these reefs seem to have been filled to spill-point, although at least two reefs are infertile of oil (Brady, Campbell and Maher, 1980).

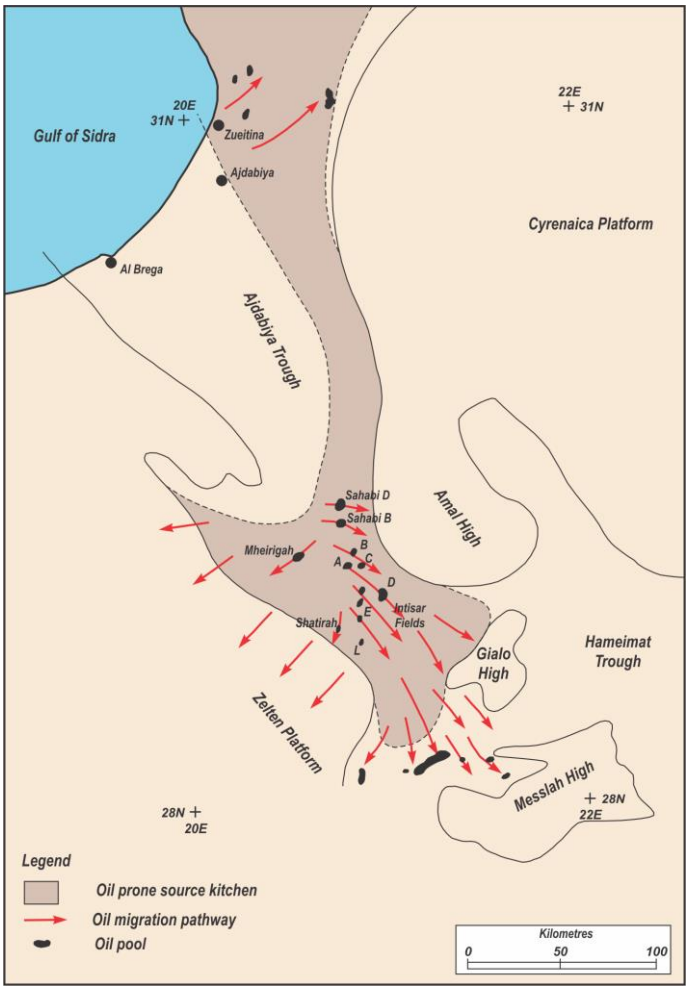

Figure 3.10. Eastern Ajdabiya trough petroleum systems (El-Alami, Rahouma and Butt, 1989; Ambrose, 2000).

3.7 Cretaceous and Tertiary Carbonate Reef Reservoirs in Libya

Carbonate reefs represent excellent oil targets because they have several petroleum elements in one place (for example; excellent porosity, effective cap and trap) and they are easily identifiable on seismic sections (Burgess *et al.*, 2013; Saqab and Bourget, 2015). Many reefs have been discovered in the Sirt basin. The *Occidental's* Augila field (Concession 102) is a fringing reef located on the Amal granitic basement high in the eastern Sirt basin (Figure 3.11). The reservoir consists of a carbonate and clastic unit and the underlying fractured and weathered granitic basement rock. The Upper Cretaceous sedimentary reservoir rocks were deposited along the crest of a paleo-high composed of upper Pre-Cambrian crystalline granitic rocks, creating a nonconformity (Williams, 1972).

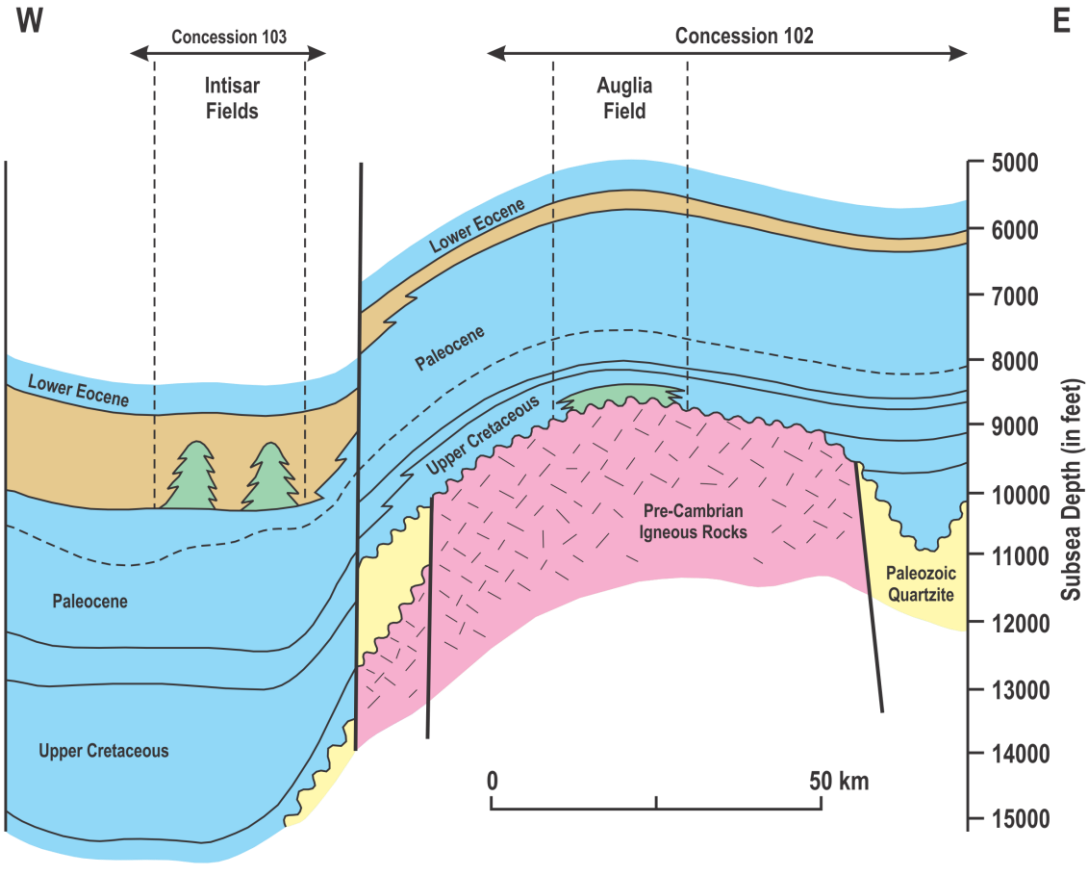

Figure 3.11. Cross section through Augila field (Williams, 1972).

The Paleocene sequences in the Sirt basin represent the Danian, Montian and Landenian stages. They consist of alternation of open marine calcareous shales and shallow water carbonates. *Occidental's* wells A1-NC29 B and C reported oil discovery from reefal limestone belonging to the Danian Upper Satal Formation organic belt.

Oasis's Bahi field produces from a reef grown on the bank edge. In wells G1-17, J1-17, H1-17 and A4-17 of the *Sirt Oil Company*. The first three wells tested oil from the Upper Satal undeveloped reef, while A4-17 produces from the Upper Satal reefoidal limestone. Wells S1, S2, A1, B1, D1 and G1 from Concession 20 encountered excellent reservoir character limestone of reefoidal nature, but with no oil accumulation being found in these wells due to lack of adequate seal rock.

A massive calcarenitic lens of the Mabruk Member (Beda Formation) was encountered in Concession NC114 (O1-32, K1-32, A1-106 and A1-24 wells). This carbonate lens, interpreted as a Montian undeveloped reef, was initiated on Danian mud-mount feature.

One of the earliest and also the largest oilfields to be discovered in the Sirt basin was Nassier, 322 km south of Benghazi. The field is located along the western edge of the Zelten platform ridge, a fault block that horst tilted downwards to the northeast. The discovery well was drilled in 1959 and the field produced nearly 193 million barrels of oil per day in 1970 from the Tertiary Zelten Member (Tiratsoo, 1976). The main reservoir of the field is a shelly limestone with pockets of reefal material; a dense, compact limestone and overlying shale unit provide an efficient cap rock for this reservoir, which has an average thickness of 350 ft and is at about 5,400 - 6,000 ft below the surface. The primary reservoir in the Nassier field is the coral-algae facies with porosities as high as 40%, resulting from freshwater diagenesis of the carbonates. The reservoir is part of a large carbonate barrier reef complex of shallow water sediments covering all of the southern area of Concession 6 and extending hundreds of kilometres to the southeast and southwest (Figure 3.12). The Nassier field reservoir contains reefal, inter-reefal and laterally associated limestone and dolomites. Limestone beds within the dolomites in the lower part of the Zelten Formation suggest that these carbonates were deposited in a broad shelf-lagoon and were later dolomitized (Tawadros, 2011). Twenty-four different depositional facies have been identified by *Esso* geologists in the field complex. Zelten lies centrally in a belt of oilfields stretching from Arshad in the north to Wahah and Defa in the south. To the west are Dahra, Hofra, Raguba and Samah, while to the east lie Amal, Nafoora, Augila and Gialo.

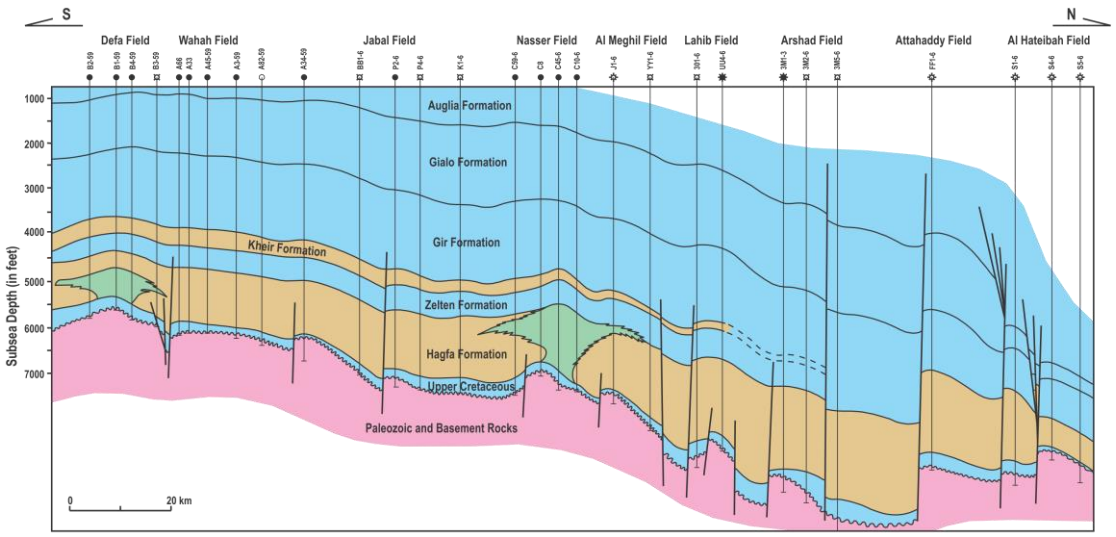

Figure 3.12. Cross section through Dafa and Nasser oil fields; modified after Roohi (1996).

From 1959 to 1961, exploring in Concession 59, south of Zaltan platform, *Oasis* made two major discoveries with their first two wells. The Al-59 well discovered the Wahah field, in which the reservoir was a late Cretaceous fringing apron of porous calcarenites, sealed by early Paleocene shales (Figure 3.12), while, the Bl-59 well discovered the Defa field (Figure 3.12), a Paleocene shoal carbonate buildup. Porosity is in the range from 25 to 30 % and permeability is commonly over 200 mD. This field contained 2000 million barrels of original reserves and over 5000 million barrels original oil in place (Hallett, 2002). The organic reef is situated on the crest of the Zelten platform ridge and rests on a high-energy Maastrichtian platform. Typically, the reef complex consists of coralline limestone, grading upwards to pelletoid algal limestone, terminating with foraminiferal calcarenite shoals. The Defa reef was probably established as a pinnacle reef, perhaps several different pinnacles are present in the initial reef complex, and later grew as a regressive reef along the Zelten ridge. Shallow-water, skeletal limestones have been found in the equivalent interval in R1-59. Whether the limestone is part of the Defa reef complex, a discreet reef in itself, or Defa derived reef debris is not presently clear. However, there is the possibility of an oil accumulation on the downthrown side of the Hagfa trough near the fault.

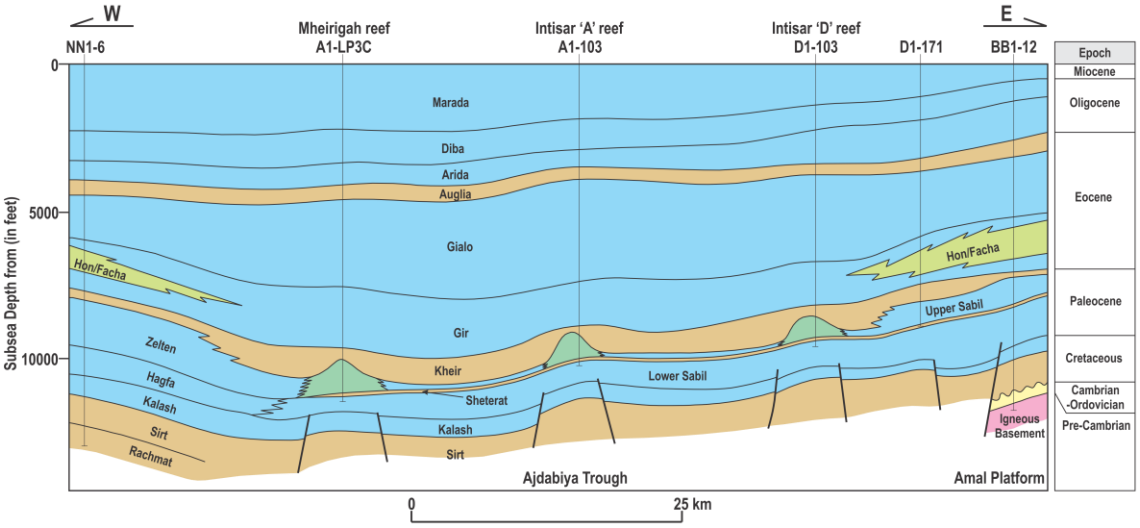

Figure 3.13. West-east cross section through Ajdabiya trough (Hallett and Clark-Lowes, 2016).

In the Eastern Sirt basin, the main producing reservoirs within the Upper Sabil Carbonate are associated with pinnacle reefs: oil has been discovered in Intisar (C103), Sahabi (NC73), Mheirigah (LP3C) and Shatirah (NC163) reefal complexes (Figure 3.13).

During 1967/68, an important group of oilfields was discovered west of the Nafoora field: the six Intisar reefs were found in a small area; two (Intisar A and D) of these reefs were found to be giants, with 1,500 and 1,200 million barrels of recoverable oil, respectively, ranked 76 and 91 among the giants of the world, by Halbouty *et al.* (1970). All were discovered from seismic reflection surveys. The total producible reserves of six of these reefal fields have been estimated as over 3 billion barrels, assuming only a 20% recovery factory. These reefs began as foraminiferal banks built up on local mounds on a shallow sea floor, and were added to by algae and coral growths (Tiratsoo, 1976).

The Intisar 'A' discovery well (A1-103) tested 43,500 barrels of oil per day, 43.5° API oil (Heatzig and Michel, 1968). A thickness of 959 ft of oil was found in one 1,349 ft thick section of Paleocene reef, and although it is only about 3 by 4 km in its greatest dimensions, it contained some 2 billion barrels of oil-in-place before production began (Tiratsoo, 1976). Terry and Williams (1969) recognized two stages in the growth of the reef: first, the development of a foraminiferal bank, loosely bound by algae; then, a period of coral-reef growth that was terminated by drowning or by smothering with argillaceous sediment. Terry and Williams (1969) also reported that the coral reef member of the bioherm has two mappable units – a coralline biomicrite overlain in general by reef limestone (Figure 3.14). It has about 15% porosity, but low

permeability, because much of the porosity is due to solution of coral skeletons and is not effective porosity. The reef limestone is 328-492 ft thick. Detrital biomicrite both in coral chambers and in the coral framework indicates that the corals had a capacity to retain sediment. The porosity of this unit is intergranular and averages about 22%. The reef is overlain by a dense biomicrite, overlain in its turn by the Upper Kheir marl (Chapman, 1983).

The Intisar 'D' discovery well (D1-103) tested 74,867 barrels of oil per day, 37.2° API oil in a maximum oil column of 995 ft, from 732 ft of reef reservoir (Heatzig and Michel, 1968). The Intisar 'D' reef is of similar size at a similar depth (Figure 3.15), roughly circular in plan with a diameter of about 5 km, and a thickness of 1,262 ft. The reef is coral and algal with grain- and mud-supported biomicrites. It differs from the other reefs in the area in that it has a lithologically homogeneous reservoir (Figure 3.16), without the noticeable layering typical of other reefs in the area (Brady, Campbell and Maher, 1980). However, its permeability varies greatly, from 4 to over 500 mD, with an average of at least 87 mD. Porosities range from 4 to 35%, with a field average of 22%, and the porosity is mostly solution and intergranular. The oil/water contact is at 9,450 ft below sea level, giving a maximum oil column of 995 ft. Original oil-in-place is estimated to be 1.8 billion barrels of recoverable oil (Chapman, 1983; Jenyon, 1990; Tawadros, 2011).

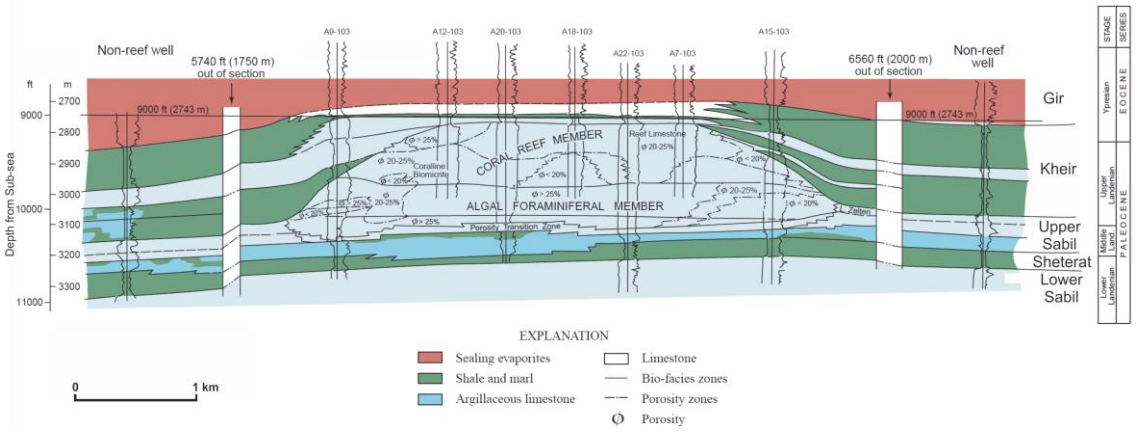

Figure 3.14. Cross-section through the Intisar 'A' reef (Terry and Williams, 1969).

The Intisar 'D' reef is full to spill point with 40°API under-saturated paraffinic crude, which is rather heavier than the oil in reefs to the north-west, and lighter than that in Intisar 'E' to the south-west. The distribution of under-saturated crudes, lightest in the north and heaviest in the south, is reminiscent of the Western Canada basin, and suggests a northerly source with southerly migration (Chapman, 1983).

The Sahabi fields are situated approximately 270 km south-southwest of Benghazi. The main pay of the Sahabi fields consists of a lower algal-foraminiferal shoal and an upper coralline reef, with average porosity 16% and permeability 3 mD. When the discovery well B1-95 in the Sahabi 'B' reef field (1,126 barrels of oil per day in 1966) was put on completion to produce oil from Upper Sabil Paleocene carbonates. The discovery well D1-95 (10,205 barrels of oil per day in 1967) encountered commercial oil accumulation in the Sahabi 'D' reef at a depth of about 10,000 ft below sea level and is approximately 1,300 ft thick, with a maximum original oil column thickness of 225 ft.

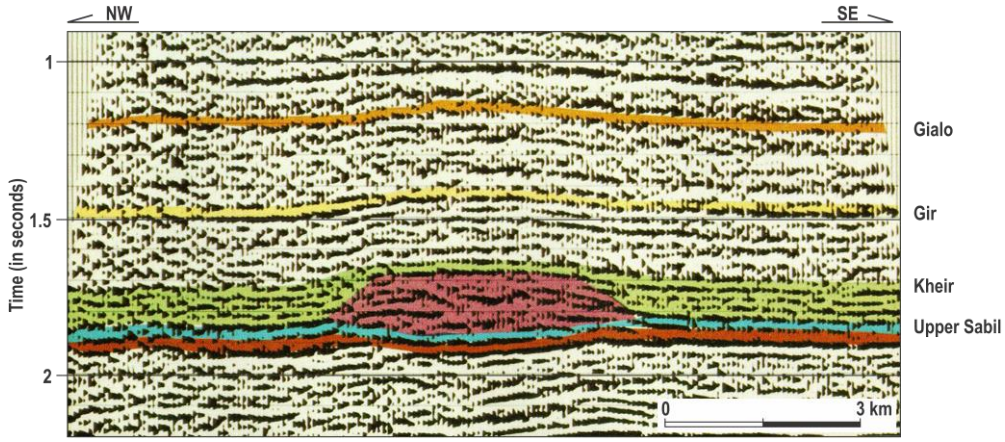

Figure 3.15. Seismic section over the crest of the Intisar 'D' reef (Brady, Campbell and Maher, 1980).

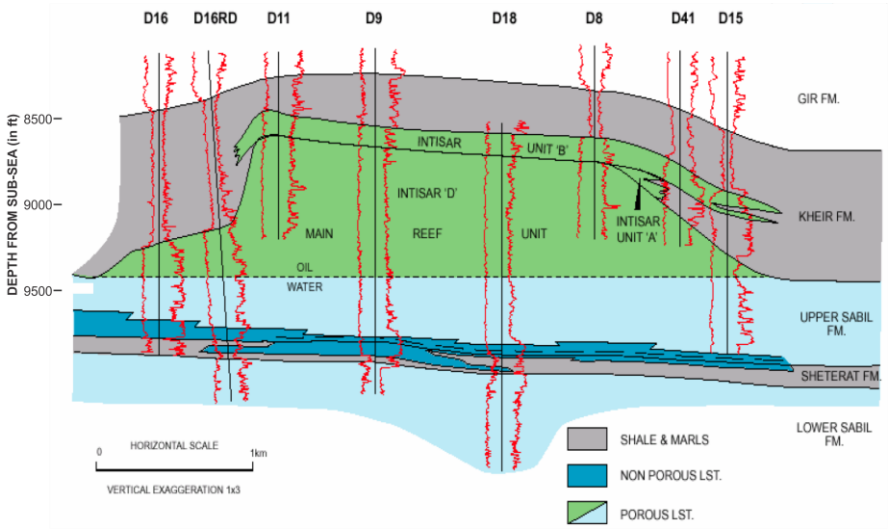

Figure 3.16. Intisar 'D' reef cross section. Gamma-ray and formation density logs were used (Brady, Campbell and Maher, 1980).

Chapter 4. Seismic Geomorphology

Chapter 4

Seismic Geomorphology

4.1 Introduction

Reef and other carbonate buildup forms are more likely to be observable on seismic sections than clastic bodies, because of the high contrast between their density and the seismic velocity of the adjacent sediments. Carbonate bodies are generally thicker than most sandstone reservoirs so that the resolution of the seismic energy does not have to be high. Carbonate is not as compactible as most clastic rocks, so draping structures which can be identified seismically are more likely to be observed over carbonate bodies than over comparable clastic entrapments (Dobrin, 1977). Finally, reefs often separate different depositional environments and reflection patterns are apt to differ on opposite sides of the reefs. This abrupt change of pattern can aid in finding reefs and differentiating between fore-reef and back-reef sides from the seismic section (McQuillin, Bacon and Barclay, 1984). Thus, stratigraphic traps in carbonates have been easier to locate by the seismic reflection method than traps in clastics.

Seismic geomorphology has been used to assess how karst features affected reservoir characterization, and to explain why Intisar ‘B’ and ‘C’ reefs are not charged. Seismic geomorphology is a useful technique to interpret seismic attribute patterns for the geomorphology of a formation, which is similar to using satellite and aerial photos of the Earth’s surface (Koson, Chenrai and Choowong, 2014). Geomorphology is the study of landforms which are produced by erosion and sedimentation. Seismic

geomorphology is defined as the application of analytical techniques pertaining to the study of topographies and buried geomorphical features as imaged by three-dimensional seismic data. This technique uses an integration of seismic attribute and horizon slices to map geomorphical surfaces as they may have formed at a specific instant in a geological period (Posamentier *et al.*, 2007).

4.2 Seismic Criteria for Reef Recognition

Several seismic reflection shapes interpreted as reefs are not unique, but may be exhibited by other geologic features similar in shape and size (e.g. igneous intrusions, salt intrusions, slump deposits, unconformity surfaces and volcanic cones). The following criteria for recognizing reefs on seismic sections (Figure 4.1) were suggested by Bubb and Hatlelid (1978); Burgess *et al.* (2013):

4.2.1 Direct Criteria

Boundary Outline: usually, reflection patterns directly define the reef boundary. These include onlap of overlying reflections onto the reef, and reflections from the flanks and top of the reef.

Onlap is related to the development of syn-depositional relief, representing subsequent burial of a reef by younger layers (Figure 4.2a). Depositional wings are high-amplitude, elongated and wedge-shape layers that thin out and extend from reefs into the adjacent layers (Figure 4.2b).

Reefs are usually noticeable by the presence of *convex-up* top reflection reliefs. However, post-depositional folding can produce similar convex-up reliefs. A general difference between reefs and tectonic folds is the vertical extent of the convex-up relief through the imaged layers. Convex-up reliefs associated with a reef should happen only within the reefs and, allowing for slight distortion produced by differences in compaction, in the directly overlying layers (Burgess *et al.*, 2013).

Seismic Facies Changes may happen in frequency, continuity and/or amplitude of seismic reflections from the area between the reef and the adjacent layers, or within the reef. Such changes would result where variances in the characteristics of bedding density, velocity and/or continuity exist between the reef and the layers surrounding the reef, or between layers within the reef (Bubb and Hatlelid, 1978).

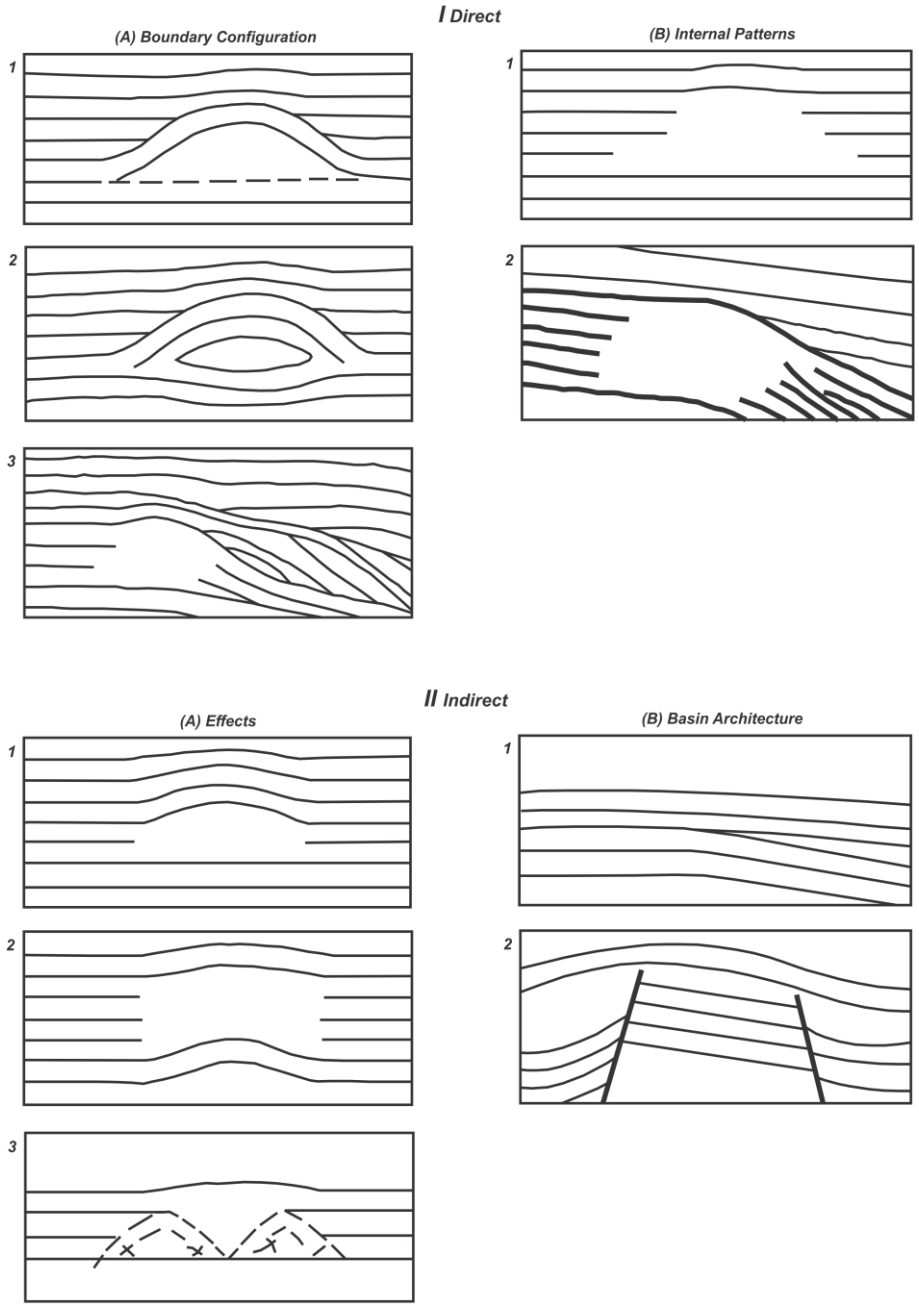

Figure 4.1 Seismic criteria for recognizing reefs. Criteria for directly outlining reefs include (A1 and A2) reflections from top and sides of reefs and (A3) onlap of overlying reflections onto reefs, and (B1 and B2) change in patterns of seismic facies between reef and enclosing strata (I-B). Criteria that indirectly outline or infer presence of reef include (A1) drape, (A2) velocity anomalies and (A3) diffraction events, and (B1 and B2) determination of optimum basin positions for reefs, include pinch out and fault (Bubb and Hatlelid, 1978).

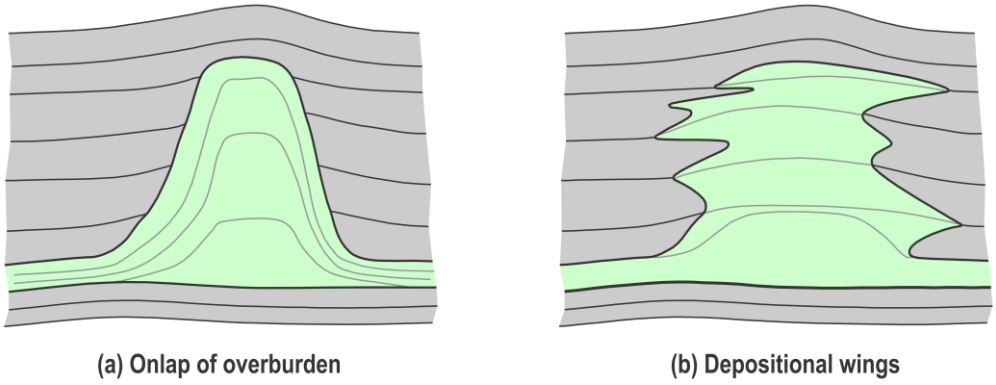

Figure 4.2 Schematic showing onlap types (Burgess *et al.*, 2013).

4.2.2 Indirect Criteria

Drape usually happens in seismic reflectors overlying the reef because of differential compaction of the reef and the enveloping layers. Reefs are usually more rigid and therefore more resistant to burial compaction than the enveloping shale layers (Burgess *et al.*, 2013). The effects of drape usually die out stratigraphically upwards.

Velocity Anomalies: reef limestones may have higher velocity than the adjacent facies (for example, back- and fore-reef shales) or they may have a lower velocity, where surrounded (for example, by denser limestones and dolomites). Both situations will give rise to velocity anomalies on a time section (Figure 4.3). Where the reef has a higher interval velocity than the adjacent strata, a velocity pull-up will develop. If the reef is draped by younger sediments, the pull-up could suggest that the overall positive feature is a deep-rooted structure (that is, pre-reef in age) and may lead to a pessimistically false geological interpretation. Alternatively, where the reef limestone has lower interval velocity than the surrounding sediments, the velocity anomaly results in a push-down; and the reef base could appear as a low on the seismic time section. This is identical to the shale push-down and the distortion on the time section is open to misinterpretation. If the lower velocity is attributed to exceptional porosity development, a push-down could have great prospective interest (Tucker and Yorston, 1973).

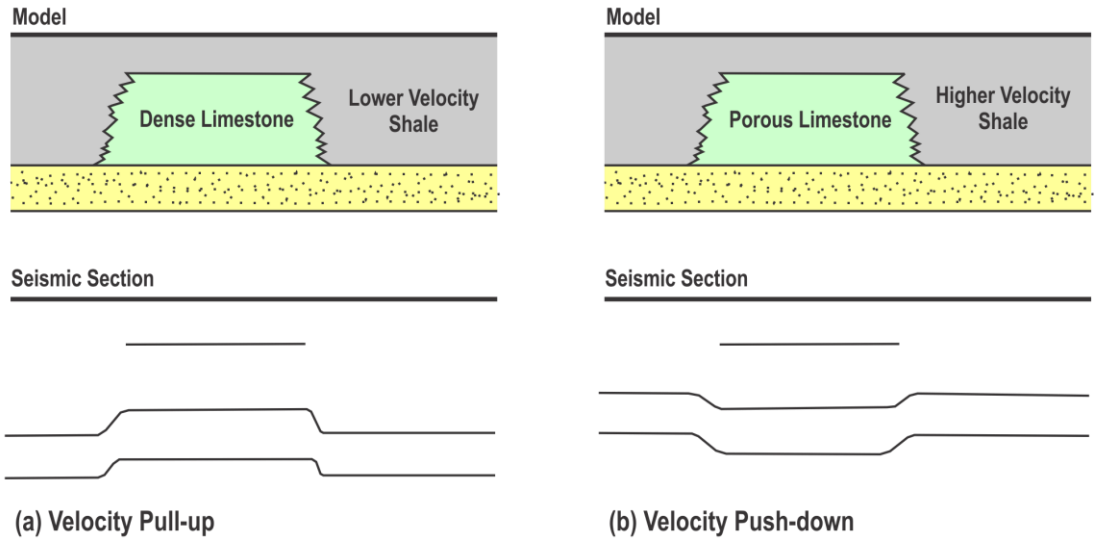

Figure 4.3 Velocity anomalies beneath reefs (Sheriff, 1980).

Spurious Events: the edges of the reef usually are noticeable by rapid changes in internal bedding geometry or the end of adjacent layers. These edges can be places for development of diffraction events. Mapping of diffractions may offer evidence for the presence and distribution of otherwise hard-to-see reefs (Bubb and Hatlelid, 1978).

Basin Architecture: understanding the geologic history of a basin allows the identification of areas where and times when environments were appropriate for reef growth. In some cases, reefs can be inferred as likely to form in a favoured place along a seismic section, based on the seismic profile and other geologic evidence of basin architecture, for example structural highs, the position of a hinge line or fault-block edges (Burgess *et al.*, 2013).

Dissolution can generate large-scale karst features, which can be recognized on seismic sections (Purdy and Waltham, 1999; Story *et al.*, 2000; Rosleff-Soerensen *et al.*, 2012), and related to an assumed subaerial exposure surface. This can support recognition of a seismic feature as a reef. However, the absence of karst should not prevent reef interpretation (Burgess *et al.*, 2013).

The interpretation is improved by a detailed study of the geologic setting of the area, and of those time-stratigraphic units which are prone to the growth of reefs. Figure 1.4 illustrates good seismic evidence for Intisar ‘A’, ‘B’ and ‘C’ reefs, interpreted as pinnacle reefs were quickly determined by (a) the convex shape at the reef top, or eye effect, (b) overlying drape, (c) break-up of data at reef edge, (d) little continuity within the reef mass, (e) being accompanied by karst features, and (f) the lower velocity of the more highly porous and fractured reef than that of the off-reef shales (which have high

interval velocity), which might be the reason for the velocity push-down seismic relief under the reef. This is a typical case in which a push-down velocity anomaly associated with a carbonate reef feature is of great significance, being often a direct indication of good porosity (Jenyon, 1990).

4.3 Well Log Analysis

Sheterat Shale is well distinguished by its positive spontaneous potential and low resistivity values. Upper Sabil Carbonate is characterized by negative spontaneous potential and generally high resistivity values, which change from the top to the base of the unit itself, due to the hydrocarbon content present in the upper part. Low resistivity is observed against some positive spontaneous potential peaks, indicating either high argillaceous content or shale streaks. The upper and lower boundaries of this unit can be defined on both the spontaneous potential curve and the resistivity log, while the Kheir Formation is characterized by positive spontaneous potential and relatively low resistivity values, with intercalations of high resistivity peaks corresponding to the limestone or dolomite bands. The spontaneous potential and resistivity logs that run across the Intisar reefs are shown in Figure 4.4. Total porosity was calculated from density logs, while, water saturation was calculated from logs using the Archie (1942) equation. A saturation gradient in Intisar ‘A’ is noted in each well having an oil-bearing section. The interval of gradually increasing water saturation normally covers the entire oil column and is due to capillary effects; its value depends on effective porosity as well.

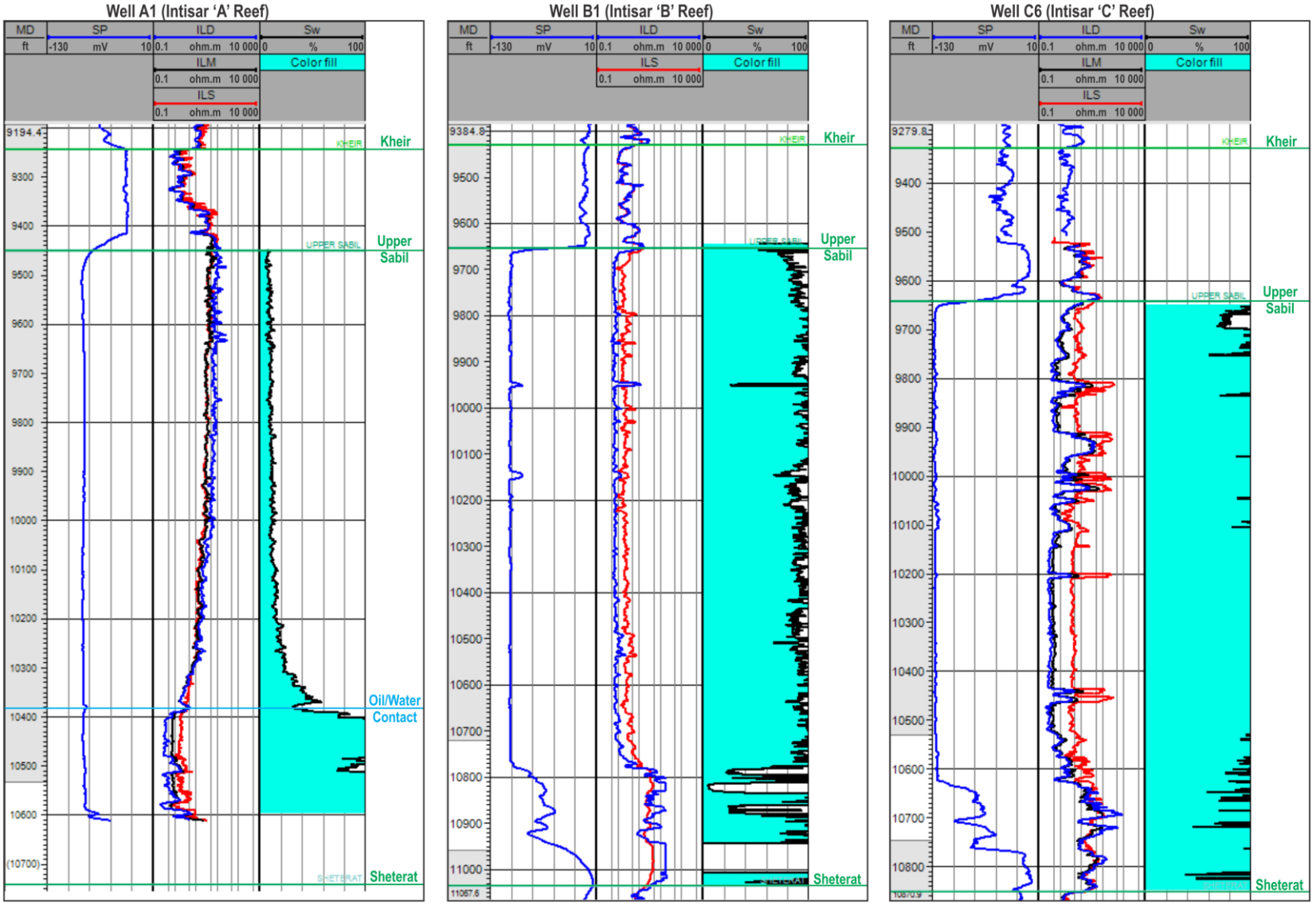

Figure 4.4. Spontaneous potential (in mV), resistivity (in ohm.m) and water saturation (in %) logs in Intisar A, B and C reefs.

The original field oil/water contact was 10,391 ft, as defined from log interpretation. The saturation values at the oil/water contacts are about 50%, while at the upper end of each reservoir the water saturations are calculated to be around 10%. The contact is distinct in most wells, with the depth of the contact varying ±20 ft from the average value. These variations are due to slight hole deviations; no tilted water table is believed to be present. The uniform resistivity separation curves indicate the homogeneous nature of the reservoir. The water saturation log in Intisar 'B' reef illustrates that the reservoir is almost completely water bearing, while Intisar 'C' reservoir rock is quite similar to that of the Intisar 'B' reef, except that it shows a non-uniform resistivity gradient because there are some more highly resistive inter-beds within the reservoir zone. The spontaneous potential logs from the three reefs show a non-porous limestone zone at the base of the reefs.

4.4 Seismic Attributes and Mapping

A seismic attribute is a quantitative measure of a seismic characteristic. This technique has been integral to seismic interpretation since the 1980's. Today, there are more than 50 different attributes measured from seismic signals and used for the understanding of petrophysical properties, geologic stratigraphy and structure (Chopra and Marfurt, 2005). Seismic attributes help to extract more information from conventional three-dimensional seismic data, which can support the interpretation of the geomorphology and the paleo-environments. Seismic attributes usually provide information relative to shape, position and amplitude of seismic waveform (Koson, Chenrai and Choowong, 2014). The seismic attributes of Intisar reefs usually display two components: time-structural relief and lateral character variations. Both components are mainly functions of the morphology of the reef and the nature of the basin in which the reef developed, and are geophysical representations of geological features.

Several seismic attributes have been generated in this study to enhance the seismic image of the reefs and to visualize the geomorphological features. A time structure map, coherence and dip illumination attributes have been used to highlight the reef features. In addition, coherence, dip illumination, edge enhancement and RMS amplitude attributes have been used to define the karst features. Variance is an edge method that measures the similarity of waveforms or traces adjacent over given lateral and/or vertical windows. It is a very effective tool for delineation of faults and reef edges. The dip illumination attribute developed by Aqrawi and Boe (2012) is a dip

exploitation attribute which calculates a dip scan estimation using a 5x5 neighbourhood of traces. This attribute consists of calculating either the dip magnitude or the directional dip (Aqrawi *et al.*, 2012). A good dip estimation can reveal a lot about various geological features on horizon slices. Edge enhancement is a volume attribute filter which performs an edge enhancement within seismic data. It applies its filter in a three-dimensional plane, rather than in lines. This attribute is a very effective tool for the delineation of reef, karst and fault features and also sequence boundaries on vertical seismic profiles. RMS amplitude calculates root-mean-squares on instantaneous traces over a specified time window. The RMS amplitude resolution can be set by changing the time window length; longer time windows produce a smoother amplitude estimation.

The study area consists of three isolated reefs that are close together: Intisar 'A', 'B' and 'C', separated by a distance of about 4 km (Figure 4.5a). The Intisar 'A' and 'C' reefs are roughly circular in plan and approximately 3 to 4 km in diameter and are about 1,349 and 1,200 ft thick at their crests, respectively. The third reef in the study area, Intisar 'B' reef, is relatively large and measures about 4.5 by 4.5 km (about 1,390 ft thick). The development of the Intisar reefs is associated with shallow-water conditions and high-energy facies deposited either along the shelf margins or on localized paleo-topographic highs (Figure 4.5b). Variance attributes have been used to reveal the geometries and dimensions of the Intisar reefs (Figure 4.6).

From the structural point of view, it appears that the Intisar 'B' reef was positioned in a slightly greater water depth where a lower energy environment existed throughout most of the growth of the reef (Figure 4.5 and Figure 4.7). In this position, the shale and micrite deposits dominated the growth of the mounds and, as a result, porosities and permeabilities are somewhat lower than for some other reefs in the region.

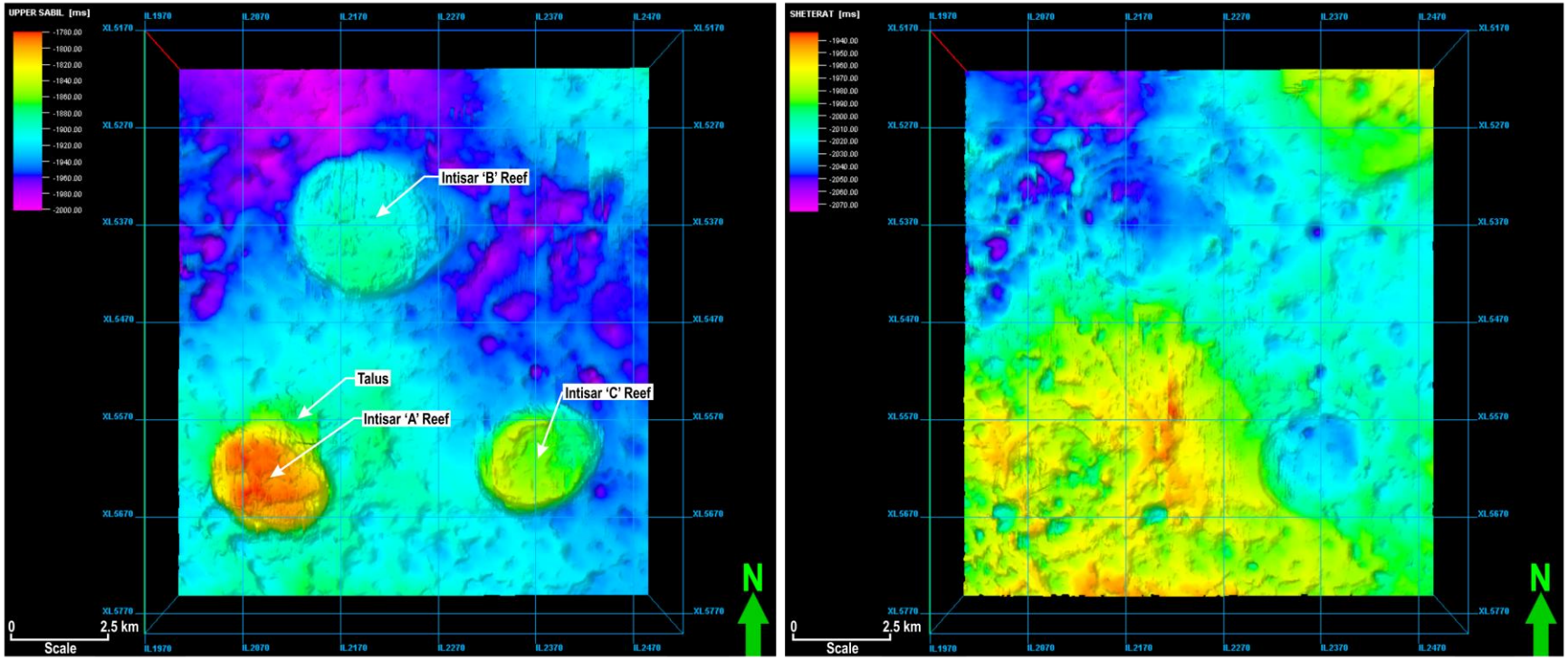

(a) Top of Upper Sabil Reflector

(b) Base of Upper Sabil Reflector

Figure 4.5. Time-structure maps: (a) top and (b) base of Upper Sabil Carbonate, and summarized lateral distribution of facies observed in the study area.

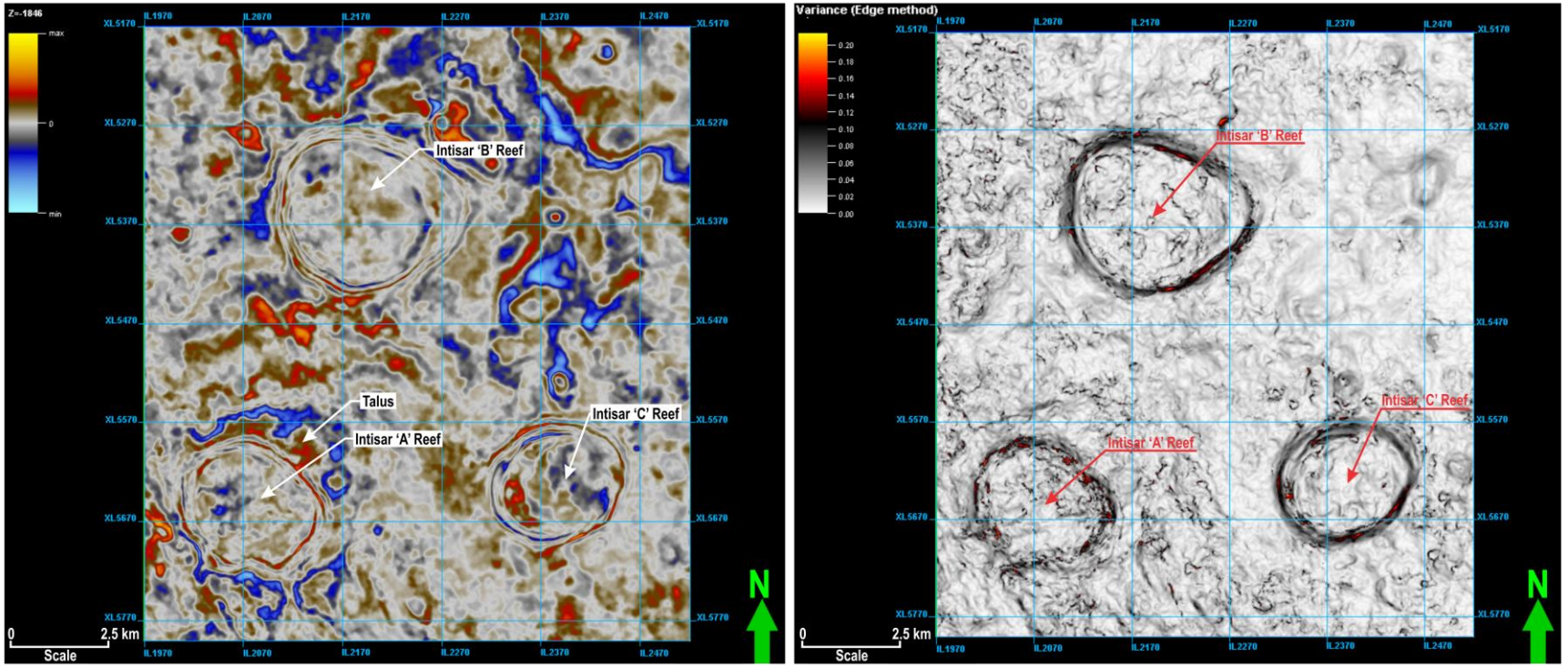

(a) Original Seismic Amplitude Time Slice (1846 milliseconds)

(b) Variance Seismic Attribute Time Slice (1860 milliseconds)

Figure 4.6. (a) Amplitude and (b) variance attributes in horizontal time slices.

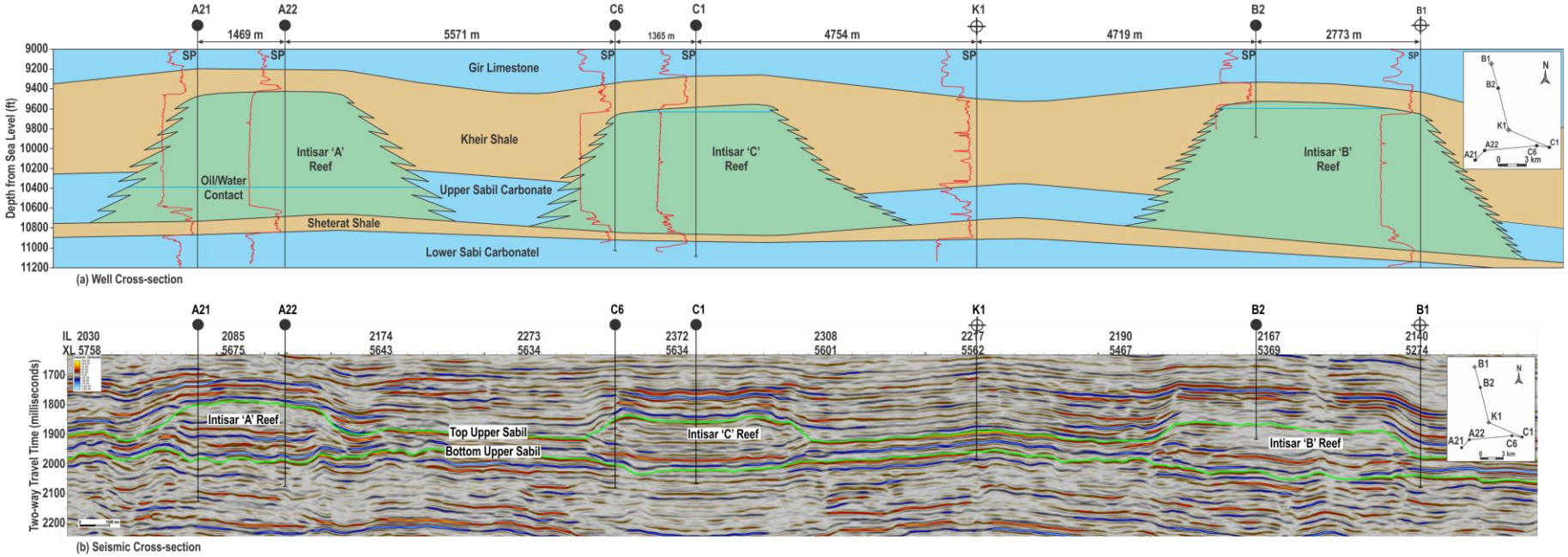

Figure 4.7. Well and Seismic cross-section through the study area.

The location of the Intisar reefs may be along the edges of individual faults within a fault complex to the immediate west of the Amal basement high. The reservoirs' source rock is mature Upper Cretaceous shales, with vertical migration along associated fault conduits (Figure 3.9). During the Miocene/Oligocene, oil migrated through the Kalash Limestone, Lower Sabil Carbonate, Sheterat Shale and into the overlying reefs. A pinnacle reef sitting on a thin carbonate platform that overlies shales is likely to undergo subsidence due to compaction. This may form a shallow rim-syncline in the surrounding and underlying rocks, sufficient to alter the path of migrating fluids (Brady, Campbell and Maher, 1980). Some of the Intisar reefs have developed rim-synclines, which might have had an effect the migration pathways. Figure 4.8 shows the presence of these rim-synclines associated with faults/fractures beneath the Intisar 'A' reef flanks. The variance and second derivative seismic attributes have been used in recognizing that the faults/fractures are most common in the south-eastern part of the Intisar 'A' reef (Figure 4.9). The model in Figure 4.10 shows fluid migration from a pinnacle reef into drape anticline beds over the reef; the highly permeable reef acts as a fluid aquifer, directing pore waters from the compacting shales upward through the reef. The overlying Kheir shale acts as the main seal and lateral side seals may be compromised by porous units. This reduces the effectiveness of the Kheir as a seal.

4.5 Analysis of Karst Features

Dissolution of limestones can generate various geomorphologic features, typically referred to as karst. Buried karst features may be cave, doline or collapse features. Large scale karst features can be recognized on seismic sections (Purdy and Waltham, 1999; Story *et al.*, 2000; Rosleff-Soerensen *et al.*, 2012). Karstification can positively or negatively affect the physical properties and geometry of reef reservoirs (Burberry, Jackson and Chandler, 2016). Dissolution throughout exposure and karstification can improve permeability and porosity. However, porosity decrease may happen as collapsed caves fill with fine-grained or brecciated material sediments (Loucks and Handford, 1996; Loucks, 1999; Loucks and Mescher, 2002). In addition, cap rock quality may be reduced because of the collapse and distortion of layers overlying karst features (Dembicki and Machel, 1996; Cerepi, Barde and Labat, 2003; Vahrenkamp *et al.*, 2004). Karst zones are usually difficult to differentiate from compacted limestone, because they commonly do not have a different seismic facies pattern (Fontaine *et al.*, 1987).

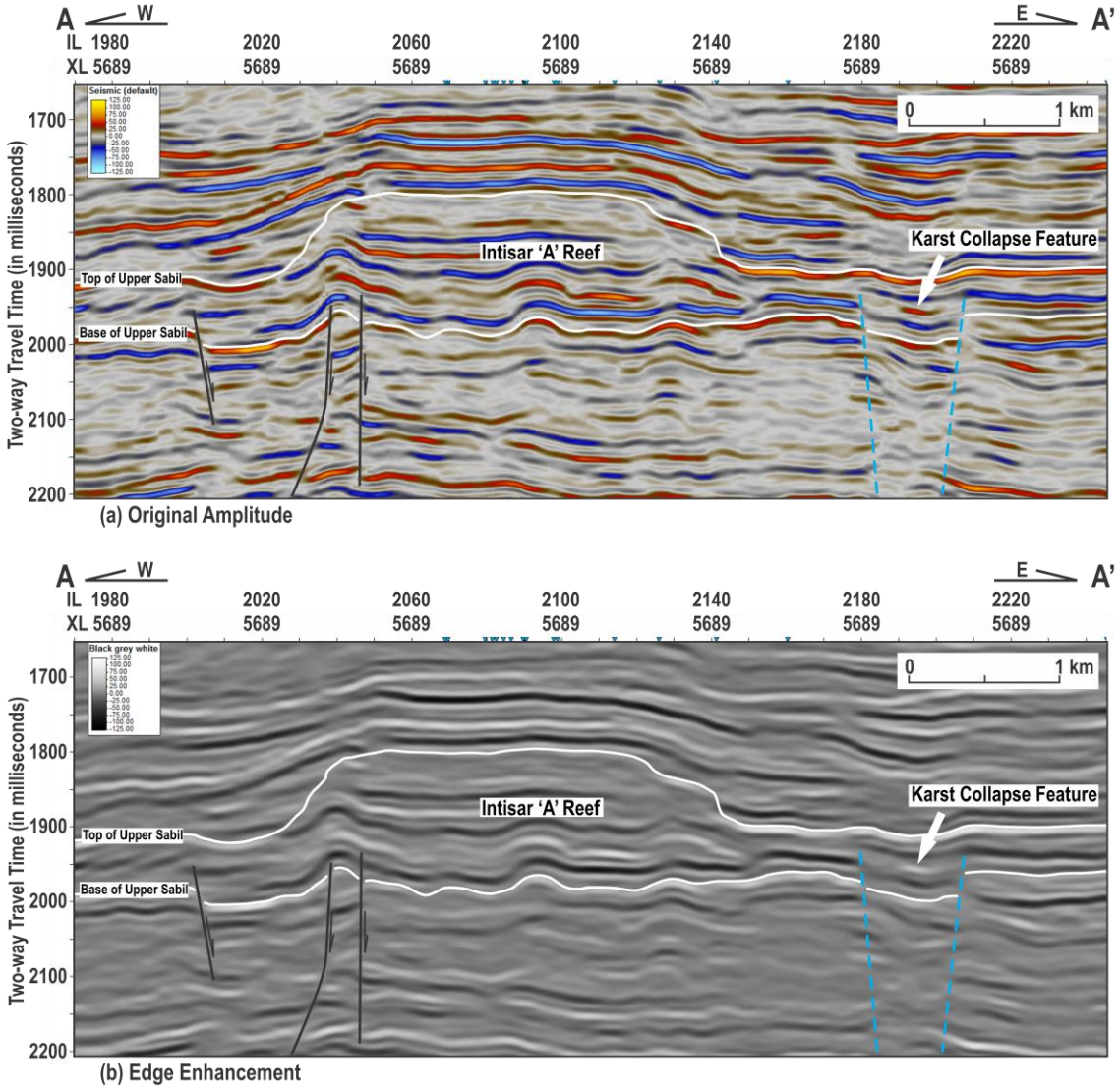

Figure 4.8. West-east seismic attribute cross sections AA´, illustrating faults beneath the Intisar 'A' reef.

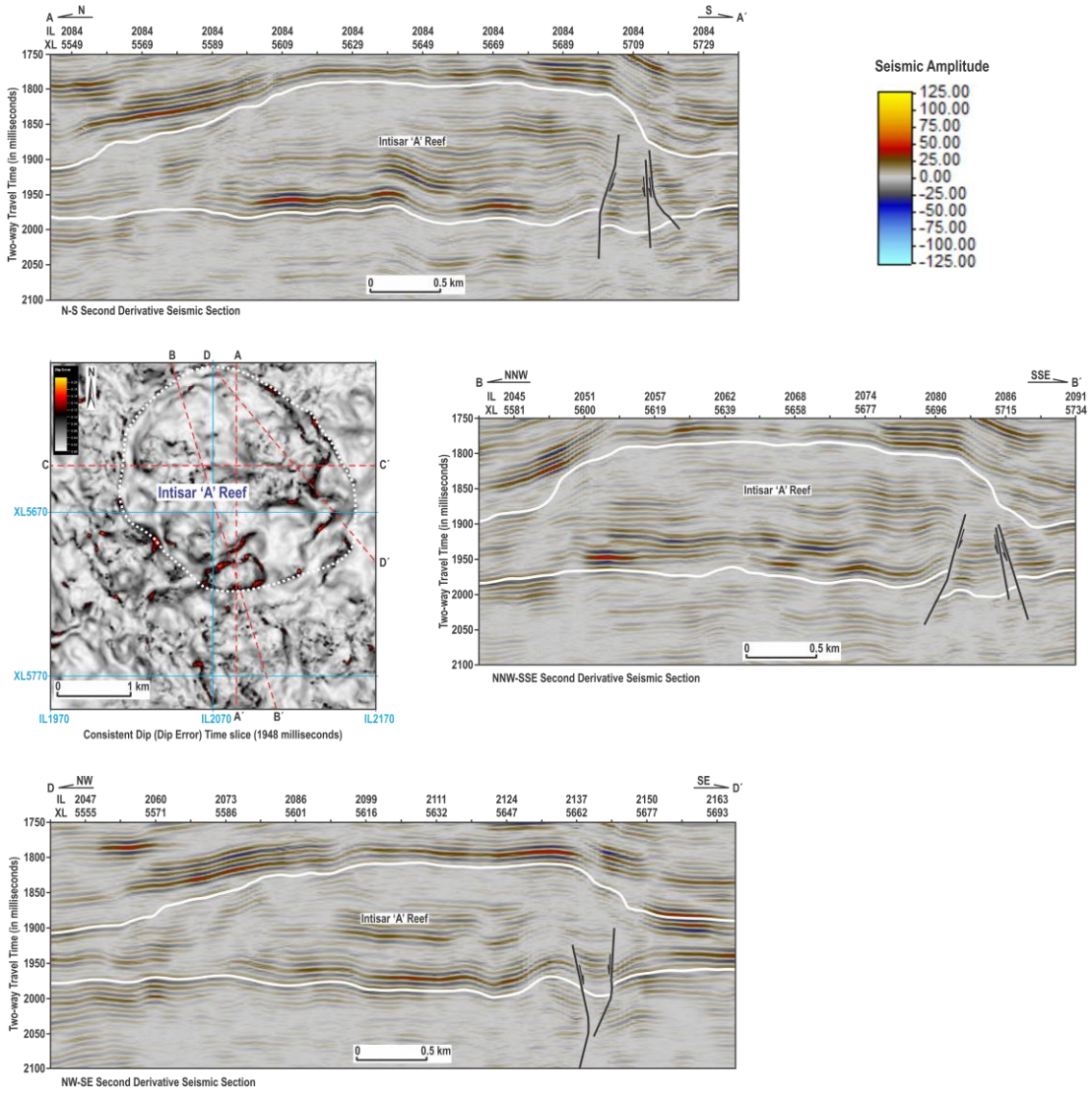

Figure 4.9. Different second derivative seismic sections with different faults illustrated beneath the Intisar 'A' reef.

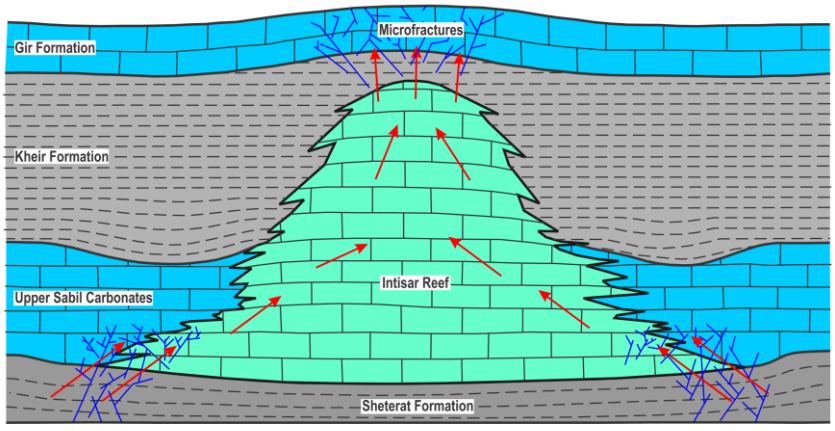

Figure 4.10. Migration into and from the Intisar reefs. Oil migration paths highlighted with red arrows.

Karst zones are usually difficult to distinguish from compact limestone on seismic data, because they do not have a distinct seismic facies. The first step in detecting karst areas is to recognize paleo-topographic highs on seismic sections (Jenyon, 1984). Amplitude analysis can be used to determine the lateral extension of a karst zone. Vandenberghe, Poggiagliolmi and Schwarz (1983) noted that the magnitude of the seismic reflection as a function of offset is affected by Poisson's ratio, and they theoretically proved that a relationship exists between values of Poisson's ratio and changes in limestone diagenesis. In addition, the relationship between the amplitudes of near and far traces on various offset stacks usually highlights these differences (Figure 4.11).

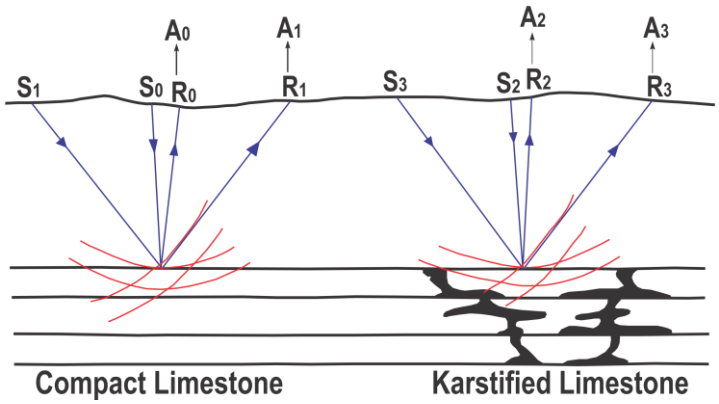

Figure 4.11. Amplitude analysis as function of offset for compact and karst limestone, where A_0, A_1, A_2 and A_3 are magnitudes of reflection for near offset (S_0-R_0) and (S_2-R_2), and far offset (S_1-R_1) and (S_3-R_3) (Fontaine *et al.*, 1987).

The seismic attributes indicate buried karst-collapse (sinkhole) features at the Intisar 'B' and 'C' reefs, in which they have an impact on reservoir quality and the production of oil within these fields (Figure 4.12 and Figure 4.13). The seismic attributes have provided the first realization of these paleo-karst features. Most karst-collapse are quite vertical pipe features, because of their genetic and spatial relationship with faults or/and fractures (Hurley and Budros, 1990; Palmer, 1991; Davies and Smith Jr, 2006; Smith Jr, 2006; Klimchouk, 2009). The karst-collapse features provide pathways for upward migration of hydrocarbons into the Gir, Gialo and Auglia reservoirs. Thus, the karst-collapse features may be the main contributing factors to the escape of hydrocarbons within Intisar 'B' and 'C' reefs. The time gain sections in Figure 4.12c and Figure 4.13c show the chaotic reflectivity associated with karst-collapse features at the reservoir level. The shale unit above the reservoir rock must be micro-fractured to allow for upward hydrocarbon migration. The major contribution to the pull-up reflectors beneath karst is from velocity distortions in the overlying

sediments. Formation porosity is reduced in the reservoir carbonates around the base of the cylindrical pipe collapse features because of the brecciated collapse material or fine-grained sediments (Figure 4.12b and Figure 4.13b). Water can move up through these karst features, which could explain the high water cuts in the Intisar 'B' and 'C' reefs. Figure 4.14 shows a horizon time slice through the dip illumination seismic attribute at the approximate top of the reefs. The karst features in the Intisar 'B' and 'C' reefs are highlighted with white arrows. The karst feature diameters are approximately 300 m and 200 m at Intisar 'B' and 'C', respectively. The residual trace of oil in these two reefs indicates that the oil migrated from these reefs after the sinkhole effects (Figure 4.4). The two karst features extended shallowly into the overlying Auglia Formation. This indicates that the collapses may have happened during the Oligocene period. The effects of the karstification processes occurred during the low stand of main sea level.

More than twenty-six large karst depressions have been identified in this area, discernible both on seismic attribute slices and in seismic attribute cross sections. Each of these features can be identified on the Upper Sabil carbonates. The seismic attribute slices indicate that the depressions are sub-circular and 0.2–1 km wide, as highlighted by the blue circles in Figure 4.15. Figure 4.16 shows the two large karst features around Intisar 'C' reef, indicated by white arrows.

These depressions breccia forms as water moves up the fault and/or fracture zones and dissolves lower formations, producing subsidence in the overlying rock mass. When the slightly acidic water reaches the limestone rocks, it continues moving through any interconnected pores, joints or fractures, as weak carbonic acid (CO_2) dissolves and enlarges any pores or cracks through which it flows, and subsequently overlying units collapse into sinkholes under differential compaction (Figure 4.17). During continued deposition, the differential compaction creates depressions over the sinkholes. However, many karst features are associated with deeper tectonic pull-apart blocks in the basement (Chopra and Marfurt, 2007).

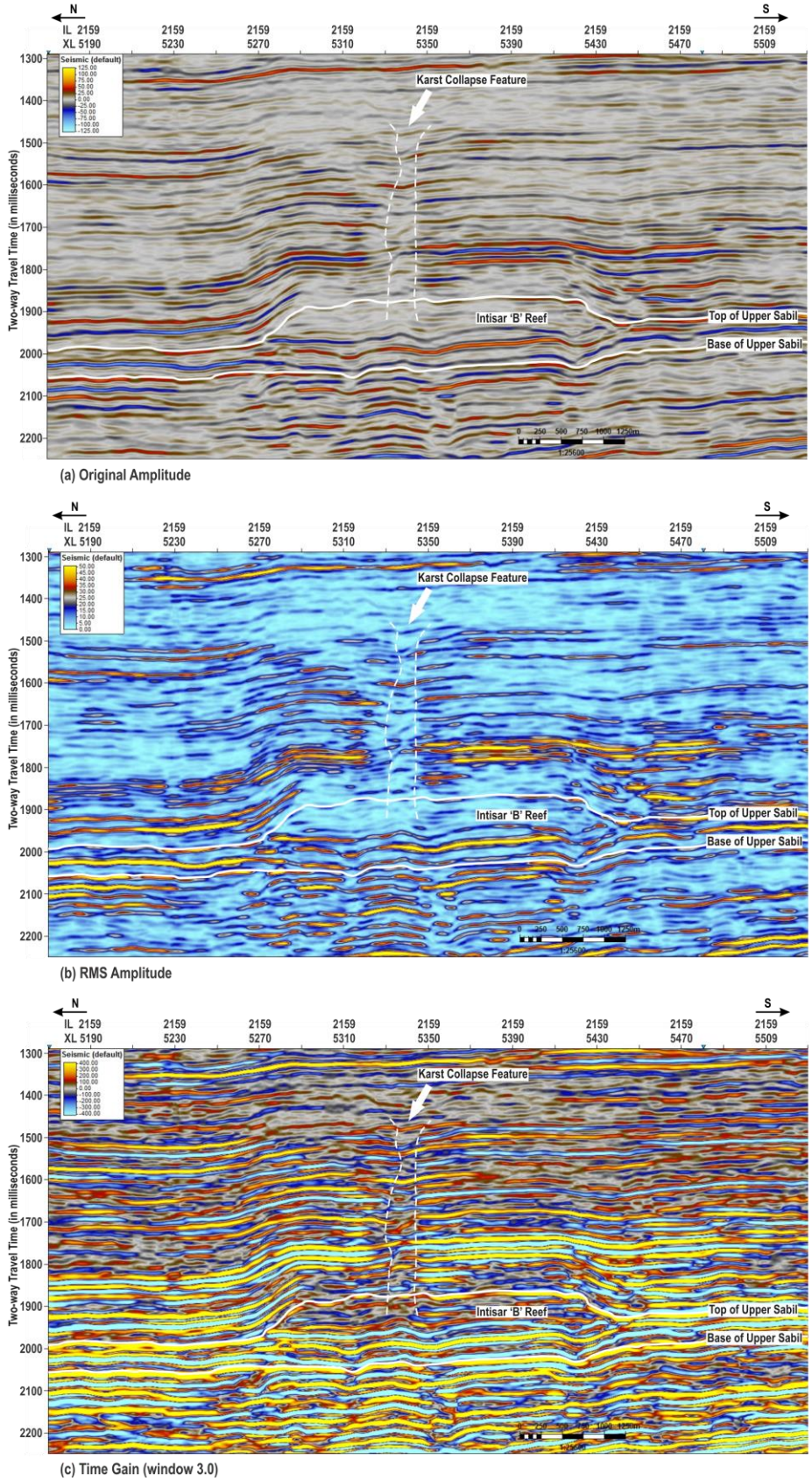

Figure 4.12. Seismic attribute sections showing karst-collapse feature in the Intisar 'B' reef field.

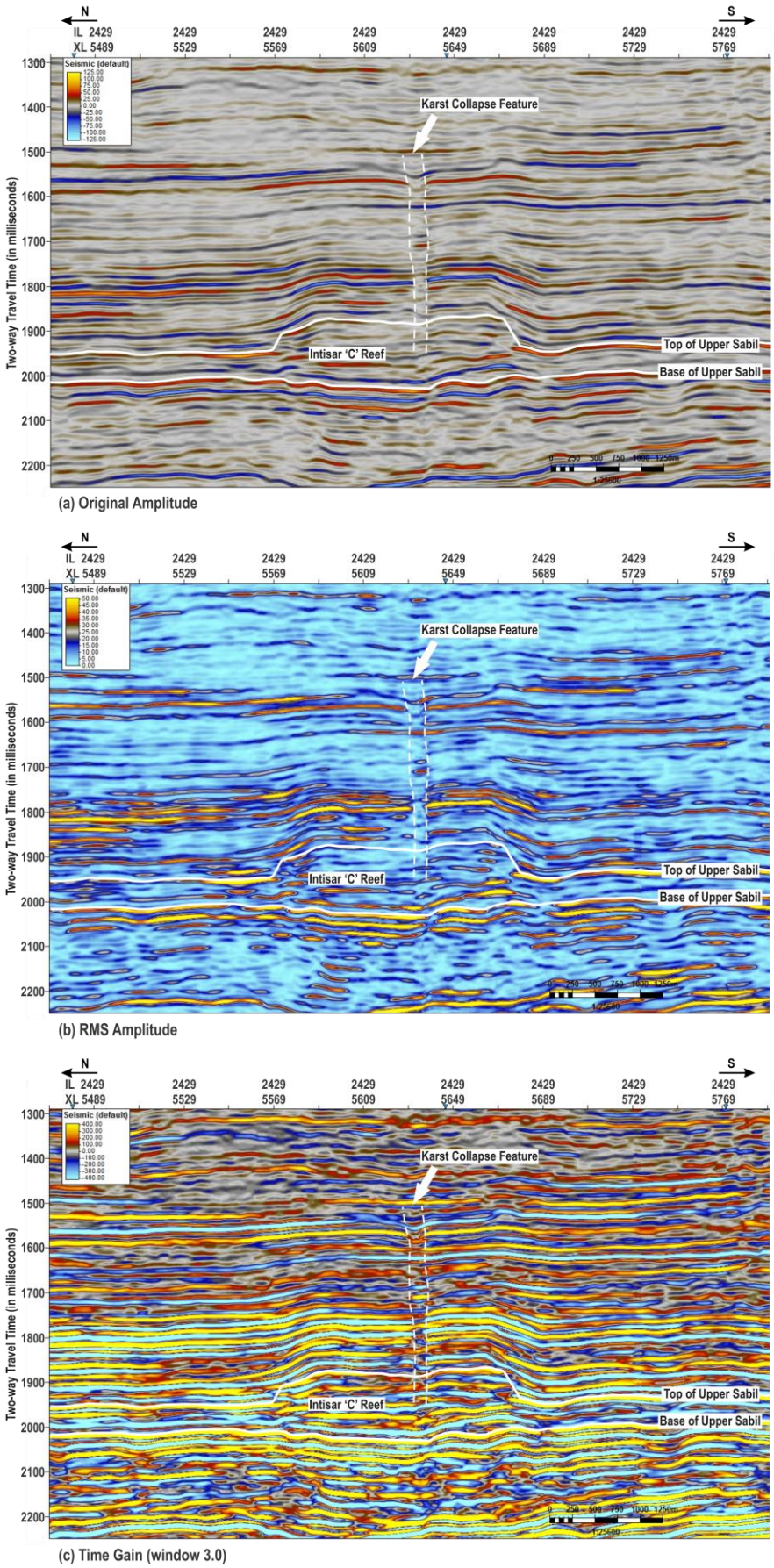

Figure 4.13. Seismic attribute sections showing karst-collapse feature in the Intisar 'C' reef field.

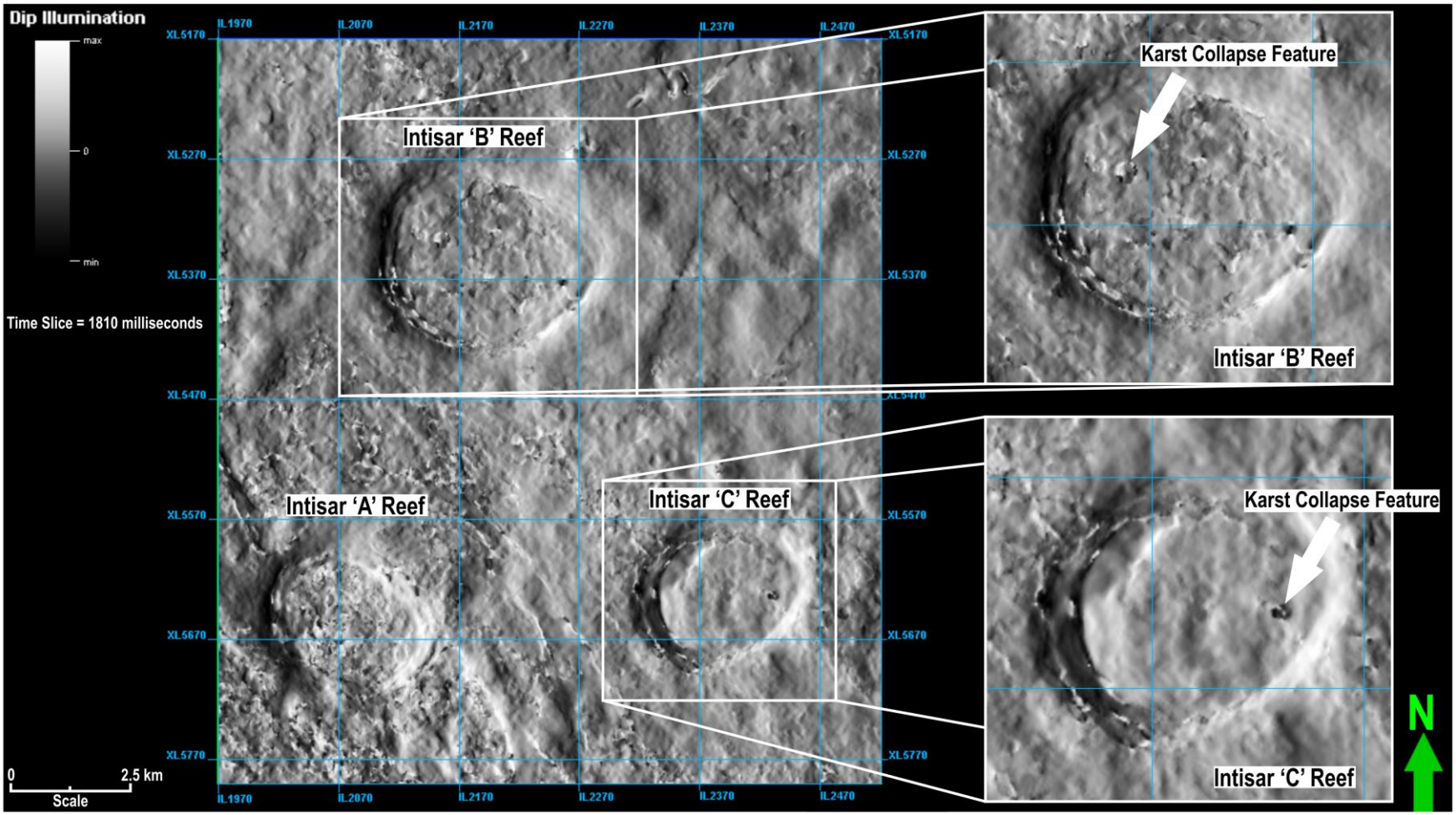

Figure 4.14. Seismic dip illumination time slice at 1810 milliseconds through the study area, showing the Intisar reefs and karst-collapse features.

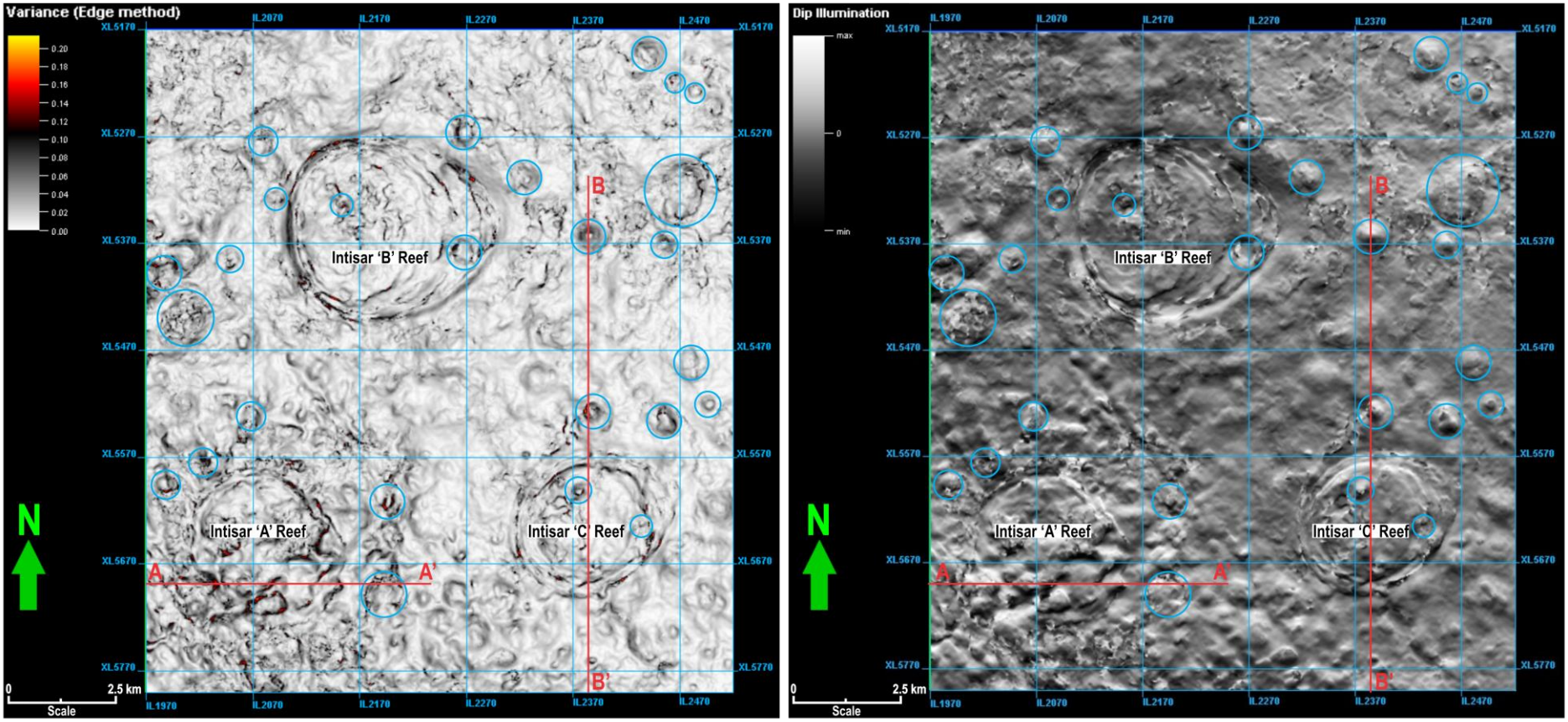

(a) Variance(1948 milliseconds slice)

(b) Dip Illumination(1948 milliseconds slice)

Figure 4.15. Seismic attribute slices of Upper Sabil Carbonate showing the distribution of sub-circular karst features. The blue circles mark the locations of karst features. AA´ and BB´ seismic cross sections are shown in Figure 4.8 and Figure 4.16, respectively.

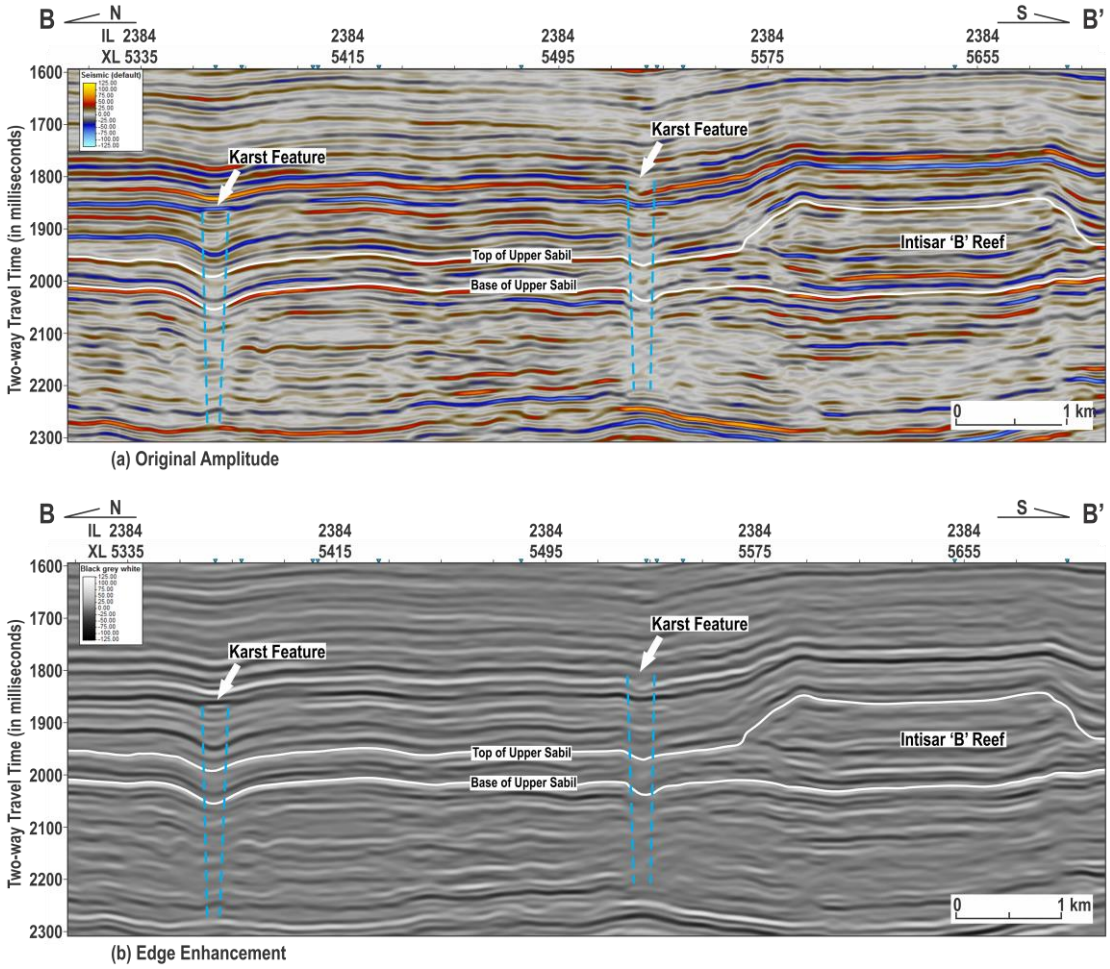

Figure 4.16. North-south seismic attribute cross section BB´ showing two sinkhole features around Intisar 'B' reef.

4.6 Summary

This chapter has used the seismic geomorphology to assess how karst features affected the reservoirs' characterization, and explained why the Intisar 'B' and 'C' reefs are not charged. The Intisar 'B' and 'C' reefs contain only residual traces of oil while Intisar 'A' has hydrocarbon fill factors as high. The seismic attributes indicate buried karst-collapse features with diameters of approximately 300 m and 200 m at the Intisar 'B' and 'C' reefs, with an impact on the reservoir quality and the production of oil within these fields. Buried karst sinkhole feature diameters are approximately 300 m and 200 m at Intisar 'B' and 'C', respectively. The residual traces of oil in these two reefs indicate that the oil has migrated from these reefs as a result of the sinkhole effects. These karst features occurred during the low stand of the main sea level, during the Oligocene time. The karst-collapse features provide pathways for upward movement

of hydrocarbons into the Eocene limestone reservoirs. This may be the main contributing factor to the escape of hydrocarbons from these two reef fields. The shale section above the reservoir is a weak cap rock and allows for upward migration of hydrocarbons. The relationship of the karst-collapse features with an abnormally large upward movement of water explains the high water cuts in these two reef fields. Some of the Intisar reefs have developed rim-synclines associated with faults/fractures which might have had an effect on the migration pathways.

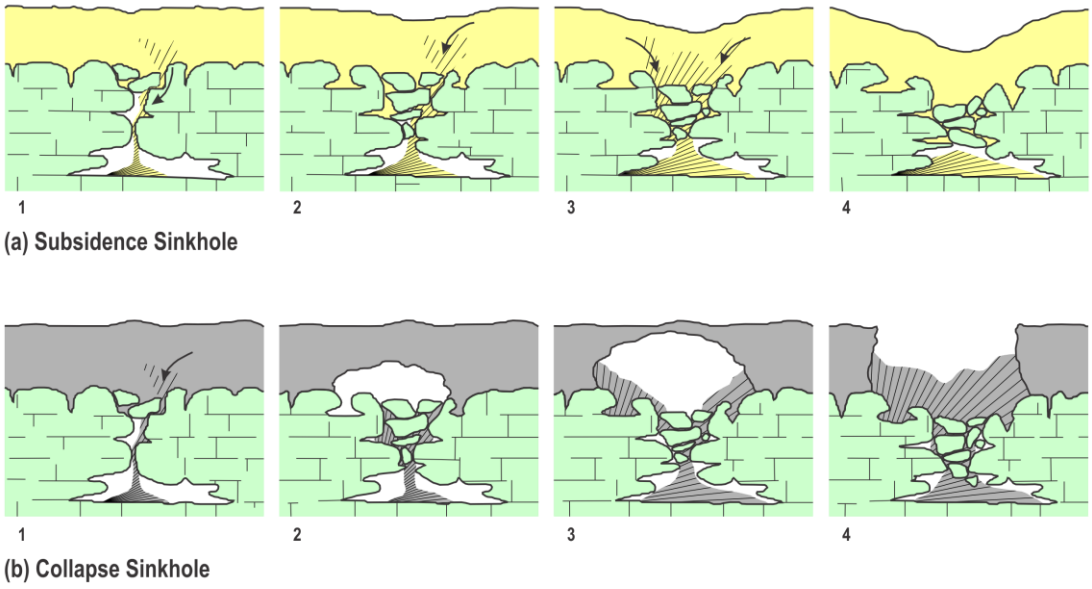

Figure 4.17. Stages of karst-collapse feature development (Culshaw and Waltham, 1987).

Chapter 5. Seismic Reservoir Characterization

Chapter 5

Seismic Reservoir Characterization

5.1 Introduction

Seismic attributes do not offer enough information about reservoir properties on a layer-by-layer basis. This information can be resulting by seismic inversion in terms of acoustic impedance (Pramanik *et al.,* 2002). The essential aim of seismic inversion is to convert seismic amplitudes into a measurable rock properties to describe the reservoir rocks (Pendrel, 2001). Seismic inversion can be categorized into pre-stack and post-stack seismic inversion. Inversion of post-stack seismic data is an estimation technique to predict earth's acoustic impedance (*AI)* through integration of well logs and post-stack seismic data. Acoustic impedance inversion was first described by Lindseth (1979). Seismic inversion techniques have been widely applied in oil exploration and development since the 1980s (Li, 2014). Various methods have been used for post-stack inversion, which include model-based, sparse-spike, and band-limited inversion techniques (Gavotti *et al.,* 2013). In this chapter the well log data is integrated with the seismic for a better defined reservoir model. This integration is accomplished by inverting the original amplitude of the seismic data to acoustic impedance properties so that correlation with the well logs is possible. The software package Hampson-Russell's Geoview® suite has been used for this study. The post-stack seismic inversion processes are summarized in Figure 5.1.

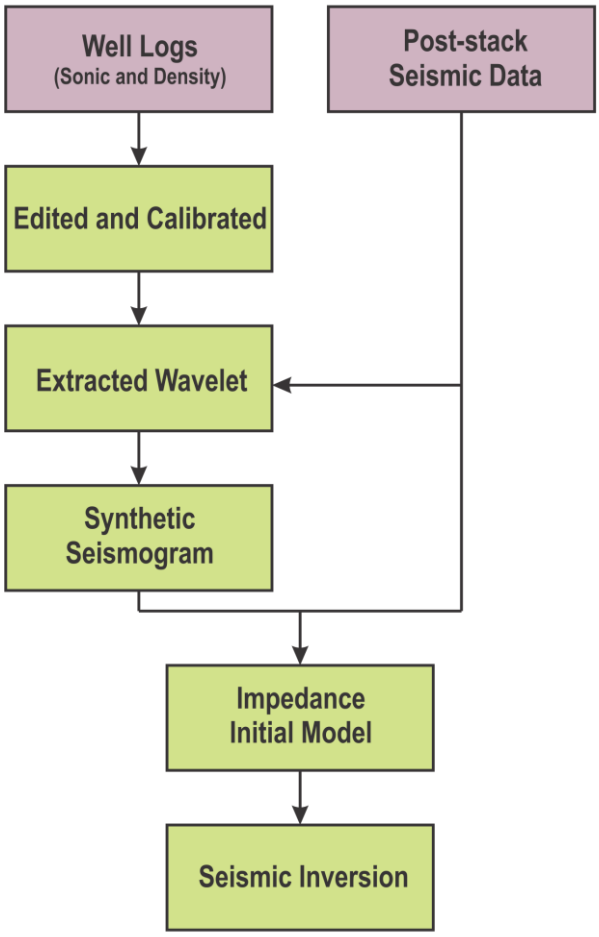

Figure 5.1. Post-stack seismic inversion workflow.

The conventional seismic interpretation has identified the Intisar 'A' pool as a reefal bioherm. However, detailed facies classification, reservoir characterization, and conditions governing oil fill-up in this reef remain unresolved. The main objectives of this chapter are to: (a) determine whether reservoir characterization can be achieved using the inversion results and whether seismic inversion is an effective technique in the evaluation of the reservoir potential of the Intisar reefs, (b) improve the geological/petrophysical models of Terry and Williams (1969) in the Intisar 'A' reservoir (Figure 3.14) using the properties estimated from the seismic inversion to control the interpolation and modelling, and (c) predict the properties of Intisar 'B' and 'C' reservoirs, where minimum well control data is available, from the post-stack seismic inversion.

5.2 Seismic Inversion Analysis

Impedance inversion is the transformation of seismic amplitudes into pseudo-acoustic impedance logs at each seismic trace; pseudo-acoustic impedance logs are acoustic impedance computed from seismic traces. Latimer, Davidson and Van Riel (2000) explained these advantages of acoustic impedance inversion: (a) the acoustic impedance model contains all the seismic information without the complicating issues produced by wavelets and adds important well log information, (b) it is closely related to pore fill, porosity, lithology, and other properties; it is common to find strong experimental relationships between impedance and at least one of these petrophysical properties, (c) it can produce sequenced stratigraphic analysis more traditional forward, and (d) it supports quick and correct interpretation, allowing for rapid delineation of geological bodies.

There are many inversion techniques for extraction of impedance from post-stack seismic volume by applying a deconvolution model to eliminate and/or minimize the tuning effects. A few theoretical methods have emerged since the 1980s, such as model-based, bandlimited (Russell and Toksöz, 1991), linear programing sparse spike (Taylor, Banks and McCoy, 1979; Cooke and Schneider, 1983; Oldenburg, Scheuer and Levy, 1983), maximum likelihood sparse spike (Chi, Mendel and Hampson, 1984), and constrained sparse spike inversions (Debeye and Riel, 1990). All these techniques determine the convolutional model components in each seismic trace. The model-based inversion begins with the low frequency (or initial) model and then this model is modified until the synthetic section best fits the real seismic section. The bandlimited inversion includes straight integration of real seismic volume to make a bandlimited inverted trace and then deriving the absent low frequency trend from the initial model. The sparse-spike inversion estimates a set of sparse reflection coefficients from the real seismic volume, constraining the reflection coefficients with the model and then inverting the reflection coefficients to produce the acoustic impedance (Russell and Toksöz, 1991).

5.3 Seismic Well Tie

The first stage of the seismic inversion procedure is to tie the seismic with the well's data, in which events recorded on the seismic are correlated with the events logged on the well logs. These events should correspond before continuing to the next stage of inversion. Seismic well tie is the best way to tie seismic data with well log data

by using a synthetic seismogram. It consists of three main workflows: calibrating and editing the density and sonic logs, generation of a synthetic seismogram, and implementing the matched (by defining the best match position and estimating the wavelet) integrated seismic well tie (White and Simm, 2003).

Before continuing to the seismic well tie stage, quality control of data is carried out, particularly in the case of well logs. Well logs often require some editing, normalization, repair and interpretation before they can be used in any reservoir characterisation study. One of the first steps in calibrating well logs is calibration of the sonic log (Figure 5.2). The aim of sonic calibration is reconciliation of seismic times from the check-shot survey and integrated sonic log times for any given depth in a well. Calibration of the sonic data is often required, because the generation of a synthetic seismogram from sonic log is a transform process that can lead to the travel time of the seismic wave error if cycle skipping and a washed-out zone effect are present in the sonic log. A check-shot survey measures a much larger cylindrical volume of rock compared with the sonic log. Additionally, sonic velocities are usually higher than check-shot velocities, because of dispersion effects; the sonic signal is a higher frequency (around 20 to 25 kHz) signal than seismic source (≈ 50 Hz) (Yadav *et al.*, 2004).

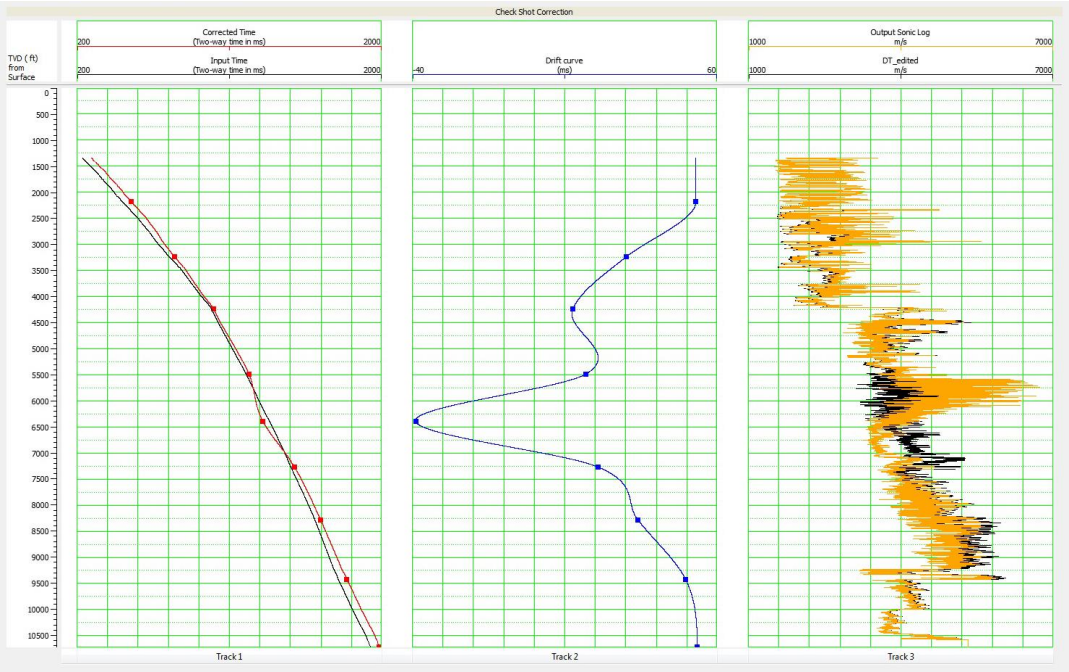

Figure 5.2. Calibration of the sonic log (depth–time) at well A1. Track 1: check-shot depth–time curve (black) and calibrated depth–time curve (red) with drift applied; Track 2: drift curve fitted to the data using spline interpolation with knee points; and Track 3: sonic velocity curve (black) and calibrated sonic velocity curve (orange).

Spikes in well log data can be caused by a number of factors, for instance: (a) ultra-thin beds, (b) fractured corridors and (c) cycle-skips. Irrespective of their origin, spikes are often undesirable in data because they represent data that are either erroneous or that are outside the log (and seismic) resolution. There are a number of ways to remove spikes from the well logs, including: (a) manually editing the section around the spiky section of the log, (b) using filters to remove questionable data, and (c) blocking a set of logs by means of replacing portions of them with one or more blocks, simplifying the logs and allowing them to be easily edited. This process can be used to remove anomalous spikes.

The drill location of the well with respect to the seismic trace may not be the correct trace to extracted the wavelet, because the best position for time-migrated data is displaced up-dip from the well (White, 1997; White and Simm, 2003). The well-seismic scanning process allows a new location to be found within a specified vicinity of the posted well location, to find the best trace location and time interval to be used to extract the wavelet (Cui and Margrave, 2014). The well-seismic scanning process allows maps to be generated showing the correlation of a synthetic with each trace in the seismic volume (or a time window of seismic data); Figure 5.3 presents the results of well-seismic scanning for well A1 that was analysed.

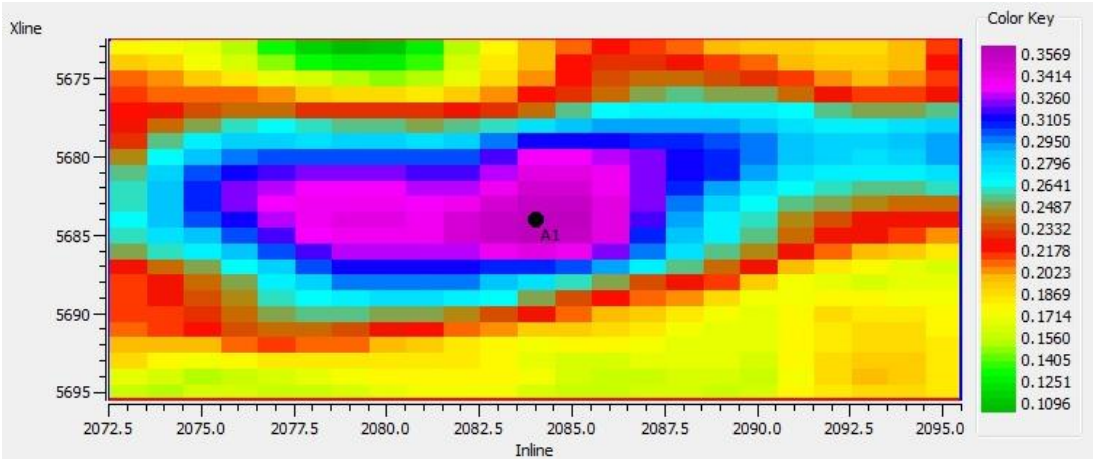

Figure 5.3. A small cube around well A1 was scanned for the best match position. Notice that the maximum energy correlation is the highest for the time window: 1750-2050 milliseconds at well A1.

Synthetic seismograms were generated for seven wells. The velocities from the calibrated sonic logs were multiplied by calibrated density logs to calculate new acoustic impedance logs. This acoustic impedance was transformed to reflectivity, which was then transformed from depth to time using a suitable wavelet to generate a

synthetic seismogram. It is equally important that the seismic data is as close as possible to a true representation of the real stratigraphy and rock properties. Subsequently, only a correlation time window of the target zone was chosen and an appropriate wavelet was predictable from real seismic data (it called a statistical wavelet) or using well logs (where it is called a wavelet using wells). After applying the suggested time shift of synthetic trace, the best-fit match was obtained with the composite trace in the time window, as shown in Figure 5.4. When a well tie is poor, it is hard to suggestion any recommendation for improving it beyond the general one of going back to apply the quality control of the seismic and calibrated log data (White and Simm, 2003).

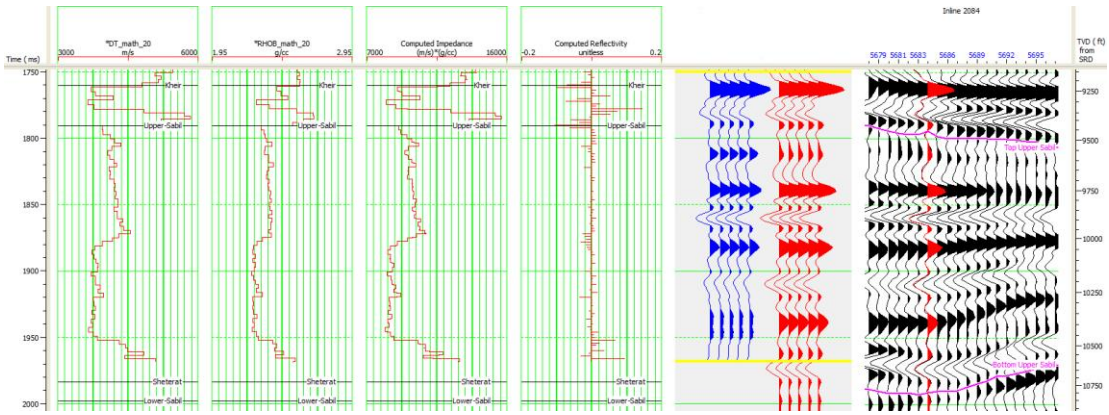

Figure 5.4. The best fit match of the composite trace (red) with synthetic trace (blue) at well A1.

Accurate determination of the wavelet is critical to the success of the inversion project. The shape of the wavelet may strongly effect the inversion results and therefore subsequent estimations of the reservoir quality. A statistical wavelet is extracted from the seismic data using statistical methods (Figure 5.5a). In this technique only the autocorrelation from the seismic data is uses; the phase is supposed to be already identified. The main limitation of this approach is that it tends to entail difficulties in estimating the right phase spectrum reliably.

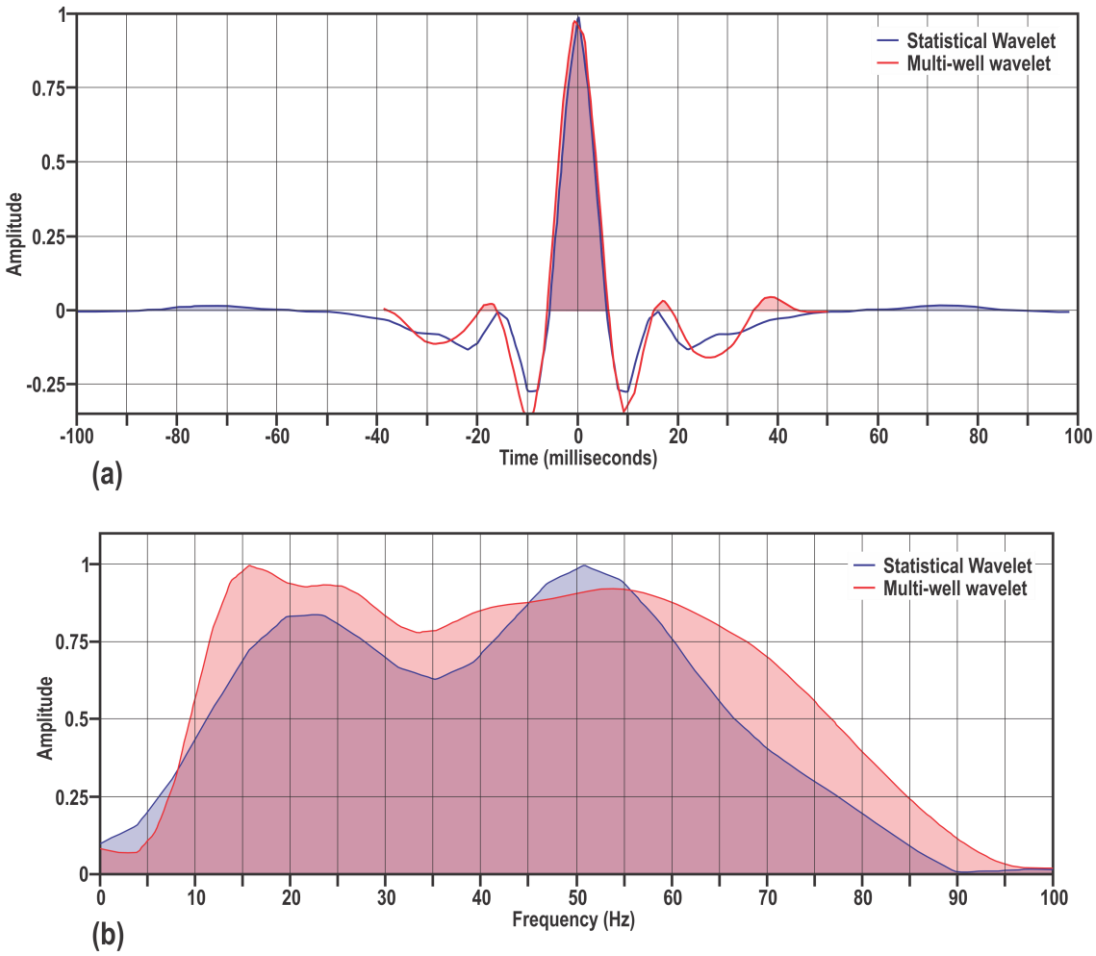

Figure 5.5. (a) Time and (b) frequency response of the seismic statistical and the multi-well wavelets.

Accurate determination of the wavelet is critical to the success of any seismic inversion. When there is more than one well, a single well-tie or individually fixing mis-ties at the various wells will not fix mis-ties at all other well locations. The solution is to perform a multi-well analysis to extract one single wavelet that is valid on the whole reservoir. The primary advantage of this approach is that it is possible to examine the quality of ties between synthetic and seismic at the selected wells for the extracted wavelet (Lucet, Déquirez and Cailly, 2000). A multi-well wavelet uses all available wells to extract one single wavelet. The Roy White algorithm method that has been used to extract the wavelet is advantageous because it extracts the wavelet's amplitude and phase. This method is described by White (1997) and White and Hu (1998). The Roy White wavelet estimation algorithms are a procedure for optimally estimating the seismic wavelet by calibrating and correlating seismic and well log data. Ideally, there are two stages in this process: (a) determining the best trace location at which to extract the wavelet using the well, and (b) given that tie's location, determine the optimal

wavelet. In this research, The Roy White algorithm method has been used to extract a multi-well wavelet (Figure 5.5b) from seven wells (A1, A2, A7, A9, A11, A51, and A52); these seven wells have sonic and check shot data. The correlation coefficients when a multi-well wavelet was used were much better than when a wavelet from an individual well was used to correlate the seismic and well log data. The correlation coefficients were enhanced by the suggested time shifting up of the synthetic traces.

5.4 Initial Model of Inversion

The inversion was started with an initial (low frequency) model of the acoustic impedance and then this model was perturbed until a good fit was obtained between the synthetic trace and real seismic trace. Four different inversion methods were applied to generate acoustic impedance logs at each seismic trace position, to create impedance-inverted models. In the current research project, two initial models were used for different inversion techniques to be analysed; the model-based and the maximum likelihood sparse spike techniques (Figure 5.6). There were number of parameters which needed to be set before building the initial model. These parameters included horizons to be displayed in the model, wells to be included, selecting the computed impedance logs used for making the model, and trace filtering options. The multi-well wavelet extracted from seven wells was used for all the inversion methods. The inversion analysis was performed for specific time window (1600-2100 milliseconds) used throughout the seismic data. The model-based method was the strongest one, as it gave more detailed results than the other methods, while, the maximum likelihood sparse spike method gave less detailed results than the other methods. A comparison has been made between the best inversion results of the two different low frequency models: model-based and linear programming sparse spike (Figure 5.6). The model-based inversion analysis at well A1 gives a very good correlation of 0.989 with error of 0.151, while, the error increases in the linear programing sparse spike inversion analysis up to 0.211, giving a correlation of 0.978, which is still not a bad correlation. Experience shows that if the correlation coefficient is less than 0.7, there is a problem with the seismic, well tie, or well log (Veeken *et al.*, 2009).

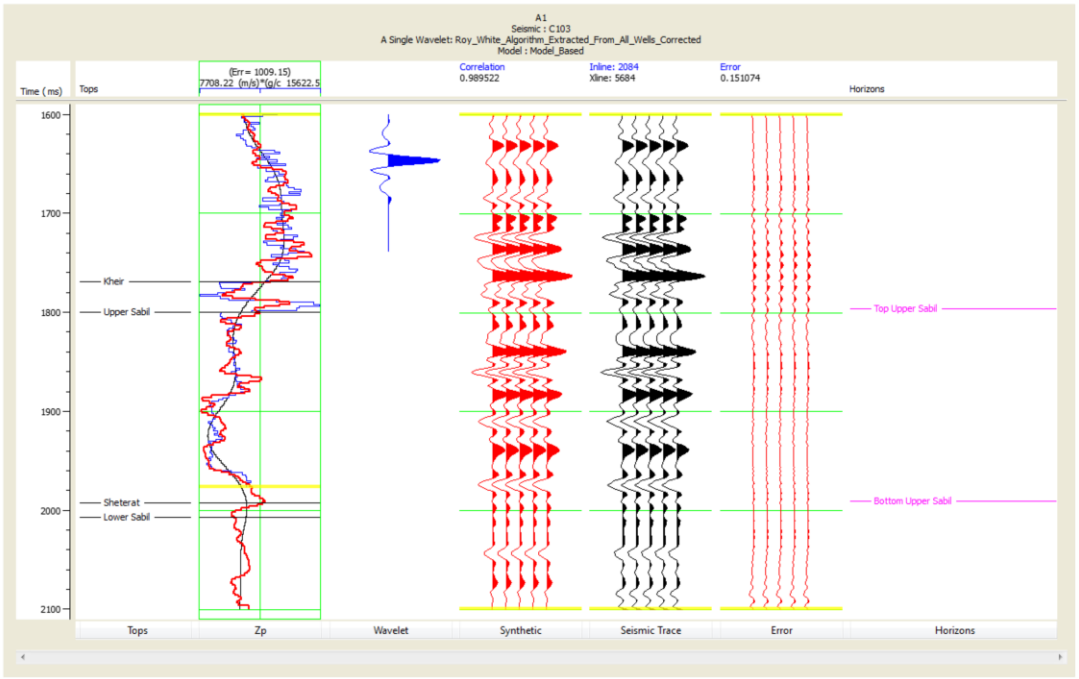

(a) Model Based

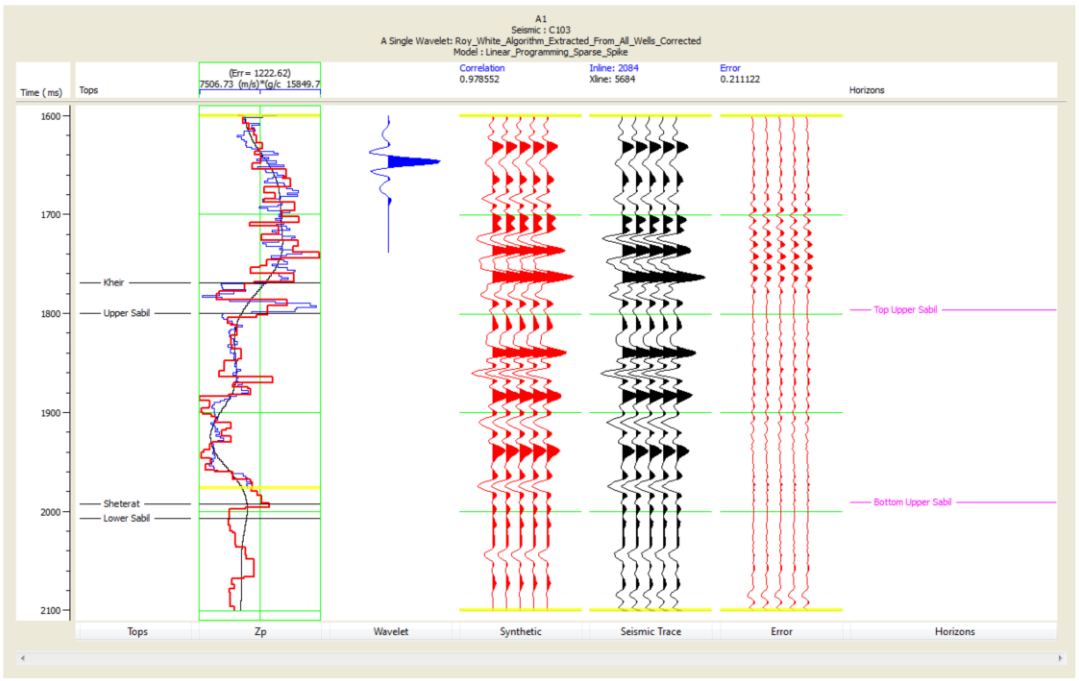

(b) Linear Programming Sparse Spike

Figure 5.6. Analysis of results for (a) model-based, and (b) linear programing sparse spike inversions at well A1.

The analysis results indicate that the model-based initial model gives the best results. Such a relatively high correlation between the predicted and original acoustic impedance logs in the model-based inversion confirms that the real seismic amplitudes are reliable to estimate inter-well impedance (Figure 5.7). By comparing the results of the two inverted models in Figure 5.8 and Figure 5.9, the acoustic impedance of the model-based inversion gives slightly better results than the linear programming sparse

spike inverted model. This is because the model-based results look relatively more reasonable geologically (blockier, with a less smoothed appearance and less dramatic swings), which simplifies the definitions of the lithological and petrophysical features. In the linear programming sparse spike inverted model, the acoustic impedance contrast is sharper as compared to the model-based impedance inversion. In addition, the impedance colour variation is less in the model-based inversion, better distinguishable that corresponds to the acoustic impedance contrast and the lithology can be distinguished better than in the linear programming sparse spike inverted model (Figure 5.8 and Figure 5.9). In this study, the model-based method has been utilized for inverting a post-stack seismic volume set into impedance volume. It remains to determine whether acoustic impedance correlates with petrophysical properties.

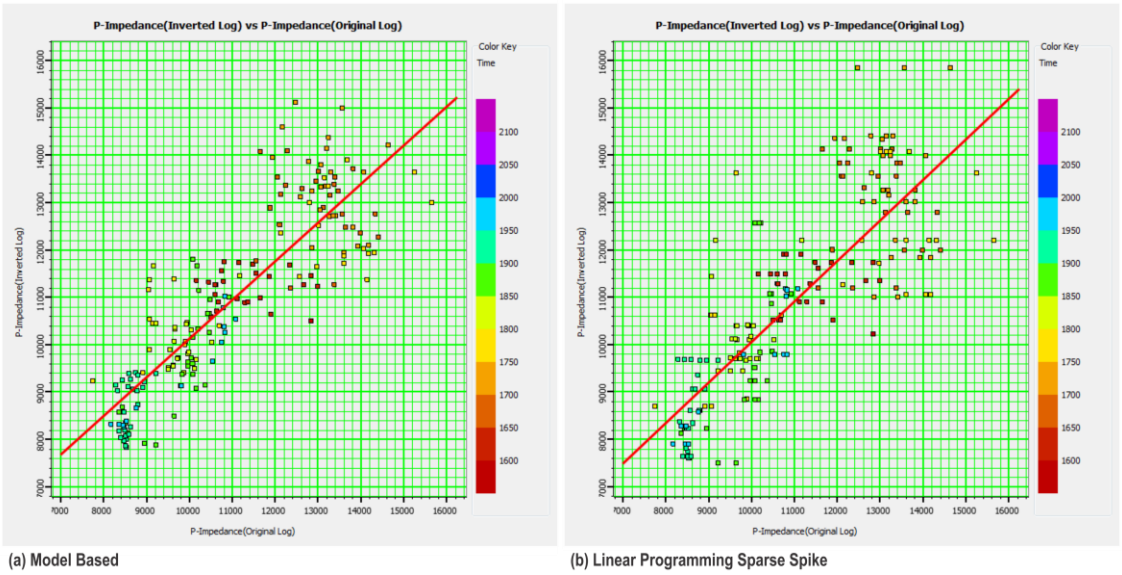

Figure 5.7. Crossplots of the acoustic impedance derived from the well logs (in *x*-axis) and the predictive acoustic impedance extracted from the seismic inversion (in *y*-axis) at well A1.

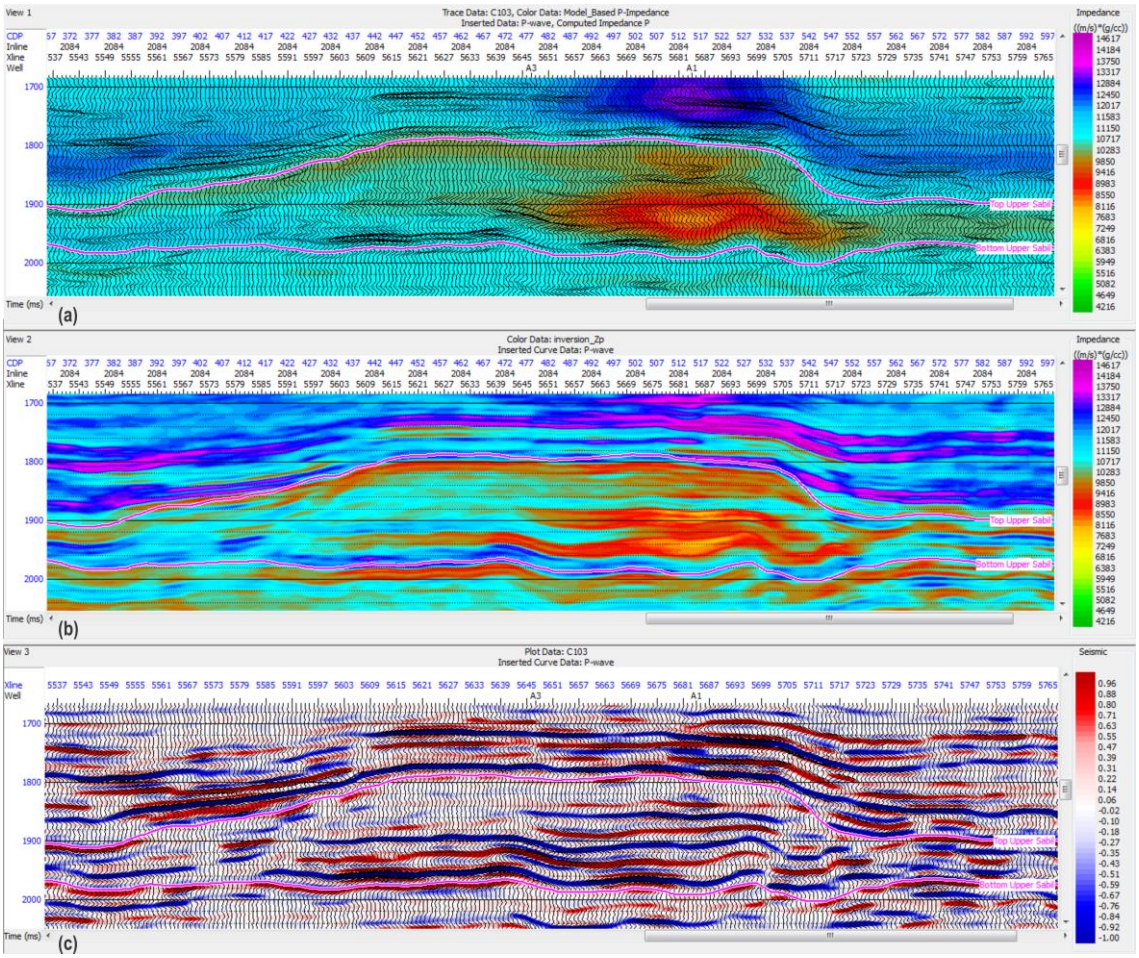

Figure 5.8. Model-based acoustic impedance initial model (at the top) generated from seismic (at the bottom) and well log data which has been inverted further for final inverted model (in the middle).

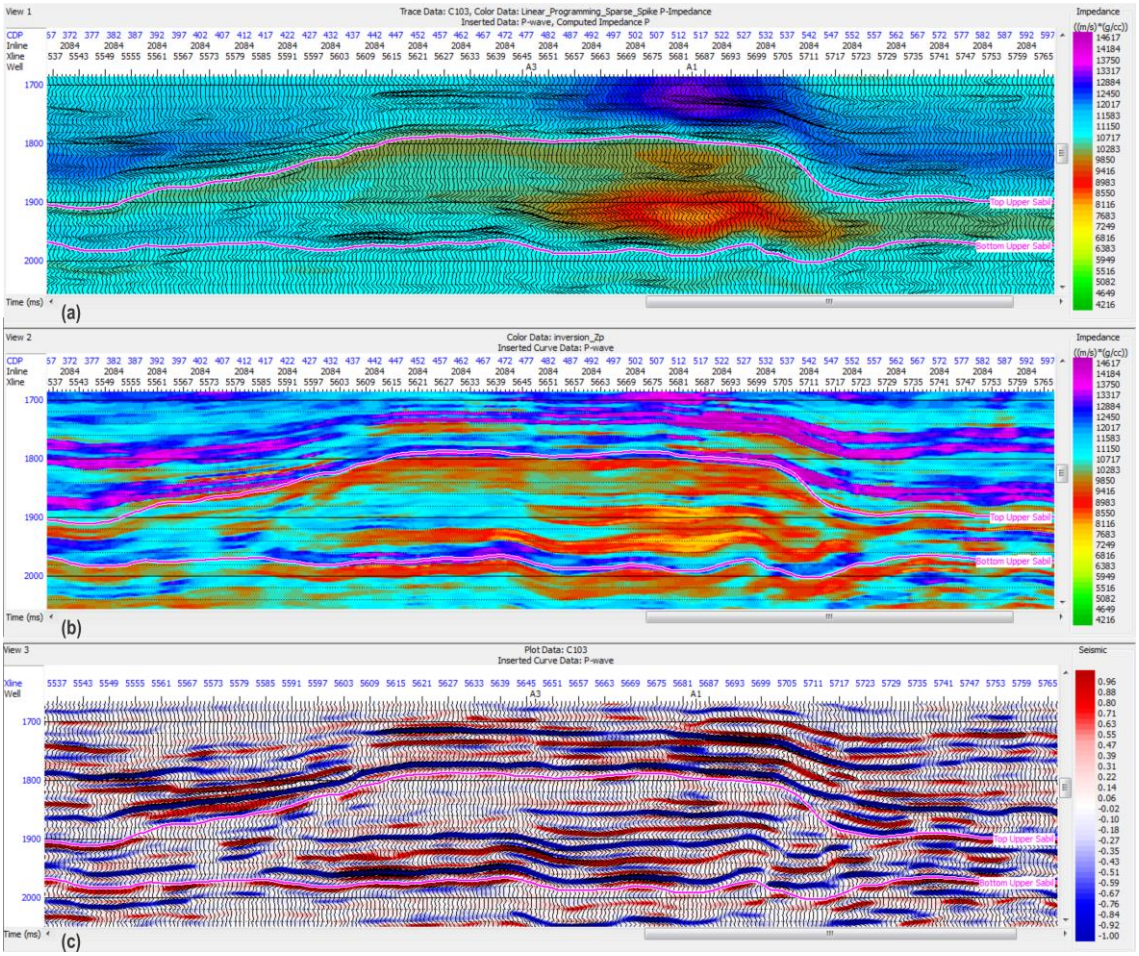

Figure 5.9. Linear programming sparse spike acoustic impedance initial model (at the top) generated from seismic (at the bottom) and well log data which has been inverted further for final inverted model (in the middle).

5.5 Analysis of Petrophysical Properties

All the well logs were analysed in detail, and generally it was observed that log qualities were good, and the calculated porosity and saturation data were considered reliable (Figure 5.10). Sheterat Shale is well characterized by positive spontaneous potential, high gamma-ray and low resistivity values. The top and the base of the Upper Sabil Carbonate unit were picked from the well logs. These boundaries are characterized by negative spontaneous potential and generally high resistivity value, which change from the top to the base of the unit itself, due to the hydrocarbon content present in the upper part. Low resistivity intercalations, however, were observed against some positive spontaneous potential peaks, indicating either high argillaceous content or shale streaks. The upper and lower boundaries of this unit can be defined on both the spontaneous potential curve and the resistivity log. The Kheir Formation is

characterized by positive spontaneous potential, high gamma-ray and relatively low resistivity values with intercalations of high resistivity peaks correspondent to the limestone or to the dolomite bands.

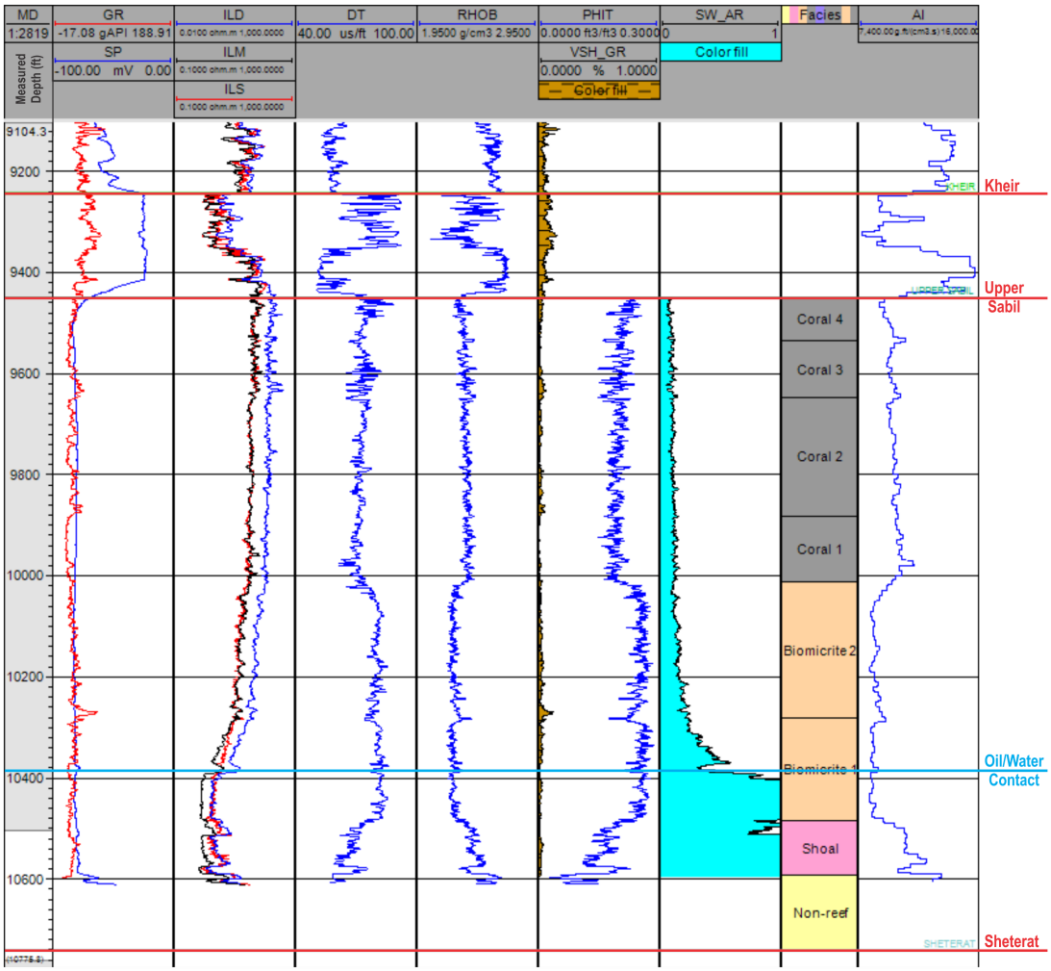

Figure 5.10. Interpreted Intisar 'A' reef facies from well A1. Well logs comprise spontaneous potential (SP), gamma-ray (GR), resistivity (ILD, ILM and ILS), sonic (DT), density (RHOB), porosity (PHIT), shale volume (V_{sh}), water saturation (S_w), and acoustic impedance (AI).

The spontaneous potential, gamma-ray, resistivity, sonic and density logs that run across the Intisar 'A' reef are shown in Figure 5.10. The oil/water contact was 10391 ft in well A1; this contact was defined from the resistivity logs. The water saturation at the oil/water contacts are about 85%, while the saturations at the upper part of reservoir were calculated to be less than 10%. The contact is distinct in most wells, with the depth of the contact varying ±20 ft from this average value. These variations are due to slight hole deviations and no tilted water table is believed to be present. The uniform resistivity separation curves indicate the homogeneous nature of the reservoir. The self-potential logs show a tight (non-porous) zone at the base of the reef body.

The Intisar ‘A’ reef reservoir rock is predominantly a limestone sequence (Figure 5.11). It consists primarily of porous calcarenite, scattered with fewer units of porous calcilutite and biomicrite that increase in rate toward the outer edges of the reef (DesBrisay and Daniel, 1972). Figure 5.10 and Figure 5.12 illustrate that there is good correlation between facies and petrophysics in the Intisar ‘A’ reef. Vertical facies variation is quite obvious and five developments of the lithofacies were distinguished during the correlation. They are characterized by different responses on the electrical well logs. These five units have different porosity, deposition and age, as described by (Terry and Williams, 1969). From bottom to top they are: (a) the non-reef unit, which is about 148 ft thick and has solution vugs usually filled with calcite cement, and characterized by lower average porosity of 9% (porosity ranges between 6-12%), (b) the shoal (algal-foraminiferal) unit, which is approximately 108 ft thick and with average porosity about 17% (porosity ranges between 14-20%), (c) a coralline reef biomicrite unit, about 472 ft thick and characterized by higher average porosity 23% (porosity ranges between 23-27%); the oil/water contact is located in this unit, (d) the coral reef limestone unit, which has good average porosity of 20% (porosity ranges between 18-23%) and is about 563 ft thick at the reef crest, and (e) the talus unit occurring toward the front-reef outer reef edges, facing the high energy area and containing debris from the reef (broken by storm waves). This unit is about 112 ft thick and has average porosity 7% in well A31 (porosity ranges between 6-20%).

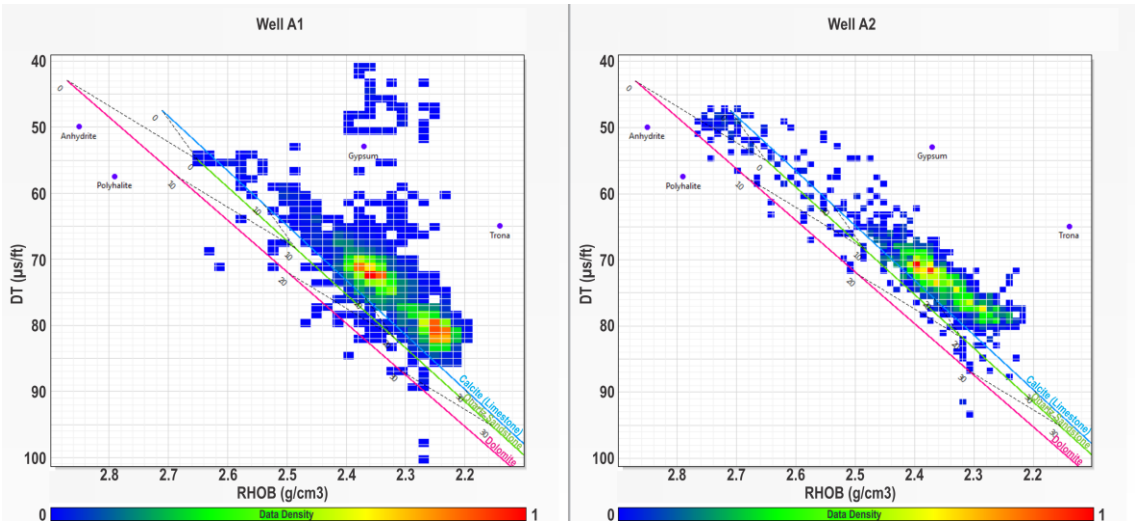

Figure 5.11. Sonic against density crossplots showing lithological components of the Intisar ‘A’ reef reservoir in wells A1 and A2.

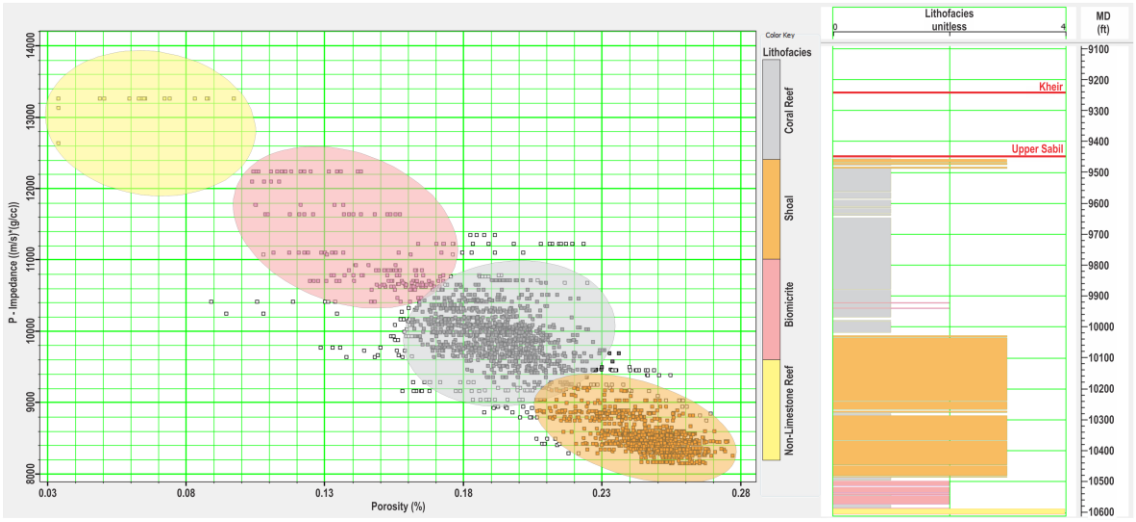

Figure 5.12. Crossplot of porosity versus acoustic impedance using well log data in Intisar 'A' reef. The various elliptical zones correspond to interpreted lithofacies units in well A1.

5.6 Seismic Attributes for Reservoir Characterization

Many reefs show a characteristic threefold division into fore-reef, the reef itself and back-reef. The reef front is a steep slope, vertical in places, with the organisms constructing reef in the upper part, passing down to a talus slope of coarse reef debris. The reef crest is the site of prolific organic growth. Behind the crest is the reef-flat. The back-reef area consists of reef debris adjacent to the reef flat, passing shoreward to a quiet-water lagoon (Tucker, 1991). Reef traps are significant oil reservoirs with the most porous facies usually found in the reef-framework and upper fore-reef facies. However, cementation is most prevalent in this zone and so porosities can be reduced from primary high values. The talus at the toe of reef slopes also makes good reservoirs. Many reefs are dolomitized, and this also enhances their reservoir qualities. In many conditions seismic data alone cannot give a whole image of the reservoir. For example, in some situations seismic data can be used to constrain reservoir porosity, but they may not provide evidence on fluid type and saturation (MacGregor, Andreis and Cooper, 2010).

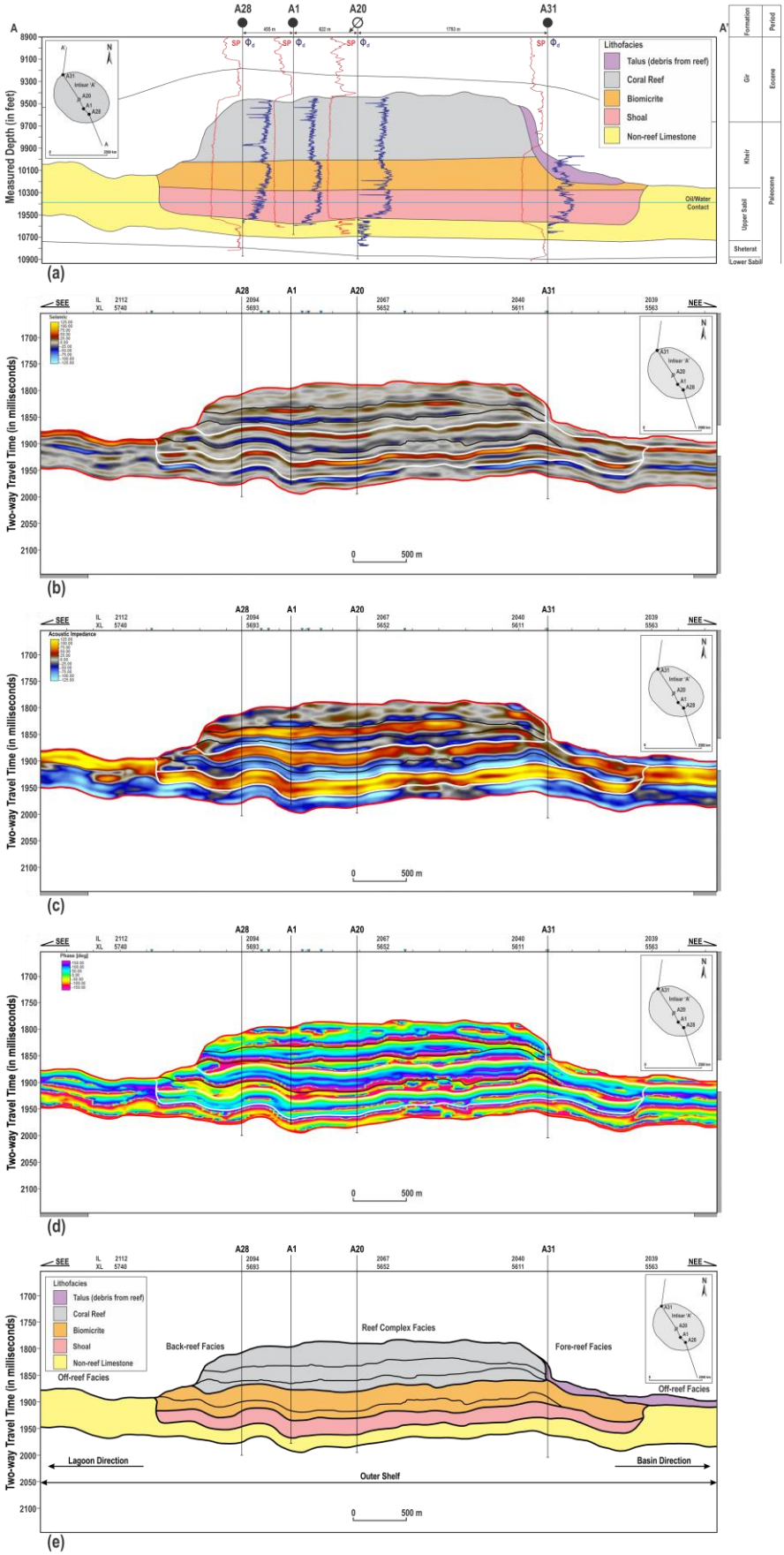

Figure 5.13. Arbitrary line across the Intisar 'A' reef showing (a) well correlation; (b) original seismic amplitude; (c) relative seismic acoustic impedance; (d) instantaneous seismic phase and (e) interpretation cross section.

The correlation between well data and seismic attributes (Figure 5.13) shows the Intisar 'A' field as a reefal/shoal complex that generally contains five facies in a layered arrangement, based on log well data and as described by Terry and Williams (1969). The seismic interpretation of the Intisar 'A' reef illustrates that conventional seismic data are insufficient to reveal the internal heterogeneity. It is interesting to note the quite marked push-down anomaly in the events beneath the reef. This suggests that the homogeneous reef material (perhaps as a consequence of having developed good secondary porosity throughout the feature) is now less dense, and with lower seismic velocity, than the adjacent off-reef carbonates. This is a typical case in which a push-down velocity anomaly associated with a carbonate reef feature is of great significance, being often a direct indication of good porosity (Jenyon, 1990).

The Intisar 'A' reef grew vertically to about 1349 ft or more, due to a progressive and gradual submergence of the area, but was finally drowned. The pattern of seismic facies changes from a back-reef of parallel and continuous reflections, to a reef facies which is nearly reflection free, to a fore-reef of parallel and continuous reflections. The talus unit is characterized by oblique, chaotic and discontinuous reflections with high amplitude. Mapping has shown lateral extension of the talus unit (prospective areas) around the Intisar 'A' reef (Figure 4.5a). The talus at the toe of the Intisar 'A' reef slopes contains debris from the reef broken by storm waves, and it has a good reservoir quality. This talus zone has not been drilled yet.

5.7 Interpretation of Seismic Inversion

The well logs are of higher resolution than the seismic data, as shown in the lower variance of acoustic impedance derived by the seismic data than that represented in the well logs. Smoothing of the well log signatures is required to be able to statistically correlate the respective information. A crossplot between acoustic impedance and porosity driven from the density log within the Intisar 'A' reef in well A1 is shown in Figure 5.14. Porosity and acoustic impedance have an inverse relationship (negative correlation coefficient). Consequently, acoustic impedance can be used as an indicator of lithofacies and porosity (Borbajo, 2010). The crossplot analysis has revealed that low acoustic impedance values within the Intisar 'A' reef can be correlated to high porosities, while higher acoustic impedance values are associated with lower porosities, but large variations are observed within the clusters; the crossplot has given around 0.63 correlation. The critical aspects in the evaluation of Intisar 'B' and 'C' reservoirs are the

assessment of these reservoirs' quality without any well coverage. This issue becomes increasingly more difficult in carbonate reservoirs, where the distribution of porosity is more unpredictable compared to clastic reservoirs (Borbajo, 2010).

The Intisar 'A' reef is seismically divided into five facies (Figure 5.14 and Figure 5.15), namely, non-reef limestone, shoal (algal foraminiferal), biomicrite (coralline biomicrite), coral reef and talus. The non-reef limestone facies generally represents high acoustic impedance and low to medium amplitude reflections. The shoal facies generally represents low to medium amplitude reflections and very high acoustic impedance, which becomes medium acoustic impedance at the fault zones in southern part of the Intisar 'A' reef. The biomicrite facies consists of pair of units and generally represents very high to medium amplitude reflections and medium acoustic impedance; this becomes very low acoustic impedance at the fault zones in the southern part of the reef. The coral reef facies consists of four of units and generally represents very high amplitude reflections and medium acoustic impedance, which becomes low to medium acoustic impedance at the fault zones in southern part of the reef. The talus facies around the Intisar 'A' reef consists of debris from the coral reef, with diverse acoustic impedance. These major units are present in the other reefs, Intisar 'B' and 'C' (Figure 5.16 and Figure 5.17). The variation in fluid content is not seismically detectable.

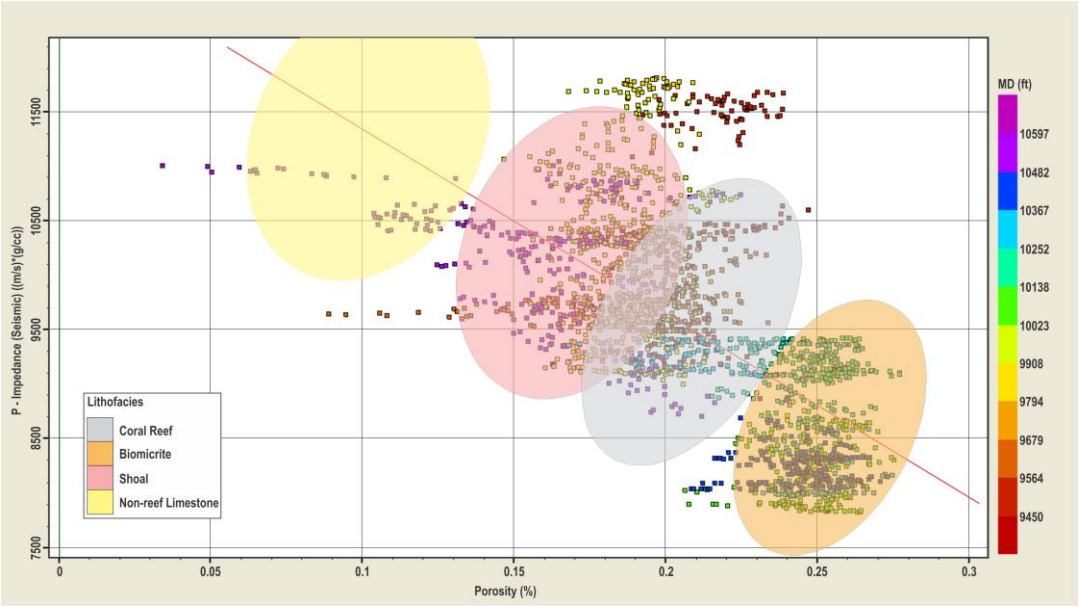

Figure 5.14. Crossplots of density-porosity log versus acoustic impedance derived from seismic data from well A1.

Carbonate sediments often fracture more easily than siliciclastic sediments. However, many fractures and karst features are associated with deeper tectonic

movements in the basement rocks. Mapping of dip magnitude has been an effective means of mapping fractures and fracture-enhanced porosity (Chopra and Marfurt, 2007). Variance and second derivative seismic attributes have been used in recognizing that the faults/fractures are most common in the south-eastern part of the Intisar 'A' reef (Figure 4.9). After comparison between the northern and southern parts of the Intisar 'A' reef, it was found that high lateral changes in acoustic impedance values within the reef ware interpreted by present faulting (Figure 5.15 and Figure 5.18). This can plausibly explain the presence of the lower acoustic impedance values and higher porosities concentrated along faults (possibly associated with fractures) in the south-eastern part of the Intisar 'A' reef.

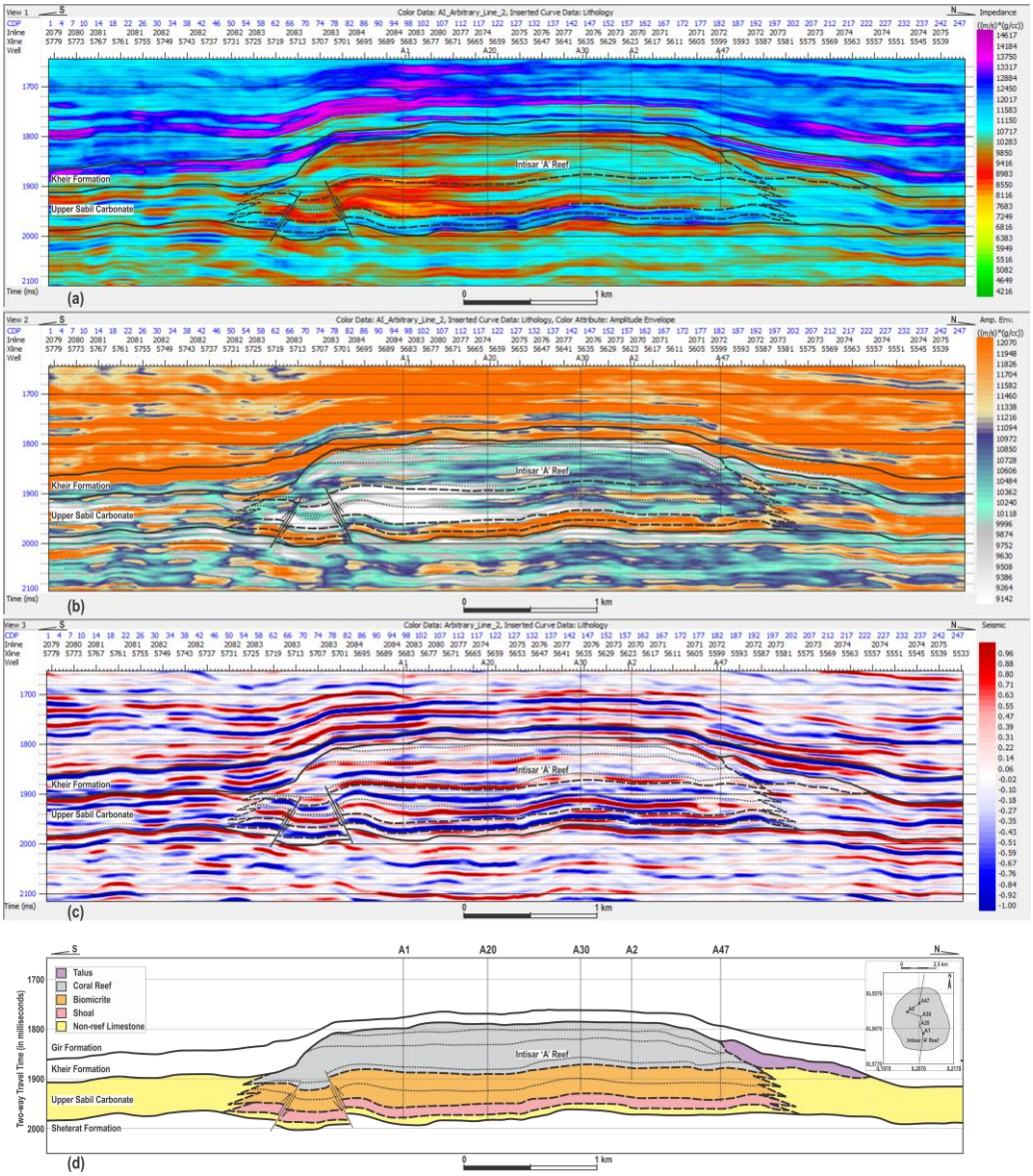

Figure 5.15. Arbitrary cross section across the Intisar 'A' reef, showing (a) acoustic impedance inversion; (b) acoustic impedance inversion amplitude envelope; (c) seismic amplitude reflections, and (d) lithofacies interpretation.

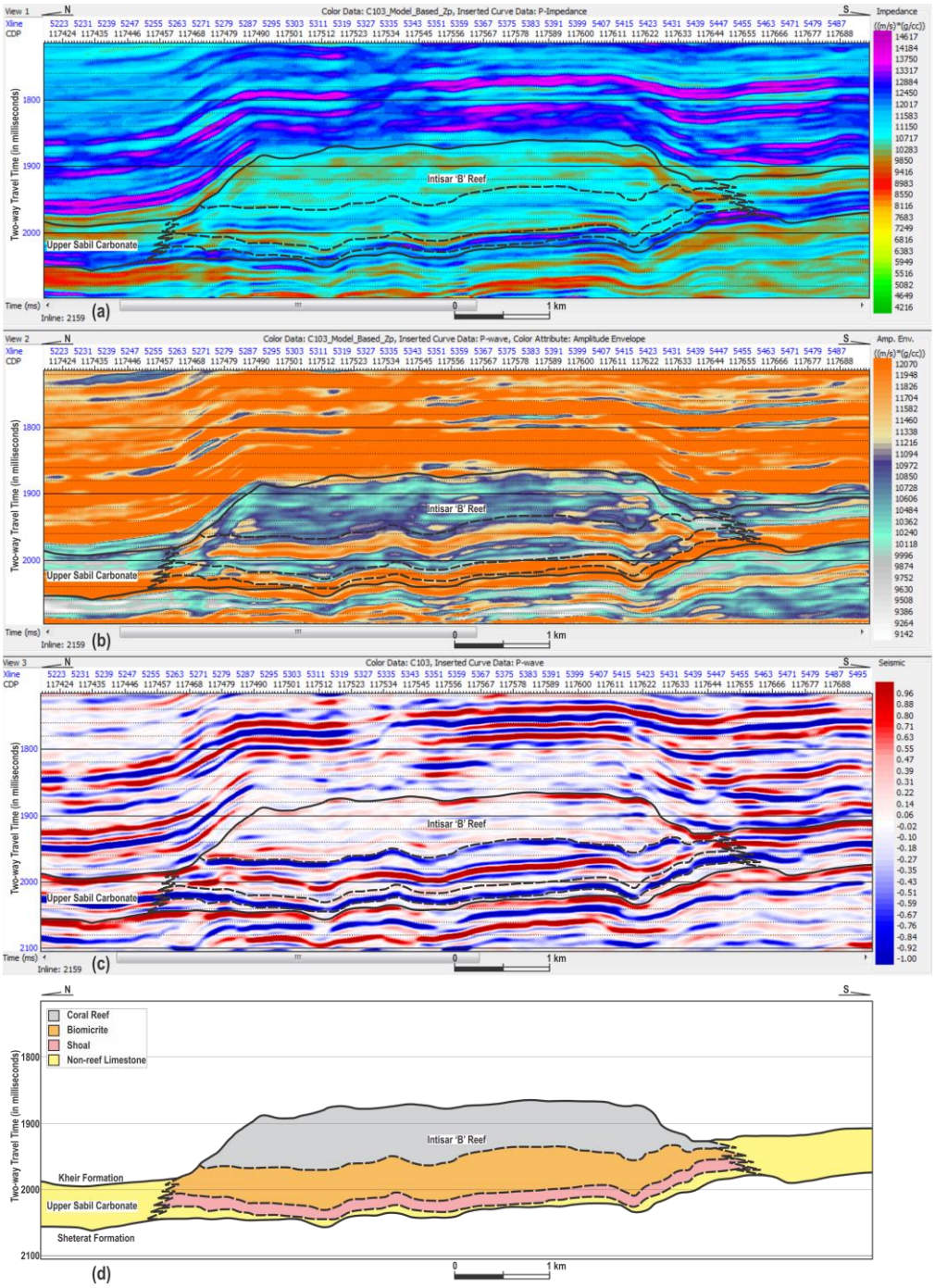

Figure 5.16. Inline cross section across the Intisar 'B' reef, showing (a) acoustic impedance inversion; (b) acoustic impedance inversion amplitude envelope; (c) seismic amplitude reflections, and (d) lithofacies interpretation.

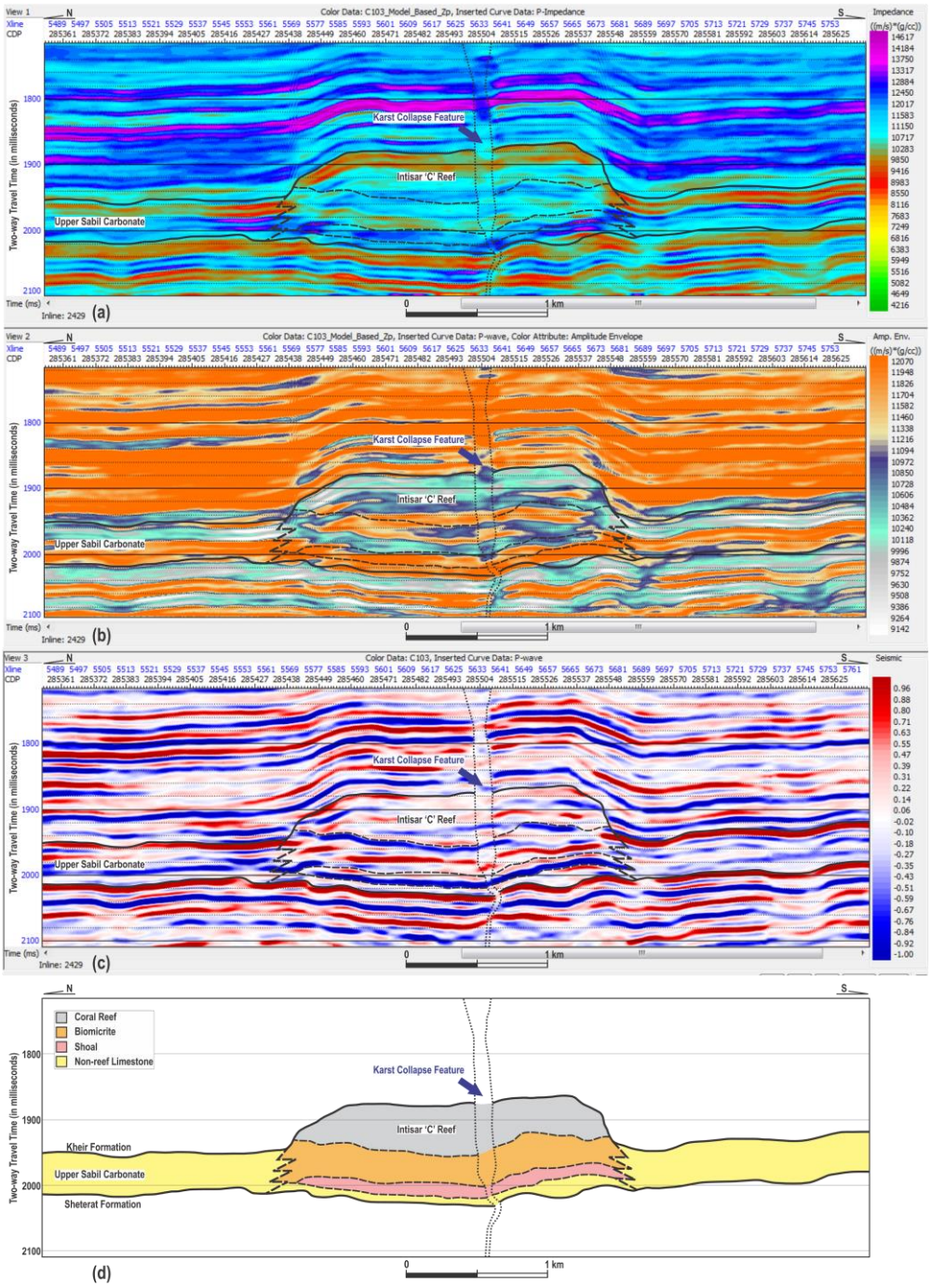

Figure 5.17. Inline cross section across the Intisar 'C' reef showing (a) acoustic impedance inversion; (b) acoustic impedance inversion amplitude envelope; (c) seismic amplitude reflections, and (d) lithofacies interpretation.

The porosity of the south-eastern part of the Intisar ‘A’ reef was significantly improved by fracturing and dissolution (Figure 5.19). In general, low-porosity limestones are the resulted of early calcite cementation and porous limestones intervals resulting from extensive dissolution. Differential compaction and movement of basement rocks generated the faults in the south-eastern part of the Intisar ‘A’ reef. These faults, associated with fractures, acted as a long-lived conduit system for movement of pressure solution and hydrocarbon migration into the Intisar ‘A’ reef during progressive burial. Macro-dissolution of calcium carbonate occurred along the flow path of the solution in association with fracturing. Dissolution of limestones and fossils has created secondary porosity (vugs and cavities) in the south-eastern part of the Intisar ‘A’ reef. These secondary pores contain variable amounts of cements but many vuggy pores are cement-free.

Well A6 on the southeast flank of the Intisar ‘A’ reef is the only remaining significant producer. It is most likely draining oil from the talus zone outside the reef (Figure 5.20), where there is likely to be significant remaining undrained potential.

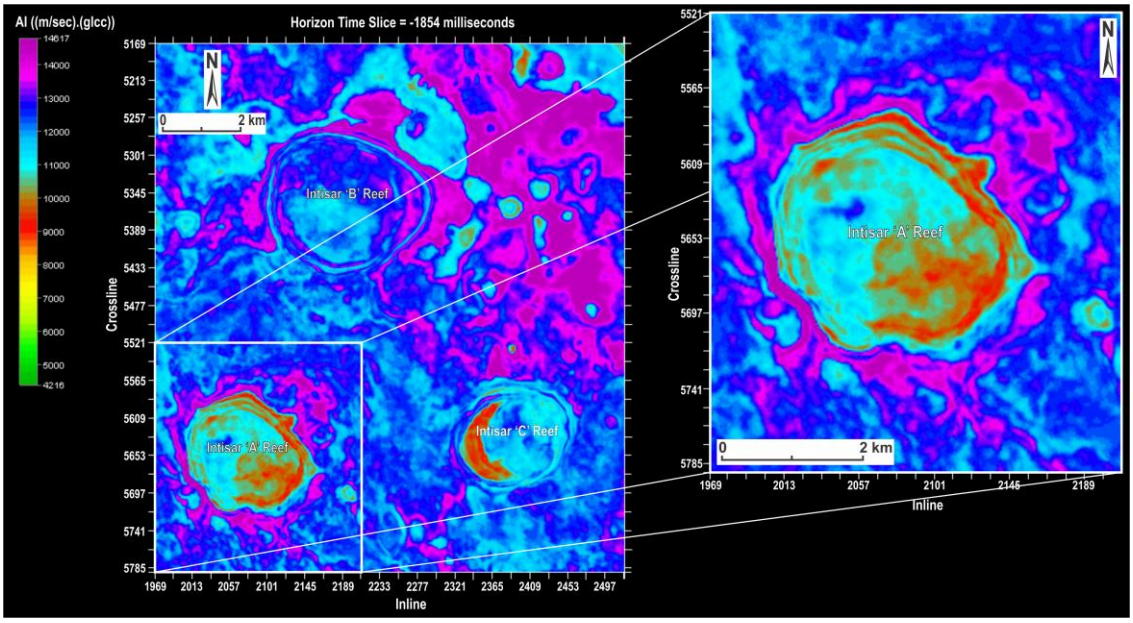

Figure 5.18. Horizontal time slice of acoustic impedance inversion, showing the high lateral changes in impedance values within the Intisar ‘A’ reef.

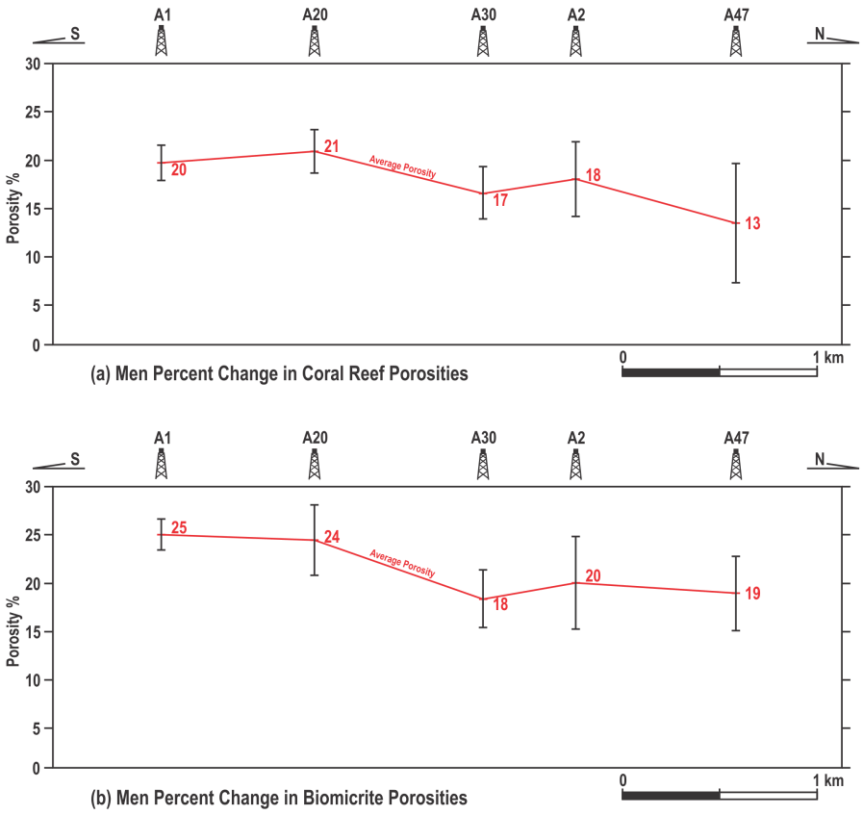

Figure 5.19. Cross section across the Intisar 'A' reef showing porosity distribution. Cross section location is shown in Figure 5.15.

The acoustic impedance time slices in Figure 5.21 reveal the occurrence of talus slope deposits on the north-eastern flank of Intisar 'A' reef. These deposits are characterized on seismic sections by a convex profile with discontinuous, oblique and chaotic reflections, with high amplitude, low acoustic impedance and high porosity values. Acoustic impedance values of the talus area range from 10077 to 11095 ((m/sec).(g/cm^3)), the lower values of acoustic impedance (lower density, lower interval velocity) indicate better reservoir properties as porosity. The talus sediments are not transgressive deposits, but they are the product of storm-related modern physical sedimentological processes (Harris and Heap, 2009). The talus is interpreted as the integrated product of storms in the region that operated during periods of lower sea level during the Paleocene. Talus deposits are mobilised throughout storm events, eroded from the reef top and deposited on the lee flank of the reef, creating the observed talus sediments. The lateral asymmetry in the talus deposits give the relative direction of storm waves and the orientation of the coast.

5.8 Summary

This chapter has improved the existing geological model of the Intisar ‘A’ reef using the properties estimated from the seismic inversion to enhance the interpolation and modelling, and has predicted the properties of the Intisar ‘B’ and ‘C’ reservoirs, where minimum well control data is available. In this study, the model-based method has been utilized for inverting a post-stack seismic volume set into impedance volume. The inverted impedance clearly highlighted facies and porosity variation in the Intisar reefs which are not apparent on the seismic data. Five vertical facies units in these reefs have been characterized by different responses on the electrical well logs. These units have different deposition and different ages; from bottom to top they are: (a) the non-reef unit, which has porosity ranging between 6-12%, (b) the shoal (algal-foraminiferal) unit, with porosity ranging between 14-20%, (c) the coralline reef biomicrite unit, with porosity ranging between 23-27%, (d) the coral reef limestone unit with porosity ranging between 18-23%, and (e) talus unit which has porosity ranging between 6-20%. The porosity of south-eastern part of the Intisar ‘A’ reef was significantly improved by faulting/fracturing and dissolution. In general, low-porosity limestone resulted from early calcite cementation and porous limestone intervals resulted from extensive dissolution. Well A6 on the southeast flank of the Intisar ‘A’ reef was the only remaining significant producer. It is most likely draining oil from the talus zone outside the Intisar ‘A’ reef, where there is likely to be significant remaining undrained potential. Talus deposits are located on the north-eastern flank of reef. The talus at Intisar ‘A’ reef has good reservoir quality, and this prospective area has not been drilled yet.

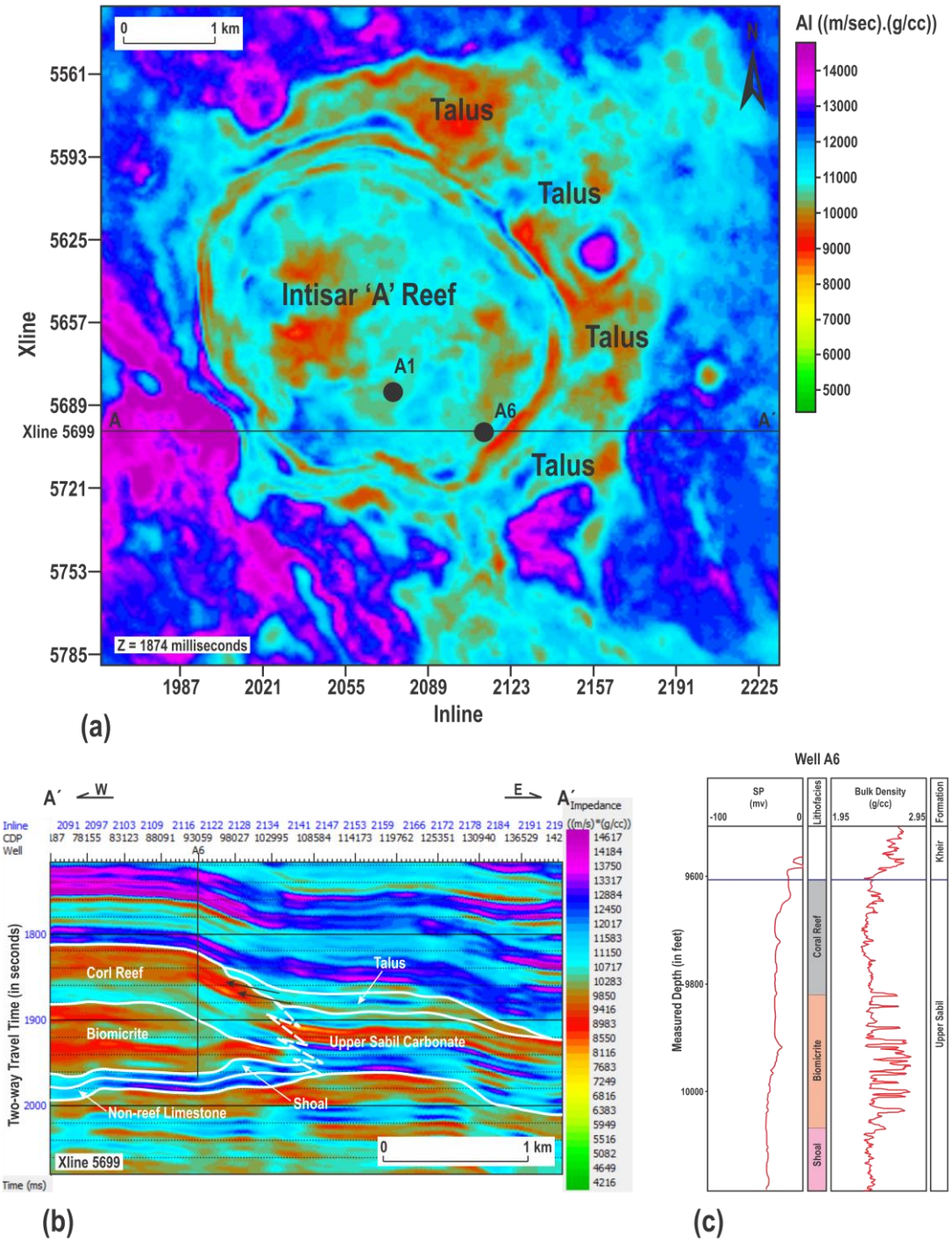

Figure 5.20. Well A6 within the Intisar 'A' reef: (a) horizontal time slice of acoustic impedance inversion over the Intisar 'A' reef; (b) acoustic impedance inversion section over the reef flank, and (c) A6 well logs.

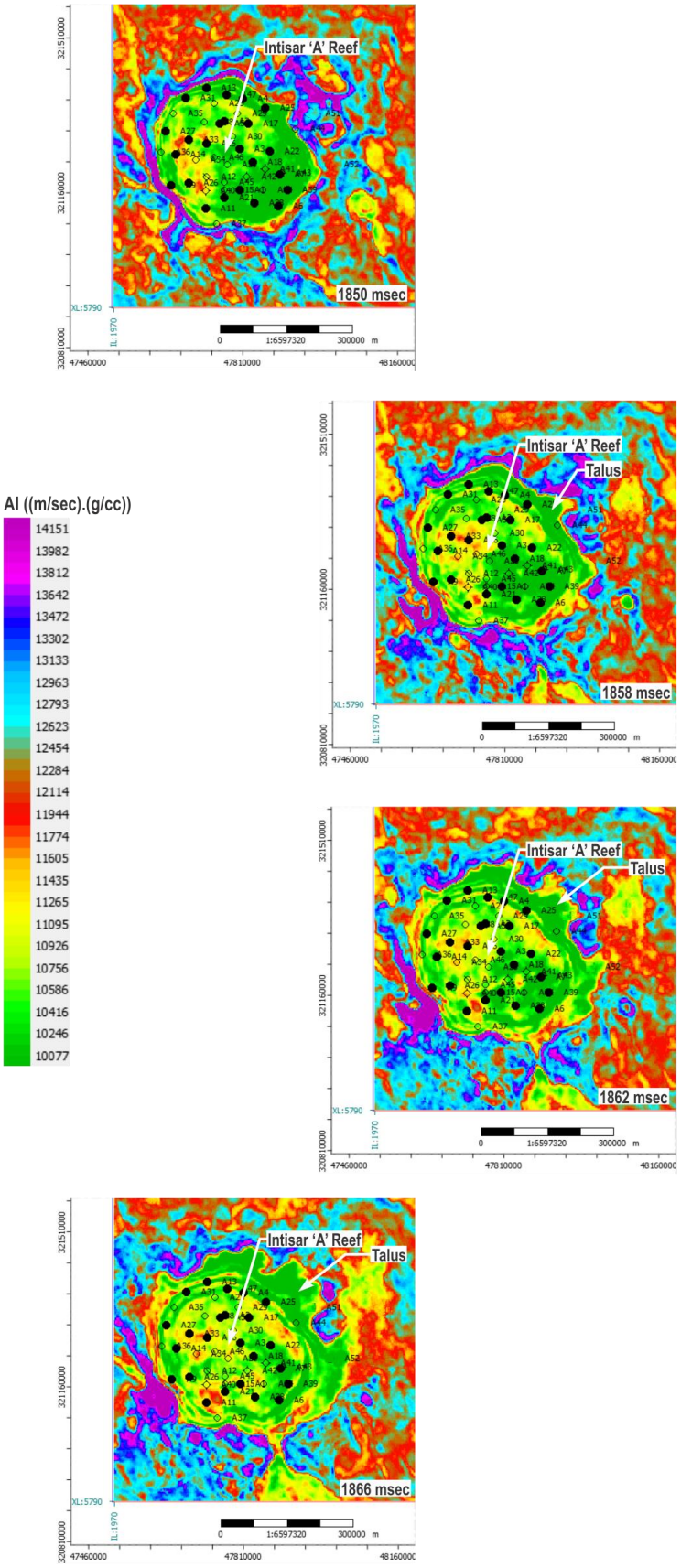

Figure 5.21. Series of acoustic impedance inversion time slices from 1850 to 1874 milliseconds, showing the Intisar 'A' pinnacle reef and its associated talus deposits.

Chapter 6. Paleoenvironmental Interpretation

Chapter 6

Paleoenvironmental Interpretation

6.1 Introduction

This chapter focuses on the seismic attribute analysis of the Paleocene carbonate shelf on the Ajdabiya trough. Three-dimensional seismic data has been used to predict, map and describe the depositional paleoenvironmental setting for Upper Sabil Carbonate by classifying the seismic facies to define the seismic attribute variations produced by geological variations. The three-dimensional seismic data covers an area of about 882 km^2, and is a merged volume of several seismic surveys obtained over several years in Concession 103 (Figure 6.1). It comprises a 25×25 m grid and a sampling interval of 2 milliseconds. This study provides the opportunity to develop and clarify an understanding of the physical controlling factors and the depositional environments affecting the distribution and the morphology of the Intisar reefs, based on the combined interpretation of multi-seismic attributes. In addition, the chapter provides the development history of Intisar pinnacle reefs and new understandings on the paleogeographic features, paleoenvironment and tectonic evolution of the Sirt basin, which remain controversial.

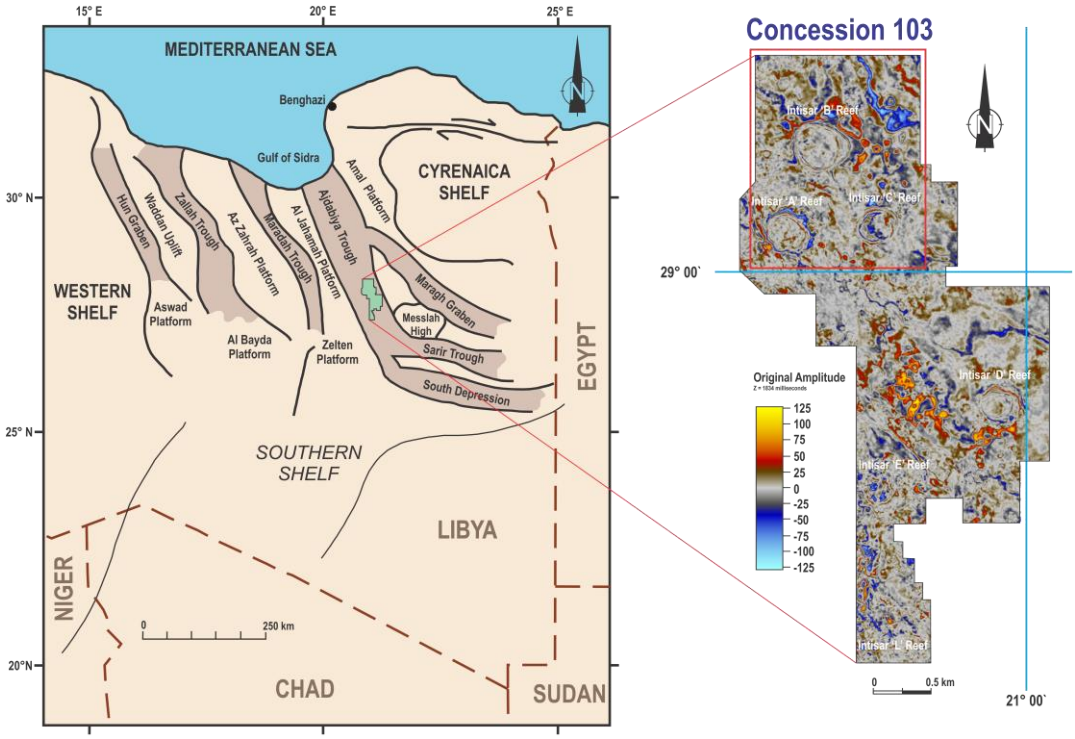

Figure 6.1. Map of Libya showing the major structural units in the Sirt basin and location of Concession 103; modified after Ambrose (2000).

6.2 Methods of Interpretation

The Upper Sabil Carbonate reflector is well defined on the seismic volume and it was interpreted and mapped. This reflector was tracked manually at every tenth crossline and inline and was then auto-tracked in the seismic volume using the selected time window. The seismic reflector was then gridded and a regional time-structure map was created. Along with conventional three-dimensional seismic time-structure and amplitude displays, dip illumination, the variance and the spectral decomposition seismic attribute time slices, and the RMS amplitude multi-attribute surface maps were created from the target horizon to see what features could be identified. The dip illumination seismic attribute is a cross-correlation dip estimation method and displays a directional view of the calculated dip. The RMS amplitude attribute is derived by calculating the square root of the sum of the squared amplitude, and then divided it by the number of samples that have been used. The variance attribute developed as a tool to improve the visibility of the discontinuity trends in the seismic data and represents the variability in trace-to-trace for a specific sample interval. The spectral decomposition attribute developed as a tool to improve the visualization of the seismic geomorphology within the areas, based on the frequency spectrum and contrast within the seismic data.

Pinnacle reefs are often seen as transgressive features, but their growth history and distribution within basins can be difficult to predict, as they respond to the interplay between several geographic, eustatic, and tectonic factors (Saqab and Bourget, 2015). Seismic attributes offer the advantage of mapping lateral variations within the study area. However, carbonate sediments are more difficult to predict laterally than are clastic sediments, using seismic data (Fontaine *et al.*, 1987). This is because the carbonate sediments are mainly controlled by the depositional environment and later diagenetic processes. These factors can make carbonate deposits extremely heterogeneous and unpredictable in the subsurface. Furthermore, carbonate sediments present challenges in seismic attributes because of poor contrasts in acoustic impedance (Skirius *et al.*, 1999). One of the key distinguishing factors between siliciclastic and carbonate transgressive systems' tracts is the ability of carbonate to aggrade rather than back-step throughout high rates of accumulation increase (Emery, 1996; Wright and Burchette, 1996; Schlager, 1999; Catuneanu *et al.*, 2009) with dome-shaped or bucket-shaped morphologies developing as illustrative architectures (Schlager, 1993; Warrlich, Waltham and Bosence, 2002; Purdy and Gischler, 2005).

6.3 Distribution of the Carbonate Depositional Environment

A summary of the main lithofacies recognized in the Eastern Sirt basin is displayed in Figure 6.2. The Cyrenaica platform and Hameimat trough areas were located in the restricted inner shelf of the lagoonal/supra-tidal zone, with deposition of dolomites and anhydrites. On the Amal platform, lagoonal dolomites persisted, with patch reefs developed over local paleo-highs. The shelf break (barrier) between the inner and outer shelf follows the geometry of the Ajdabiya trough. The margin of the shelf was an area of high energy conditions, with deposition of shoaling carbonates, patch reefs and generally abundant biogenic activity, resulting in the development of a porous carbonate belt barrier reef. Pinnacle reefs developed within the low energy outer-shelf environment in the protected southern embayment of the Ajdabiya trough. Local topographic highs, perhaps related to Lower Sabil Carbonate paleo-highs and deeper structure, produced higher energy conditions and more favourable sites for increased biogenic activity and reef growth. Pinnacle reef growth kept pace with subsidence, resulting in the deposition of reef building carbonates. Growth of the reef was terminated when the subsidence or rate of sea-level rise exceeded the rate at which the reef could build. Patch reefs grow similarly to pinnacle reefs, where they both reach

mean sea-level, but their rise from the substrate varies: while patch reefs have < 20 m depth, the pinnacle reefs reach > 20 m in relief (Blanchon, 2011).

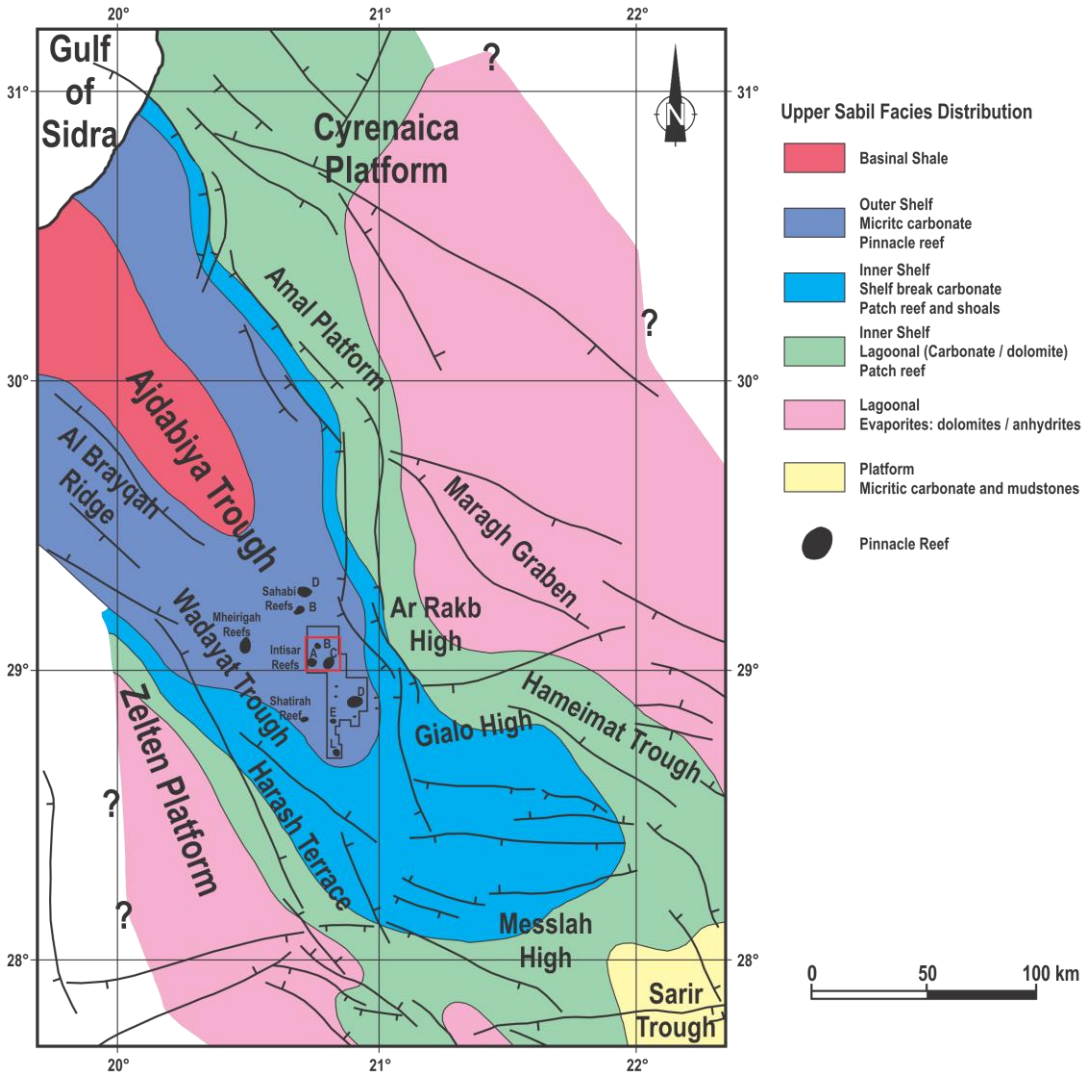

Figure 6.2. Distribution of the main lithofacies in the Eastern Sirt basin; modified after Terry and Williams (1969); Brady, Campbell and Maher (1980); Gumati (1992); Bezan (1996); Hallett and Clark-Lowes (2016).

The Intisar pinnacle reefs developed within the outer-shelf environment in the protected southern embayment of the Ajdabiya trough. Figure 6.3 shows a schematic model of shelf edge facies development, and well data suggest that the shoal-rimmed model appears to best fit the sequences recorded from the Ajdabiya trough area (Spring and Hansen, 1998). The Intisar reefs' development is associated with shallow-water conditions and high-energy facies, deposited either along the shelf margins or on localized paleo-topographic highs.

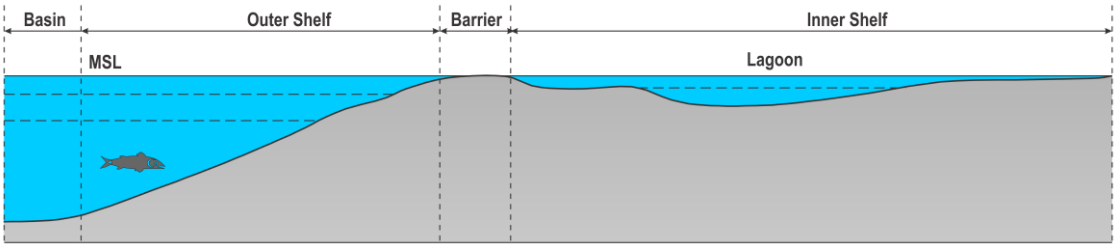

Figure 6.3. Standard facies on a rimmed shelf (Spring and Hansen, 1998).

6.4 Seismic Interpretation of Carbonate Depositional Environments

The regional time-structure map, seismic attributes horizon time slices, and multi-attribute surfaces for the Upper Sabil Carbonate allow investigation of the geometries and depositional architecture within the depositional unit. Studying the seismic geomorphologies associated with the Intisar reefs also helps to understand the developments at the origin of this depositional unit. An important consideration when running a seismic attribute is whether to apply it to a surface of interest and then extract it as a time slice. A surface attribute along a picked horizon forces the attribute to be dependent upon the interpreter's picking and in this sense is not an entirely objective process.

The time structural map (Figure 6.4) displays the geomorphology of the Upper Sabil Carbonate. This map is derived from the interpreted horizon. The map presents a surface morphology which shows six large, isolated, circular pinnacle reefs; Intisar 'A', 'B', 'C', 'D', 'E' and 'L'. These pinnacle reefs relatively have the same size and age. The map also shows a relatively flat topography with slight to no large surface karst features, but it shows a gradual dipping towards the northwest. The dipping is interpreted as representing the direction of the major depocenter of the Paleocene shale basin. In the time-structure map of Upper Sabil Carbonate, it appears that the Intisar 'A', 'B' and 'C' reefs were located on a down-dip and positioned in a slightly greater water depth where a lower energy environment existed throughout most of the growth of the reef. In this position, the shale and micrite deposits dominated the growth of the mounds and, as a result, porosities and permeabilities are somewhat lower than those of same other reefs in the region. The distribution of the Intisar pinnacle reefs in the Ajdabiya trough is probably controlled by the topography of the Lower Sabil Carbonate paleo-highs. However, we cannot confirm the existence of subtle topographic features that are below the limit of seismic resolution.

The Paleocene succession of the Ajdabiya trough is characterized by a carbonate system that developed from a rimmed shelf. The time structural map shows that the

average shelf slope is approximately 5° at this location. A tilt is considered to be by faulting, causing a consequent linear saddle and hump (barrier reef) between the Intisar 'A', 'B', 'C' and 'D' reefs' group, and the other two reefs' group (Figure 6.5). The circular depression karst features observed in the most of the Upper Sabil Carbonate shelf (Figure 6.6), strongly suggests a karst origin of the structures. These karst features are interpreted as sinkholes and dolines, which occurred during the low stand of main sea level.

Variance and dip illumination seismic attribute image discontinuities (for example: faults and karst features) can also provide map views of the carbonate depositional environment. These seismic attributes are particularly useful for finding faults, including reefal and basement fault blocks that could affect facies development (Skirius *et al.*, 1999). A study of the variance and dip illumination seismic attributes of the Upper Sabil Carbonate reveals several probable faults as dark, and two major faults on the central part of the study area; the orientation of these faults indicates a NW to SE trend (Figure 6.6). A horst block bounded saddle forms a strong positive morphology, generally oriented in the NW-SE direction, and has developed parallel to the shelf break. It has an average width of about 9 km and is several kilometres long. This saddle can be easily tracked over the whole shelf area within the seismic attributes slices (Figure 6.6 and Figure 6.7) as well as in cross-sections (Figure 6.5). The barrier reef is characterized by a mound-shaped morphology, draping of overlying reflectors, push-down effects, onlaps at the edges and diffraction hyperbola (Figure 6.5). The reflection configuration in the internal part of the barrier reef comprises hummocky medium amplitude reflectors. The association of the geometry and position of the barrier reef with its precedent topographies is evident. The linear configuration of this reef suggests a structural control. The Intisar 'E' and 'L' reefs may have been developed along the inner shelf margin. The growth of the reefs' succession happened on a paleo-high topography developed by the faulting.

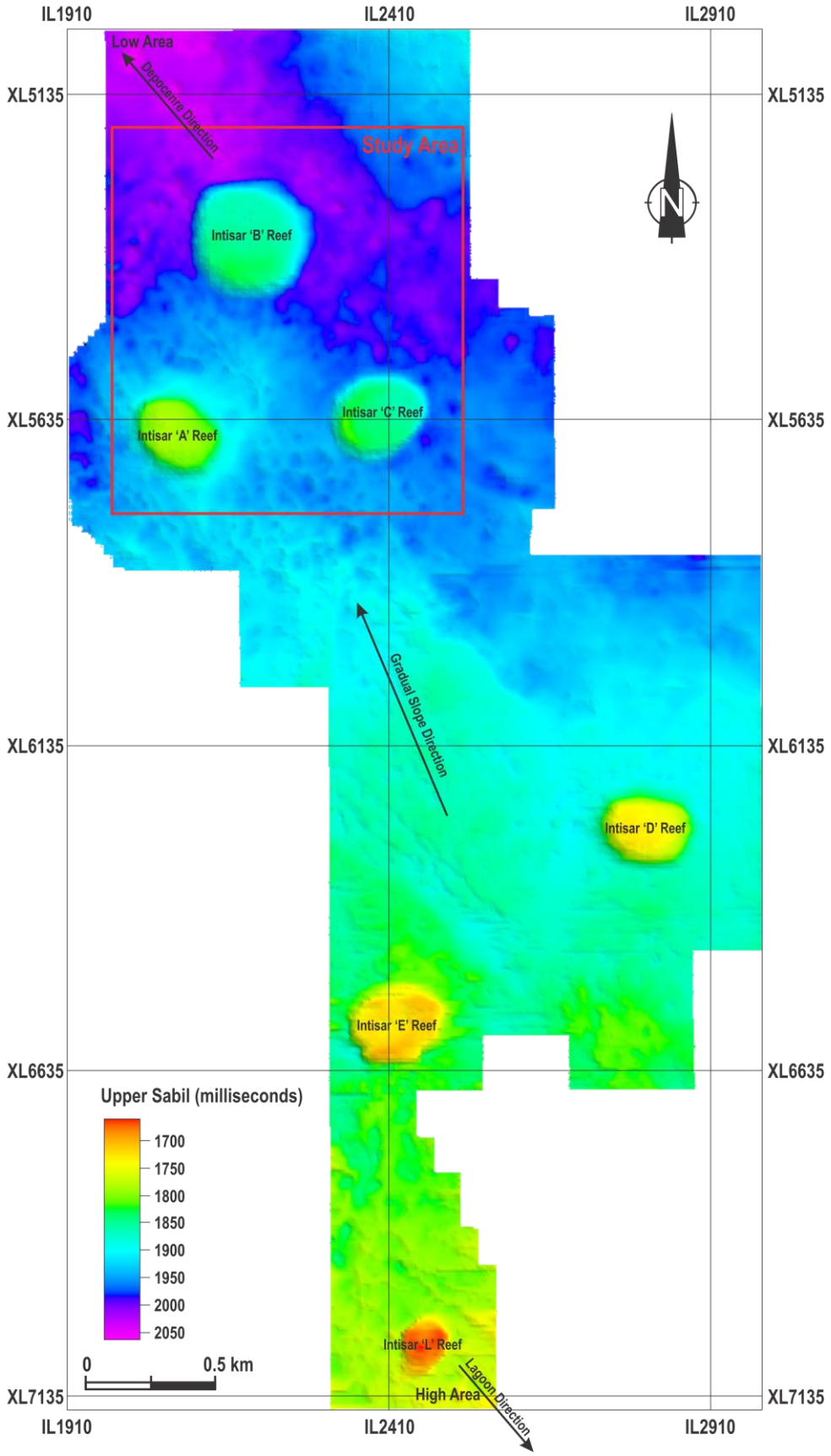

Figure 6.4. Regional time-structure map of Upper Sabil Carbonate derived from three-dimensional seismic data, showing the Intisar pinnacle reefs.

The talus slope around the Intisar ‘A’ reef does not show a significant asymmetry (Figure 6.7). Only the extended side of the east reef appears to form a slightly steeper inclining slope than the short sides. According to Betzler *et al.* (2009), the steep slopes on the extended sides of the current-shaped pinnacle reefs can be caused by sediment winnowing by these currents.

The lateral distribution of the carbonate facies units is shown in the depositional environments map (Figure 6.8). The Upper Sabil Carbonate shelf break between the outer (high amplitude), and inner (low amplitude) shelf zones is well-defined and parallel to the general strike direction of the shelf (Figure 6.7). In general, the high-energy conditions resulted in the development and growth of the isolated pinnacle reefs, and shoals were situated immediately basin-ward of the high amplitude zone of Upper Sabil Carbonate. Behind the shelf break, lagoonal condition predominated with deposition of low energy dolomites, lime-mudstones and anhydrites resulting in the development of patch reefs. In some cases, pinnacle reefs may have developed along the inner shelf margin. The closure of the barrier reef controls the depositional environment in the inner shelf zone distributed by the patch reefs, while behind the barrier reef lagoonal sediments dominate. The increasing concentration of the pinnacle reefs’ growth on the inner bounding barrier reef possibly represents the increasing constraint of the open marine environment conditions behind it, so the patch reefs were limited. The broken discontinuous barrier reef complex has initiated a semi-lagoonal open marine area: the ideal condition for the continued growth of Intisar ‘E’ and ‘N’ pinnacle reefs in the inner shelf area (Figure 6.9). The Paleocene section in the Ajdabiya trough area is represented by two discontinuous carbonate cycles: (a) the Lower Sabil Carbonate, which was deposited in a shallow-water and quite low-energy condition, with occasional periods of emergence, and (b) the Upper Sabil Carbonate, which was deposited in a high-energy, shallow-water environment. A thin narrow sheet of Sheterat Shale separated the two Sabil carbonate cycles.

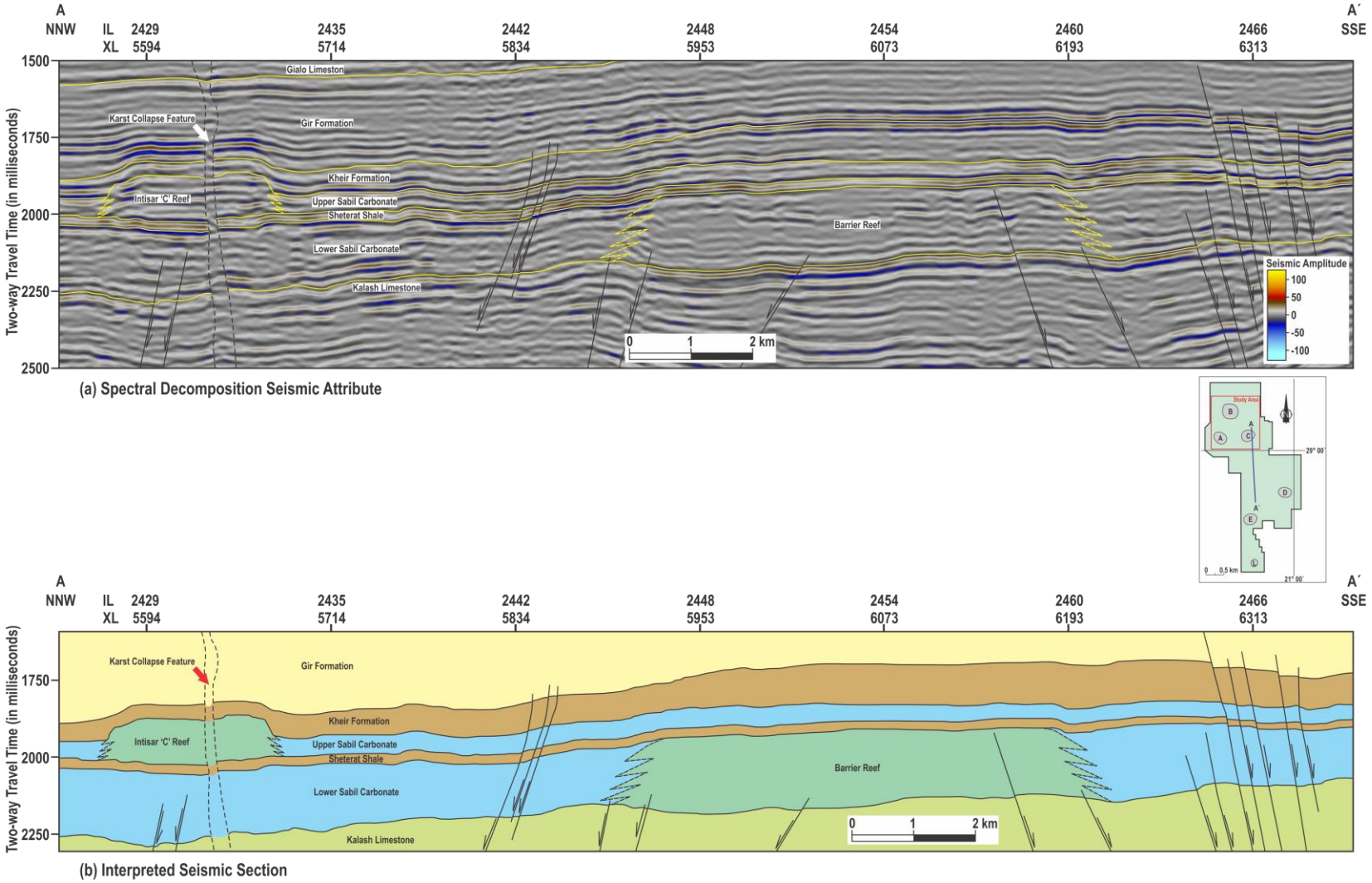

Figure 6.5. Regional NNW-SSE seismic cross-section showing the main geological features in the study area.

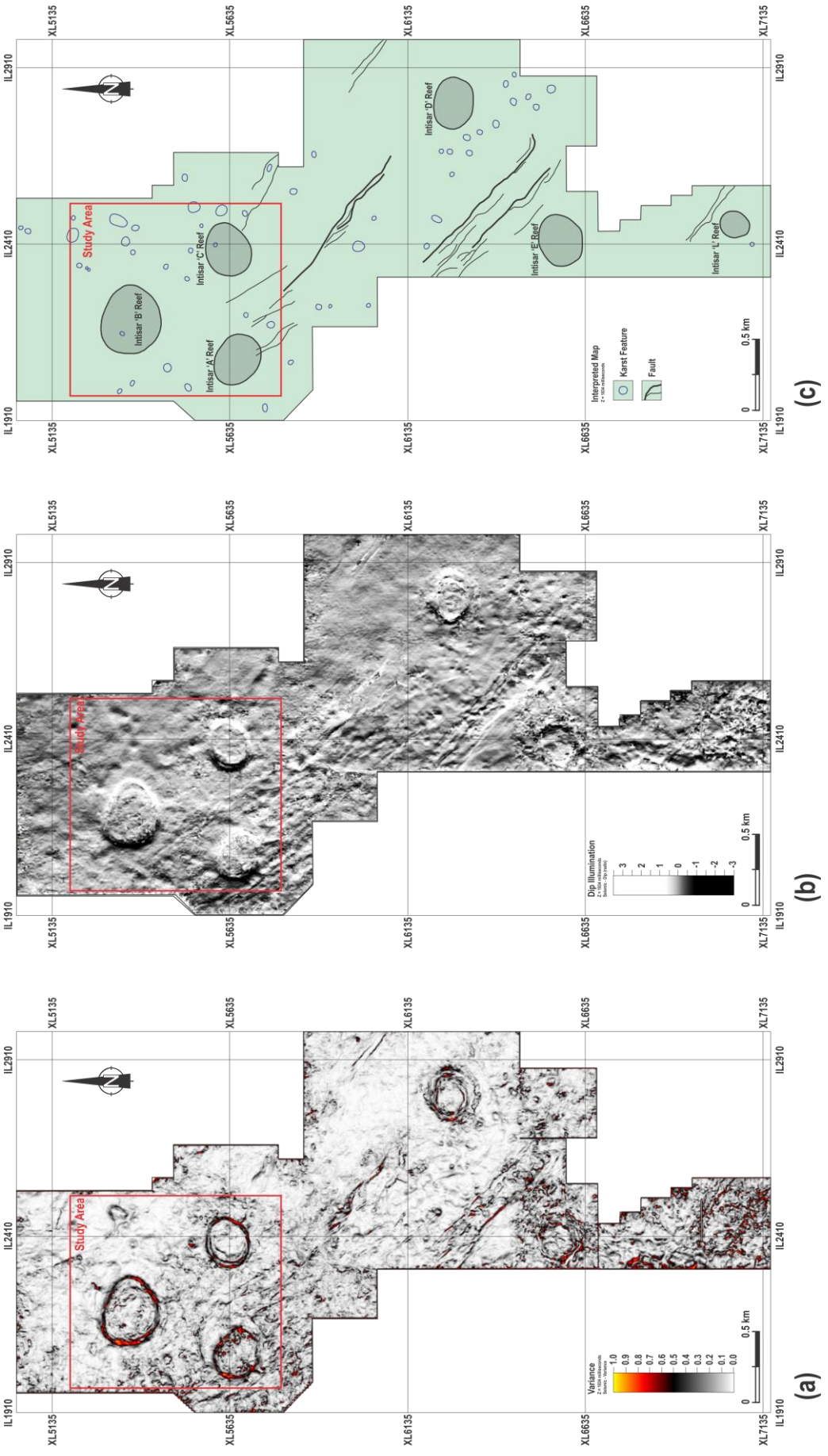

Figure 6.6. (a) Variance attribute time slice, (b) dip illumination attribute horizon time slice, and (c) the interpreted map.

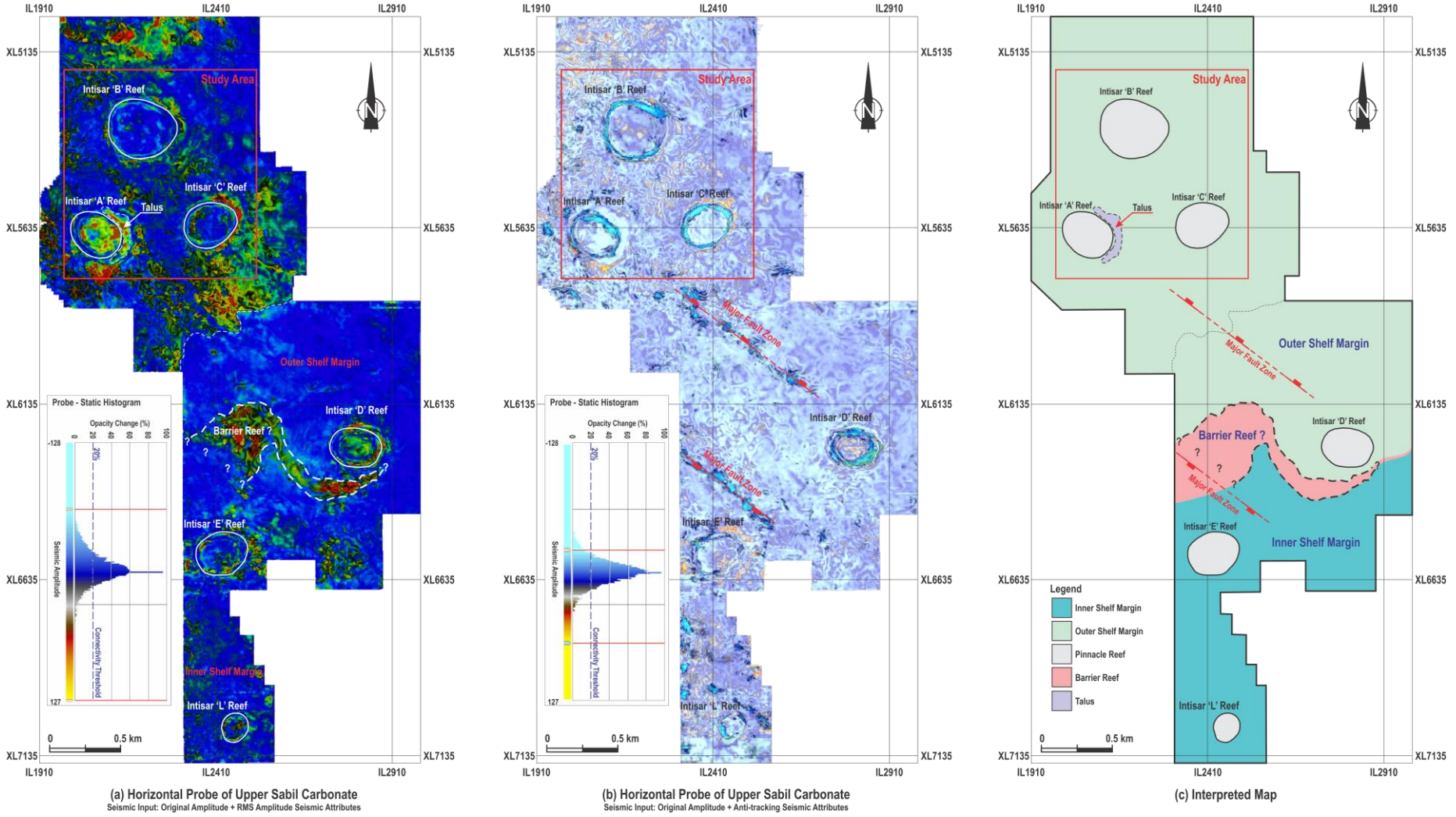

Figure 6.7. Multi-attribute surface maps and the main facies elements of Upper Sabil Carbonate.

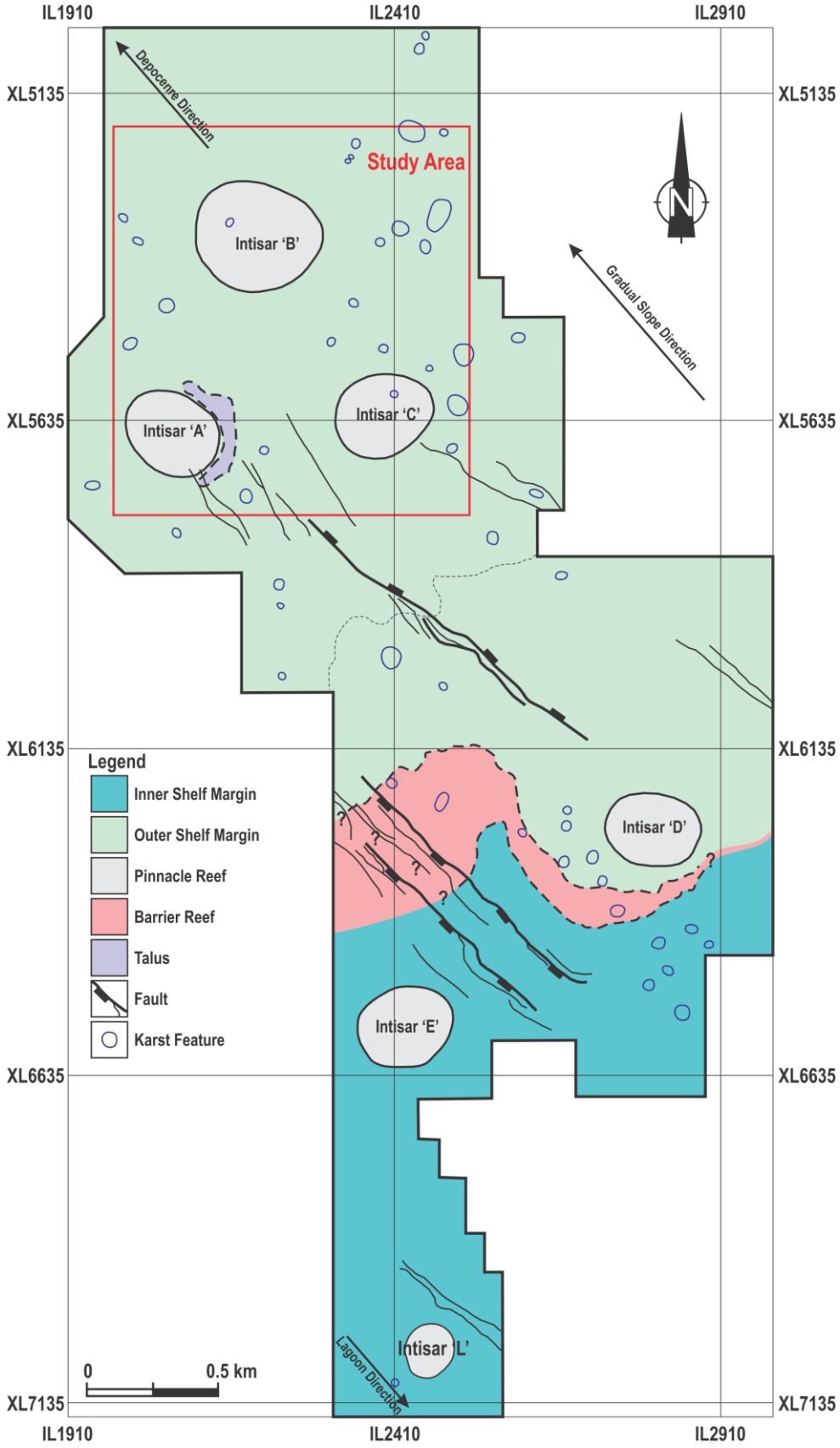

Figure 6.8. Paleogeographic map of Upper Sabil Carbonate.

6.5 Theory of Growth of Intisar Reefs

The physical controlling factors on carbonate depositional systems have been long known since Darwin (1842) exposed the effect of marine currents, winds and sea waves on the growth of reefs. The history of the Intisar reefs fits the Darwin transgressive type theory very well, because there are no evaporite sediments within, surrounding or overlying these reefs and no evidence of a change in facies between the fore-reef and the back-reef sediments. Darwin explained how reef growth is favoured through the rise of the shoreline. The first stage is an idealized hypothetical case of the Intisar 'B' reef growing upward because of a slow rise in sea level (Figure 6.10). Clearly, if the sea level were to stay steady throughout a long period, the reef would grow laterally toward the open marine zone (Link, 1950). In the second stage such a reef is indicated, as the Intisar 'E' started its growth throughout the last stages of the Intisar 'B', the latter now being dead and enclosed with shales. Sustained drowning would also finish the growth of Intisar 'E', and the sequent reefs indicated as Intisar 'L' would give rise to a complex case progressing toward the shore. With sustained drowning all these reefs would finally be enclosed by shale, and thus be closed completely, so that any of the hydrocarbons would be in completely isolated reservoirs. The reef growth was shifted more and more landwards, which indicates a continuously rising relative sea level. However, carbonate aggradation is normally associated with periods of relative sea level rise (Kendall and Schlager, 1981; Emery and Myers, 2009; Courgeon, Bourget and Jorry, 2016).

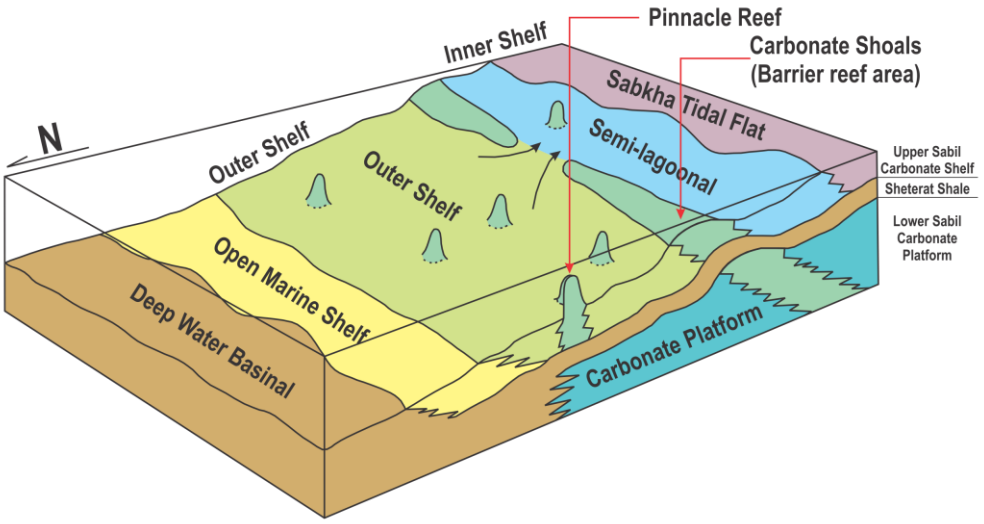

Figure 6.9. Three-dimensional depositional model of the Upper Sabil Carbonate shelf margin. Note: not to scale.

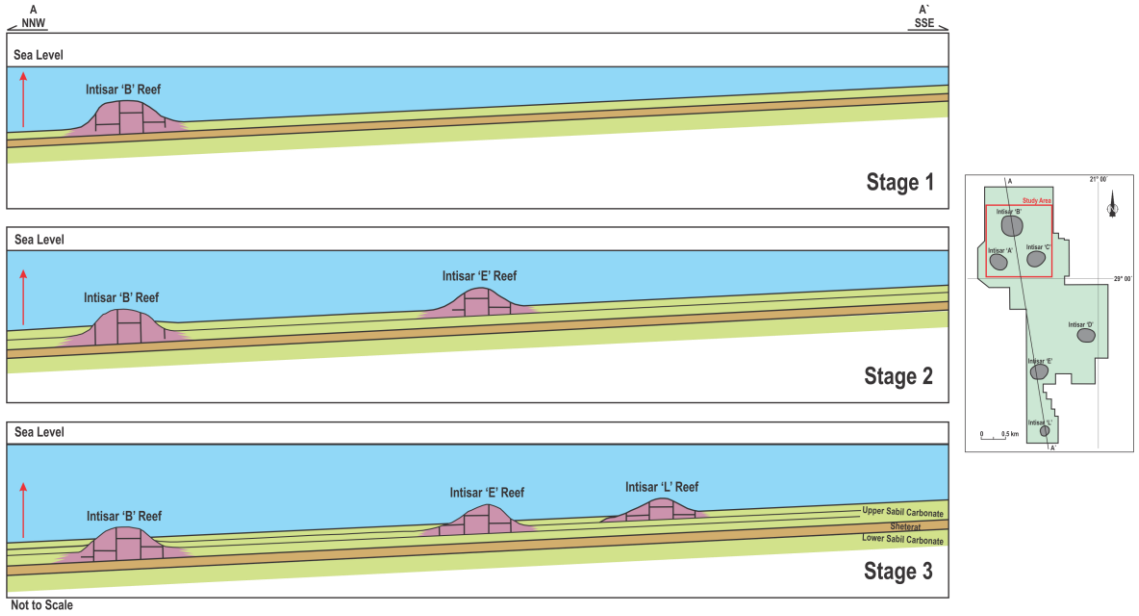

Figure 6.10. Intisar reef development during transgression of sea. Note: not to scale.

6.6 Development History of Intisar 'A' Reef

It was possible to unravel the development of the Intisar reefs in Sirt basin based on the integrated interpretation of all the seismic attributes, seismic inversion and well log data, for the first time. A practical geological model has been proposed that describes the evolution of the Intisar 'A' reef (Figure 6.11). In the central Sirt basin during Paleocene time, the Lower Sabil Carbonate was deposited in a low energy, shallow marine environment (Figure 6.11a). In the very early Upper Paleocene time, the major marine transgression is marked by the influx of the Sheterat Shale (Figure 6.11b). With the return of clear-water conditions during the remaining part of the Upper Paleocene, the sea-level began a very slow fall, due to variable subsidence of the underlying strata due to compaction or slight deep fault movements (Gumati and Kanes, 1985; Ghanoush, Imber and McCaffrey, 2014). The result over the Sheterat Shale was a deposition of micrite: the lower part of the Upper Sabil Carbonate (Figure 6.11c). As water continued to shoal, that accounted for an increase in foraminifera and algae constituents over the high areas of the lower part of the Upper Sabil Carbonate, and continued to build upward into moderate energy levels (Figure 6.11d). The rise in sea level is obvious from the foraminiferal fauna (Rosleff-Soerensen *et al.*, 2012). Under the proper local circumstances, the isolated Intisar 'A' reef was born (Figure 6.11e). The rate of subsidence was very slow, and the coral reef had a significant upward growth (Figure 6.11f). Since the Intisar 'A' reef was high on the sea floor and it was affected by

storm waves, the talus zone was formed around the reef. Early upward fluid flow (pressure solution) through the south-eastern part of the reef resulted in an overall enhancement of the original porosity by solution processes that both enlarged the pre-existing porosity and dissolved skeletons and fossils along fault zones (Figure 6.11g). At the end of the Paleocene, a major transgression happened, and the consequent deepening of the water in the area drowned and killed the Intisar 'A' reef and capped it with Kheir Shale (Figure 6.11h). The subsidence of the basin continued to the Eocene epoch (Gumati and Kanes, 1985; Abadi *et al.*, 2008). A sequence of carbonates and evaporates more than 13000 ft thick was deposited during the Eocene, as the Gir, Gialo and Augila Formations (Wang *et al.,* 2016). The migration of hydrocarbons into the Intisar 'A' reef occurred during Oligocene/Miocene time, when the reef was buried to a deep depth (Terry and Williams, 1969) (Figure 6.11i). There are about twenty known isolated reefs in the Ajdabiya trough; all of these have relatively the same size, shape and history as the Intisar 'A' reef.

6.7 Summary

In this chapter, the Upper Sabil carbonate shelf has been described and clarified and an understanding of the depositional processes has been developed based on the combined interpretation of seismic attributes. The time structural map of Concession 103 presents a surface morphology of Upper Sabil Carbonate which shows six large isolated circular pinnacle reefs which have similar sizes and age. The map also shows a relatively flat topography, with a gradual dipping towards the northwest. The map shows that the Intisar 'A', 'B' and 'C' reefs were located on the down-dip and positioned in a slightly greater water depth. The multi-attribute surface maps of the Upper Sabil Carbonate show two major faults in the centre of the study area and their orientation indicates an NW to SE trend. A horst block bounded saddle forms a strong positive morphology, and generally develops parallel to the shelf break between the Intisar 'A', 'B', 'C' and 'D' reefs' group, and the other two reefs. The Intisar 'E' and 'L' reefs may have been developed along the inner shelf margin. The growth of the reefs' succession took place on a paleo-high topography developed by the faulting. The Upper Sabil Carbonate shelf break between the outer and inner shelf zones is well-defined and parallel to the general strike direction of the shelf. In general, the high-energy conditions resulted in the development and growth of the isolated pinnacle reefs and shoals were situated immediately basin-ward of the high amplitude zone of Upper

Sabil Carbonate. Behind the shelf break, lagoonal conditions predominated with deposition of low energy dolomites, lime-mudstones and anhydrites, which resulted in the development of patch reefs. In some cases, pinnacle reefs may have developed along in the inner shelf margin. The closure of the barrier reef controls the depositional environment in the inner shelf zone distributed by the patch reefs, while behind the barrier reef lagoonal sediments dominate. The increasing concentration of pinnacle reefs growing on the inner bounding barrier reef possibly represents the increasing constraint of the open marine environment conditions behind it, so that the development of patch reefs was limited. The broken discontinuous barrier reef complex has initiated a semi-lagoonal open marine area; this was the ideal condition for the continued growth of the Intisar ‘E’ and ‘N’ pinnacle reefs within the inner shelf area.

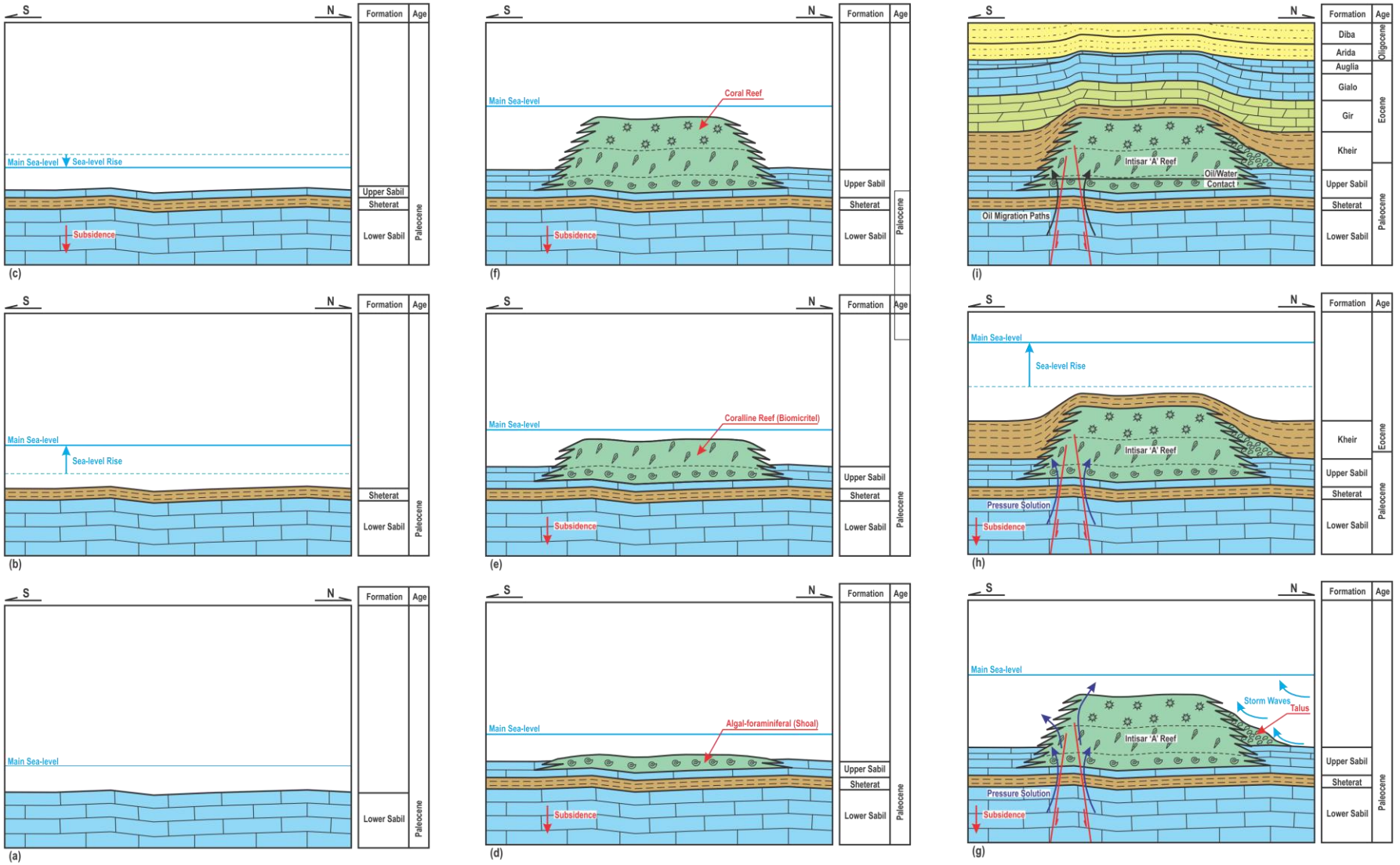

Figure 6.11. Geologic model of the evolution of the Intisar 'A' reef. Note: not to scale.

Chapter 7. Conclusions and Recommendations

Chapter 7

Conclusions and Recommendations

The study area is situated on Ajdabiya trough, in the eastern part of the Sirt basin, north-central Libya. The main play is Upper Sabil Carbonate, within large pinnacle reef traps. About twenty pinnacle reefs have been identified in the Ajdabiya trough within the Paleocene carbonates, some of which are oil bearing. The reservoirs are charged from the underlying mature Upper Cretaceous shales via faults and fractures. This study aims to improve our understanding of the depositional and geomorphological processes, the reservoir characterization, and the paleogeographic environment of the Paleocene reefs in the Sirt basin. In addition, it aims to provide better understandings on the evolution of Sirt basin, which remain controversial. The present study is based on three-dimensional post-stack seismic and well logs. Well data has been used to indicate the lithological and petrophysical variations within the reefs. The Seismic geomorphology has been used to assess how karst features affected reservoir characterization. The existing Intisar 'A' geological model has been updated using the properties estimated from the seismic inversion, to enhance the interpolation and modelling, and to predict the properties of Intisar 'B' and 'C' reservoirs, where minimum well control is available. The study has also provided a description of the Paleocene carbonate shelf

and the opportunity to clarify and develop an understanding of the depositional processes, based on the combined interpretation of seismic attributes.

In the Late Jurassic to Early Cretaceous, a drift-way movement over a fixed mantle hot-spot produced an extension and consequent collapse of what had been the Sirt uplift. The elasticity and stretch of the crust made the massive blocks of the Sirt arch move downward and break along the weak planes, forming a system of horsts and grabens. The Ajdabiya trough is the largest and deepest of the troughs in the Sirt basin. The trough is the most prolific part of the Sirt basin. The main play in the southern part of the Ajdabiya trough is Paleocene carbonates, within large pinnacle reef traps. The reefs within this section form productive oil reservoirs at the Sahabi, Intisar, Shatirah and Mheirigah oilfields; more than twelve pinnacle reefs have been discovered in the Ajdabiya trough, most of them are oil bearing. The reefs were developed in the Upper Sabil Carbonate with the Kheir Marl as top seal. These reservoirs are charged from the underlying mature Upper Cretaceous shales via faults and fractures.

The Intisar pinnacle reefs were controlled by two major marine transgressions which occurred across the Sirt basin shelves during the Paleocene period. The first major marine transgression, occurred in the very early Upper Paleocene period, while the second major marine transgression occurred in the remaining part of the Upper Paleocene. The Paleocene sequence is represented by two discontinuous carbonate cycles: Lower and Upper Sabil Carbonates, and the two cycles were separated by a thin narrow sheet-like unit of Sheterat Shale. The Paleocene succession of the Ajdabiya trough is characterized by a carbonate system that developed from a rimmed shelf. It was found that the average shelf slope is approximately 5° at this location. The Intisar pinnacle reefs developed within the outer-shelf environment in the protected southern embayment of the Ajdabiya trough. The development of these reefs is associated with shallow-water conditions and high-energy facies, deposited either along the shelf margins or on localized paleo-topographic highs of Lower Sabil Carbonate; these paleo-highs and deeper structure produced higher energy conditions and more favourable sites for increased biogenic activity and reef growth. However, the existence of subtle topographic features that are below the limit of seismic resolution cannot be confirmed. The Intisar pinnacle reefs started as algal-foraminiferal banks and the growth of the reef was terminated when subsidence or the rate of sea-level rise exceeded the rate at which the reef could build. The history of these reefs fits the Darwin submergence theory very well, as these pinnacle reefs have relatively same size and age. It was possible to unravel the evolution of the Intisar reefs in the Sirt basin based on the integrated

interpretation of all the seismic attributes, seismic inversion and well log data for the first time. Thus, a practical geological model has been proposed that describes the evolution of the Intisar reefs.

The Intisar ‘A’ reef, which is roughly circular in plan, grew vertically about 1390 ft, and is approximately 4.5 by 4.5 km in diameter. The Intisar ‘A’ and ‘C’ reefs are approximately 3 by 4 km in diameter, respectively. The third reef is the relatively large Intisar ‘B’ reef, which measures about 4.5 by 4.5 km in diameter. The Intisar reefs are interpreted as pinnacle reefs, and can be seen on seismic data by: (a) the convex shape at the reef top or eye effect, (b) drape, (c) break-up of data at the reef edge, (d) little continuity through the reef, (e) the low velocity of the higher porous and fractured reef than off-reef shales, which are more probably the cause of the velocity push-down of the seismic relief under the reef, and (f) associated with karst features. There are no evaporites within, overlying or surrounding these reefs and there is no any evidence of change in facies between the back-reef and fore-reef sediments. Some of the Intisar reefs have developed rim-synclines associated with faults/fractures which might have had an effect the migration pathways. The fluid migrates from the Intisar reefs into drape anticline beds over the reefs, the highly permeable reefs acting as fluid aquifers, directing pore waters from the compacting shales upward through the reefs. The overlying Kheir shale acts as the main seal and lateral side seals may be compromised by porous units, which reduce the effectiveness of the Kheir as a seal.

The Intisar ‘B’ and ‘C’ reefs contain only residual traces of oil whereas Intisar ‘A’ has hydrocarbon fill factors as high as 85%. More than twenty-six 0.2–1-km wide karst depressions can be identified in the Upper Sabil carbonates in this area. The seismic attributes indicate buried karst-collapse features at the Intisar ‘B’ and ‘C’ reefs, which are approximately 300 m and 200 m in diameter respectively, with an impact on the reservoir quality and production of oil within these fields. The residual trace of oil in these two reefs indicates that the oil migrated from these reefs after the sinkhole effects. These karst features occurred during the low stand of main sea level, during the Oligocene period. The karst-collapse features provide pathways for upward movement of hydrocarbons into the Eocene limestone reservoirs. This may be the main contributing factor to the escape of hydrocarbons from these two reef fields. The shale section above reservoir is a weak cap rock and allows for upward hydrocarbon migration. The relationship of the karst-collapse features with an abnormally large upward movement of water explains the high water cuts in these two reef fields.

The inversion of seismic data to acoustic impedance has allowed for a better determination of the main lithofacies units. In this study, the model-based method has been utilized for inverting a post-stack seismic volume set into impedance volume. The impedance colour variation is less in the model-based inversion, which is better distinguishable and corresponds to the acoustic impedance contrast and the lithology. The combination of seismic attributes' interpretation and seismic inversion together with log interpretation and petrographical study has improved our understanding and determination of the Intisar reefs reservoirs. The inverted impedance clearly highlighted facies and porosity variation in the Intisar reefs which are not apparent on the seismic data. Five vertical facies units in these reefs were characterized by different responses on the electrical well logs. These units have different deposition and different ages; from bottom to top they are: (a) the non-reef unit with porosity ranging between 6-12%, (b) the shoal (algal-foraminiferal) unit which has porosity ranging between 14-20%, (c) the coralline reef biomicrite unit that has porosity ranging between 23-27%, (d) the coral reef limestone unit that has porosity ranging between 18-23%, and (e) the talus unit, with porosity ranging between 6-20%.

The porosity of the south-eastern part of Intisar 'A' reef was significantly improved by faulting/fracturing and dissolution. In general, low-porosity limestone resulted from early calcite cementation and porous limestone intervals resulted from extensive dissolution. Well A6 on the southeast flank of the Intisar 'A' reef was the only remaining significant producer. It was most likely draining oil from the talus zone outside the Intisar 'A' reef, where there was likely to be significant remaining undrained potential. Talus deposits are located on the north-eastern flank of reef. These are not transgressive deposits but are the product of storm-related modern physical sedimentological processes. They are the integrated product of storms in the region that have operated during periods of lower sea level through the Paleocene. Sediments are mobilized throughout storm wave events, eroded from the reef top and deposited on the lee side of reef, forming the observed talus deposits. The lateral asymmetry in the talus deposits give the relative direction of storm waves and the orientation of the coast. The talus at Intisar 'A' reef has good reservoir quality, and this prospective area has not been drilled yet.

The time structural map of Concession 103 presents a surface morphology of Upper Sabil Carbonate, which shows six large isolated circular pinnacle reefs with similar size and age. The map also shows a relatively flat topography with a gradual dipping towards the northwest. From the map, it appears that the Intisar 'A', 'B' and 'C'

reefs were located on the down-dip and positioned in a slightly greater water depth. The multi-attribute surface maps of the Upper Sabil Carbonate show two major faults on the centre of the study area; the orientation of these faults indicates an NW to SE tend. A horst block bounded saddle forms a strong positive morphology, which generally develops parallel to the shelf break between the Intisar 'A', 'B', 'C' and 'D' reef group, and the other two reefs. The Intisar 'E' and 'L' reefs may have developed along in the inner shelf margin. The growth of the reefs' succession happened on a paleo-high topography developed by the faulting. The Upper Sabil Carbonate shelf break between the outer and inner shelf zones is well-defined and parallel to the general strike direction of the shelf. In general, the high-energy conditions resulted in the development of the isolated pinnacle reefs and shoals were situated immediately basin-ward of the high amplitude zone of Upper Sabil Carbonate. Behind the shelf break, lagoonal condition predominated with deposition of low energy dolomites, lime-mudstones and anhydrites which resulted in the development of patch reefs. In some cases, pinnacle reefs may have developed along in the inner shelf margin. The closure of the barrier reef controls the depositional environment in the inner shelf zone distributed by the patch reefs, while behind the barrier reef lagoonal sediments dominate. The increasing concentration of pinnacle reefs on the inner bounding barrier reef possibly represents the increasing constraint of the open marine environment conditions behind it, so the formation of patch reefs was limited. The broken discontinuous barrier reef complex initiated a semi-lagoonal open marine area; this was the ideal condition for the continued growth of the Intisar 'E' and 'N' pinnacle reefs in the inner shelf area.

On the basis of the current research work, the following recommendations have been proposed for future work: (a) To improve the seismic interpretation by using the pre-stack seismic data; pre-stack simultaneous inversion will enhance the inversion interpretation. The obtained results can be compared with the results from post-stack seismic inversion, using elastic impedance. (b) A detailed rock property modelling exercise, aided by pre-stack seismic inversion, could help in better reservoir properties estimation, thus enhancing well planning, particularly in the talus zones around the Intisar reefs. (c) Quantitative reinterpretation of the Upper and Lower Sabil Carbonate sections from seismic data, to define any other small isolated build-ups in the concession. Further integration with more borehole logs and perhaps well testing would help to characterize static reservoir connectivity. (d) Interpretation of Bougeur gravity and aeromagnetic data could enhance the imaging of the Lower Sabil paleo-highs, faults and basement rocks' features beneath the Intisar reefs.

Appendix A. Determination of Shale Content

Simple shaly formations are made up of a single matrix rock, either sandstone, limestone or dolomite mixed with shale. Because shales are more radioactive than sands or carbonates, gamma-ray logs can be used to calculate the shale fraction V_{Sh}, in selected formations. The first step in the calculation of shale volume is the determination of the gamma-ray index I_{GR}. This is accomplished using:

Equation A.1

$$I_{GR} = \frac{GR_{\log} - GR_{\min}}{GR_{\max} - GR_{\min}}$$

where GR_{log} is the gamma-ray reading at the depth of interest, GR_{min} is the minimum gamma-ray reading from clean carbonate (4.16 API), and GR_{max} is the maximum gamma-ray reading from shale (156.28 API).

Many petrophysicists then assume that $V_{sh}=I_{GR}$. To extract the shale content in rocks, a linear or non-linear relation is used to convert a gamma-ray index I_{GR}, to shale volume V_{sh}, because local sands or limestones contain radioactive components and the shales may vary with depth. The shale may be deposited as dispersed (clay distributed through the rock and pore space), laminated (thin layers of shale cutting the sand beds),

or structural form (an original depositional granular form). However, to be correct, the value of I_{GR} should be entered into the chart shown in Figure A.7.1. The Larionov (Tertiary Rocks) relation is used to convert a gamma-ray index I_{GR} to shale volume V_{sh}:

Equation A.2

$$V_{Sh} = 0.083 \times [\, 2^{(3.7 * I_{GR})} - 1]$$

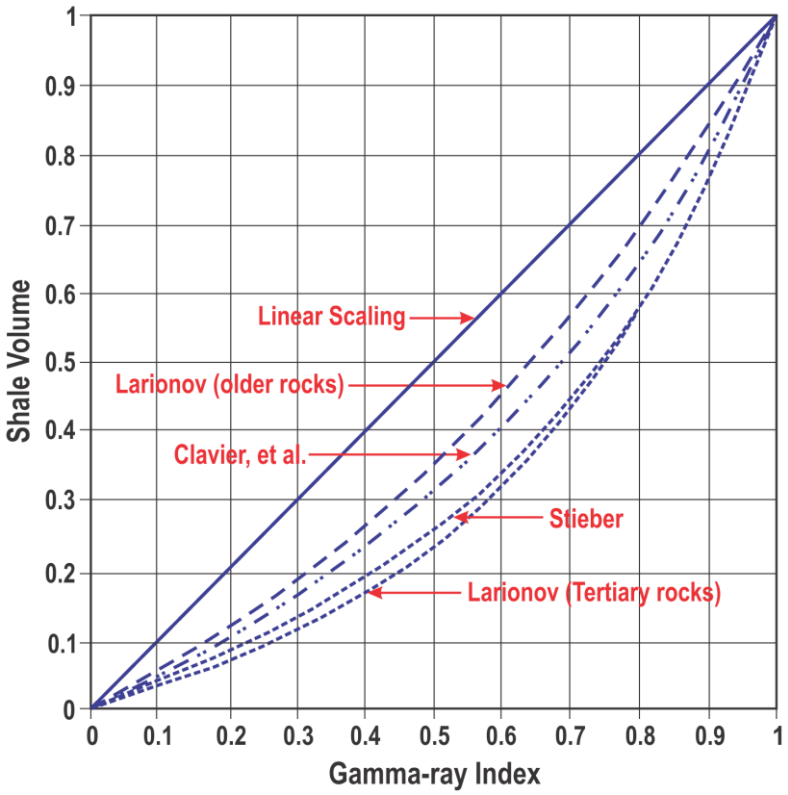

Figure A.7.1. Reported gamma-ray index (I_{GR}) to shale volume (V_{Sh}) conversion (Bigelow, 1995).

Appendix B. Determination of Porosity

Porosity is the pore volume per bulk volume of formation. Porosity may be estimated in three ways: directly from cores, indirectly from well logs or at high resolution from seismic data (Schlumberger, 1989). Porosity was calculated from the density log when available or from the sonic. The density is more likely to respond to the total porosity than the sonic log and therefore it was selected in all cases, if available. The neutron and density logs are responses to pores of all sizes. When a secondary porosity exists, i.e. of the vuggy type or when there are fractures, the sonic porosity that is read primary porosity. Total porosity was calculated from density logs by using the standard equation:

Equation A.3

$$\Phi_T = \frac{\rho_{ma} - \rho_b}{\rho_{ma} - \rho_f}$$

where ρ_b is the bulk density reading at the depth of interest, ρ_{ma} is the matrix density (2.71 gm/cm^3 for limestone), and ρ_f is the fluid density – usually mud filtrate (1.0 gm/cm^3). A fluid density of 1.0 gm/cm^3 was used because freshwater base mud was used in the drilling fluid. Shale also affects the accuracy of the density-derived porosity of the reservoir. Moreover, several minerals have anomalous densities, the log traces of

which may affect porosity values. Notable among these minerals are mica, siderite, and pyrite (Selley and Sonnenberg, 2014). Porosity can be corrected for the shale effect, so that an effective porosity can be computed as compared to a total porosity which includes the shale effect. Therefore, an effective porosity ($\Phi_{effective}$) can be defined as:

Equation A.4

$$\Phi_{effective} = \Phi_T - V_{Sh} \times \Phi_{Sh}$$

Appendix C. Determination of Water Saturation

Water saturation is the fraction (or percentage) of the pore volume of the reservoir rock that is filled with water. Water saturation values were calculated from logs using Archie's water saturation equation:

Equation A.5

$$S_w^n = \frac{F \times R_w}{R_t}$$

where R_w is the formation water resistivity, R_t is the true formation resistivity, F is the formation resistivity factor, and n is the saturation exponent. Archie examined the way that the formation factor F changes from rock to rock, and noticed that the following rule commonly holds true:

Equation A.6

$$F = \frac{a}{\Phi^m}$$

where Φ is porosity, a is the cementation constant, and m is the cementation exponent. In these equations, the saturation exponent n is usually taken as 2. It is assumed that a

and m are constant. In carbonates, $F=1/\Phi^2$ is usually used, with $a=1$ and $m=2$ (Schlumberger, 1989).

The value of formation water resistivity R_w was estimated using a Pickett plot (resistivity function of porosity) within the water zone of the reservoir. The Pickett plot shows the values of the formation resistivity R_t versus the effective porosity on a logarithmic scale. On this plot the hydrocarbon-bearing zones can be distinguished from the water-bearing ones. The data form straight lines with a gradient equal to the cementation exponent $m=2$. As shown on Figure A.7.2; at B1 well (Figure A.7.2), for a 100% water saturation formation $S_w=1$, $R_t=R_0=0.74$ ohm.m and $\Phi=23\%$, where R_0 is 100% water-saturated formation water resistivity. Hence, $F = 1/\Phi^2 = 1/(0.23)^2 = 18.9$. From Equation A.5, $R_w = R_0/F = 0.74/18.9 = 0.03$ ohm.m.

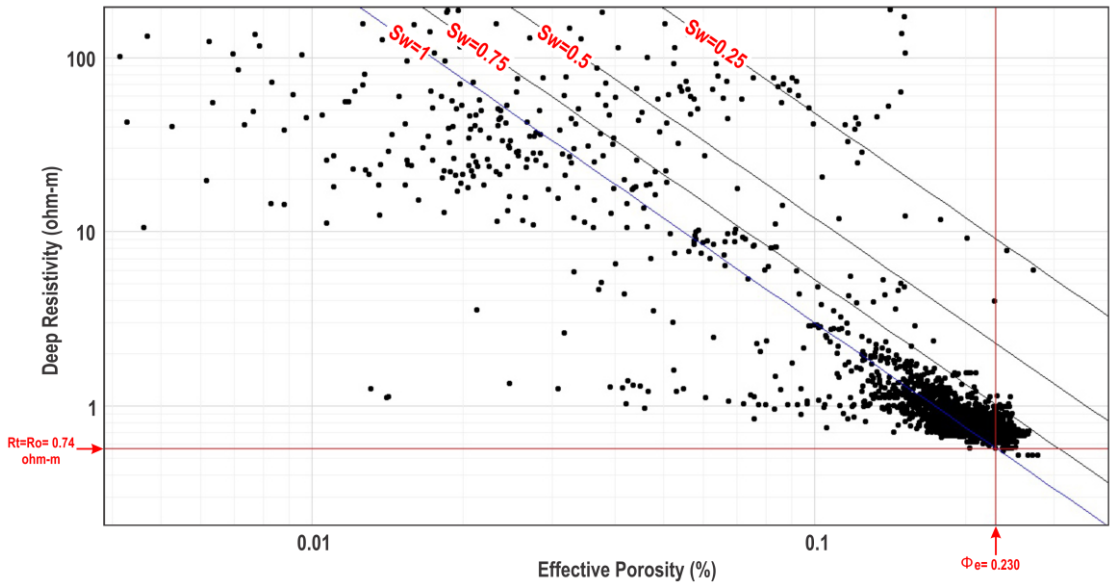

Figure A.7.2. Determining *m* and R_w at B1 well from Pickett plot.

Appendix D. Acoustic Impedance

Inversion of seismic data is the process to produce an estimate of the earth's acoustic impedance. The way in which the reflectivity can be extracted from the seismic is based on the convolutional model of the seismic trace according to:

Equation A.7

$$S = W * R + n$$

where S is the seismic trace, W is the wavelet, * is denotes convolution, R is the reflectivity time series, and n is the noise. R

A reflectivity time series is defined as the contrast in acoustic impedance (Z) between two interfaces:

Equation A.8

$$R_i = \frac{Z_{i+1} - Z_i}{Z_{i+1} + Z_i}$$

where the acoustic impedance is simply the product of interval velocity ($V_{int.}$) and bulk density (ρ_{bulk}):

Equation A.9

$$Z = V_{\text{int.}} \times \rho_{bulk}$$

Band-limited impedance inversion is commonly used with a classical recursive inversion algorithm, which ignores the effect of the seismic wavelet, and treats the trace as a set of reflection coefficients (Lindseth, 1979). The inversion of seismic data is based upon rearranging the terms of Equation A.8 to give the impedance series:

Equation A.10

$$Z_{i+1} = Z_i \left(\frac{1+R_i}{1-R_i}\right)$$

The inversion requires the initial value of Z to be known and the inherent bandwidth characteristic of the seismic adds a limitation to this technique. The low-frequency component missing in the seismic must be added from another source, such as calibrated sonic logs, to assure a more realistic result (Lindseth, 1979).

Appendix E. Multi-well Wavelet Estimation

Malkin and Canning (2008) summarized the multi-well wavelet estimation workflow, which includes the following steps: (1) Estimate wavelet amplitude spectrum $A(\omega)$ from seismic data. (2) For each well, from a selected set calculate a 4D correlation cube $\rho(\Delta x, \Delta y, \Delta t, \theta)$. Each point of the cube $\rho_{ijkl} = \rho(\Delta x_i, \Delta y_j, \Delta t_k, \theta_l)$ represents a normalized correlation for time shift Δt_k between synthetics (generated with a wavelet with predefined amplitude spectrum $A(\omega)$ and phase rotation angle θ_l), and seismic trace, extracted along the well trajectory and shifted relatively to the well position by Δx_i inlines and Δy_j crosslines. (3) By scanning the correlation cube for each i^{th} well, find the maximum correlation coefficient C_i and the corresponding best extracted trace position Δx_i, Δy_i. (4) Find a vector λ, maximizing the objective function:

Equation A.11

$$F(\boldsymbol{\lambda}) = \sum_{i=1}^{M} C_i R_i(\boldsymbol{\lambda})$$

where $R_i(\lambda)$ is the maximum of the cross-correlation between synthetics for the i^{th} well, generated with a wavelet with predefined amplitude spectrum $A(\omega)$ and phase spectrum $\theta(\omega, \lambda)$ defined by the equation

Equation A.12

$$\theta(\omega) = \sum_{k=1}^{N} \lambda_k \varphi_k(\omega)$$

and the seismic trace is extracted from the input volume along the well trajectory at the best position, Δx_i, Δy_i. Correlation coefficients C_i are used as weighting factors, reducing the contribution to the objective function from the bad wells.

Appendix F. Model Based Inversion Analysis

Well A1

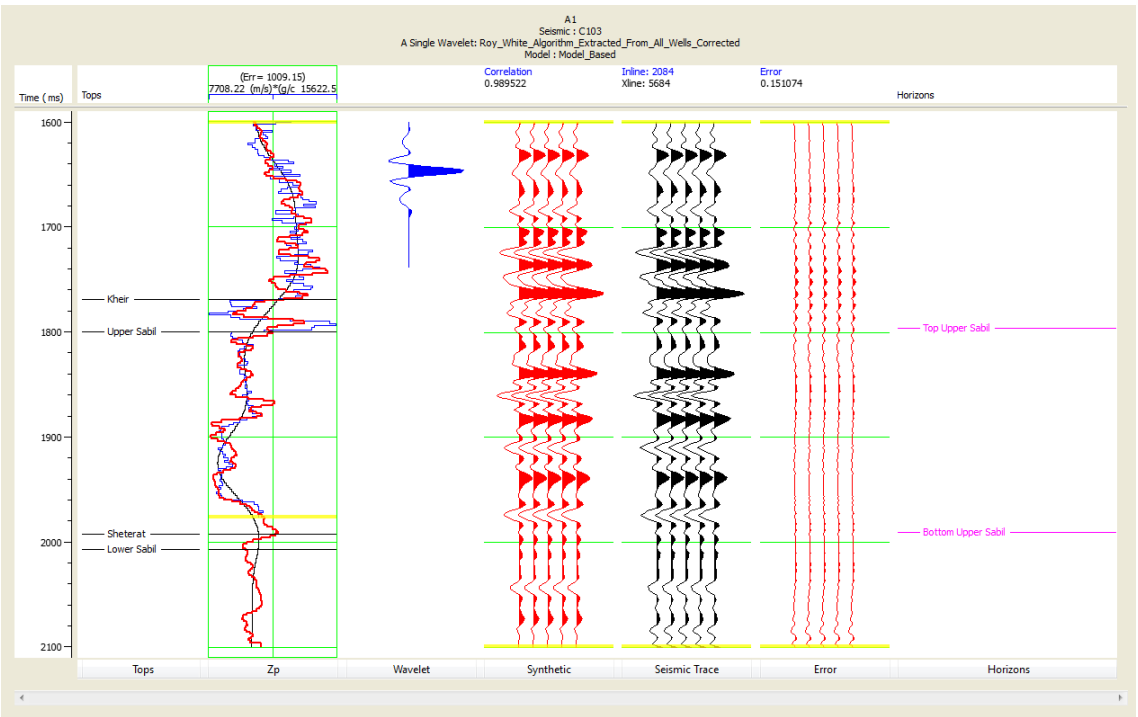

Well A2

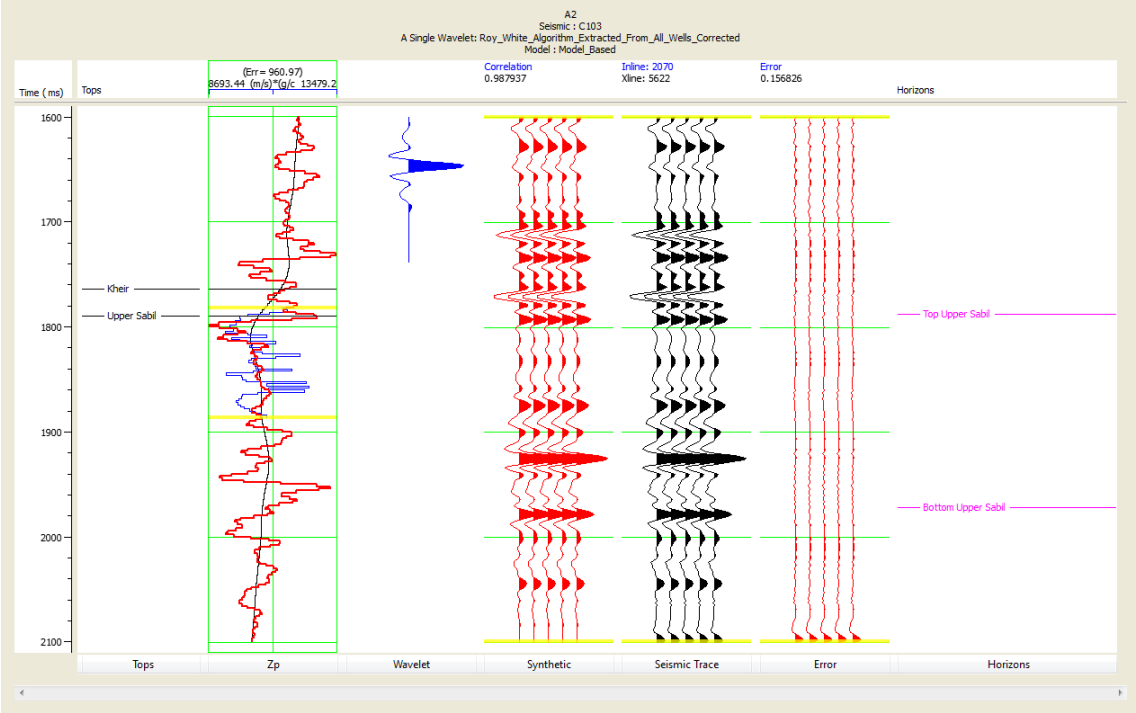

Well A7

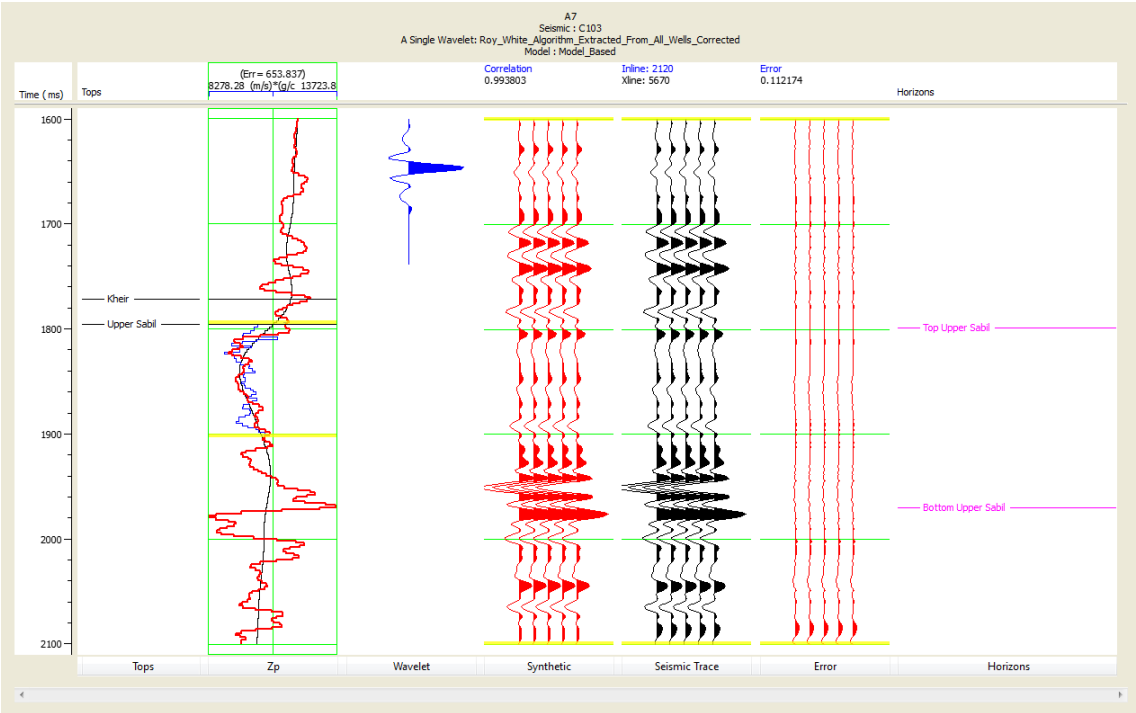

Well A9

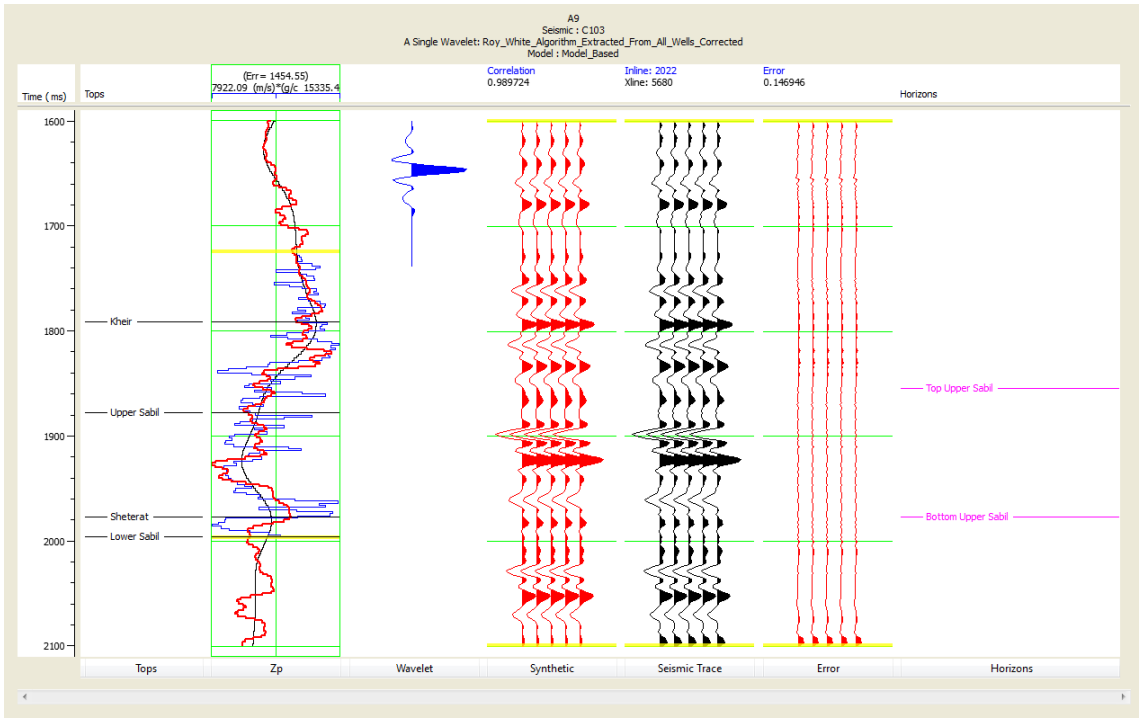

Well A11

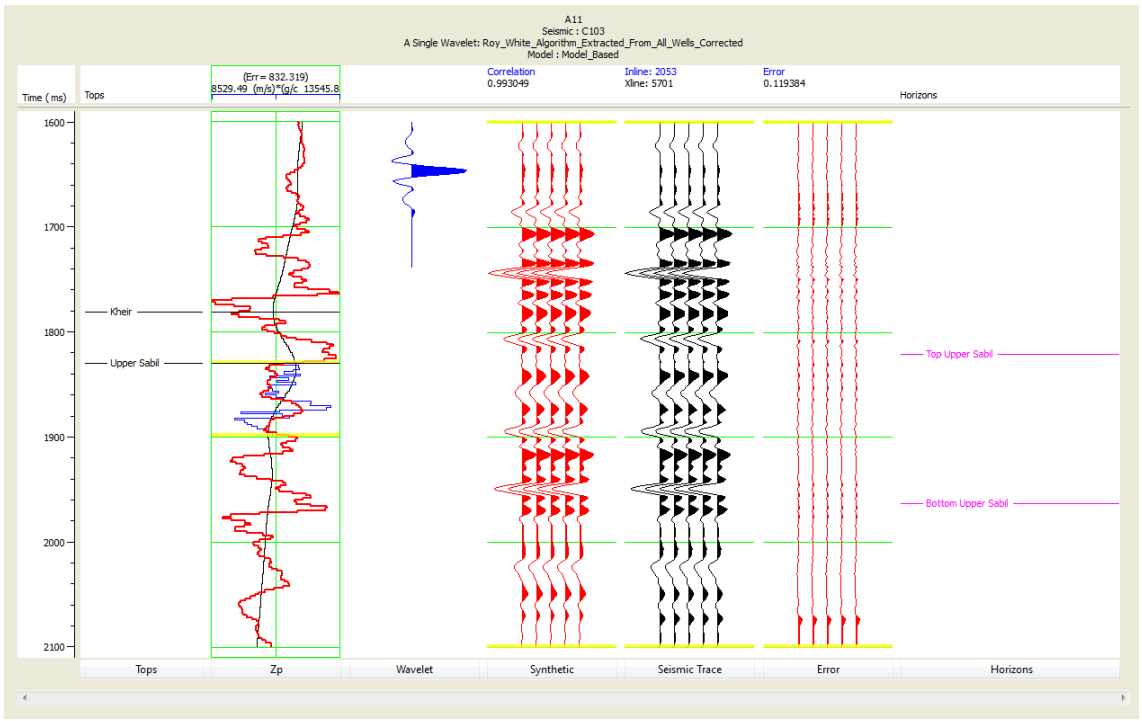

Well A51

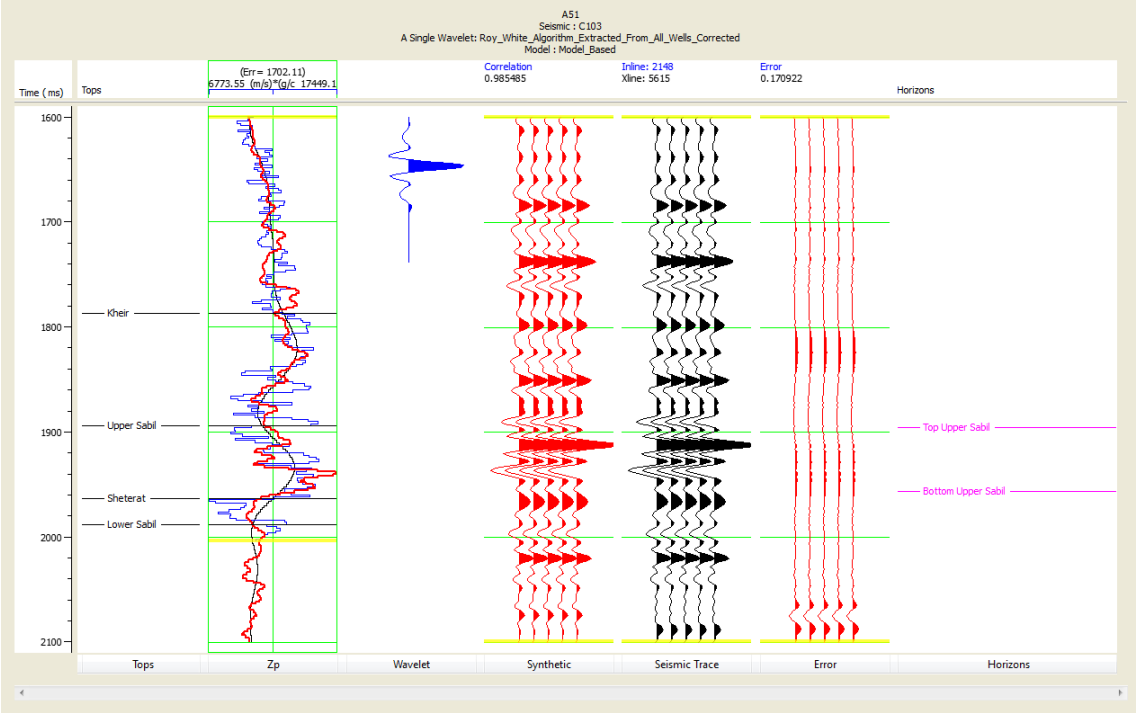

Well A52

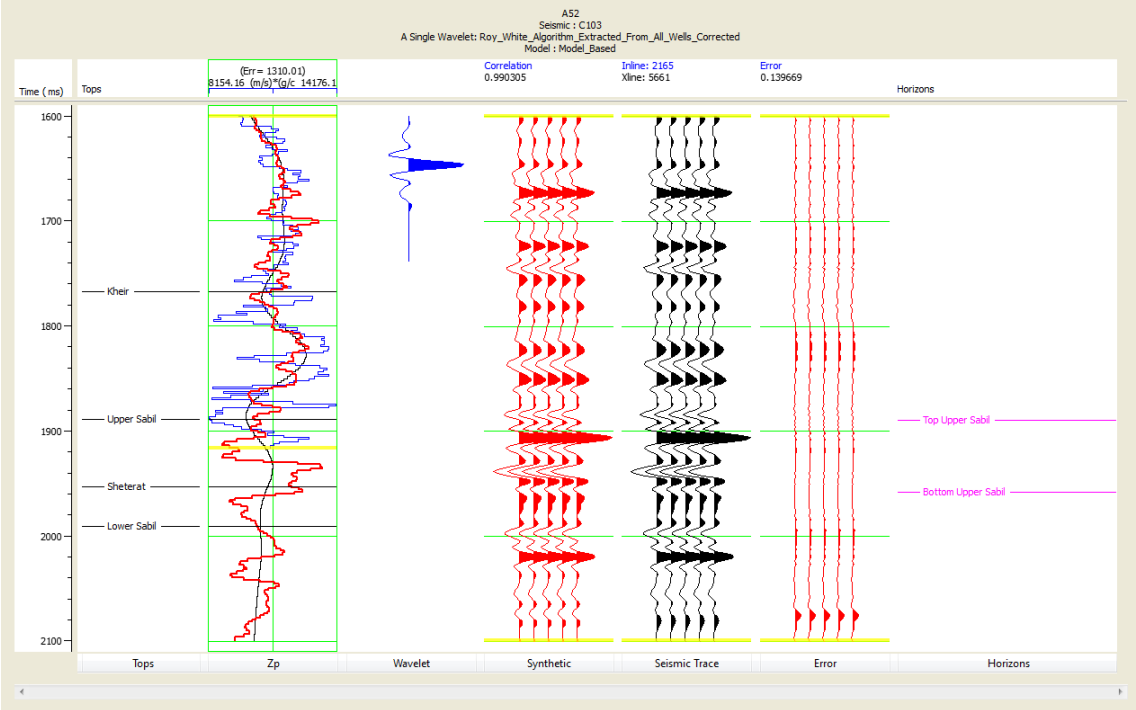

References

Abadi, A. M., van Wees, J.-D., van Dijk, P. M. and Cloetingh, S. A. P. L. (2008) 'Tectonics and subsidence evolution of the Sirt Basin, Libya', *AAPG bulletin*, 92(8), pp. 993-1027.

Ahr, W. M. (1973) 'The carbonate ramp: an alternative to the shelf model', *GCAGS Transactions*, 23, pp. 221-225.

Ahr, W. M. (2008) *Geology of carbonate reservoirs*. Wiley publication.

Ambrose, G. (2000) 'The geology and hydrocarbon habitat of the Sarir Sandstone, SE Sirt Basin, Libya', *Journal of Petroleum Geology*, 23(2), pp. 165-191.

Anketell, J. M. (1996) 'Structural history of the Sirt Basin and its relationship to the Sabratah Basin and Cyrenaican Platform, northern Libya', *The Geology of the Sirte Basin*, 3(Part 5), pp. 57-87.

APRC (2004) *Arab Oil & Gas Directory 2004*. Arab Petroleum Research Center, Paris, France.

Aqrawi, A. A. and Boe, T. H. (2012). SEG.

Aqrawi, A. A., Weinzierl, W., Daber, R. and Boe, T. H. (2012) *2012 SEG Annual Meeting*. Society of Exploration Geophysicists.

Archie, G. E. (1942) 'The electrical resistivity log as an aid in determining some reservoir characteristics', *Transactions of the AIME*, 146(01), pp. 54-62.

Badley, M. E. (1985) *Practical seismic interpretation*. Boston: International Human Resources Development Corporation.

GP501 Basic Interpretation (1984) Directed by Badley, M. E. and Anstey, N. A.

Bagnold, R. A. (1933) 'A further journey through the Libyan Desert', *Geographical Journal*, pp. 103-126.

Banerjee, S. (1980) *Stratigraphic lexicon of Libya*. Socialist People's Libyan Arab Jamahiriya, Industrial Research Centre.

Barr, F. T. and Weegar, A. A. (1972) *Stratigraphic Nomenclature of the Sirte Basin, Libya*. The Petroleum Exploration Society of Libia.

Betzler, C., Hübscher, C., Lindhorst, S., Reijmer, J. J., Römer, M., Droxler, A. W., Fürstenau, J. and Lüdmann, T. (2009) 'Monsoon-induced partial carbonate platform drowning (Maldives, Indian Ocean)', *Geology*, 37(10), pp. 867-870.

Bezan, M. A. (1996) 'The Paleocene sequence in Sirt Basin', in M. J. Salem, A. J. M. a. O. S. H. (ed.) *The geology of the Sirt Basin*. Amsterdam: Elsevier Science Ltd, pp. 97-118.

Bigelow, E. L. (1995) *Introduction to wireline log analysis: Western Atlas International*. Inc., Houston, Texas.

Blanchon, P. (2011) 'Geomorphic zonation', in *Encyclopedia of Modern Coral Reefs*. Springer, pp. 469-486.

Bonnefous, J. (1972) 'Geology of the Quartzitic Gargarf Formation in the Sirte Basin, Libya', *Bull. Cent. Rech. Pau.*, 6, pp. 256-261.

Borbajo, R. M. (2010) 'Reservoir Characterization of the Nido Limestone in the Northwest Palawan Basin Using Seismic Inversion', *Bulletin of Earth Sciences of Thailand (BEST), International Journal of Earth Sciences*, 3(2), pp. 45-48.

Brady, T. J., Campbell, N. D. J. and Maher, C. E. (1980) 'Intisar 'D' oil field, Libya', in *Giant Oil and Gas Fields of the Decade 1968-1978*. AAPG, pp. 543-564.

Braithwaite, C. J. R. (1973) 'Reefs: just a problem of semantics?', *AAPG Bulletin*, 57(6), pp. 1100-1116.

Bubb, J. N. and Hatlelid, W. G. (1978) 'Seismic stratigraphy and global changes of sea level, part 10: seismic recognition of carbonate buildups', in *Seismic stratigraphy - applications to hydrocarbon exploration*. Memoir 62: AAPG, pp. 772-791.

Burberry, C. M., Jackson, C. A.-L. and Chandler, S. R. (2016) 'Seismic reflection imaging of karst in the Persian Gulf: Implications for the characterization of carbonate reservoirs', *AAPG Bulletin*, 100(10), pp. 1561-1584.

Burgess, P. M., Winefield, P., Minzoni, M. and Elders, C. (2013) 'Methods for identification of isolated carbonate buildups from seismic reflection data', *AAPG bulletin*, 97(7), pp. 1071-1098.

Burk, K. and Dewey, J. F. (1974) 'Two plates in Africa during the Cretaceous?', *Nature*, 249, pp. 313-316.

Burwood, R., Cope, M. and Redfern, J. (2000) 'Petroleum System of the Eastern Sirte Basin, Libya', *Symp. on petrol. systems and evolving technol. in Afr. E&P, Geol. Soc. London, May 2000. Book of abstracts*, pp. 50-51.

Campbell Jr, R. L. (1968) 'Stratigraphic Applications of Dipmeter Date in Mid-Continent', *AAPG Bulletin*, 52(9), pp. 1700-1719.

Catuneanu, O., Abreu, V., Bhattacharya, J. P., Blum, M. D., Dalrymple, R. W., Eriksson, P. G., Fielding, C. R., Fisher, W. L., Galloway, W. E., Gibling, M. R., Giles, K. A., Holbrook, J. M., Jordan, R., Kendall, C. G. S. C., Macurda, B., Martinsen, O. J., Miall, A. D., Neal, J. E., Nummedal, D., Pomar, L., Posamentier, H. W., Pratt, B. R., Sarg, J. F., Shanley, K. W., Steel, R. J., Strasser, A., Tucker, M. E. and Winker, C. (2009) 'Towards the standardization of sequence stratigraphy', *Earth-Science Reviews*, 92(1), pp. 1-33.

Cerepi, A., Barde, J.-P. and Labat, N. (2003) 'High-resolution characterization and integrated study of a reservoir formation: the danian carbonate platform in the Aquitaine Basin (France)', *Marine and petroleum geology*, 20(10), pp. 1161-1183.

Chapman, R. E. (1983) *Petroleum geology*. Amsterdam: Elsevier Science Publishers B.V.

Chi, C.-Y., Mendel, J. M. and Hampson, D. (1984) 'A computationally fast approach to maximum-likelihood deconvolution', *Geophysics*, 49(5), pp. 550-565.

Chopra, S. and Marfurt, K. J. (2005) 'Seismic attributes—A historical perspective', *Geophysics*, 70(5), pp. 3SO-28SO.

Chopra, S. and Marfurt, K. J. (2007) *Seismic attributes for prospect identification and reservoir characterization*. Edited by Hill, S. J. SEG.

Choquette, P. W. and Pray, L. C. (1970) 'Geologic nomenclature and classification of porosity in sedimentary carbonates', *AAPG bulletin*, 54(2), pp. 207-250.

Cooke, D. A. and Schneider, W. A. (1983) 'Generalized linear inversion of reflection seismic data', *Geophysics*, 48(6), pp. 665-676.

Courgeon, S., Bourget, J. and Jorry, S. J. (2016) 'A Pliocene–Quaternary analogue for ancient epeiric carbonate settings: The Malita intrashelf basin (Bonaparte Basin, northwest Australia)', *Aapg Bulletin*, 100(4), pp. 565-595.

Craig, J., Rizzi, C., Said, F., Thusu, B., Luning, S., Asbali, A. I., Keeley, M. L., Bell, J. F., Durham, M. J. and Eales, M. H. (2008) 'Structural styles and prospectivity in the Precambrian and Palaeozoic hydrocarbon systems of North Africa', *The Geology of East Libya*, 4, pp. 51-122.

Cui, T. and Margrave, G. F. (2014) 'Seismic wavelet estimation', *the 26th Annual Report of the CREWES Project*.

Culshaw, M. G. and Waltham, A. C. (1987) 'Natural and artificial cavities as ground engineering hazards', *Quarterly Journal of Engineering Geology and Hydrogeology*, 20(2), pp. 139-150.

Cumings, E. R. (1932) 'Reefs or bioherms?', *Geological Society of America Bulletin*, 43(1), pp. 331-352.

Darwin, C. (1842) *The structure and distribution of coral reefs*. D. Appleton and company.

Davies, G. R. and Smith Jr, L. B. (2006) 'Structurally controlled hydrothermal dolomite reservoir facies: An overview', *AAPG bulletin*, 90(11), pp. 1641-1690.

Davis, R. A. (1983) *Depositional systems: A genetic approach to sedimentary geology*. Prentice-Hall Upper Saddle River.

Debeye, H. W. J. and Riel, v. P. (1990) 'Lp-norm deconvolution', *Geophysical Prospecting*, 38(4), pp. 381-403.

Dembicki, E. A. and Machel, H. G. (1996) 'Recognition and delineation of paleokarst zones by the use of wireline logs in the bitumen-saturated Upper Devonian Grosmont Formation of northeastern Alberta, Canada', *AAPG bulletin*, 80(5), pp. 695-712.

DesBrisay, C. L. and Daniel, E. L. (1972) 'Supplemental Recovery Development of The Intisar "A" and "D" Reef Fields, Libyan Arab Republic', *Journal of Petroleum Technology*, 24(07), pp. 785-796.

Desio, A. (1935) *Studi geologici sulla Cirenaica, sul Deserto Libico, sulla Tripolitania e sul Fezzan orientali.Missione scientifica della Reale Accademia d'Italia a Cufra, 1931*.

Dobrin, M. B. (1976) *Introduction to geophysical prospecting*. 3rd edn. McGraw-hill.

Dobrin, M. B. (1977) 'Seismic exploration for stratigraphic traps', in *Seismic Stratigraphy--Applications to Hydrocarbon Exploration*. AAPG, pp. 329-351.

Doveton, J. H. (1986) *Log analysis of subsurface geology: concepts and computer methods*. Canada: John Wiley & Sons Inc.

Dunham, R. J. (1962) 'Classification of carbonate rocks according to depositional textures', *Classification of Carbonate Rocks—a symposium: Tulsa, OK, AAPG*, Memoir 1, pp. 108-121.

Dunham, R. J. (1970) 'Stratigraphic reefs versus ecologic reefs', *AAPG Bulletin*, 54(10), pp. 1931-1932.

El-Alami, M., Rahouma, S. and Butt, A. (1989) 'Hydrocarbon habitat in the Sirte Basin, northern Libya', *Petroleum Research Journal*, 1, pp. 19-30.

Elag, M., Vur, C. T., Sefunc, A. and Sharif, A. (2014) 'Application of Seismic Attributes and Facies Modeling to Analyze The Reservoir Characterization In Intisar "103A" Field, Sirt Basin, Libya', *International Conference and Exhibition*. Istanbul, Turkey, September 14-17, 2014. AAPG.

Emery, D. (1996) 'Carbonate systems', *Sequence stratigraphy*, pp. 211-237.

Emery, D. and Myers, K. (2009) *Sequence stratigraphy*. John Wiley & Sons.

Faraj, M. A. M., Knudsen, T. Š., Nytoft, H. P. and Jovančićević, B. (2016) 'Organic geochemistry of crude oils from the Intisar oil field (East Sirte Basin, Libya)', *Journal of Petroleum Science and Engineering*, 147(November), pp. 605-616.

Finetti, I. (1982) 'Structure, stratigraphy and evolution of central Mediterranean', *Boll. Geofis. Teor. Appl*, 24(96), pp. 247-312.

Fitton, J. C. and Long, J. A. (1967) 'Reef interpretation by frequency analysis', *Canadian Journal of Exploration Geophysics*, 3, pp. 5-23.

Flügel, E. (2004) *Microfacies of carbonate rocks*. Springer, Berlin.

Folk, R. L. (1962) 'Spectral subdivision of limestone types', *Classifi cation of Carbonate Rocks—a symposium. Tulsa, OK, AAPG*, Memoir 1, pp. 62-84.

Fontaine, J. M., Cussey, R., Lacaze, J., Lanaud, R. and Yapaudjian, L. (1987) 'Seismic interpretation of carbonate depositional environments', *AAPG bulletin*, 71(3), pp. 281-297.

Gavotti, P., Lawton, D., Margrave, G. and Isaac, H. (2013) 'Poststack inversion of broadband seismic data from Alberta, Canada', in *SEG Technical Program Expanded Abstracts 2013*. Society of Exploration Geophysicists, pp. 3149-3153.

Gerdes, K. D., Winefield, P., Simmons, M. D. and Van Oosterhout, C. (2010) 'The influence of basin architecture and eustacy on the evolution of Tethyan Mesozoic and Cenozoic carbonate sequences', *Geological Society, London, Special Publications*, 329(1), pp. 9-41.

Ghanoush, H. B., Imber, J. and McCaffrey, K. (2014) 'Cenozoic Subsidence and Lithospheric Stretching Deformation of the Ajdabiya Trough Area, Northeast Sirt Basin, Libya', *Search and Discovery Article #10695*.

Gumati, Y. D. (1992) 'Lithostratigraphy of Oil-Bearing Tertiary Bioherms in the Sirte Basin, Libya', *Journal of Petroleum Geology*, 15(2), pp. 305-318.

Gumati, Y. D. and Kanes, W. H. (1985) 'Early Tertiary subsidence and sedimentary facies--northern Sirte Basin, Libya', *AAPG Bulletin*, 69(1), pp. 39-52.

Gumati, Y. D., Kanes, W. H. and Schamel, S. (1996) 'An evaluation of the hydrocarbon potential of the sedimentary basins of Libya', *Journal of Petroleum Geology. Scientific Press, U.K*, 19(1), pp. 95-112.

Halbouty, M. T., Meyerhoff, A. A., King, R. E., Dott Sr, R. H., Klemme, H. D. and Shabad, T. (1970) 'World's giant oil and gas fields, geologic factors affecting their formation, and basin classification: Part I: Giant oil and gas fields', *Geology of Giant Petroleum Fields*, Memoir 14, pp. 502-528.

Hallett, D. (2002) *Petroleum geology of Libya*. Elsevier.

Hallett, D. and Clark-Lowes, D. (2016) *Petroleum geology of Libya*. 2nd edn. Elsevier.

Hallett, D. and El Ghoul, A. (1996) 'Oil and Gas Potential of the Deep Trough Area in the Sirt Basin, Libya', *The Geology of Sirt Basin*, pp. 97-118.

Haq, B. U., Hardenbol, J. and Vail, P. R. (1987) 'Chronology of fluctuating sea levels since the Triassic', *Science*, 235(4793), pp. 1156-1167.

Harding, T. P. (1984) 'Graben hydrocarbon occurrences and structural style', *AAPG Bulletin*, 68(3), pp. 333-362.

Harris, P. T. and Heap, A. D. (2009) 'Cyclone-induced net sediment transport pathway on the continental shelf of tropical Australia inferred from reef talus deposits', *Continental Shelf Research*, 29(16), pp. 2011-2019.

Haye, E. F. (1967) 'Lateral density contrast-Key to finding reefs with gravity', *Canadian Journal of Exploration Geophysics*, 3, pp. 24-30.

Heatzig, G. and Michel, R. (1968) 'Petroleum Developments in North Africa in 1967', *AAPG Bulletin*, 52(8), pp. 1489-1511.

Hurley, N. F. and Budros, R. (1990) 'Albion-Scipio And Stoney Point Fields-USA, Michigan Basin'.

James, N. P. (1983) 'Reef environment', in Scholle, P. A., Bebout, D. G., and Moore, C. H. (ed.) *Carbonate Depositional Environments*. AAPG, pp. 346-462. 8.

Jankowsky, W. (1970) 'Empirical investigation of some factors affecting elastic wave velocities in carbonate rocks', *Geophysical Prospecting*, 18(1), pp. 103-118.

Jenyon, M. K. (1984) 'Seismic response to collapse structures in the Southern North Sea', *Marine and Petroleum Geology*, 1(1), pp. 27-36.

Jenyon, M. K. (1990) 'Oil and gas traps', *Aspects of their seismostratigraphy, morphology and development. John Wiley&Sons*.

Kendall, C. G. S. C. and Schlager, W. (1981) 'Carbonates and relative changes in sea level', *Marine Geology. Elsevier Scientific Publishing Company, Amsterdam*, 44(1), pp. 181-212.

Klimchouk, A. B. (2009) 'Principal features of hypogene speleogenesis', *Hypogene Speleogenesis and Karst Hydrogeology of Artesian Basins (ped. Klimchouk, AB, Ford, DC).–Simferopol: Ukrainian Institute of Speleology and Karstology*, pp. 7-16.

Klitzsch, E. (1970) 'Die Strukturgeschichte Der Zentral-Sahara: Neue Erkenntnisse Zum Bau Und Zur Palaeogeographic Eines Tafellandes', *Geol. Rundsch*.

Klitzsch, E. (1971) *Symposium on the geology of Libya: Tripoli, Faculty of Sciences, University of Libya*.

Koson, S., Chenrai, P. and Choowong, M. (2014) 'Seismic Attributes and Their Applications in Seismic Geomorphology', *Bulletin of Earth Sciences of Thailand*, 6(1), pp. 1-9.

Latimer, R. B., Davidson, R. and Van Riel, P. (2000) 'An interpreter's guide to understanding and working with seismic-derived acoustic impedance data', *The leading edge*, 19(3), pp. 242-256.

Lees, A. (1975) 'Possible influence of salinity and temperature on modern shelf carbonate sedimentation', *Marine Geology. Elsevier B.V.*, 19(3), pp. 159-198.

Li, M. (2014) *Geophysical Exploration Technology: Applications in Lithological and Stratigraphic Reservoirs*. Elsevier.

Lindseth, R. O. (1979) 'Synthetic sonic logs-a process for stratigraphic interpretation', *Geophysics*, 44(1), pp. 3-26.

Link, T. A. (1950) 'Theory of transgressive and regressive reef (bioherm) development and origin of oil', *AAPG Bulletin*, 34(2), pp. 263-294.

Loucks, R. G. (1999) 'Paleocave carbonate reservoirs: origins, burial-depth modifications, spatial complexity, and reservoir implications', *AAPG bulletin*, 83(11), pp. 1795-1834.

Loucks, R. G. and Handford, C. R. (1996) 'Origin and recognition of fractures, breccias and sediment fills in paleocave-reservoir networks', *PUBLICATIONS-WEST TEXAS GEOLOGICAL SOCIETY*, pp. 207-220.

Loucks, R. G. and Mescher, P. K. (2002) 'Paleocave facies classification and associated pore types'.

Lowenstam, H. A. (1950) 'Niagaran reefs of the Great Lakes area', *the Journal of Geology. The University of Chicago Press*, 58(4), pp. 430-487.

Lucet, N., Déquirez, P.-Y. and Cailly, F. (2000) *2000 SEG Annual Meeting*. Society of Exploration Geophysicists.

Lucia, F. J. (2007) *Carbonate reservoir characterization: an integrated approach*. Springer Science & Business Media.

MacGregor, L., Andreis, D. and Cooper, R. (2010) *EGM 2010 International Workshop*.

Machel, H. G. (2004) 'Concepts and models of dolomitization: a critical reappraisal', *Geological Society, London, Special Publications*, 235(1), pp. 7-63.

Malkin, A. and Canning, A. (2008) *2008 SEG Annual Meeting*. Society of Exploration Geophysicists.

Mancini, E. A., Parcell, W. C. and Har, B. S. (2006) *T-R Cycle Characterization and Imaging: Advanced Diagnostic Methodology for Petroleum Reservoir and Trap Detection and Delineation*.

Massa, D. and Delort, T. (1984) 'Evolution Du Bassin De Syrte (Libya) Du Cambrien Au Cretace Basal', *Bull. Soci. Geol. France*.

McQuillin, R., Bacon, M. and Barclay, W. (1984) *An introduction to seismic interpretation-Reflection seismics in petroleum exploration*. Graham & Trotman Limited.

Meckel Jr, L. D. and Nath, A. K. (1977) 'Geologic considerations for stratigraphic modeling and interpretation', in *Seismic Stratigraphy--Applications to Hydrocarbon Exploration*. AAPG, pp. 417-438.

Mikbel, S. R. (1977) 'Basement configuration and structure of Western Libya', *Libyan Journ. Sci*, 7, pp. 19-34.

Mikbel, S. R. (1979) 'Structural and configuration map of the basement of east and central Libya: Neues Jahrbuch fur Geol', *Palaont. Abhhan dlungen*, 158(2), pp. 209-220.

Mitchum Jr, R. M. and Vail, P. (1977) 'Seismic Stratigraphy and Global Changes of Sea Level: Part 7. Seismic Stratigraphic Interpretation Procedure', *Seismic Stratigraphy--Applications to Hydrocarbon Exploration*, AAPG Memoir(26), pp. 135-143.

Mitchum Jr, R. M., Vail, P. R. and Sangree, J. B. (1977) 'Seismic stratigraphy and global changes of sea level: Part 6. Stratigraphic interpretation of seismic reflection patterns in depositional sequences', *Seismic Stratigraphy--Applications to Hydrocarbon Exploration*, AAPG Memoir(26), pp. 117-133.

Mitchum Jr, R. M., Vail, P. R. and Thompson III, S. (1977) 'Seismic stratigraphy and global changes of sea level: Part 2. The depositional sequence as a basic unit for stratigraphic analysis', *Seismic Stratigraphy--Applications to Hydrocarbon Exploration*, AAPG Memoir(26), pp. 53-62.

Moore, C. H. and Wade, W. J. (2013) *Carbonate Reservoirs: Porosity and diagenesis in a sequence stratigraphic framework*. Newnes.

Mouzughi and Taleb (1981) *Tectonic Elements of Libya*, 1:2 000 000. National Oil Corporation, Libya.

Nelson, H. F., Brown, C. W. and Brineman, J. H. (1962) 'Skeletal limestone classification', *Classification of Carbonate Rocks. AAPG Special Volumes*, Memoir 1, pp. 224-252.

Oldenburg, D. W., Scheuer, T. and Levy, S. (1983) 'Recovery of the acoustic impedance from reflection seismograms', *Geophysics*, 48(10), pp. 1318-1337.

Palmer, A. N. (1991) 'Origin and morphology of limestone caves', *Geological Society of America Bulletin*, 103(1), pp. 1-21.

Parsons, M. G., Zagaar, A. M. and Curry, J. J. (1980) 'Hydrocarbon occurrences in the Sirte basin, Libya', *Facts and Principles of World Petroleum Occurrence*, Memoir 6, pp. 723-732.

Pendrel, J. (2001) 'Seismic inversion—The best tool for reservoir characterization', *CSEG Recorder*, 26(1), pp. 18-24.

Peterson, J. A. (1986) 'Geology and Petroleum Resources of North-Central and Northeast Africa', *Am. Assoc. Pet. Geol., Bull.;(United States)*, 70(CONF-860624-).

Pickett, G. R. (1973) 'Pattern recognition as a means of formation evaluation', *The Log Analyst*, 14(04).

Pomar, L. (2001) 'Types of carbonate platforms: a genetic approach', *Basin Research*, 13(3), pp. 313-334.

Posamentier, H. W., Davies, R. J., Cartwright, J. A. and Wood, L. (2007) 'Seismic geomorphology-an overview', *Seismic geomorphology: applications to hydrocarbon exploration and production*, 277(1).

Pramanik, A. G., Srivastava, A. K., Singh, V. and Katiyar, R. (2002) 'Stratigraphic interpretation using post stack seismic inversion: Case histories from Indian Basins', in *SEG Technical Program Expanded Abstracts 2002*. Society of Exploration Geophysicists, pp. 1758-1761.

Prothero, D. R. and Schwab, F. (2004) *Sedimentary geology*. Macmillan.

Purdy, E. G. (1974) 'Reef configurations: cause and effect', *Special Publications of SEPM*, 18, pp. 9-76.

Purdy, E. G. and Gischler, E. (2005) 'The transient nature of the empty bucket model of reef sedimentation', *Sedimentary Geology*, 175(1), pp. 35-47.

Purdy, E. G. and Waltham, D. (1999) 'Reservoir implications of modern karst topography', *AAPG bulletin*, 83(11), pp. 1774-1794.

Roohi, M. (1996) 'A geological view of source-reservoir relationships in the western Sirt Basin', *The geology of Sirt Basin: Amsterdam, Elsevier*, 2, pp. 323-336.

Rosleff-Soerensen, B., Reuning, L., Back, S. and Kukla, P. (2012) 'Seismic geomorphology and growth architecture of a Miocene barrier reef, Browse Basin, NW-Australia', *Marine and Petroleum Geology*, 29(1), pp. 233-254.

Rusk, D. C. (2001) 'Libya, Petroleum Potential of the Underexplored Basin Centers--A Twenty-First-Century Challenge', *AAPG Memoir*, 74, pp. 429–452.

Russell, B. and Toksöz, M. N. (1991) *1991 SEG Annual Meeting*. Society of Exploration Geophysicists.

Saheel, A. S., Bin Samsudin, A. R. and Bin Hamzah, U. (2010) 'Regional geological and tectonic structures of the Sirt basin from potential field data', *American Journal of Scientific Industrial Research*, 1(3), pp. 448-462.

Salem, Y. A. A. (1996) 'Dix Stacking Velocity Interpretation in the Intisar "D" Field', *The Geology of Sirt Basin*, III, pp. 243-265. Elsevier, Amterdam.

Sangree, J. B. and Widmier, J. M. (1977) 'Seismic Stratigraphy and Global Changes of Sea Level: Part 9. Seismic Interpretation of Clastic Depositional Facies', *Seismic Stratigraphy--Applications to Hydrocarbon Exploration*, AAPG Memoir(26), pp. 165-184.

Saqab, M. M. and Bourget, J. (2015) 'Controls on the distribution and growth of isolated carbonate build-ups in the Timor Sea (NW Australia) during the Quaternary', *Marine and Petroleum Geology*, 62, pp. 123-143.

Schlager, W. (1993) 'Accommodation and supply—a dual control on stratigraphic sequences', *Sedimentary Geology*, 86(1-2), pp. 111-136.

Schlager, W. (1999) 'Sequence stratigraphy of carbonate rocks', *The Leading Edge*, 18(8), pp. 901-907.

Schlumberger (1989) *Log Interpretation Principles/Applications*. Houston, Texas: Schlumberger Educational Services.

Selley, R. C. and Sonnenberg, S. A. (2014) *Elements of petroleum geology*. Academic Press.

Sheriff, R. (1980) 'Seismic stratigraphy: IHRDC'.

Sheriff, R. E. (1991) *Encyclopedic dictionary of exploration geophysics*. Society of Exploration Geophysicists (SEG), Tulsa.

Sheriff, R. E. (1997) 'Seismic Resolution a key element', *AAPG Explorer*, 18(10), pp. 44-51.

Skirius, C., Nissen, S., Haskell, N., Marfurt, K., Hadley, S., Ternes, D., Michel, K., Reglar, I., D'Amico, D. and Deliencourt, F. (1999) '3-D seismic attributes applied to carbonates', *The Leading Edge*, 18(3), pp. 384-393.

Smith Jr, L. B. (2006) 'Origin and reservoir characteristics of Upper Ordovician Trenton–Black River hydrothermal dolomite reservoirs in New York', *AAPG bulletin*, 90(11), pp. 1691-1718.

Smith, R. G. and Baker, J. D. (1983) *Proceedings of the Eighth international joint conference on Artificial intelligence-Volume 1*. Morgan Kaufmann Publishers Inc.

Spring, D. and Hansen, O. P. (1998) 'The influence of platform morphology and sea level on the development of a carbonate sequence: the Harash Formation, Eastern Sirt Basin, Libya', *Geological Society, London, Special Publications*, 132(1), pp. 335-353.

Story, C., Peng, P., Heubeck, C., Sullivan, C. and Lin, J. D. (2000) 'Liuhua 11-1 field, south China sea: a shallow carbonate reservoir developed using ultrahigh-resolution 3-D seismic, inversion, and attribute-based reservoir modeling', *The Leading Edge*, 19(8), pp. 834-844.

Tawadros, E. (2011) *Geology of North Africa*. CRC Press.

Taylor, H. L., Banks, S. C. and McCoy, J. F. (1979) 'Deconvolution with the ℓ 1 norm', *Geophysics*, 44(1), pp. 39-52.

Teichert, C. and Fairbridge, R. W. (1948) 'Some Coral Reefs of the Sahul Shelf', *Geographical Review*, 38(2), pp. 222-249.

Telford, W. M., Geldart, L. P. and Sheriff, R. E. (1990) *Applied geophysics*. 2nd edn. Cambridge, UK: Cambridge University Press.

Terry, C. E. and Williams, J. J. (1969) 'The Idris 'A' bioherm and oilfield Sirte Basin Libya–its commercial development regional Paleocene geologic setting and stratigraphy', *The exploration for petroleum in Europe and North Africa: London, Inst. Petroleum*, pp. 31-48.

Tiratsoo, E. N. (1976) *Oilfields of the World*. England: Scientific Press Ltd.

Tucker, M. E. (1991) *Sedimentary petrology: an introduction to the origin of sedimentary rocks*. John Wiley & Sons.

Tucker, M. E. and Wright, V. P. (1990) *Carbonate Sedimentology*. Oxford, United Kingdom, Blackwell Scientific Publications.

Tucker, P. M. and Yorston, H. J. (1973) *Pitfalls in seismic interpretation*. SEG Books.

Vahrenkamp, V. C., David, F., Duijndam, P., Newall, M. and Crevello, P. (2004) 'Growth architecture, faulting, and karstification of a middle Miocene carbonate platform, Luconia Province, offshore Sarawak, Malaysia'.

Van Houten, F. B. (1983) 'Sirte Basin, north-central Libya: Cretaceous rifting above a fixed mantle hotspot?', *Geology*, 11(2), pp. 115-118.

Vandenberghe, N., Poggiagliolmi, E. and Schwarz, E. (1983) *European geothermal update. International seminar. 3*.

Veeken, P. C., Priezzhev, I. I., Shmaryan, L. E., Shteyn, Y. I., Barkov, A. Y. and Ampilov, Y. P. (2009) 'Nonlinear multitrace genetic inversion applied on seismic data across the Shtokman field, offshore northern Russia', *Geophysics*, 74(6), pp. WCD49-WCD59.

Wang, Y., Eichkitz, C. G., Schreilechner, M. G., Heinemann, G., Davis, J. C. and Gharsalla, M. (2016) 'Seismic attributes for description of reef growth and channel system evolution—Case study of Intisar E, Libya', *Interpretation*, 4(1), pp. SB1-SB11.

Warrlich, G. M. D., Waltham, D. A. and Bosence, D. W. J. (2002) 'Quantifying the sequence stratigraphy and drowning mechanisms of atolls using a new 3-D forward stratigraphic modelling program (CARBONATE 3D)', *Basin Research*, 14(3), pp. 379-400.

White, R. (1997) *1997 SEG Annual Meeting*. Society of Exploration Geophysicists.

White, R. and Simm, R. (2003) 'Tutorial: Good practice in well ties', *First Break*, 21(10).

White, R. E. and Hu, T. (1998) 'How accurate can a well tie be?', *The Leading Edge*, 17(8), pp. 1065-1071.

Williams, J. J. (1972) 'Augila Field, Libya: Depositional Environment and Diagenesis of Sedimentary Reservoir and Description of Igneous Reservoir', *Stratigraphic Oil and Gas Fields-Classification, Exploration Methods and Case Histories. AAPG Memoir*, 16, pp. 623-632.

Wilson, J. L. (1975) *Carbonate Facies in Geologic History*. Springer-Verlag, New York.

Wright, V. P. and Burchette, T. P. (1996) *Shallow-water carbonate environments*. Edited by Reading, H. G. Blackwell Science, Oxford.

Wyllie, M. R. J., Gregory, A. R. and Gardner, L. W. (1956) 'Elastic wave velocities in heterogeneous and porous media', *Geophysics*, 21(1), pp. 41-70.

Yadav, L., Ghosh, D., Maurya, S. N. and Bhattacharya, A. N. (2004) 'Calibration of Sonic Logs for Seismic Applications in Upper Assam', *Conference & Exposition on Petroleum Geophysics*. Hyderabad, India. pp. 154-161.

Yungul, S. H. (1961) 'Gravity prospecting for reefs: effects of sedimentation and differential compaction', *Geophysics*, 26(1), pp. 45-56.